PNNL-27452 Rev. 1

Pacific Northwest NATIONAL LABORATORY

Potential Impacts of Accelerated Climate Change

Third Annual Report of Work for NRC Agreement Number NRC-HQ-60-14-D-0025

April 2019

LR Leung
R Prasad

U.S. DEPARTMENT OF ENERGY

Prepared for the U.S. Nuclear Regulatory Commission
under an Interagency Agreement with the U.S. Department of Energy
Contract DE-AC05-76RL01830

PACIFIC NORTHWEST NATIONAL LABORATORY
operated by
BATTELLE
for the
UNITED STATES DEPARTMENT OF ENERGY
under Contract DE-AC05-76RL01830

Printed in the United States of America

Available to DOE and DOE contractors from the
Office of Scientific and Technical Information,
P.O. Box 62, Oak Ridge, TN 37831-0062;
ph: (865) 576-8401
fax: (865) 576-5728
email: reports@adonis.osti.gov

Available to the public from the National Technical Information Service
5301 Shawnee Rd., Alexandria, VA 22312
ph: (800) 553-NTIS (6847)
email: orders@ntis.gov <http://www.ntis.gov/about/form.aspx>
Online ordering: http://www.ntis.gov

This document was printed on recycled paper.

(8/2010)

PNNL-27452 Rev. 1

Potential Impacts of Accelerated Climate Change

Third Annual Report of Work for NRC Agreement Number NRC-HQ-60-14-D-0025

April 2019

LR Leung
R Prasad

Prepared for the U.S. Nuclear Regulatory Commission
under an Interagency Agreement with the U.S. Department of Energy
Contract DE-AC05-76RL01830

Pacific Northwest National Laboratory
Richland, Washington 99352

Abstract

This study is part of the U.S. Nuclear Regulatory Commission's (NRC) Probabilistic Flood Hazard Assessment (PFHA) research program. This current report summarizes Year 3 activities, which focused on reviewing region-specific scientific findings about climate change for the Midwest Region. The Midwest Region comprises eight states—Illinois, Indiana, Iowa, Michigan, Minnesota, Missouri, Ohio, and Wisconsin—which is consistent with the regional makeup used in the Third and Fourth National Climate Assessments (NCA3 and NCA4). Except for Indiana, the states in the Midwest Region have operating nuclear power plants and new nuclear power reactor permit and license applications have been submitted to the NRC for sites located in two midwestern states.

Climatic features relevant to the NRC for the Midwest Region include temperature and precipitation extremes,[1] severe storms, riverine flooding, low flows and seasonal streamflow, and Great Lakes water-level, storm surge, and ice-cover changes. Drawing primarily from the NCA reports and peer-reviewed literature, this Year 3 annual report summarizes the regional climate, including observed trends and projected changes, as well as 21st century hydrologic impacts. The Midwest Region has experienced long-term warming trends with acceleration occurring in the later years of the 20th century and into the 21st century. Warming is projected to continue in the future. Extreme rainfall events and flooding have increased during the last century; annual precipitation magnitude increased by 0.31 in./decade, with much of the increase resulting from intensification of the heaviest rainfalls. For example, the increased frequency of longer-lived mesoscale convective systems has contributed to the increased extreme rainfall in the past 35 years. Daily precipitation at the 5-percent annual exceedance probability is projected to increase by 10 to 20 percent between the mid-century and late-century for the lower and higher emissions scenarios. Precipitation change projections are more robust across models for winter; summer change projections have larger uncertainty because most global models are not able to simulate intense summer rainfall that contributes significantly to the seasonal mean. Severe weather is projected to increase in the future as the convective available potential energy increases with warmer temperatures and increasing atmospheric moisture. Projecting the water level of the Great Lakes remains challenging because of modeling limitations.

Flood frequency in the Midwest Region is projected to increase in the future, as warming increases the ratio of rainfall to total precipitation in the cold season and increases extreme rainfall in the warm season. However, uncertainties associated with hydrologic modeling can significantly affect estimates of flood magnitudes. Site-specific flood assessments, which is the current NRC practice for application reviews, that incorporate insights of the climate research community with hydrologic engineering practice can incorporate these uncertainties for consideration in decision-making.The authors of this report note that the climate research community has not focused on evaluating trends and impacts of meteorological (and by extension, hydrologic) events of exceedance probabilities that are of interest to the NRC for permitting and licensing. Current climate models have significantly larger uncertainties for events whose exceedance probabilities approach those of interest to the NRC. These uncertainties are carried through and combined with uncertainties in hydrologic and hydraulic modeling approaches employed in hydrologic engineering assessments including PFHAs. Therefore, a consistent framework for enumerating, attributing, and incorporating these uncertainties, both in climate models and in hydrologic engineering assessments, should be used in site-specific PFHAs for permitting and licensing.

Pacific Northwest National Laboratory staff presented updates summarizing these findings at the Third Annual PFHA Research Workshop, which took place from December 4–6, 2017, at NRC Headquarters in Rockville, Maryland.

[1] The precise meaning of the term "extreme" can vary between the climate research community and the nuclear regulatory community. More details are provided in Section 1.2 of this report.

Executive Summary

The study reported here is part of the U.S. Nuclear Regulatory Commission's (NRC's) Probabilistic Flood Hazard Assessment (PFHA) research program that aims to develop regulatory tools and guidance to support and enhance the NRC's capacity to perform thorough and efficient reviews of license applications and license amendment requests.The NRC asked Pacific Northwest National Laboratory (PNNL) to prepare a summary of the current state of climate research and results regarding hydrometeorological phenomena that are of interest in safety assessments and environmental impact assessments for commercial nuclear power plants. In Year 1, PNNL staff prepared an annual report that summarized recent scientific findings about global and regional climate change, focusing in particular on climatic elements across the conterminous United States that are relevant to NRC concerns broadly (i.e., increasing air and water temperatures, decreasing water availability, increasing frequency and intensity of storms and flooding, and sea-level rise). In Year 2, PNNL staff summarized recent research findings about climate change for the Southeast Region of the United States (i.e., historical and projected changes in air temperature, precipitation, hurricanes, sea-level rise, storm surge, tornadoes, flooding, and low flows). This report summarizes Year 3 activities, which focused on reviewing region-specific scientific findings about climate change for the Midwest Region. Consistent with the U.S. Global Change Research Program Third National Climate Assessment (NCA3) and the Fourth National Climate Assessment (NCA4), this current report defines the Midwest Region to comprise eight states—Illinois, Indiana, Iowa, Michigan, Minnesota, Missouri, Ohio, and Wisconsin. Except for Indiana, the states in the Midwest Region have operating nuclear power plants. Further, new nuclear power reactor permit and license applications have been submitted to the NRC in the recent past for sites located in two of the Midwest Region states. Therefore, having an improved understanding of potential climate change and resulting hydrologic impacts in the Midwest Region is important to informing the PFHA research program.

Climatic features relevant to the NRC for the Midwest Region include temperature extremes,[1] precipitation extremes, severe storms, flooding, low flows, seasonal streamflow, and water-level and ice-cover changes in the Great Lakes. Drawing primarily from the NCA reports and peer-reviewed literature, this Year 3 annual report summarizes the observed climate, its past changes, and its projected changes, as well as 21st century hydrologic impacts in the Midwest Region. The Midwest Region exhibits long-term warming trends with acceleration occurring the later years of the 20th century and into the 21st century. Warming is projected to continue in the future. The annual number of days with daily maximum temperature above 95°F is projected to increase by up to 30 days when the 1980 to 2000 period is compared to projections for the 2041 to 2070 period. Extreme rainfall events and flooding increased during the last century by up to 20 percent in some locations; annual precipitation magnitude increased by 0.31 in./decade, with much of the increase resulting from intensification of the heaviest rainfalls. For example, increased frequency of longer-lived mesoscale convective systems have contributed to the increased extreme rainfall in the past 35 years. Daily precipitation at the 5-percent annual exceedance probability is projected to increase by 10 to 20 percent between the mid-century and late-century for the lower and higher emissions scenarios. Projected changes in daily peak precipitation are quite robust across the global climate models in the Coupled Model Intercomparison Project Phase 5 for winter, showing an increase of about 32 percent over the 2017 to 2100 period compared to the 1950 to 2005 period. For summer, however, the projected changes have large uncertainty; models show both increases and decreases, leading to a multimodel ensemble mean decrease of about 6 percent. Uncertainty in projecting summer precipitation changes is related to the inability of most global models to simulate the

[1] The precise meaning of the term "extreme" can vary between the climate research community and the nuclear regulatory community. More details are provided in Section 1.2 of this report.

intense summer rainfall, which also leads to warm biases and uncertainty in projecting summer temperature changes.

More than half of the 24-hour 1-percent annual exceedance probability rainfall events east of the Rocky Mountains in the period from 2002 through 2011 were associated with mesoscale convective systems (MCSs). Analysis of observations indicates that the precipitation frequency and lifetime of MCSs occurring during the period from April through June in the north-central United States (including the Midwest Region) have increased by 11 percent per decade and 4 percent per decade, respectively, from 1979 to 2014. More frequent and longer-lived MCSs occurring over the past 35 years are associated with enhanced moisture transport by the Great Plains low-level jet because there is more warming over land than over the adjacent ocean. Climate simulations that explicitly resolve deep convection project MCS precipitation to be more intense and cover larger areas in a warmer climate due to enhanced convective available potential energy and stronger updraft supported by enhanced moisture transport by the low-level jet into the Central and Midwest Regions. Severe weather is also projected to increase in the future as convective available potential energy increases with warmer temperatures and increased atmospheric moisture. Using convection-permitting simulations made feasible by advances in computing resources, several studies have provided new insights into changes in hazardous convective weather beyond those derived from traditional analysis of the changes in severe storm environments.

After remaining below long-term mean levels in the first decade of the 21st century, mean annual water levels for the five Great Lakes have been recovering in the last few years. Projections of the future water levels in the Great Lakes range from a slight decrease to a slight increase. Projecting the Great Lakes water level remains challenging because of limitations in modeling the complex processes that influence the Great Lakes water budget. Recent studies have shown that models largely overestimate evapotranspiration in the Great Lakes, which significantly impacts modeled water levels. Flood frequency in the the Midwest Region has been increasing (over the last five decades), but no significant changes in flood magnitude have been observed over the same period. Flood frequency is projected to increase in the future, as warming increases the ratio of rainfall to total precipitation in the cold season and increases extreme rainfall in the warm season. However, many other hydrometeorologic parameters that influence flood generation are not addressed directly in the NCAs. Additionally, uncertainties associated with hydrologic modeling can significantly affect estimates of flood magnitudes, particularly for floods of exceedance probabilities of interest to the NRC. Site-specific flood assessments, which is the current NRC practice for application reviews, that incorporate insights of the climate research community with hydrologic engineering practice can assist in quantifying these uncertainties for decision-making.

PNNL staff presented updates summarizing these findings at the Third Annual PFHA Research Workshop, which took place from December 4 to 6, 2017, at NRC Headquarters in Rockville, Maryland.

Glossary

Bermuda High	The Bermuda High (also known as the North Atlantic Subtropical High and the Azores High) is a semi-permanent, subtropical area of high pressure in the North Atlantic Ocean off the East Coast of North America that migrates east and west with varying central pressure. When it is displaced westward, during the Northern Hemispheric summer and fall, the center is located in the western North Atlantic, near Bermuda. In the winter and early spring, it is primarily centered near the Azores in the eastern part of the North Atlantic. The summer westward extension of the Bermuda High enhances the Great Plains low-level jet that transports moisture northward into the Midwest Region, causing increased precipitation.
Clausius-Clapeyron relationship	The Clausius-Clapeyron relationship describes the discontinuous transition between two phases of matter of a single constituent. In meteorology and climatology, this relationship is used to calculate the change in saturation water vapor pressure per unit change in air temperature. Based on this relationship and under typical atmospheric conditions, saturation water vapor pressure changes approximately exponentially with temperature and the water-holding capacity of the atmosphere increases by about 7 percent for every 1 degree Celsius rise in temperature.
climate change	Changes in average weather conditions that persist over multiple decades or longer. Climate change encompasses both increases and decreases in temperature, as well as shifts in precipitation, changing risk of certain types of severe weather events, and changes in other features of the climate system.
climate variability	Natural changes in climate that fall within the observed range of extremes for a particular region, as measured by temperature, precipitation, and frequency of events. Drivers of climate variability include the El Niño-Southern Oscillation and other phenomena.
convective available potential energy (CAPE)	CAPE is the amount of energy a parcel of air would have if lifted a certain distance vertically through the atmosphere. CAPE effectively represents the positive buoyancy of an air parcel and is an indicator of atmospheric instability that can lead to convective storms.
convective inhibition (CIN)	CIN is a measure of the amount of energy that will prevent an air parcel from rising from the surface to the level of free convection. The negatively buoyant energy is a result of the air parcel being cooler than the air that surrounds it, causing a downward acceleration of the air parcel. Typically, an area with a high convection inhibition is considered stable and has very little likelihood of developing a thunderstorm. Conceptually, it is the opposite of CAPE.

convection-permitting simulations	Convection-permitting simulations are atmospheric simulations performed at fine horizontal resolution, such that deep convection is explicitly resolved instead of using convection or cumulus parameterization (typically grid spacings of 4 km or less).
El Niño	El Niño and La Niña are opposite phases of what is known as the El Niño-Southern Oscillation (ENSO) cycle. The ENSO cycle describes the fluctuations in temperature between the ocean and atmosphere in the east-central Equatorial Pacific. El Niño is sometimes referred to as the warm phase of ENSO and La Niña the cold phase of ENSO. These deviations from normal surface temperatures can have large-scale impacts not only on ocean processes, but also on global weather and climate.
enhanced Fujita scale	An update of the original Fujita scale (F-scale), the Enhanced Fujita (EF) scale rates the intensity of tornadoes based on the observed damage they cause. The EF scale was adopted by the National Weather Service on February 1, 2007.
extreme event	An extreme event is defined by its frequency of occurrence or return period. The definition of “extreme” is a statistical concept that varies depending on the location, season, and length of the historical record. For example, 99^{th} percentile precipitation, which refers to the precipitation that has an annual exceedance probability of 1/100, is one definition of extreme precipitation used in this report. In practice, the exceedance probability considered to be extreme depends on the application. For example, an event considered to be extreme in the context of climate studies, agricultural applications, or design of typical civil infrstrucure such as roads and bridges may not be extreme in the context of critical infrastructure such as high-hazard dams or nuclear power plants.
(climate) forcing	Factors that affect the Earth’s climate. For example, natural factors such as volcanoes and human factors such as the emission of heat-trapping gases and particles through fossil fuel composition.
greenhouse gases	Gases that absorb heat in the atmosphere near the Earth’s surface, preventing it from escaping into space. If the atmospheric concentrations of these gases increase, the average temperature of the lower atmosphere will gradually increase—a phenomenon known as the greenhouse effect. Greenhouse gases include, for example, carbon dioxide, water vapor, and methane.
global climate models (GCM)	Mathematical models that are used to numerically simulate the physics, chemistry, and biology that influence the global climate system.

Hadley cell	The Hadley cell is a global-scale tropical atmospheric circulation that features air rising near the equator, flowing poleward at 10 to 15 kilometers above the surface, descending in the subtropics, and then returning equatorward near the surface. This circulation creates the trade winds, tropical rain-belts and hurricanes, subtropical deserts, and the jet streams.
hazardous convective weather (HCW)	Tornadoes, hail, and damaging winds are events collectively referred to as hazardous convective weather. HCW is rare and most often does not occur even when the atmospheric environment is favorable because HCW requires initiation. Nevertheless, identifying large-scale environments that are favorable for HCW has helped advance understanding of how it may change in the future.
heat wave	A period of abnormally hot weather lasting days to weeks.
La Niña	La Niña is a coupled ocean-atmosphere phenomenon that is the counterpart of El Niño as part of the broader El Niño-Southern Oscillation climate pattern. During a period of La Niña, the sea surface temperatures across the equatorial Eastern Central Pacific Ocean will be lower than normal by 3 to 5°C. In the United States, the effects of La Niña persist for at least five months. La Niña has extensive effects on the weather in North America, even affecting the Atlantic and Pacific hurricane seasons.
land cover	The physical characteristics of the land surface, such as soils, crops, trees, or impervious surface.
land use	Activities taking place on land, such as growing food, cutting trees, or building cities (strongly connected with land cover).
mesoscale convective system (MCS)	MCSs are complexes of thunderstorms that become organized on a scale larger than individual storms (but smaller in scale than tropical cylones). They produce precipitation that covers a horizontal scale of hundreds of kilometers and lasts up to 24 hours. MCSs contribute about 60 percent of warm season precipitation and over half of the extreme 24-hour precipitation in the Midwest Region.
Representative Concentration Pathway (RCP)	These are four greenhouse gas concentration (not emission) trajectories adopted by the Intergovernmental Panel on Climate Change (IPCC) for its fifth Assessment Report (AR5) in 2014, which supersedes the Special Report on Emissions Scenarios (SRES) published in 2000. The four scenarios are RCP2.6, RCP4.5, RCP6, and RCP8.5, all of which are possible. They are named after a possible range of radiative forcing values in the year 2100 relative to pre-industrial values (+2.6, +4.5, +6.0, and +8.5 Wm^{-2}, respectively).

tornado outbreak	A tornado outbreak is the occurrence of multiple tornadoes over a region, usually spawned by thunderstorms embedded in the same synoptic-scale weather system. The number of tornadoes required to qualify as an outbreak is at least 6 to 10. The tornadoes usually occur within the same day, or continue into the early morning hours of the succeeding day, and within the same region. Tornado outbreaks usually occur from March through June in the Great Plains of the United States and Canada, the Midwestern United States, and the Southeastern United States.
wave train	A superposition of waves propagating in the same direction and with almost equal phase speeds.
wet-bulb temperature	The wet-bulb temperature is the temperature that a parcel of air would have if it were cooled to saturation by the evaporation of water into it. It is largely determined by both the air temperature and the amount of moisture in the air. The wet-bulb temperature is the lowest temperature that may be achieved by evaporative cooling of a water-wetted, ventilated surface.

Acronyms and Abbreviations

7Q2	50 percent exceedance probability lowest 7-day average streamflow
7Q10	90 percent exceedance probability lowest 7-day average streamflow
AEP	annual exceedance probablility
AMO	Atlantic Multidecadal Oscillation
AWSSI	accumulated winter season severity index
BASINS	Better Assessment Science Integrating Point and Non-point Sources
BCSD	bias-correction spatial disaggregation
CAM	Community Atmosphere Model
CAPE	convective available potential energy
CC	Clausius-Clapeyron relation
CGLRRM	Coordinated Great Lakes Regulation and Routing Model
CHARM	Coupled Hydrosphere Atmospheric Research Model
CIN	convective inhibition
CMIP	Coupled Model Intercomparison Project
CMIP3	Coupled Model Intercomparison Project Phase 3
CMIP5	Coupled Model Intercomparison Project Phase 5
CNRM-CM5	Centre National de Recherches Météorologiques Coupled Global Climate Model, version 5
CRCM	Canadian Regional Climate Model
CSSR	Climate Science Special Report
DJF	December-January-February
EA	energy adjustment
ECB	(USACE) Engineering and Construction Bulletin
EF	Enhanced Fujita (scale that measures the intensity of a tornado based on wind speed and related damage to structures, vegetation, etc.)
ENSO	El Niño-Southern Oscillation
EPA	U.S. Environmental Protection Agency
F	Fujita (scale that measures the intensity of a tornado based on damage to structures, vegetation, etc.)
FI	Flood Index
FRT	extratropical cyclone near a front
GCM	global climate model
GEM	Global Environmental Multiscale Model
GEV	Generalized Extreme Value
GFDL	Geophysical Fluid Dynamics Laboratory
GHCN-Daily	Global Historical Climatology Network-Daily
GHG	greenhouse gases

GLC	Great Lakes Commission
GLERL	Great Lakes Environmental Research Laboratory
GLM-HMD	GLERL monthly hydrometeorological database
GLRCM	Great Lakes Regional Climate Model
GLSHyFS	Great Lakes Seasonal Hydrologic Forecasting System
GR4J	Modèle du Génie Rural à 4 Paramètres Journalier
HEC-HMS	Hydrologic Engineering Center-Hydrologic Modeling System
HCW	hazardous convective weather
HUC	Hydrologic Unit Code
IGLD	International Great Lakes Datum
IJC	International Joint Commission
IPCC	Intergovernmental Panel on Climate Change
IUGLS	International Upper Great Lakes Study
IUGLSB	International Upper Great Lakes Study Board
JJA	June-July-August
L2SWBM	Large Lake Statistical Water Balance Model
LBRM	large basin runoff model
LCL	lifting condensation level
LLTM	large lake thermodynamic model
MAM	March-April-May
MCC	mesoscale convective complex
MCS	mesoscale convective system
MESH	Environment Canada's Modélisation Environnementale – Surface et Hydrologie
MIROC5	Model for Interdisciplinary Research on Climate, version 5
MMF	multiscale modeling framework
MODIS	Moderate Resolution Imaging Spectroradiometer
NAO	North Atlantic Oscillation
NARCCAP	North American Regional Climate Change Assessment Program
NARR	North American Regional Reanalysis
NASA	National Aeronautics and Space Administration
NASEM	National Academies of Science, Engineering, and Medicine
NBS	net basin supply
NCA	National Climate Assessment
NCA3	Third National Climate Assessment
NCA4	Fourth National Climate Assessment
NCDC	(NOAA) National Climatic Data Center
NCEI	(NOAA) National Centers for Environmental Information (formerly NCDC)
NDSEV	number of days with severe-thunderstorm environment

NOAA	National Oceanic and Atmospheric Administration
NLCD	National Land Cover Database
NLDAS	North American Land Data Assimilation System
NOAA	National Oceanic and Atmospheric Administration
NRC	U.S. Nuclear Regulatory Commission
NSE	Nash-Sutcliffe efficiency
NTC	Number of tropical cyclones
P-E	precipitation minus evaporation
PDF	probability density function
PDI	Power Dissipation Index
PDO	Pacific Decadal Oscillation
PFHA	Probabilistic Flood Hazard Assessment
PGW	pseudo-global warming
PI	pre-industrial
PNA	Pacific-North American
PNNL	Pacific Northwest National Laboratory
PRISM	Precipitation Elevation Regression on Independent Slopes Model
PRMS	Precipitation-Runoff Modeling System
PT	modified temperature adjustment
RCP	representative concentration pathways
RE	relative error
RegCM4	Regional Climate Model, version 4
SCE	snow cover extent
SLR	sea-level rise
SNR	signal-to-noise ratio
SOI	Southern Oscillation Index
SON	September-October-November
SPCAM	Superparameterized Community Atmosphere Model
SRES	Special Report on Emissions Scenarios
STEnv	severe-thunderstorm environment
TA	temperature adjustment
TC	tropical cyclone
USACE	U.S. Army Corps of Engineers or Corps
USGCRP	U.S. Global Change Research Program
USGS	U.S. Geological Survey
UVV	upward vertical velocity
WBT	wet-bulb temperature
WRF	Weather Research and Forecasting (model)

Contents

Figures

Tables

1.0 Introduction

This report is part of the U.S. Nuclear Regulatory Commission's (NRC) Probabilistic Flood Hazard Assessment (PFHA) research program that aims to develop regulatory tools and guidance to support and enhance the NRC's capacity to perform thorough and efficient reviews of license applications and license amendment requests. The report summarizes current climate research and results regarding hydrometeorological phenomena that are of interest in safety assessments and environmental impact assessments for commercial nuclear power plants. This report is the third in a series of reports. The first report summarized scientific findings about global and regional climate change, focusing in particular on climatic elements relevant to NRC concerns broadly across the conterminous United States (i.e., increasing air and water temperatures, decreasing water availability, increasing frequency and intensity of storms and flooding, and sea-level rise). In the second report, PNNL staff summarized research findings about climate change for the Southeast Region of the United States, including projected changes in air temperature, precipitation, hurricanes, sea-level rise, storm surge, tornadoes, and impacts on flooding, and low flows. This current report summarizes region-specific scientific findings for the Midwest Region.

The U.S. Global Change Research Program (USGCRP) Third National Climate Assessment (NCA3) discussed the regional climate, historical trends, and future changes in 10 climate regions (Melillo et al. 2014). In the Fourth National Climate Assessment (NCA4), similar regions are used in the Climate Science Special Report except that the Great Plains are divided into northern and southern Great Plains and the Caribbean Islands are separated from the Southeast Region (USGCRP 2017). The region of interest for the purpose of this report consists of eight midwestern states—Illinois, Indiana, Iowa, Michigan, Minnesota, Missouri, Ohio, and Wisconsin (hereafter, the Midwest Region) (USGCRP 2017; Figure 1.1). Except for Indiana, the states within the Midwest Region have operating nuclear power plants (Figure 1.2). In addition, a new nuclear power reactor early site permit was approved by the NRC on March 15, 2007, for the Clinton site in Illinois, that hosts a currently operating reactor. A combined operating license for a new nuclear power reactor was approved on May 1, 2015, for the Fermi site in Michigan, which also hosts a currently operating reactor (Figure 1.3).

To support the NRC's (1) PFHA research program in developing a risk-informed licensing framework for flood hazards and design standards, (2) environmental reviews at existing and proposed facilities, and (3) significance determination tools for evaluating potential flood hazards and their protection at plant facilities, this report summarizes key findings available in the broad climate research literature about observed regional climate trends and projected climate change, as well as observed and potential hydrologic impacts in the Midwest Region. The contents are drawn from published reports including the National Oceanic and Atmospheric Administration (NOAA) Technical Report NESDIS 142-3, *Regional Climate Trends and Scenarios for the U.S. National Climate Assessment Part 3: Climate of the Midwest U.S.* (Kunkel et al. 2013b) and *Climate Change Impacts in the United States, Chapter 18: Midwest* (Pryor et al. 2014) for NCA3; the NCA4 (USGCRP 2017, NCA4 Volume I; USGCRP 2018, NCA4 Volume II); papers published in peer-reviewed journals; NOAA websites; and other sources including information available from the Midwestern Regional Climate Center website.

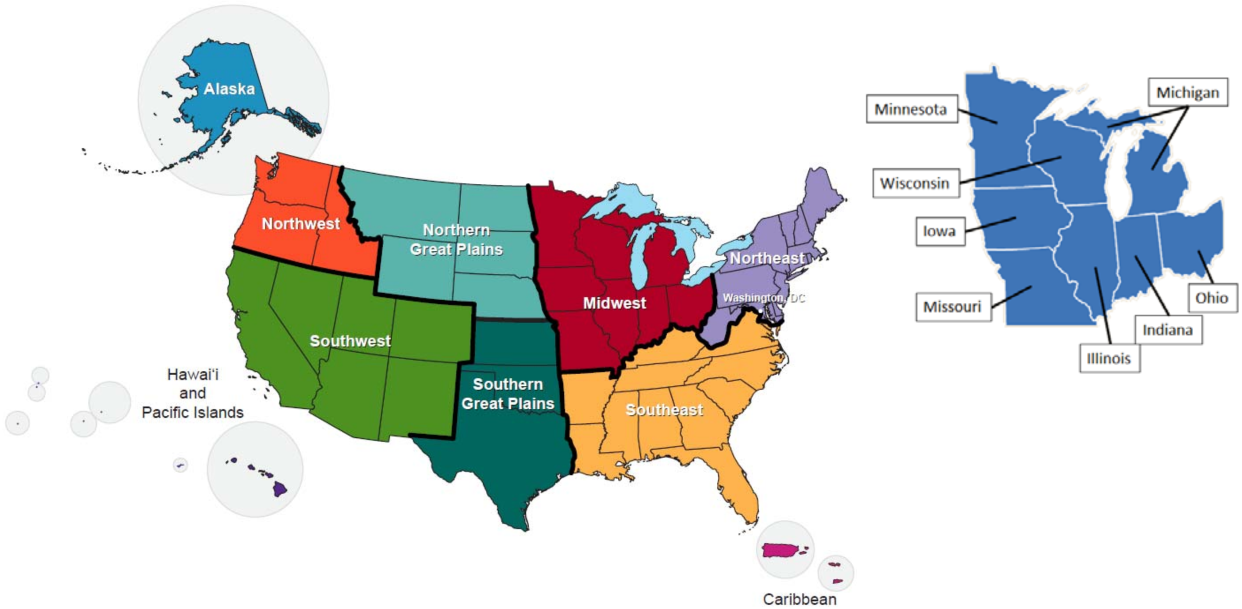

Figure 1.1. USGCRP NCA4 climate regions and the states composing the Midwest Region. (Source: USGCRP 2017)

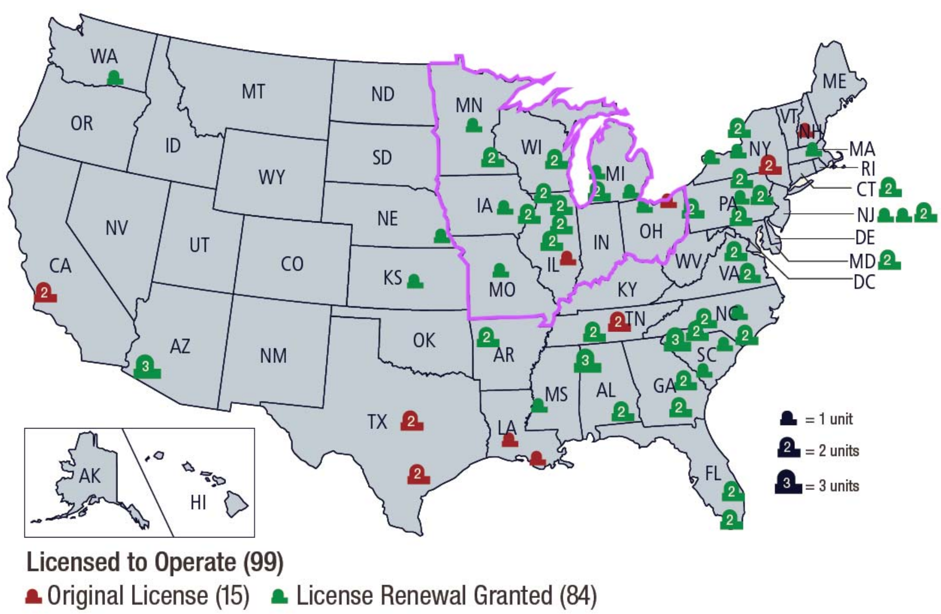

Figure 1.2. Operating nuclear power reactors in the United States as of July 2017. (Source: NRC 2017)

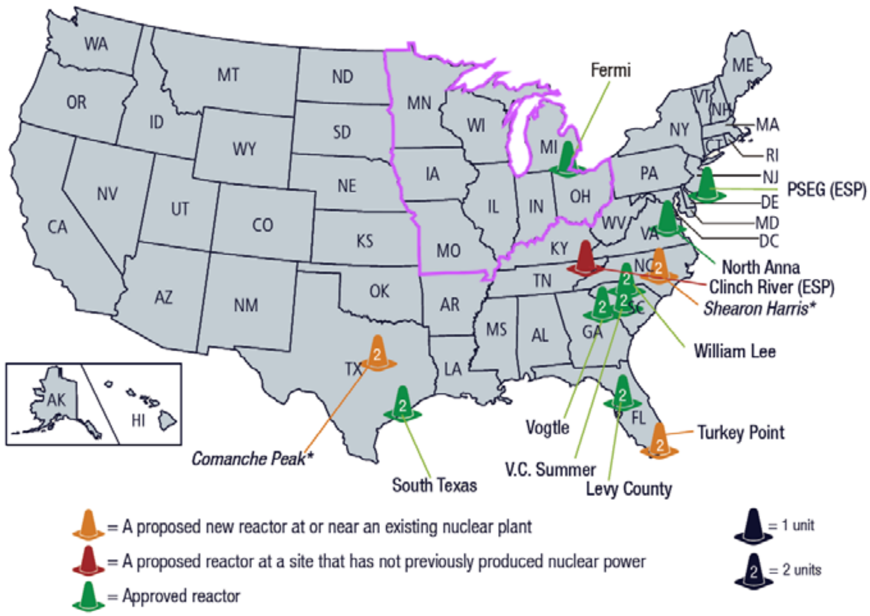

Figure 1.3. Proposed nuclear power reactors in the United States as of July 2017. An early site permit was also approved for another reactor at the Clinton site in Illinois (single-reactor site in Illinois shown on Figure 1.2), which is not shown on this map. Additionally, the Grand Gulf site in Mississippi also has an approved early site permit (also not shown on this map), although the Grand Gulf site is outside the Midwest Region. (Source: NRC 2017)

As summarized in Chapter 1 of the Year 2 report and in Table 1.1 of that report, information used in NCA3 is mainly derived from (1) multimodel global climate simulations of the Coupled Model Intercomparison Project Phase 3 (CMIP3); (2) regional climate projections from the North American Regional Climate Change Assessment Project (NARCCAP), in which regional climate models were used to dynamically downscale a subset of CMIP3 models; and (3) statistically downscaled products at $^{1}/_{8}$-degree resolution for the United States developed using the bias-correction spatial disaggregation (BCSD) method applied to the CMIP3 simulations. Future projections highlighted in NCA3 are associated with lower emissions (B1) and higher emissions (A2) that correspond to a mitigation scenario and a business-as-usual scenario, respectively. In contrast to NCA3, NCA4 draws information mainly from (1) multimodel global climate simulations of the Coupled Model Intercomparison Project Phase 5 (CMIP5; Taylor et al. 2012), (2) a limited number of high-resolution global climate simulations at ~25 km resolution, and (3) statistically downscaled products at $^{1}/_{16}$-degree resolution for the United States developed using the Localized Constructed Analogs method applied to the CMIP5 simulations.

Table 1.1. Comparison of climate information used in NCA3 and NCA4

	NCA3	NCA4
Global climate simulations	CMIP3	CMIP5 and a limited number of high-resolution global simulations
Emissions and land use land cover scenarios	B1, A2	RCP4.5, RCP8.5
Downscaling of global climate simulations	Dynamical dowscaling: NARCCAP (50 km) Statistical downscaling: BCSD (1/8-degree)	Statistical downscaling: LOCA (1/16-degree)

Two scenarios, RCP4.5 and RCP8.5, that are comparable to the lower and higher emissions scenarios of B1 and A2, are used. These scenarios correspond to a global radiative forcing of 4.5 and 8.5 Wm^{-2} by the end of the 21st century.

1.1 Report Contents and Organization

This annual report discusses the climate change projections for the Midwest Region of the United States summarized in both NCA3 and NCA4, so emissions scenarios B1 and A2 used in CMIP3 and RCP4.5 and RCP8.5 used in CMIP5 are discussed throughout the report. Chapter 2 provides an overview of the regional temperature characteristics of the Midwest Region, including current climatology, observed trends and projected future changes. Chapter 3 summarizes current climatology, observed trends and projected changes in annual mean, seasonal mean, and extreme precipitation. Storms that produce the extreme precipitation most relevant to NRC PFHAs are generally not captured in global climate simulations because of their relatively coarse spatial resolution, so Chapter 3 also summarizes the characteristics of a few recent flooding events in the Midwest to provide context for extreme precipitation useful for NRC's consideration. Chapter 4 discusses current climatology, observed trends, and projected changes in severe storms including mesoscale convective systems (MCSs) and severe weather events. Chapter 5 describes current climatology, observed trends, and projected changes in Great Lakes water levels, which influence both water supply and flooding. Chapter 6 summarizes studies of observed and projected hydrologic changes including floods and droughts in the Midwest. Chapter 7 summarizes recent U.S. agency activities related to climate change and its impacts. Finally, Chapter 8 lists references cited in this report.

1.2 Climate Terminology Relative to NRC Permitting and Licensing

We note that the terminology used in the broad climate research community is not aligned with that used in the NRC permitting and licensing context. For example, Kunkel et al. (2013b, Figure 18) describe trends in "extreme" precipitation events in the Midwest Region using the 24-hour, 0.2 annual exceedance probability precipitation events. In contrast, the NRC's interest in extreme events spans a much lower range of annual frequencies of exceedance—10^{-3} and lower (NRC 2016). The flood events of interest to the NRC may be generated by precipitation at a range of timescales—from 5 minutes to several days. Therefore, research results developed by the climate community should be carefully evaluated and interpreted for use in the NRC permitting and licensing context. This misalignment between climate scientists and hydrologic engineers with respect to definition of extremes also impacts other areas of critical infrastructure design such as dams and coastal flood protection. As far as possible, this report endeavors to explicitly state the event time scales and the annual exceedance probabilities or frequencies reported in the reviewed literature.

2.0 Temperature in the Midwest Region

This chapter summarizes available information related to characteristics of observed temperatures in the Midwest Region (e.g., annual and seasonal mean temperatures and hot and cold extremes) and their historical trends (Section 2.1), and summarizes the projected changes over the 21st century (Section 2.2) derived from peer-reviewed scientific journal papers and agency reports.

2.1 Observed Temperature and Historical Trends

- Observations indicate that the Midwest Region is experiencing a long-term warming trend. Warming rates show acceleration in the later parts of the 20th century and into the 21st century.
- Warming in the Midwest Region has been more rapid at night and during winter.
- Indices designed to represent heat-wave and cold-wave events do not exhibit statisitically significant trends over the period from 1895 through 2011.

2.1.1 30-Year Climate Normals

The average value of a meteorological quantity over 30 years is defined as a climatological normal. The normal climate helps in describing the climate and is used as a base to which current conditions can be compared. Every 10 years, the NOAA National Centers for Environmental Information (NCEI) computes new 30-year climate normals for selected temperature and precipitation elements for a large number of U.S. climate and weather stations. The NCEI currently uses an averaging period of 1981 through 2010[1] to create climatology maps (NCEI 2016a).

Vose et al. (2014) described the details of how climate normals are currently computed. Using this methodology, the NCEI publishes climatology and monthly time series maps for minimum and maxium temperatures and precipitation. The methodology uses daily temperature and precipitation data from the Global Historical Climatology Network-Daily (GHCN-Daily) dataset. The GHCN-Daily dataset contains data from several observing networks in North America, six of of which were used. Two primary networks—the Cooperative Observer and the Automated Surface Observing System—were supplemented by four additional networks—National Interagency Fire Center's Remote Automatic Weather Station network, U.S. Department of Agriculture's Snow Telemetry network, Environment Canada's network, and Mexico's Servicio Meteorologico Nacional network. Daily data, adjusted for changes in observation time, station location, instrumentation, and siting conditions were used to compute monthly values. Climate normals data (referred to as climate normals) were computed for each station, month, and element (minimum and maximum temperatures and precipitation). Climate normals are simple averages of 30 monthly values if the station had a complete record for the whole base period (1980 through 2010). For stations with incomplete records, missing monthly values were estimated before computing climate normals. Climate normals grids were created on a 5-km resolution by climatologically-aided interpolation

[1] The Third National Climate Assessment used the 1971–2000 normals.

employing the thin-plate smoothing spline method.[1] Two other grids—the anomaly grid and the composite grids—also were developed for each element. These grids were developed in three steps:

1. Computing station anomalies from climate normals for each year and month
2. Creating anomaly grids using invese-distance weighting
3. Creating composite grids by combining the normal and anomaly grids.

This process resulted in the following products from NCEI (2016a):

1. Climate normal grids for minimum and maximum temperatures and precipitation, available as annual and month-by-month "Climatology" maps
2. Monthly time series for minimum and maximum temperatures and precipitation, available as month-by-month maps for the period from 1895 through 2016.

The annual average minimum temperatures (as represented by annual minimum temperature climate normals) in the Midwest Region fall into three bands: (1) the 40s (in degrees Fahrenheit) for a southern tier that comprises most of Missouri, Illinois, Indiana, and Ohio; (2) the 20s for an upper tire comprising the far northern parts of Minnesota, Wisconsin, and Michigan; and (3) the 30s for a middle tier comprising Iowa, and most of Minnesota, Wisconsin, and Michigan. (Figure 2.1, top left panel). The annual average maximum temperatures (as represented by annual maximum temperature climate normals) exhibit a similar pattern: 60s in the southern tier, 50s in the middle tier and 40s in the northern tier (Figure 2.1, top right panel). On average, January is the coolest month (Figure 2.1, bottom-left panel) and July is the warmest month (Figure 2.1, bottom-right panel). Average minimum January temperatures are lower than 10°F for an upper tier comprising Minnesota, most of Wisconsin, northern Michigan and northern Iowa. They are in the 20s for a tier comprising roughly the southern half of Missouri, Illinois, Indiana, and Ohio. A middle tier comnprising the lower peninsula of Michigan, the lower half of Iowa and the upper halves of Missouri, Illinois, Indiana and Ohio exhibit average minimum January temperature in the 20s. Average maximum July temperatures are in the 80s for almost the entire region. A northern tier comprising the northern half of Minnesota, and northern thirds of Wisconsin and Michigan exhibit average maximum July temperature in the 70s.

Record high temperatures in the Midwest Region can range from 47°F in January to 115°F in July (NCEI 2016b). Across the Midwest Region, maximum daily average temperatures can exceed 90°F for periods from 1 to 15 days in July and up to 14 days in August (NCEI 2016b). Record low temperatures in the Midwest Region can range from 51°F in July to -55°F in January (NCEI 2016b). In the Midwest Region, minimum daily average temperatures can fall below freezing during all months and can fall below freezing for all days in December and January (NCEI 2016b).

[1] Thin-plate smoothing spline is a data interpolation and smoothing technique that was originally used in geometric design (Duchon 1976) and has been extensively applied in geospatial problems (e.g., Wahba and Wendelberger 1980, Wahba 1990, Hutchinson 1991, Gu and Wahba 1993, Zheng and Basher 1995, Dodson and Marks 1997, Hulme and New 1997, Price et al. 2000, Smith et al 2003, McVicar et al. 2005, Hancock and Hutchinson 2006, DeGaetano and Belcher 2007, Trossman et al. 2011, Rahman et al. 2018).

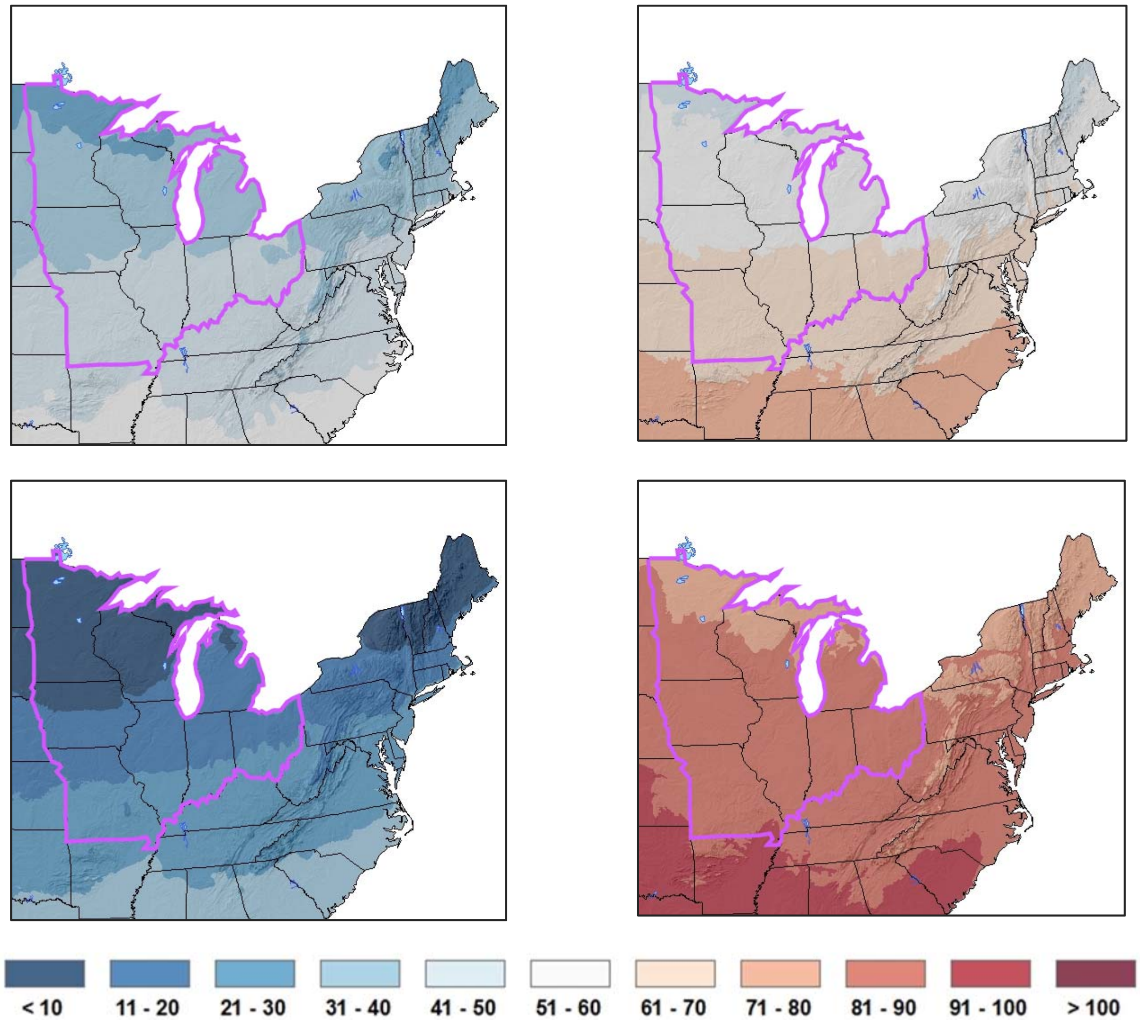

Figure 2.1. Annual average minimum (top left) and maximum (top right) temperatures (°F) and average minimum January (bottom left) and maximum July (bottom right) temperatures (°F) based on the 1981 through 2010 normals. (Source: NCEI 2016a)

2.1.2 Observed Trends

2.1.2.1 Annual Averages and Averages in Annual, Seasonal, and Daily Exteremes

As summarized in the NCA4 Climate Science Special Report (CSSR, Vose et al. 2017), annual average temperatures over the contiguous United States have increased by 1.2°F for the 1986 through 2016 period relative to the 1901 through 1960 period, and the surface observation and satellite data have consistently shown a rapid warming since 1979. The change in annual average temperature for the same periods for the Midwest Region was reported as 1.26°F (see Figure 2.2), while the change in annual average maximum temperature was 0.77°F and the change in annual average minimum temperature was 1.75°F.

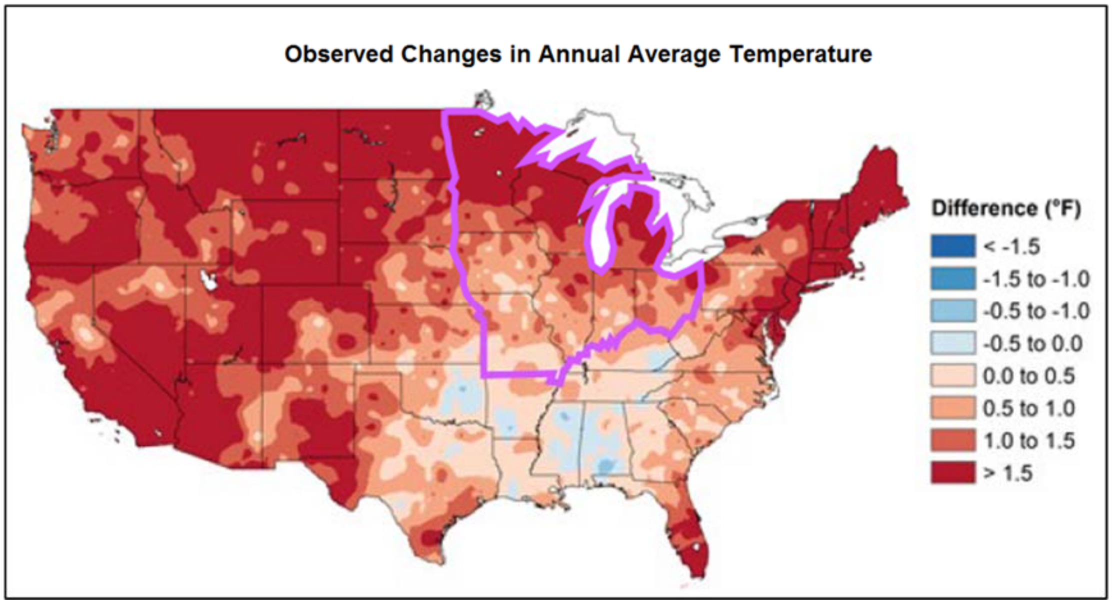

Figure 2.2. Observed changes in annual average temperature (°F). Changes are the difference between the average for present day (1986 to 2016) and the average for the first half of the last century (1901 to 1960). (Source: Vose et al. 2017)

The coldest daily temperature of the year has increased at most locations within the contiguous United States over the last 30 years compared to the first six decades of the 20th century (Figure 2.3a, left panel). The regional average increase in the temperature of the coldest day of the year for the Midwest Region was 2.93°F. In contrast, the warmest daily temperature of the year showed a decrease for all eastern U.S. regions (Figure 2.3a, right panel); for the Midwest Region, the regional average warmest daily temperature of the year decreased by 2.22°F. It is also noticeable that the warming of the coldest daily temperature shows a spatial pattern—the warming increases from the south to the north within the Midwest Region. The change in warmest daily temperatures show no such spatial trend (Figure 2.3a). The report provides a few possible reasons why the average present-day (1986 through 2016) warmest daily temperatures show a decrease from the corresponding average for 1901 through 1960. The main reason appears to be the strong influence of 1930s Dust Bowl era of elevated temperatures (Figure 2.3b, right panel). Other reasons stated are the forcings from aerosols that may have reduced summer temperatures during 1950 through 1975 (Mascioli et al. 2017) and intensification of agriculture that may have suppressed the hottest extremes (Mueller et al. 2016). The report also states that across the United States, the frequency of cold waves has decreased since the early 1900s and the frequency of heat waves has increased since the 1960s. The report mentions that the number of high-temperature records set in the past two decades far exceeds the number of low-temperature records.

Based on analysis of gridded NOAA Cooperative Observer Network weather data, Kunkel et al. (2013b) reported that the Midwest Region showed a rising trend in temperature anomalies (deviations from the 1901 through 1960 average) throughout the 20th century that has continued into the 21st century (Figure 2.4). Most of the increase occurred during winter and spring (see middle panels of Figure 2.4). Annual trend in temperature anomaly was significant at 95 percent confidence level and was estimated to be +0.14°F/decade. The spring trend also was significant at 95 percent confidence level and estimated to be +0.17°F/decade. Using the University of East Anglia Climate Research Unit (CRUTEM3) data set (Brohan et al. 2006), Kunkel et al. (2013b) calculated temperature anomaly trends for three time periods:1900 through 2010, 1950 through 2010, and 1979 through 2010 (Figure 2.5). Linear trend fits to the three periods showed increasing positive trends of 0.059, 0.116, and 0.264°C/decade (0.11, 0.21, and 0.48°F/decade).

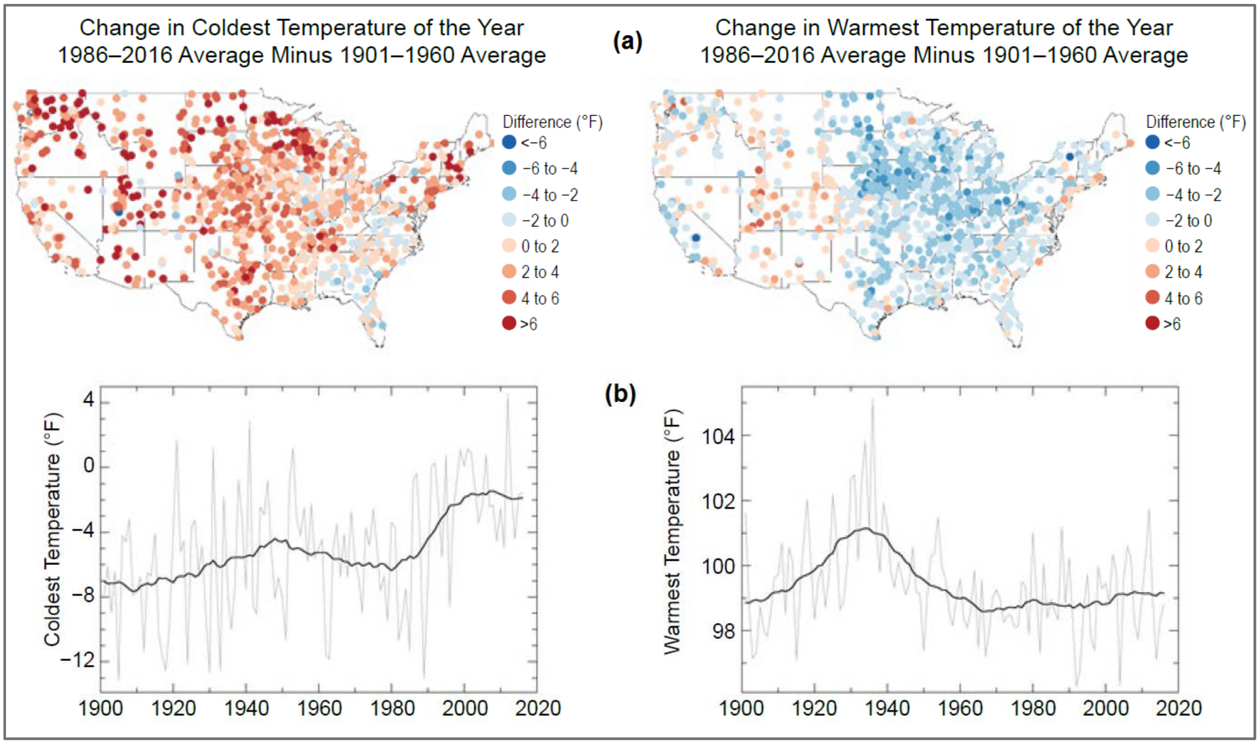

Figure 2.3. (a) Changes in the average coldest and warmest daily temperatures between the 1986 through 2016 and 1901 and 1960 periods. (b) Area-weighted time series of the coldest and warmest average daily temperatures over the contiguous United States. (Source: Vose et al. 2017)

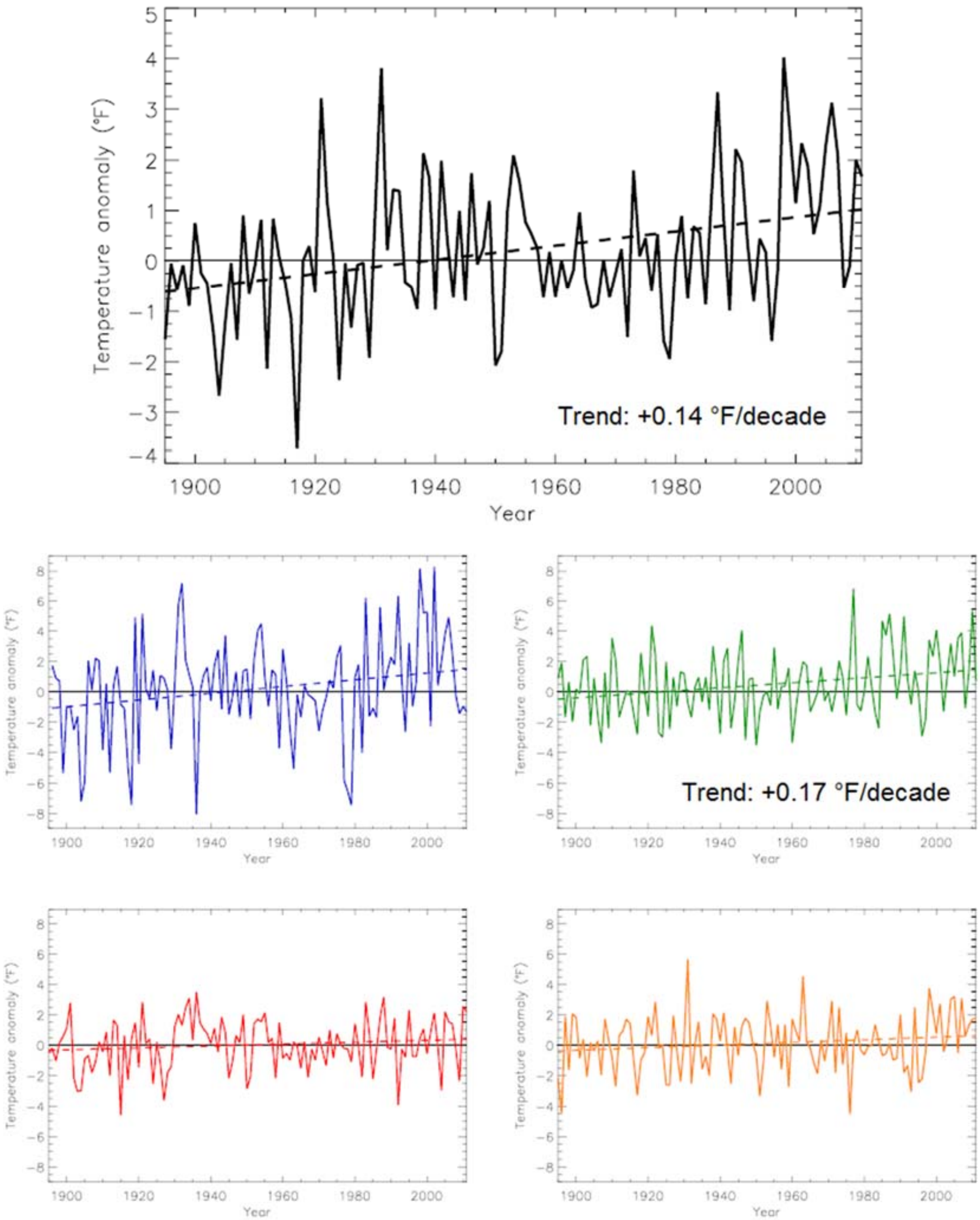

Figure 2.4 Trends in observed temperature anomalies (deviations from the 1901 through 1960 average) in the Midwest Region based on Gridded NOAA Cooperative Observer Network Data. The top panel shows the annual temperature anomalies, middle-left panel shows the winter temperature anomalies, middle-right panel shows the spring temperature anomalies, bottom-left panel shows the summer temperature anomalies, and the bottom-right panel shows the fall temperature anomalies. (Source: Kunkel et al. 2013b)

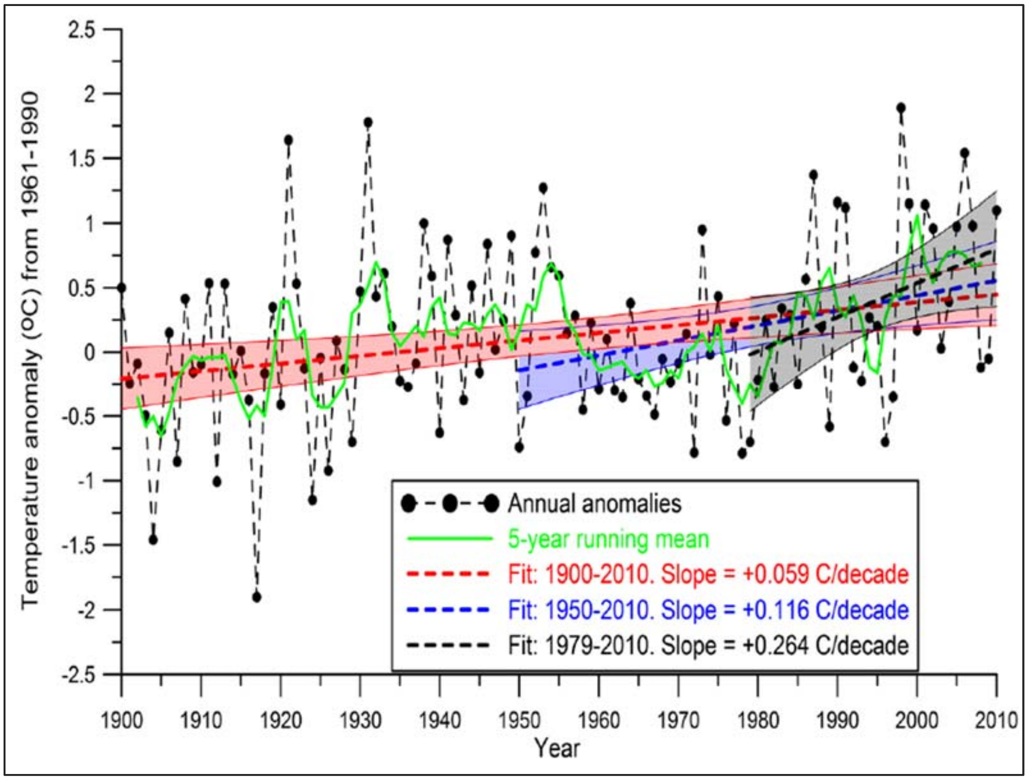

Figure 2.5. Annual temperature anomalies for the Midwest Region based on the University of East Anglia Climate Research Unit (CRUTEM3) data set. The linear fits to the 1900 through 2010, 1950 through 2010, and 1979 through 2010 time periods are shown along with the respective 95 percent confidence intervals. (Source: Kunkel et al. 2013b)

2.1.2.2 Heat Waves and Cold Waves

Historical information and analysis on heat and cold waves in the Midwest Region has been developed to support NCA4 (Kunkel et al 2103b). The average frequency of days exceeding 100°F ranges from one every two years to an average of two per year in the Midwest Region (temperatures exceeding 90°F are considered hot by Midwest Region residents). Cities in the region (Chicago, Cincinnati, Cleveland, Detroit, Des Moines, Indianapolis, Milwaukee, Minneapolis-St. Paul, and St. Louis) experience an average of 7 to 36 days during which temperatures exceed 90°F each year. Notable heat waves have occurred in the region during the early 1900s, multiple years in the 1930s and 1950s, 1988, 1995, and 2012. The 1995 heat wave, which resulted in 700 fatalities in Chicago, had seven consecutive days with maximum daily temperatures exceeding 90°F and two days exceeding 100°F. During the hottest days, minimum daily temperatures also exceeded 80°F (Kunkel et al. 2013b).

Kunkel et al. (2013b) used time series of indices to represent heat and cold-wave events based on daily Cooperative Observer Program data from long-term stations in the Global Historical Climate Network station dataset. Heat or cold-wave events were identified by ranking all 4-day mean temperatures and selecting the highest and lowest fifth of the values at each station (i.e., events are defined as 4-day periods that are hotter or colder than the threshold for 1 in 5-year recurrence). The number of events for all stations in each 1° × 1° box was averaged for each year. The regional average of all grid boxes was taken as the index for that year. The heat-wave and cold-wave indices are shown in Figure 2.6. The heat waves of the 1930s stand out. Kunkel et al. (2013b) also noted that since 2000, there have been relatively few cold waves. However, the trends were not statistically significant.

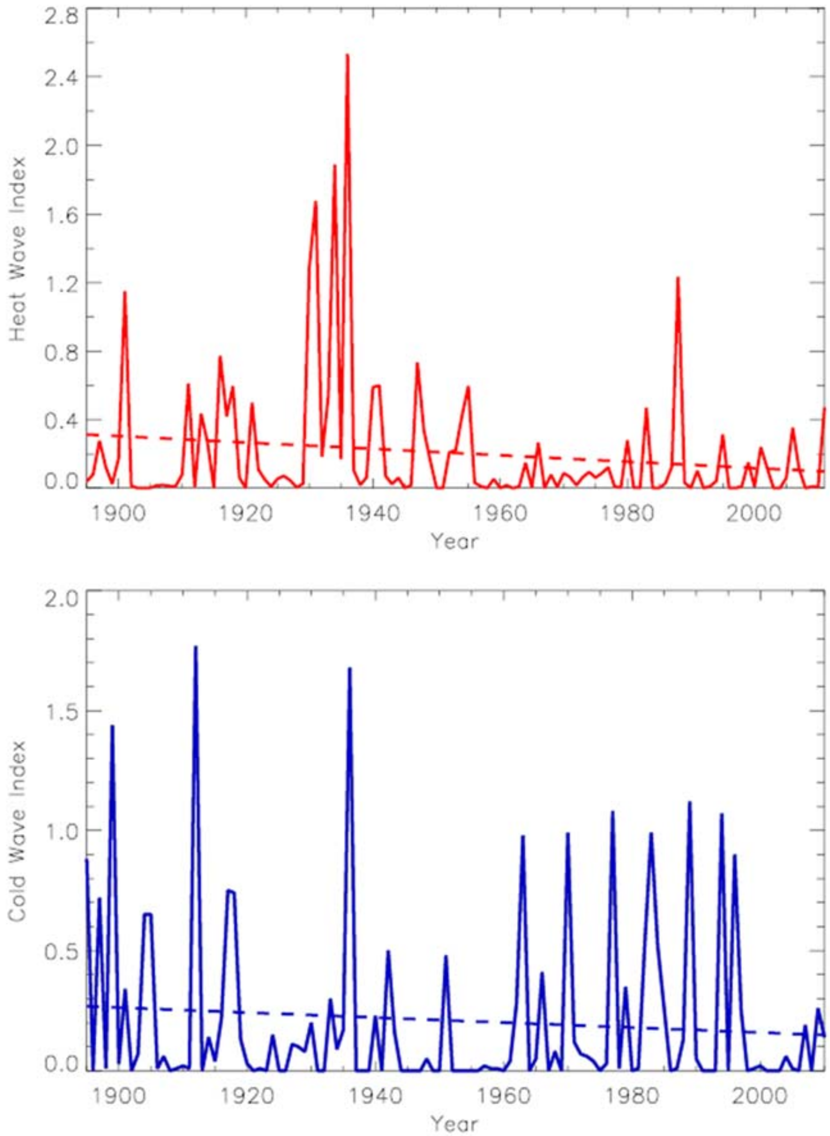

Figure 2.6. Time series of heat- and cold-wave indices. The dashed lines represent the linear fits. The trends were not statistically significant. (Source: Kunkel et al. 2013b)

An increase in temperature and humidity may lead to an increase in wet-bulb temperature (WBT), which has serious implications for human health and the economy. Raymond et al. (2017) investigated the spatiotemporal patterns of WBT and factors that influence extreme WBT in the United States. More specifically, they analyzed the top 100 extreme WBTs from May to October across the United States using data for the 1981 through 2015 period from weather stations and North American Regional Reanalysis (NARR). In the Midwest Region, the median value of the top 100 WBT daily maximums is between 26°C and 30°C (Figure 2.7).

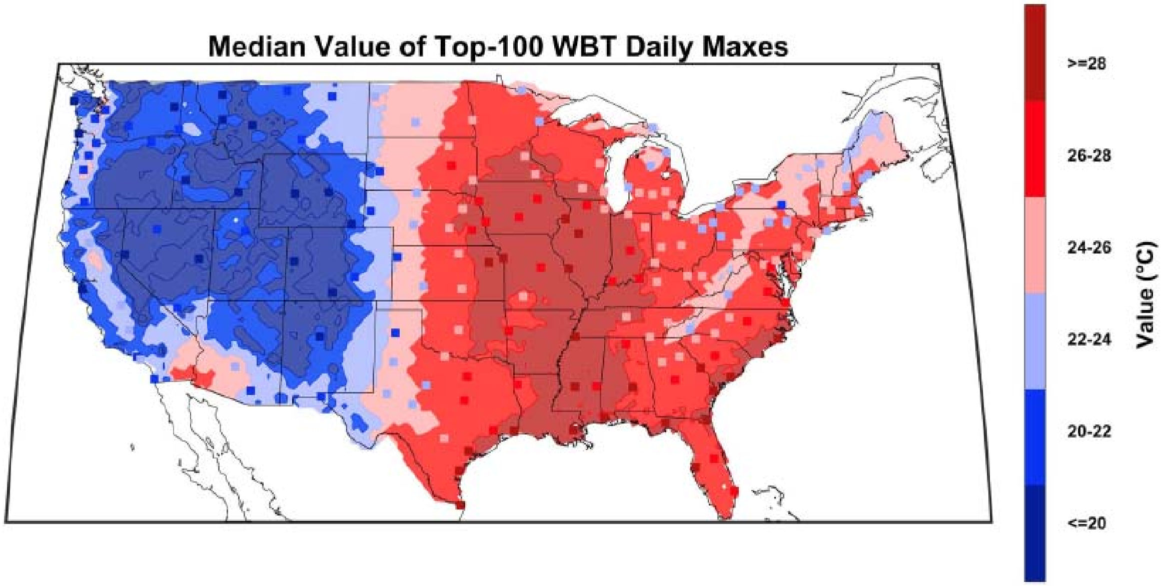

Figure 2.7. The median value of the 100 extreme WBT daily maximums for each station (squares) and NARR grid cells (shading), computed using data from May through October of each year in 1981 through 2015. (Source: Raymond et al. 2017)

Raymond et al. (2017) found that specific humidity anomalies have a greater influence on extreme WBT than extreme temperature. Extreme WBTs in the Midwest Region is associated with westward expansion of the Bermuda High and strong low-level southerly flow that enhances moisture transport into the region (top panel of Figure 2.8). Furthermore, at the upper level, an extreme WBT is associated with a wave train that originates from eastern Asia and propagates across the Pacific Ocean. The wave train induces a ridge over the Midwest that creates a surface temperature anomaly in that region (bottom panel of Figure 2.8. The wave train, which is similar to that discussed in Teng and Branstator (2017), has the ridge over the Midwest Region apparently by 10 days prior to the extreme WBT, suggesting long range weather predictability for the extreme event. As discussed by Raymond et al. (2017), extreme WBT occurences may increase in the future as both mean and extreme temperature and specific humidity increase with increasing greenhouse gas concentrations. Because there is a greater nonlinearity in the relationship between WBT with moisture than with temperature, changes in moisture may play a greater role in determining changes in extreme WBTs in the future.

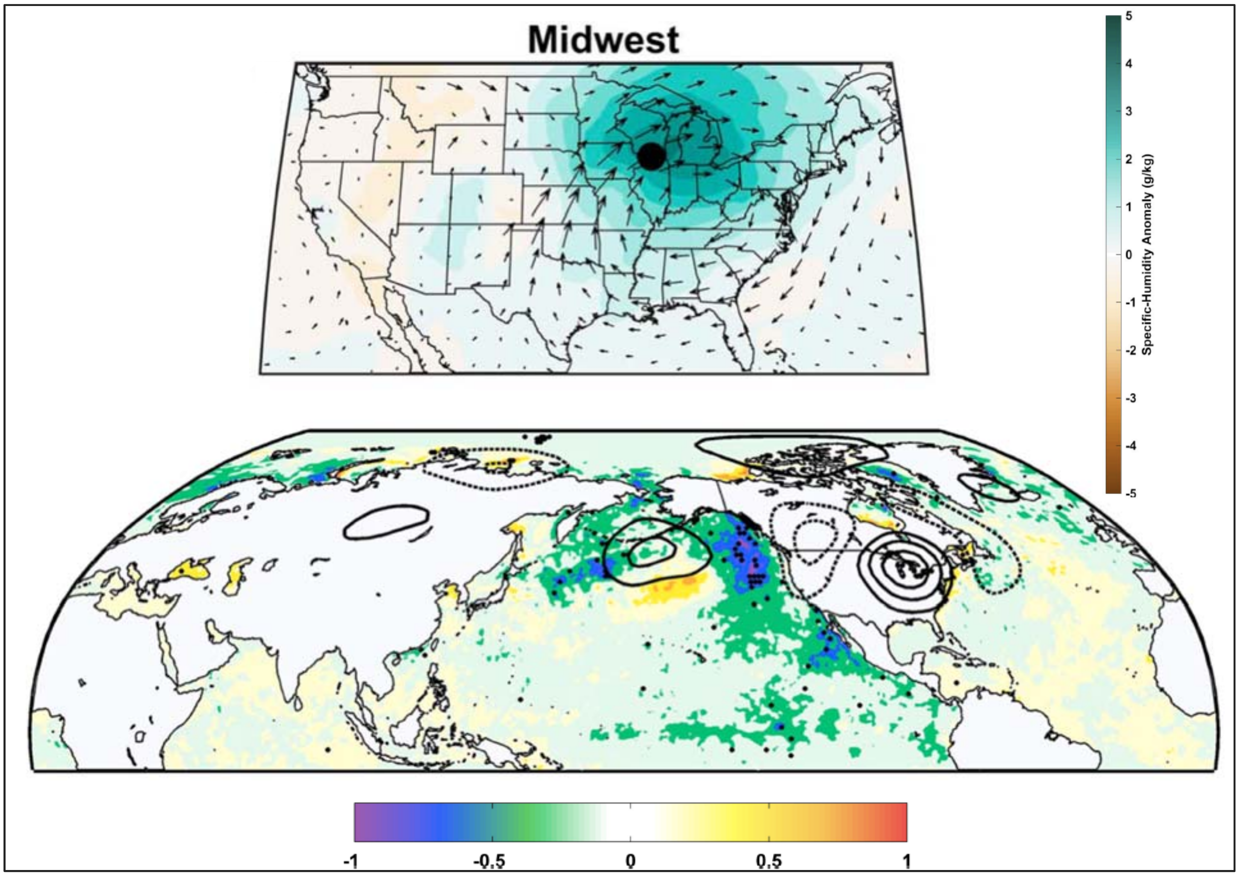

Figure 2.8. Composites of (top) daily anomalies of 850 hPa specific humidity (shading) and 850 hPa wind (vectors) and (bottom) daily 500 hPa height anomalies (contours at 20 m intervals) and sea surface temperature anomalies (shading in units of °C, stippled at 95 percent significance) from the North American Regional Analysis for the top 100 extreme-WBT days from May to October across the U.S. using data for 1981–2015 from weather stations. (Source: Raymond et al. 2017)

2.2 Projected Temperature Changes

- The mean annual temperature is projected to increase by 4.5°F to 6.5°F and 7.5°F to 9.5°F under the B1 and A2 scenarios, respectively, by 2085.
- Projected warming is rather uniform spatially across the Midwest Region; greater warming occurs in winter and summer than in spring and fall.
- The annual number of days with daily maximum temperatures >95°F is projected to increase by up to 30 days comparing 2041–2070 with 1980–2000.

Consistent with the projections of global surface warming, temperatures in the Midwest Region are projected to increase in the future with greater warming in the higher emissions A2 scenario than in the lower emissions B1 scenario. **Error! Reference source not found.** (left panel) shows the projected mean annual temperature changes from the CMIP3 multimodel ensemble mean for three future periods and the NARCCAP-projected mean annual and mean seasonal temperature changes for the mid-century.

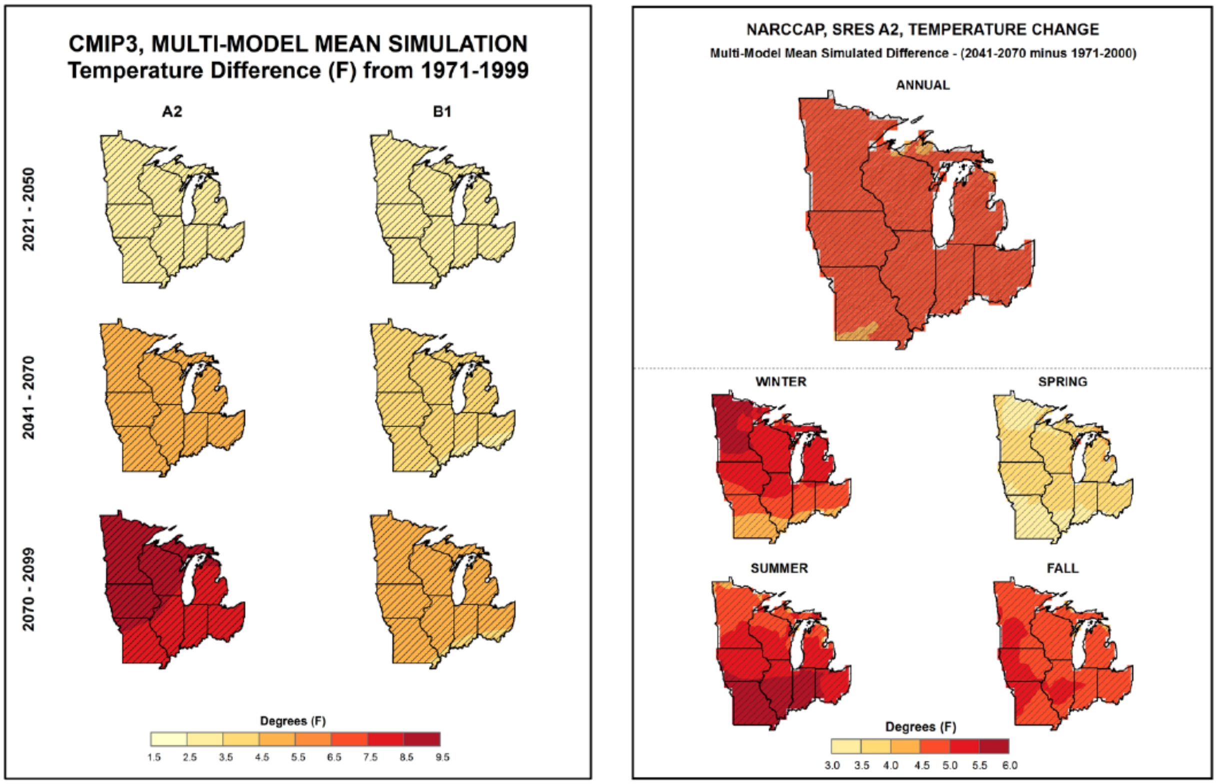

Figure 2.9. (Left) simulated differences in annual mean temperatures (°F) for the Midwest Region, for each future time period (2021 through 2050, 2041 through 2070, and 2070 through 2099) with respect to the reference period of 1971 through 1999, based on the multimodel means for the A2 and B1 emissions scenarios from the CMIP3 Global Climate Simulations. Color with hatching indicates that more than 50 percent of the models show a statistically significant change in temperature, and more than 67 percent agree on the sign of the change. (Right) Similar to the left panel A2 scenario, except that the simulations are from NARCCAP instead of CMIP3, for 2041 through 2070 relative to 1980 through 2000 for the annual mean and four seasons. Color with hatching has the same meaning as that of the left panel (Source: Kunkel et al. 2013b)

In general, spatial variations of the warming signals are small, except for greater warming in the northwestern part of the region by the late 21st century. The NARCCAP-projected mean annual warming for the 2041–2070 period (Figure 2.9, right panel) is comparable to that of the CMIP3 global simulations for the same period. Larger spatial variations are noted in the seasonal mean temperature changes; greater warming is projected for winter and summer than for spring and fall. The differences between the two scenarios are generally small before mid-century, then they increase over time. In 2085, warming in the A2 scenario is between 7.5 and 9.5 °F compared to between 4.5 and 6.5 °F for the B1 scenario.

Figure 2.10 shows the spatial distribution of the NARCCAP multimodel mean change in the average annual number of days with a maximum temperature exceeding 95°F between 2041 and 2070 and the reference period of 1980 through 2000.

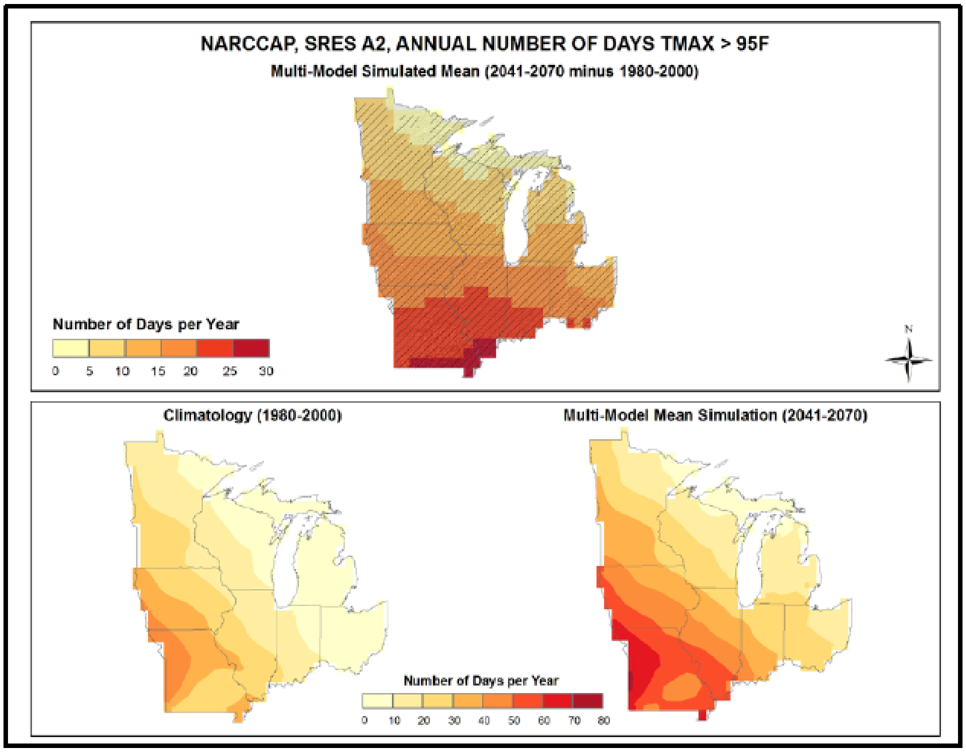

Figure 2.10. (Top) Simulated difference in the annual mean number of days with maximum temperatures greater than 95°F for the Midwest Region, for the 2041 to 2070 period with respect to the reference period of 1980 through 2000, based on the multimodel means from eight NARCCAP Regional Climate Simulations for the HIGH (A2) emissions scenario. Color with hatching indicates that more than 50 percent of the models show a statistically significant change in temperature, and more than 67 percent agree on the sign of the change. (Bottom) The simulated mean annual number of days with a maximum temperature greater than 95°F for the 1980 through 2000 period (left) and the 2041 through 2017 future periods (right). (Source: Kunkel et al. 2013b)

The Southern Region sees the largest increase (more than 30 days), and there is a large north-south gradient in the change pattern. The changes are statistically significant across almost the entire Midwest Region. Corresponding to the warming, the average annual number of days with a minimum temperature of less than 10°F decreases throughout the region, and the largest decrease of up to 25 days occurs in Minnesota, Wisconsin, and Michigan. As shown in Figure 2.5 of the Year 2 report, Diffenbaugh and Ashfaq (2010) found a substantial increase in heat waves by two to three events per year in the 2030–2039 period compared to 1951 through 1999 period in the Midwest Region. In Chapter 21 of the NCA4 report on the Midwest, Swanston et al. (2017) noted that exposure to high temperatures poses a particular risk for the Midwest Region. Currently, days over 100°F are rare in the City of Chicago, but the annual number of days above 100°F is projected to increase throughout the 21st century in both the lower emissions (RCP4.5) and higher emissions (RCP8.5) scenarios (Figure 2.11).

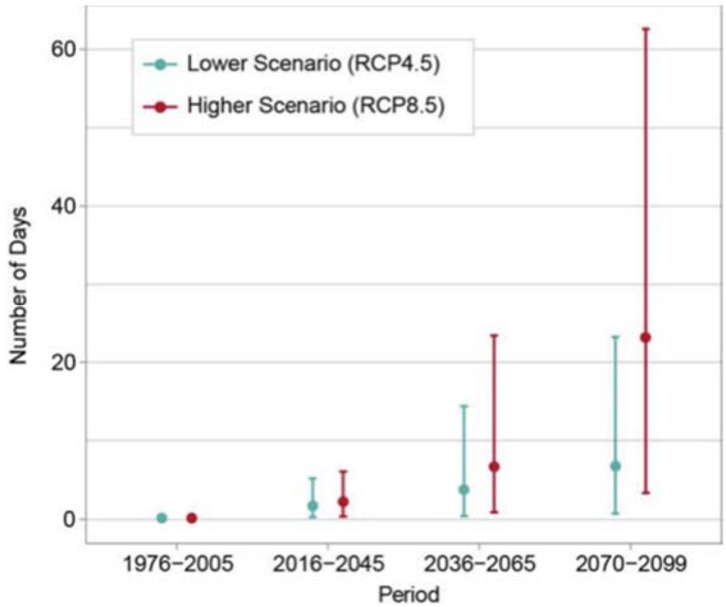

Figure 2.11. The annual number of days above 100°F for Chicago projected throughout the 21st century for a lower scenario (RCP4.5) and a higher scenario (RCP8.5) using statistically downscaled data from 32 models. (Source: University of Illinois, NOAA NCEI, and Cooperative Institute for Climate and Satellites, North Carolina)

Lopez et al. (2018) used a hierarchical clustering algorithm to study heat extremes in the United States using the ERA-20C reanalysis daily surface temperature data for the 1900–2010 period. They identified eight major regional heat-wave clusters and focused on four of them that affect the largest U.S. population, including the western United States, Northern Great Plains, Southern Great Plains, and the Great Lakes regions. Applying the same clustering method to CMIP5 projections under RCP8.5, they found increasing trends in the ratio of warm-to-cold extremes over the western United States and the Great Lakes regions, but changes in the northern and southern Great Plains are not significant. Figure 2.12 shows the heat waves (2 m temperature anomaly) of the Great Lakes cluster and the probability distribution of 21st century Great Lakes heat-wave events, exhibiting a statistically significant increase in the signal-to-noise ratio (SNR), which is defined as the ratio of the change in heat-wave events to the natural variability of heat-wave events.

To understand the differences in the projected change in SNR among the four heat-wave clusters, Lopez et al. (2018) analyzed the changes in atmospheric circulation that can influence heat waves and the changes in soil moisture that may influence surface temperature through land-atmosphere interactions. They found that heat waves are strongly negatively correlated with atmospheric transient eddies (an indicator of storminess) in the western and northeastern United States (Figure 2.13a). Storm activities in both regions are projected to decrease during summer in the future, as was also found by Lehmann et al. (2014). Because storms bring moist and cool air from the oceans to the continents, a weakening of the storm tracks in the western and northeastern United States may explain the increase in heat-wave events in the western U.S. and Great Lakes heat-wave clusters in the future. For the northern and southern Great Plains, they found that strengthening of the Great Plains low-level jet enhances moisture transport into the Great Plains, which increases precipitation and soil moisture and reduces surface temperature. In summary, Lopez et al. (2018) attributed the robust increase in warm-temperature extremes in the western U.S. and Great Lakes regions to the projected significant reduction of storminess during summer. With anthropogenic climate change dominating heat-wave occurrence over the western U.S. and Great Lakes regions, they found that the time of emergence (i.e., when SNR >1) could occur as early as the 2020s and 2030s for the respective regions.

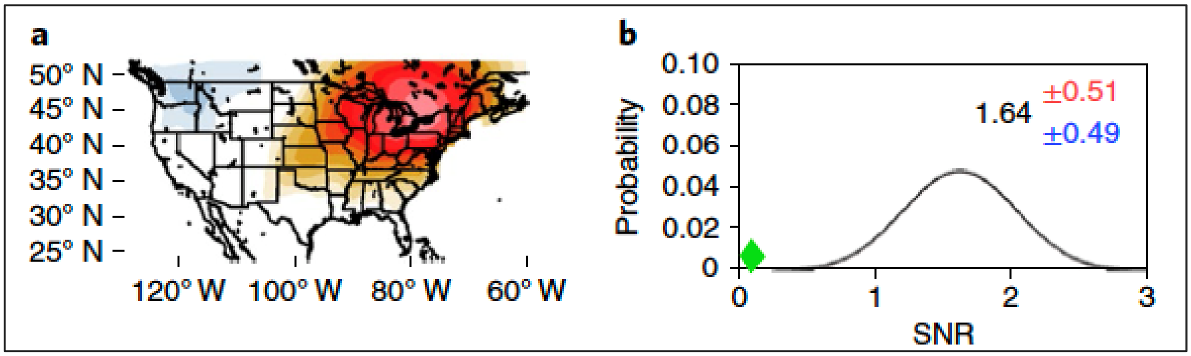

Figure 2.12. Geographic distribution of the 20th century 2 m temperature anomaly (a) and 21st century probability density function of the SNR of heat-wave events for the Great Lakes cluster from the ensemble mean of CMIP5 models. The SNR probability density function (PDF) is obtained by randomly selecting eight models (ensembles) 1000 times from the CMIP5 simulations. The mean SNR is shown in black and 95 percent confidence interval in red (blue) from the CMIP5. The 20th century SNR is shown by green diamonds. (Source: Lopez et al. 2018)

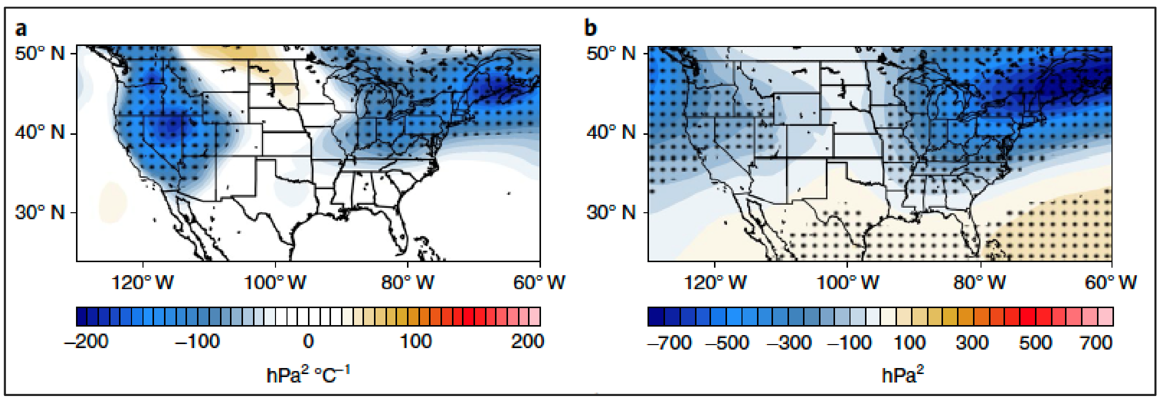

Figure 2.13. Regression of (a) June-July-August transient eddies and 2 m temperature (hPa^2 $°C^{-1}$) and (b) projected changes of June-July-August transient eddies (hPa^2) from the CMIP5 ensemble. The stipple areas indicate the 95 percent level based on a Student's t-test and an F-test, respectively. (Source: Lopez et al. 2018)

3.0 Precipitation in the Midwest Region

This chapter includes information related to characteristics and historical trends in observed precipitation in the Midwest Region (Section 3.1) and summarizes projected changes in mean and extreme[1] precipitation (Section 3.2). Information summarized was obtained from the NOAA NCEI, the CSSR report, U.S. Geological Survey (USGS), and from published papers and reports in the broad climate research community.

- Extreme rainfall events and flooding increased during the last century. Annual precipitation increased by 0.31 in./decade, with a statistically significant trend found only in summer. Much of this increase resulted from intensification of the heaviest rainfall events.
- The frequency of snowfall events equaling or exceeding the 90th percentile is decreasing over the Midwest. Snow-covered area also shows a decreasing trend.

3.1 Observed Precipitation

3.1.1 Current Climatology

Similar to the temperature climatology discussed in the previous section, NOAA NCEI Climate Atlas summarizes precipitation in the form of climatology maps (1981-2010 Normals) (NCEI 2016a). Average annual precipitation in the Midwest Region generally decreases from south to north and from east to west (see Figure 3.1). Annual average precipitation varies from 20 to 30 in. in the northwest portion of the Midwest Region to 40 to 50 in. in the south and east portion (Figure 3.1). On average, precipitation in the western portion of the region occurs once every 7 days and in the southeastern portion once every 3 days (Pryor et al. 2014). More than 30 percent of annual precipitation in the Midwest Region occurs during the 10 wettest days of the year (Kunkel et al. 2013b , see Figure 3.2).

MCSs contribute about 60 percent of warm season precipitation and over half of the extreme 24-hour precipitation in the Midwest Region (Schumacher and Johnson 2006; Stevenson and Schumacher 2014). MCSs form when cumulonimbus clouds aggregate and develop into a single entity. MCS precipitation can cover a horizontal scale of hundreds of kilometers and last up to 24 hours (Houze 2004). Some MCSs also are associated with severe weather such as tornadoes that produce damaging winds in the Midwest Region. Hence, understanding how MCSs have changed in the past and how they will change in the future is critically important for projecting changes in severe storms in the Midwest Region. This is discussed in more detail in Chapter 4, which focuses on past and future changes in severe storms in the Midwest Region.

[1] The precise meaning of the term "extreme" can vary between the climate research community and the nuclear regulatory community. More details are provided in Section 1.2 of this report.

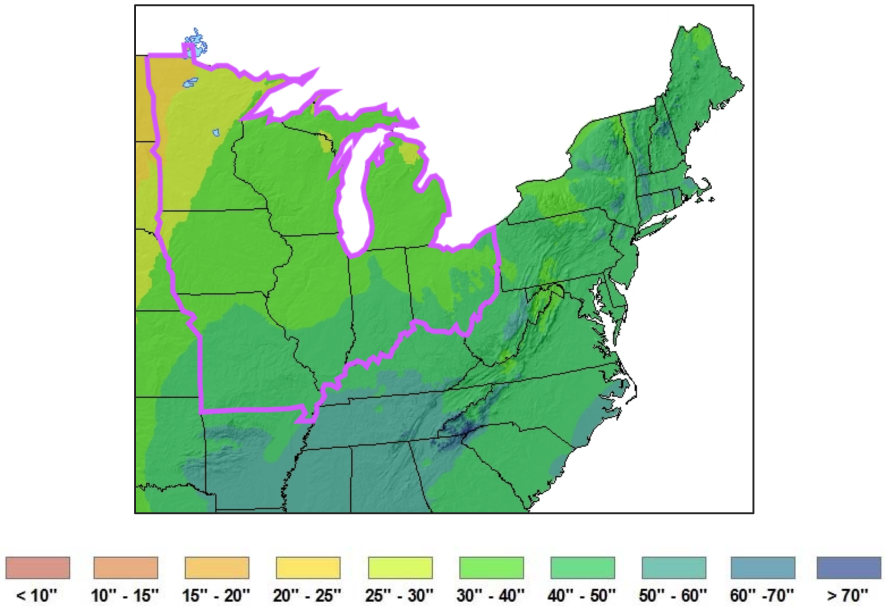

Figure 3.1. Average Annual Precipitation (1981 through 2010 normals) (Source: NCEI 2016a).

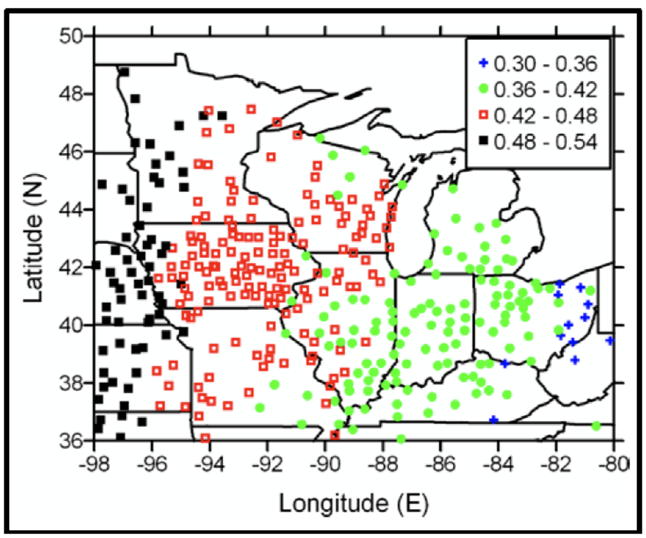

Figure 3.2. Fraction of annual precipitation at NOAA Cooperative Observer Network stations from the top 10 wettest days during the 1971 through 2000 period. The fraction increases from east (30 percent) to west (over 50 percent). (Source: Kunkel et al. 2013b)

3.1.2 Observed Trends

Annual average precipitation shows an increasing, statistically significant trend (+0.31 in./decade) at 95 percent confidence level over the observed record (see Figure 3.3). Over 90 percent of the increase in the annual precipitation resulted from increases in spring, summer, and fall precipitation; a statistically significant trend in seasonal precipitation was found only for summer. Despite high station-to-station variability in large rainfall events, 22 percent of meteorological stations exhibited a statistically significant increasing trend over the 1901–2000 period in the total precipitation from 10 wettest days (Figure 3.4).

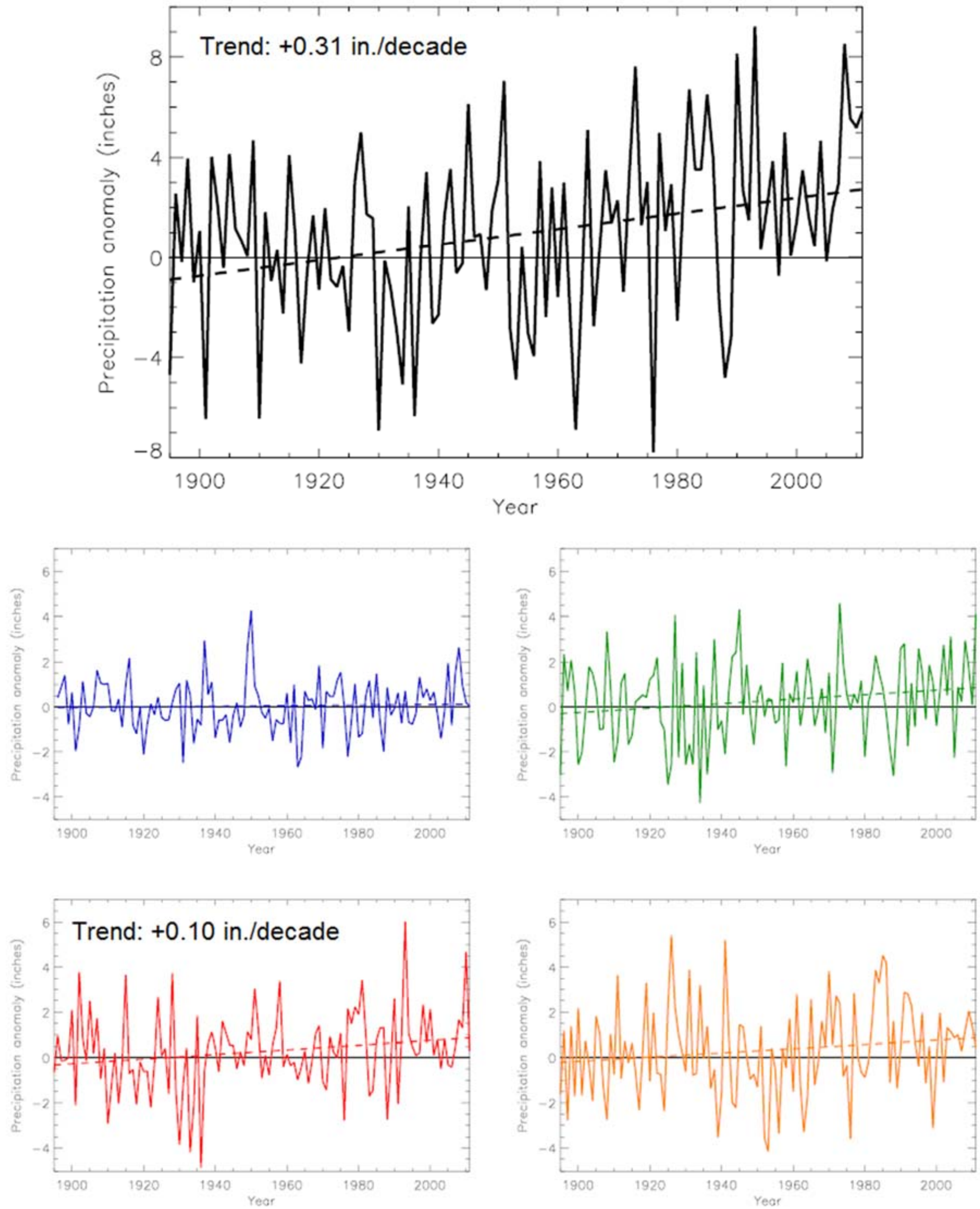

Figure 3.3. Trends in observed precipitation anomaly from 1895–2011 (deviations from 1901–1960 means) in the Midwest Region based on gridded NOAA Cooperative Observer Network Data. The top panel shows the annual precipitation anomalies, the middle-left panel shows the winter precipitation anomalies, the middle-right panel shows the spring precipitation anomalies, the bottom-left panel shows the summer precipitation anomalies, and the bottom-right panel shows the fall precipitation anomalies. Significant trends at the 95 percent confidence level were only found for the annual and summer precipitation anomalies. (Source: Kunkel et al. 2013b)

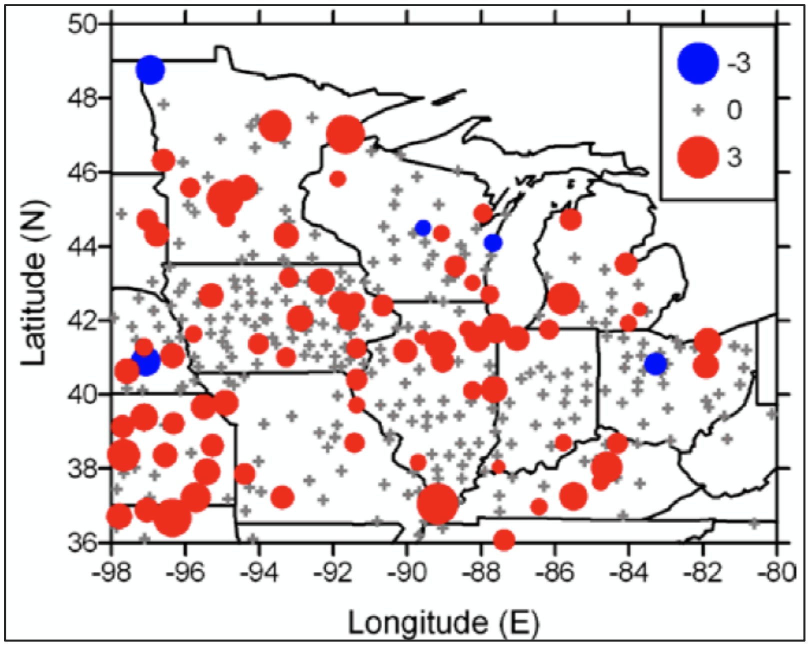

Figure 3.4. Trend in total precipitation (percent per decade) from the top 10 wettest days in the Midwest Region. Red circles indicate statistically significant increasing trends, blue circles indicate statistically significant decreasing trends, and gray pluses indicate trends that are not statistically significant. (Source: Kunkel et al. 2013b)

Figure 3.5 shows the observed change in the 5-percent annual exceedance probablility (AEP) value of daily precipitation by season between 1948 and 2015. In the Midwest Region, larger changes are observed in fall (0.27 in.), although a positive trend is seen in all seasons.

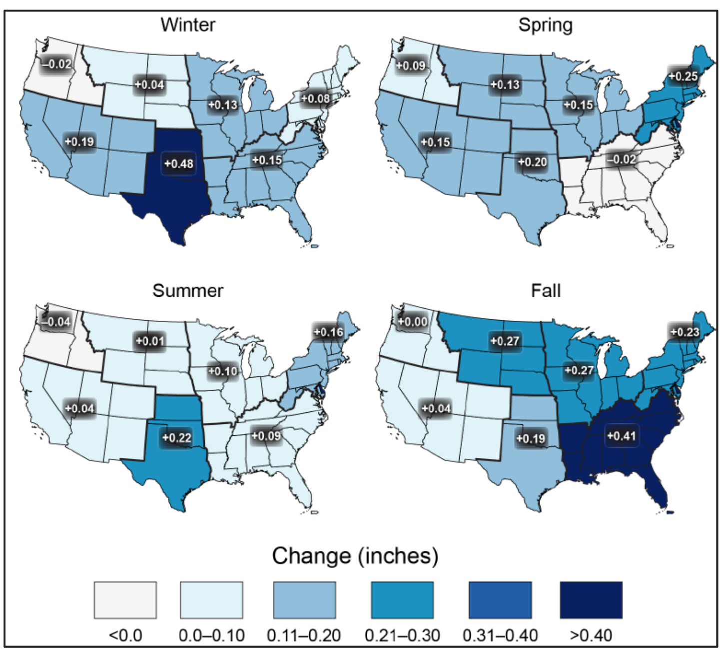

Figure 3.5. Observed changes in the 5-percent AEP value of the seasonal daily precipitation totals over the period from 1948–2015 using data from the Global Historical Climatology Network data set. (Source: Easterling et al. 2017)

Figure 3.6 shows the change in several metrics of precipitation over two periods (1901–2016 and 1958–2016). For each metric, the numerical value is the percent change over the entire period (1901–2016 or 1958–2016). The percentages are first calculated for individual stations, then averaged over 2° latitude by 2° longitude grid boxes, and finally averaged over each NCA4 region The metrics include (1) the maximum daily precipitation in consecutive 5-year blocks for the 1901–2016 period; (2) daily precipitation in the top 1 percent of all days for 1958–2016; and (3) the number of 2-day events exceeding the 20-percent AEP threshold for 1958–2016 and 1901–2016. Changes over the Midwest Region are generally positive; increases of 42 percent in the amount of precipitation falling during daily events exceed the 99th percentile of non-zero precipitation days. The number of 2-day events exceeding the 20-percent AEP threshold shows an increase of 63 percent for the 1901–2016 period and of 53 percent for the 1958–2016 period, and the difference may be due to multi-decadal variability.

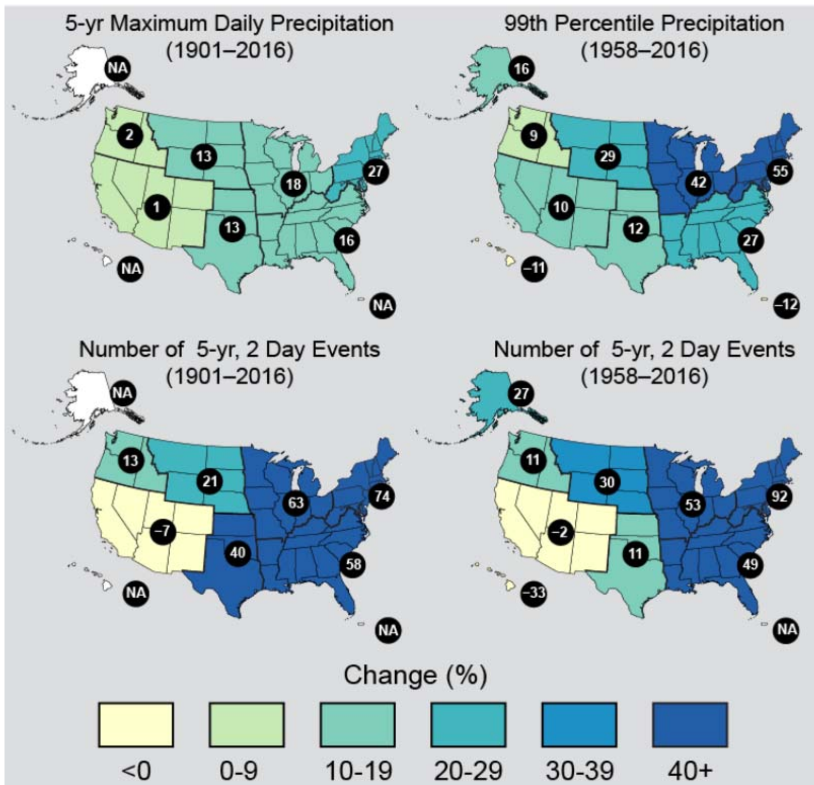

Figure 3.6. The change in several metrics of precipitation by NCA4 region, including (upper left-hand panel) the maximum daily precipitation in consecutive 5-year blocks; (upper right-hand panel) the amount of precipitation falling in daily events that exceeds the 99th percentile of all non-zero precipitation days; (lower left-hand panel) the number of 2-day events exceeding the 20-percent AEP threshold, calculated over 1901–2016; and (lower right-hand panel) the number of 2-day events exceeding the 20-percent AEP threshold, calculated over 1958–2016. The numerical value is the percent change over the entire period, either 1901–2016 or 1958–2016. The percentages are first calculated for individual stations, then averaged over 2° latitude by 2° longitude grid boxes, and finally averaged over each NCA4 region. (Source: Easterling et al. 2017)

Last, Figure 3.7 shows a linear increasing trend in an extreme precipitation index (occurrence of 20-percent AEP daily precipitation events) in the Midwest Region of the United States. Events are first identified for each individual station by ranking all daily precipitation values and choosing the top one-fifth (N/5) of the events, where N is the number of years of data for that particular station. Then, event numbers for each year are averaged for all stations in each 1° × 1° grid box. Finally, a regional average is determined by averaging the values for the individual grid boxes. This regional average is the extreme precipitation index shown in Figure 3.7, in which a statistically significant increasing trend is depicted.

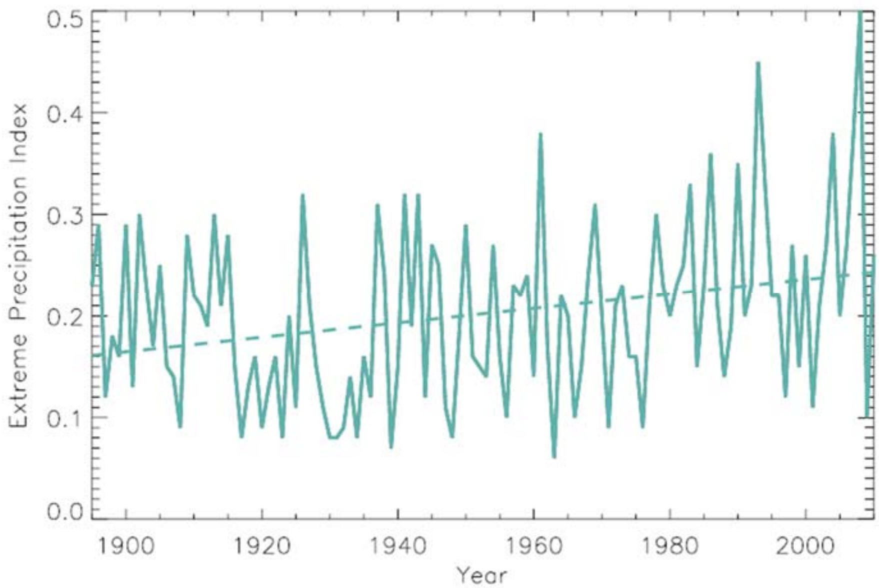

Figure 3.7. Time series of an extreme precipitation index for the Midwest Region (occurrence of 20-percent AEP daily precipitation events). The dashed line indicates the best linear fit by minimizing the chi-square error statistics. Based on daily Cooperative Observer Network data from long-term stations in the National Climatic Data Center's Global Historical Climate Network data set. (Source: Kunkel et al. 2013a)

3.1.3 Snowfall Climatology and Trends

Snowfall varies across the Midwest Region; less than 10 percent of total precipitation is snowfall in the south and more than 50 percent is snowfall in the north (Pryor et al. 2014). Accumulated snowfall averaged over calendar years 1981–2010, obtained from the Midwestern Regional Climate Center are shown in Figure 3.8. Average annual snowfall varies from less than 25 in. in the southern portion to over 200 in. in the northern portion of the Midwest Region. Figure 3.9 shows the average number of days with accumulated snow depths equal to or exceeding 1 in. during any month of the year for the period 1961-2017. As expected, the number of days with accumulated snow depths equal to or exceeding 1 in. varies from about 10 in the southern parts to over 148 in the northern parts of the Midwest Region. The Midwestern Regional Climate Center also provides climatology of the accumulated winter season severity index (AWSSI, Boustead et al. 2015).[1] The AWSSI is also updated on an ongoing basis.

[1] The AWSSI is an accumulated index of winter severity that takes into account temperature, snowfall, snow depth, and duration of winter-weather conditions (Boustead et al. 2015). AWSSI has a temperature component and a snow component that are calculated separately using daily data and is accumulated through a winter season. Onset of winter is defined as the earliest occurrence of one of (1) daily maximum temperature less than or equal to 32°F,

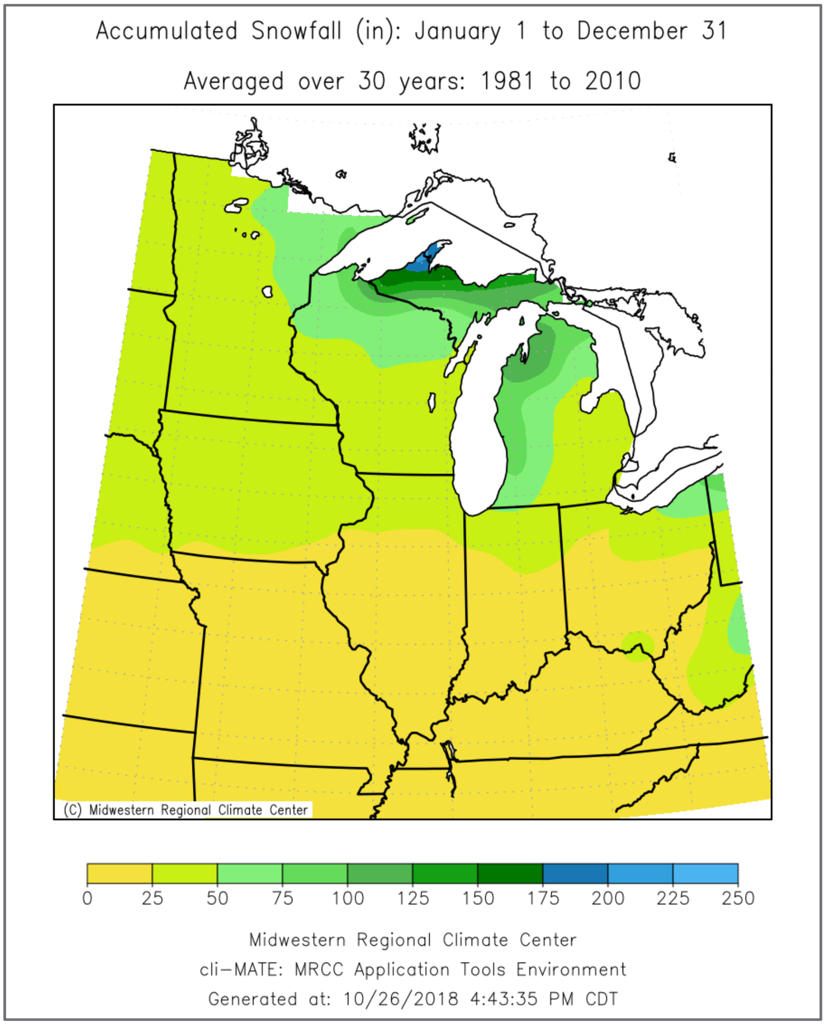

Figure 3.8. Average accumulated snowfall (in.) from 1981–2010. (Source: Midwestern Regional Climate Center)

(2) daily snowfall greater than or equal to 0.1 in., and (3) December 1. Winter ends at the last occurrence of one of (1) daily maximum temperature less than or equal to 32°F, (2) daily snowfall greater than or equal to 0.1 in., (3) snow depth greater than or equal to 1 in., and (4) last day of February. Daily AWSSI is a score assigned to the day based on thresholds of daily maximum and minimum temperatures, snowfall, and snow depth; scores in all categories are summed to obtain AWSSI for the day. Because snow data can contain significant uncertainties and are of limited record, AWSSI is also calculated using estimated snowfall from precipitation and temperature data. A degree-day approach is used to compute snowmelt and a compaction factor approach is used to estimate daily snow depths.

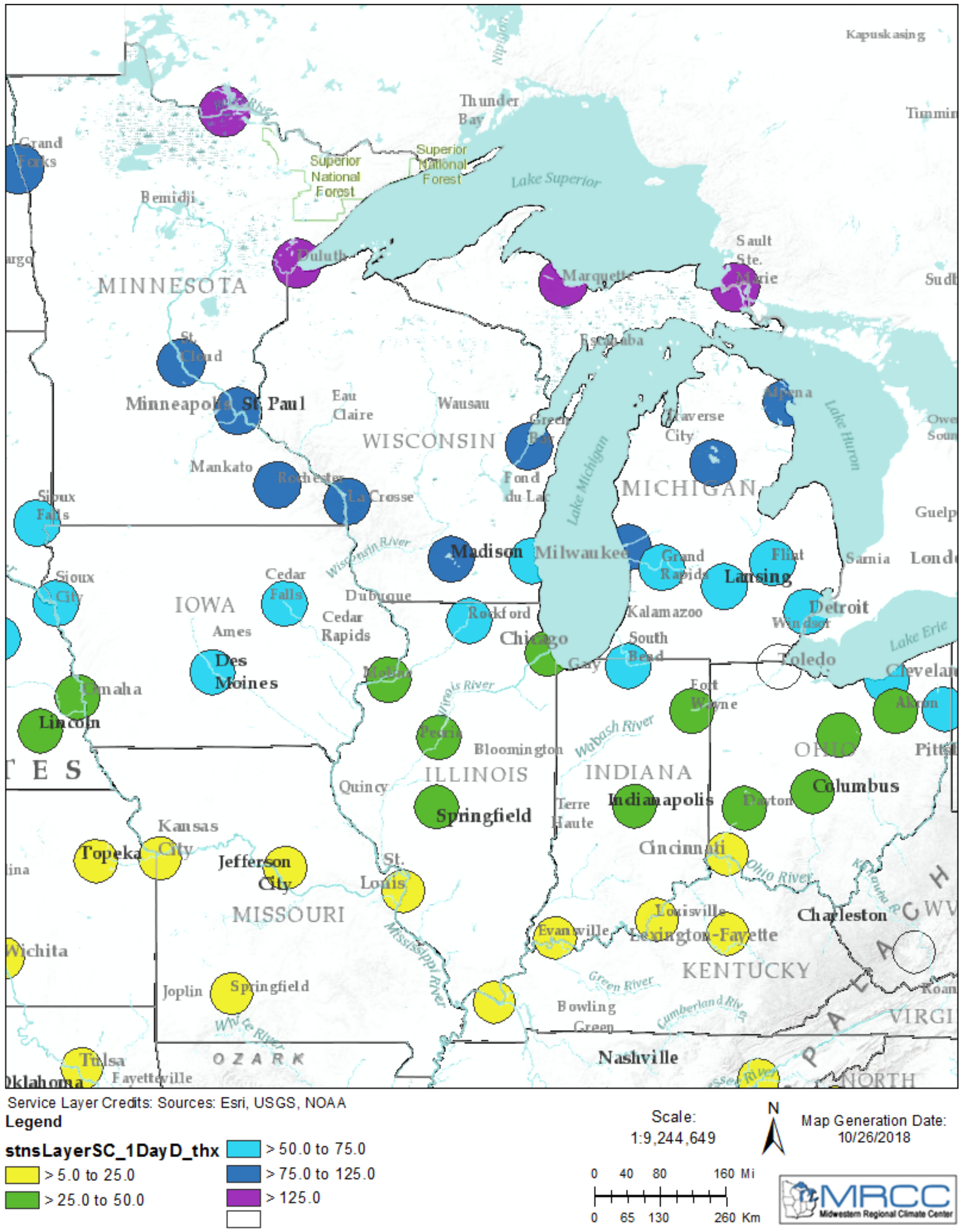

Figure 3.9. Average number of days with snow depth equal to or exceeding 1 in. based on the period 1961-2017. (Source: Midwestern Regional Climate Center)

Figure 3.10 shows the average AWSSI computed using 1980–2014 data. The AWSSI in itself provides little information; however, it is a useful measure to compare among winters at a given location, including the onset of winter and its length. The temperature and snow portions of the AWSSI can also be used to distinguish between how a particular winter progressed, as represented by temperature and snow accumulation, respectively. These indices can be useful in quantifying antecedent and transient conditions for regions where floods may result from rain-on-snow events.

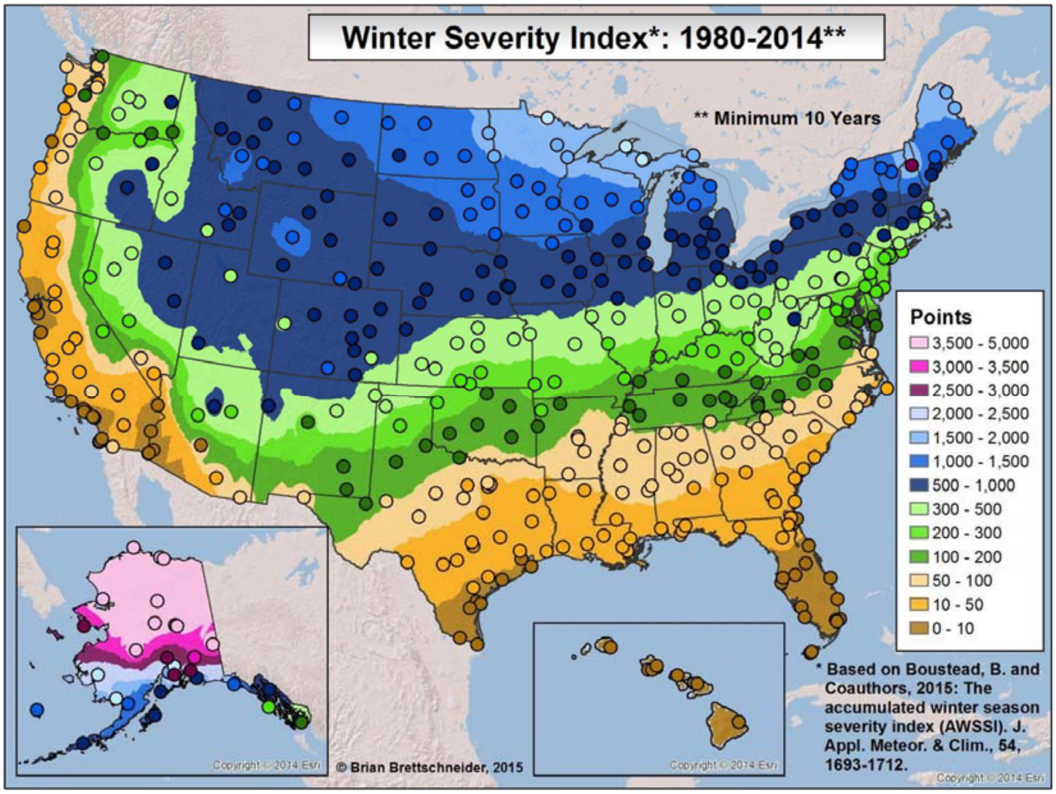

Figure 3.10. Average AWSSI computed for the 1980–2014 period. (Source: Midwestern Regional Climate Center)

Figure 3.11 shows the 2017–2018 end-of-season AWSSI categories. The categories are: minimum to 20th percentile – mild, 21st to 40th percentile – moderate, 41st to 60th percentile – average, 61st to 80th percentile – severe, 81st percentile and above – extreme. It should be noted that the categories are determined based on the station data; that is, a mild AWSSI categorization at one location does not mean that it was less severe in absolute terms than another location whose AWSSI category may have been average. The categories reflect how the current winter compares with the climatology of that location.

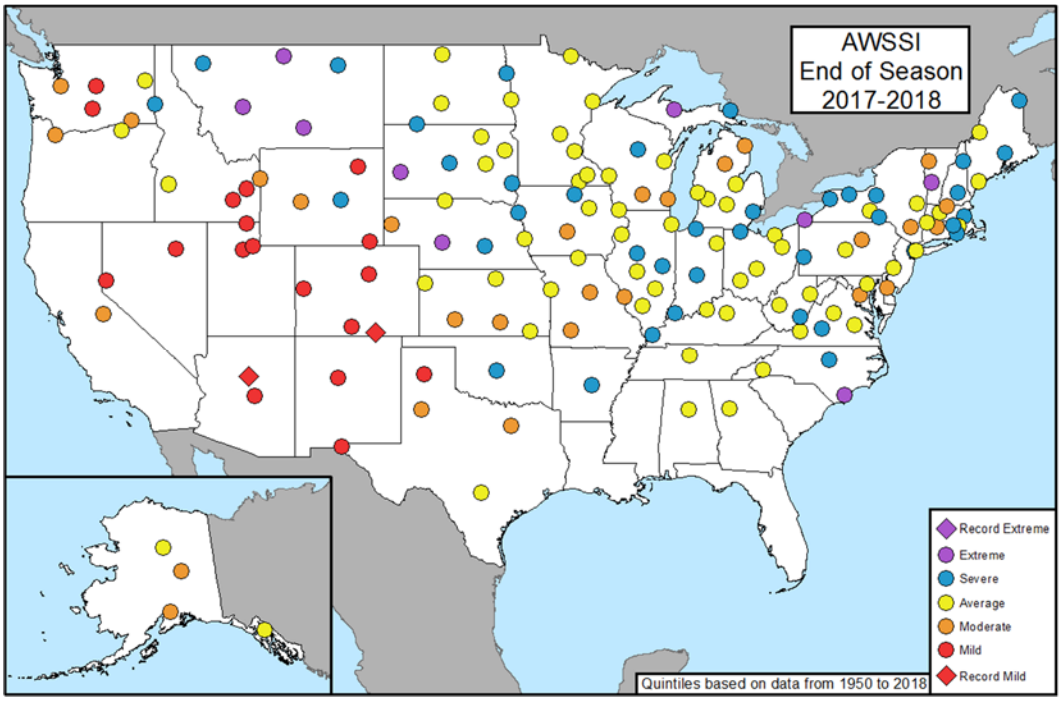

Figure 3.11. AWSSI computed for the 2017–2018 season. (Source: Midwestern Regional Climate Center)

The AWSSI for the 2017–2018 season for Urbana-Champaign, Illinois, is shown in Figure 3.12. In the top panel, the shaded portion shows the accumulation of AWSSI through the 2017–2018 winter. The solid black line is the 1951–2014 average AWSSI and the dashed black lines denote ±1 standard deviation spread. A few other selected years are also shown; for example, 1977–1978 had the highest end-of-season AWSSI, and 2011–2012 had the lowest end-of-season AWSSI at Urbana-Champaign. Winter can "begin" between late October and early December and "end" between early March and mid-April.

The bottom panel of Figure 3.12 shows the progression of 2017–2018 AWSSI at Urbana-Champaign, Illinois, in relation to the years with the highest and lowest end-of-season AWSSI, 1977–1978 and 2011–2012, respectively. The color shadings show the categories throughout the winter season. The 2017–2018 winter started out mild in early December, but between Christmas and mid-January, temperatures quickly dropped into severe to extreme categories (Figure 3.13, top panel). Snowfall and accumulation also occurred during this period, taking the snow component of AWSSI into the severe category (Figure 3.13, bottom panel). The 2017–2018 end-of-season AWSSI was severe for temperatures but average for snow, and the end-of-season total AWSSI was slightly above the long-term average (Figure 3.12, top panel).

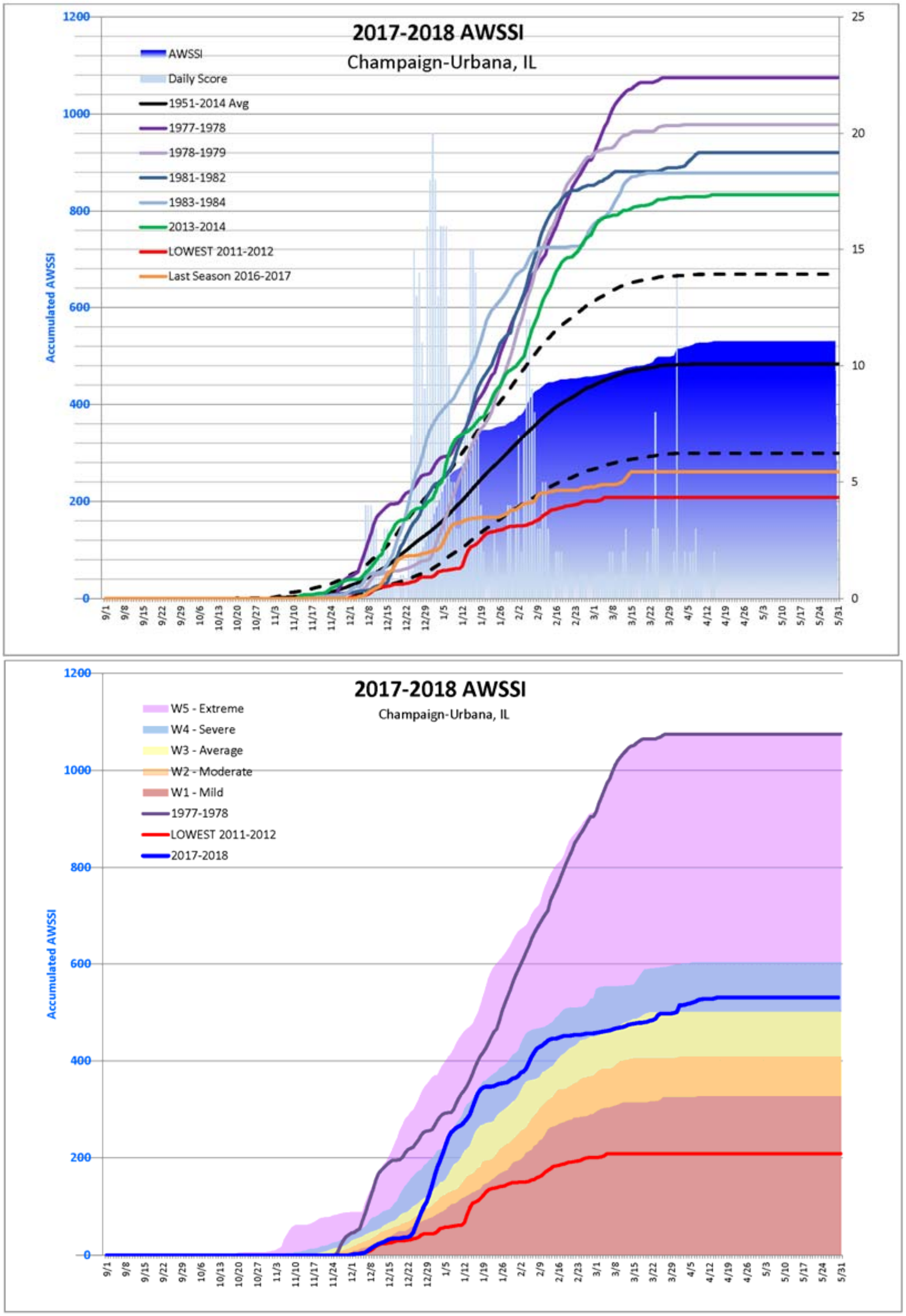

Figure 3.12. AWSSI computed for the 2017–2018 season at Urbana-Champaign, Illinois. Top panel: The left vertical axis shows accumulated AWSSI, and the right vertical axis shows the daily (incremental) AWSSI. (Source: Midwestern Regional Climate Center)

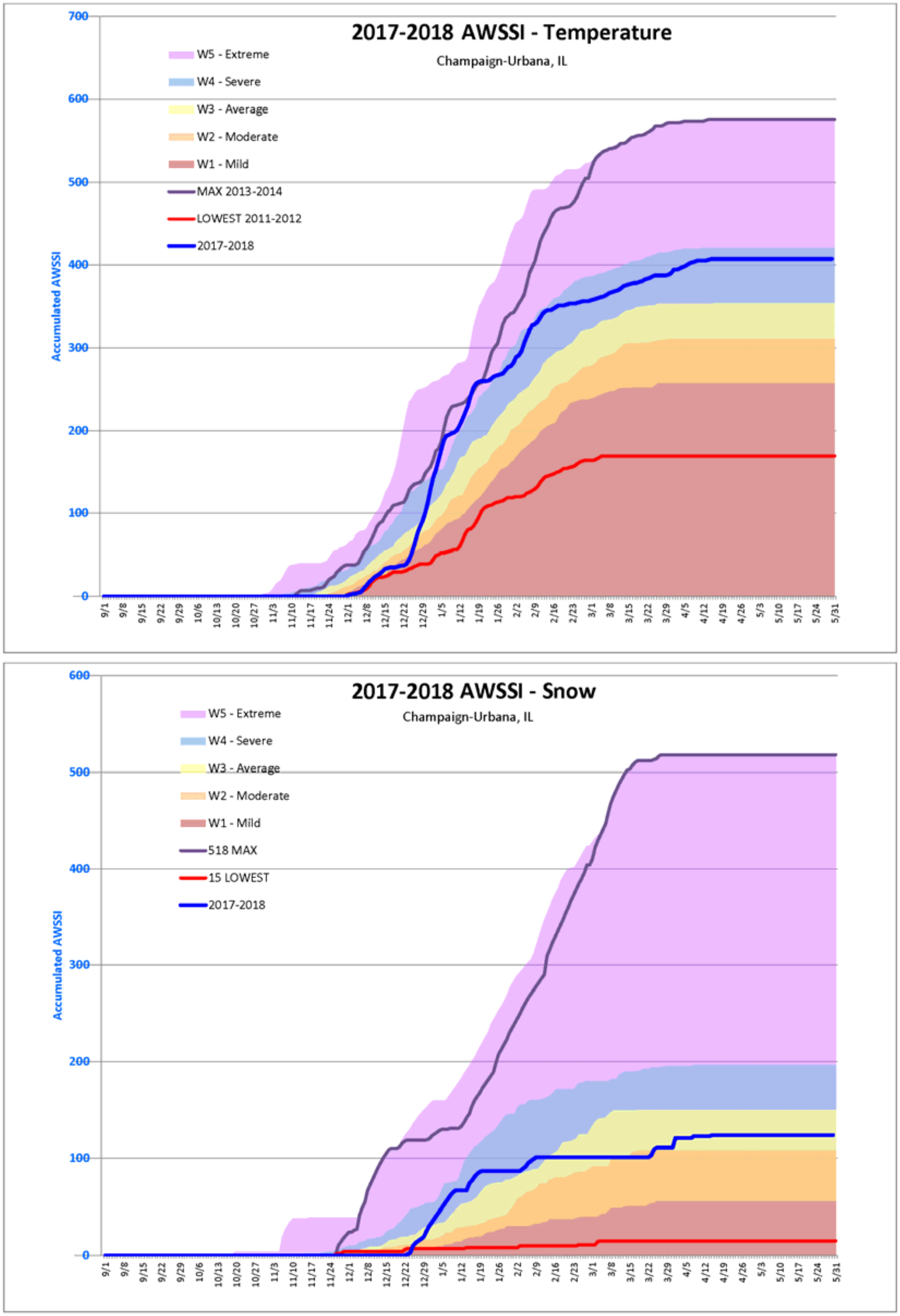

Figure 3.13. The temperature (top panel) and snow (bottom panel) components of 2017–2018 AWSSI at Urbana-Champaign, Illinois (note that the vertical AWSSI scales are different between the two panels). (Source: Midwestern Regional Climate Center)

Kunkel et al. (2009) analyzed the percentage of stations where winter-centered annual snowfall totals were equal to or greater than the 90th percentile (high-extreme snowfall) and were equal to or less than the 10th percentile (low-extreme snowfall) for National Climatic Data Center (NCDC) standard regions depicted in Figure 3.14; the time period used was 1937–1938 through 2006–2007 for this analysis. The east north-central and northern part of central NCDC standard regions compose the Midwest Region defined by NCA4. The estimated 1900–2006 trend for the high-extreme snowfall for the Midwest Region ranged from a decrease of 8.4 percent (east north-central NCDC standard region) to an increase of 0.8 percent (central NCDC standard region), but was not statistically significant. The estimated 1950–2006 trend for the high-extreme snowfall for the Midwest Region ranged from a decrease of 5.9 percent (east north-central NCDC standard region, not statistically significant) to a decrease of 19.4 percent (central NCDC standard region, statistically significant). The estimated 1900–2006 trend for the low-extreme snowfall for the Midwest Region ranged from a decrease of 14.5 percent (east north-central NCDC standard region, statistically significant) to an increase of 6.7 percent (central NCDC standard region, not statistically significant). The estimated 1950–2006 trend for the low-extreme snowfall for the Midwest Region ranged from a decrease of 5.2 percent (east north-central NCDC standard region) to an increase of 11.4 percent (central NCDC standard region), but was not statistically significant.

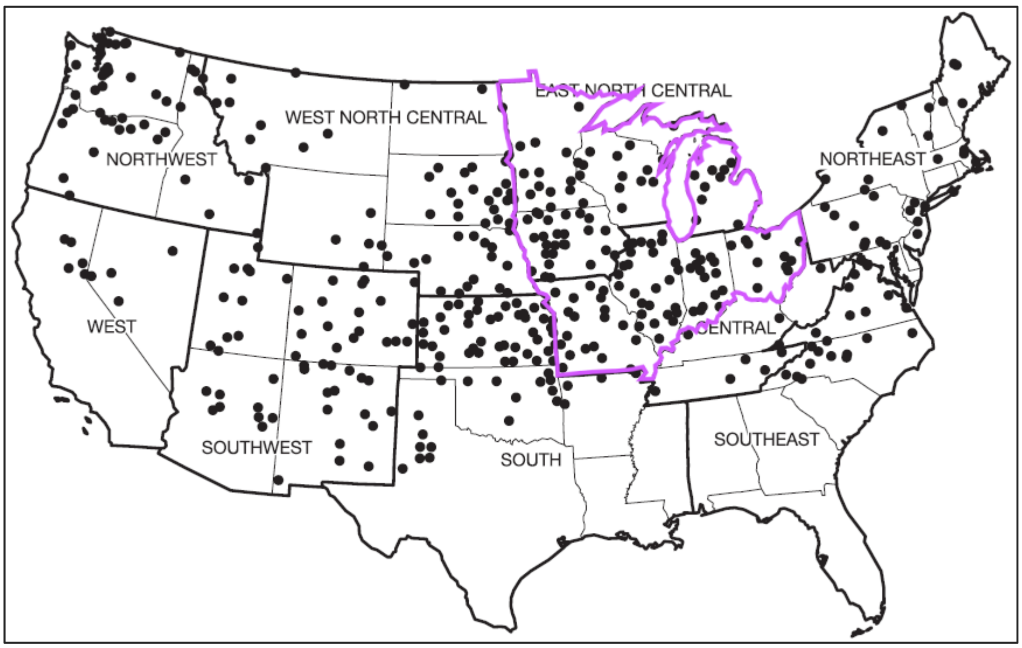

Figure 3.14. NCDC climate regions used by Kunkel et al. (2009).

The time series of the percentage of stations with high-extreme and low-extreme snowfall for the two NCDC standard regions that mostly comprise the Midwest Region are shown in Figure 3.15. Since 1975, there seems to be a decreasing trend in the high-extreme snowfall frequency. The trends in the low-extreme since 1975 is less clear (east north-central shows fluctuations and central shows an increasing trend). However, taken together, they indicate a reduction in high-extreme snowfall frequency over the midwest. Kunkel et al. (2009) concluded that November-March air temperatures are key to the frequency of both metrics.

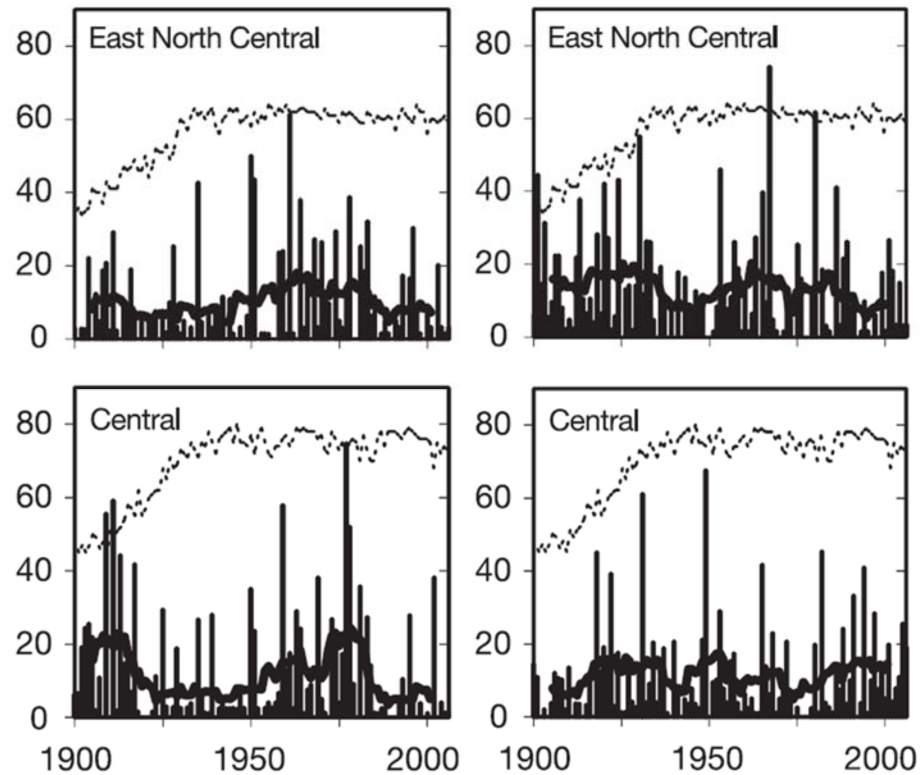

Figure 3.15. Regional average percentage of snowfall stations that are equal to or greater than the 90th percentile (left panel) and equal to or less than the 10th percentile annual snowfall. The percentile thresholds were estimated using data from 1937–1938 through 2006–2007. The thick black line is a moving 11-year average and the dashed line indicates the number of active stations. (Source: Kunkel et al. 2009)

Since the 1960s, when snow cover data from satellites became available, northern hemisphere snow cover extent (SCE) has not changed significantly during winter but has increased in the fall and decreased in spring (Easterling et al. 2017). Partly due to higher temperatures, the decrease in spring SCE is larger than the increase in fall SCE. Since 2010, 7 of the 45 highest monthly SCE values occurred in fall or winter (November and December), while 9 of the 10 lowest monthly SCE values occurred in May and June, which indicates a trend toward earlier snowmelt, particularly at high latitudes (Kunkel et al. 2016). Using NOAA’s Global Historical Climatology Network Daily data set to analyze northern hemisphere snow depths, Kunkel et al. (2016) also stated that while most of the trends in snow depths across the United States were not statistically significant, most grids exhibited negative trends (Figure 3.16).

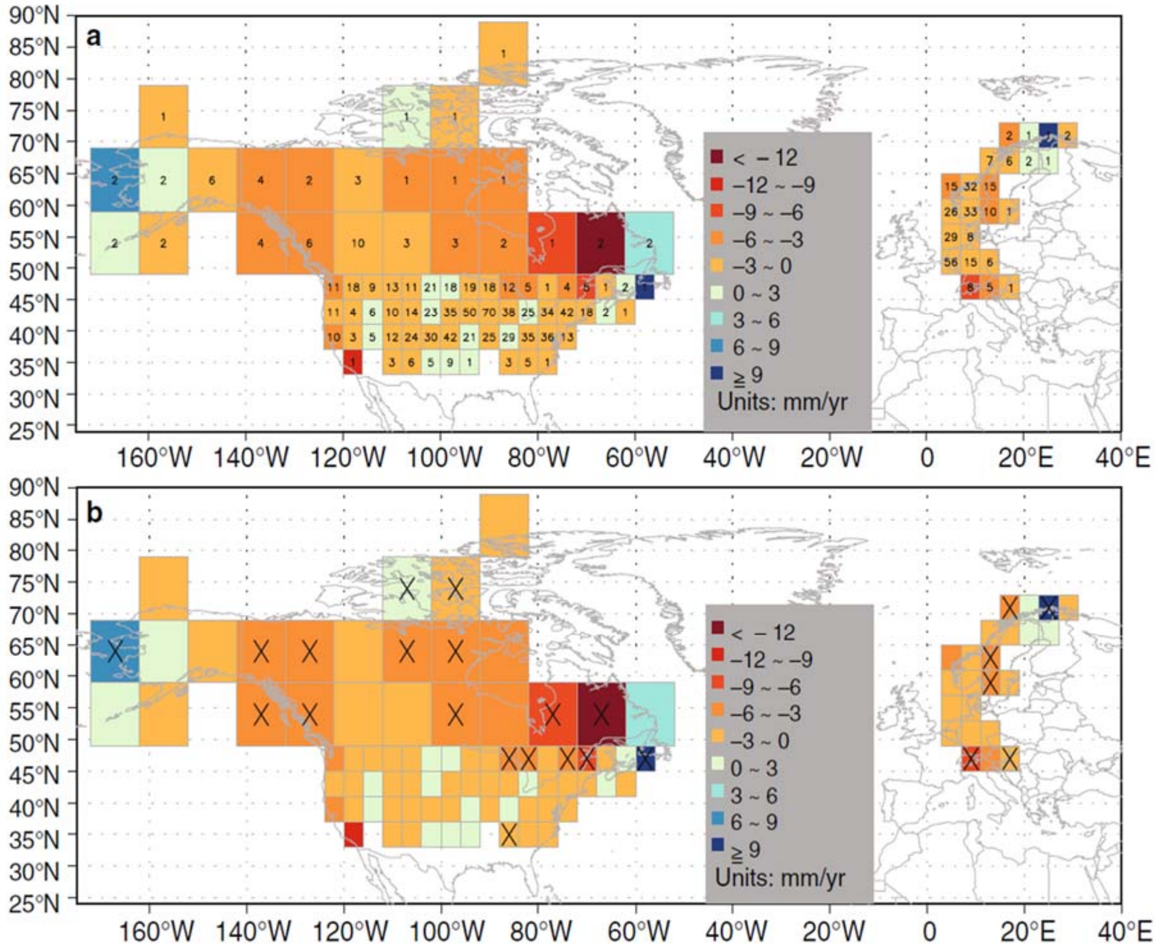

Figure 3.16. Trends in annual maximum snow depths for the period 1960–1961 through 2014–2015. The top panel indicates the number of stations available in the grid cell and the check marks in the bottom panel indicate statistically significant trends. (Source: Kunkel et al. 2016)

3.2 Future Changes in Precipitation

- Projected changes in annual mean precipitation have a general south-north gradient with the greatest increases seen in the north by up to 9–12 percent under the high emissions scenario by 2085.
- The daily, 20-year extreme precipitation is projected to increase by 10 to 20 percent in the Midwest Region between the mid-century and late-century for the lower and higher emissions scenarios.
- In the 2080s under the higher emissions scenario, daily peak precipitation is projected to increase by 32.75 percent during winter and decrease by 6.65 percent during summer.

The projected changes in annual and seasonal mean precipitation from the CMIP3 global models and NARCCAP regional models are shown in Figure 3.17. From the CMIP3 models, there is a general south-north gradient in precipitation changes; the greatest increases are seen in the north by up to 9–12 percent in northern Minnesota under the A2 scenario by 2085. While the changes are generally not statistically significant for the 2035 time period, models mostly agree on the precipitation increase north of the Missouri-Iowa border under the high emissions scenario. The downscaled projections by the NARCCAP models also show a general south-north gradient of mean annual precipitation changes. The south-north gradient in annual precipitation changes is more dominated by the cold season changes consistent with a northward shift of the jet stream (Barnes and Polvani 2013) and storm tracks (Chang et al. 2012) associated with an expansion of the Hadley cell (Lu et al. 2007). The spring increase in precipitation is also associated with the strengthening of the Great Plains low-level jet that transports more moisture to the Midwest Region and enhances precipitation there (Cook et al. 2008). From the NARCCAP simulations, seasonal precipitation changes are more spatially variable, particularly in the wetter seasons of summer and fall. Increases are found throughout the region for all seasons except for summer when drying is projected in the southern part of the region. As discussed later, the summer drying is projected by many models, but CMIP models have common large warm and dry biases in the central and Midwest Regions during summer, which may have implications for projecting changes in the future.

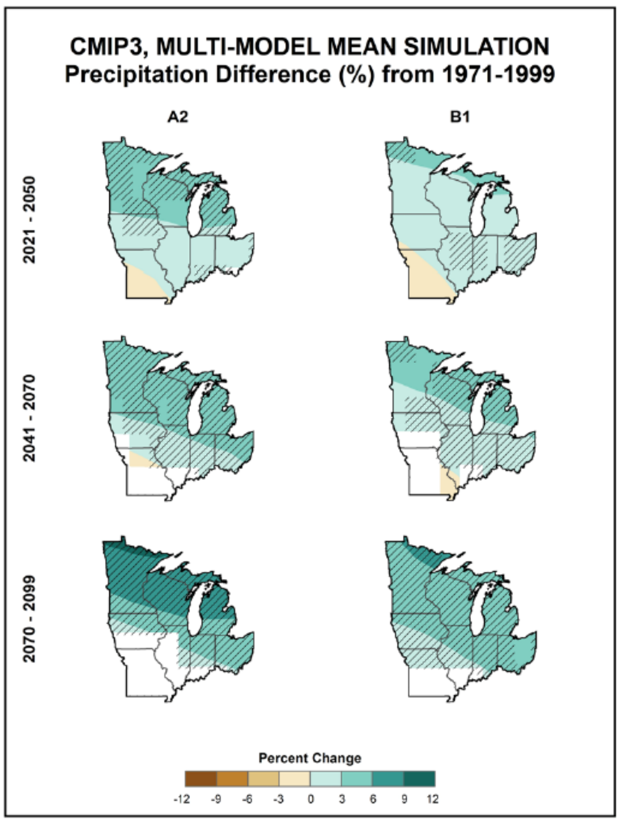

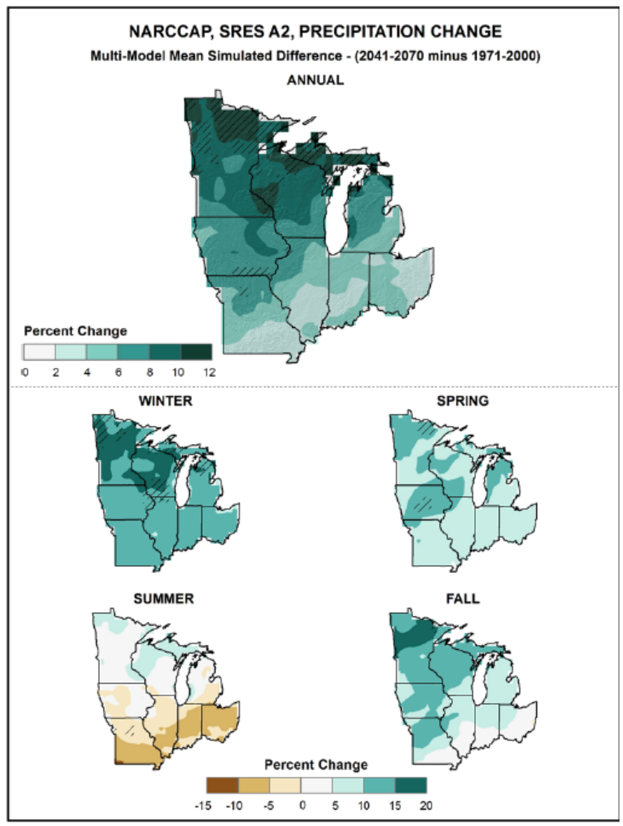

Figure 3.17. (Left) Simulated difference in annual mean precipitation (percent) for the Midwest Region, for 2021–2050, 2041–2070, and 2070–2099 with respect to the reference period of 1971–1999 from the CMIP3 global models for the A2 and B1 emissions scenarios. (Right) Simulated difference in annual and seasonal mean precipitation (percent) for 2041–2070 with respect to the reference period of 1971–2000 from the NARCCAP regional simulations for the A2 emissions scenario. In both panels, color with hatching indicates that more than 50 percent of the models show a statistically significant change in precipitation, and more than 67 percent agree on the sign of the change. (Source: Kunkel et al. 2013b)

As the atmospheric water-holding capacity increases with warming following the Clausius-Clapeyron relationship, extreme precipitation is generally projected to increase even in the absence of changes in atmospheric large-scale circulation. In NCA3, extreme precipitation changes were assessed by comparing the annual number of days with precipitation greater than 1 in. using the NARCCAP regional climate projections (Figure 3.18). Climatologically, there is a strong south-north gradient in extreme precipitation with the southern region showing more than 6 days per year with precipitation greater than 1 in. There are increases throughout the Midwest Region in the 2041–2070 period compared to the 1980–2000 period. However, except for the northern region that featured increases up to 60 percent, the projected changes are not statistically significant in other parts of the Midwest because the changes are small relative to the year-to-year variations.

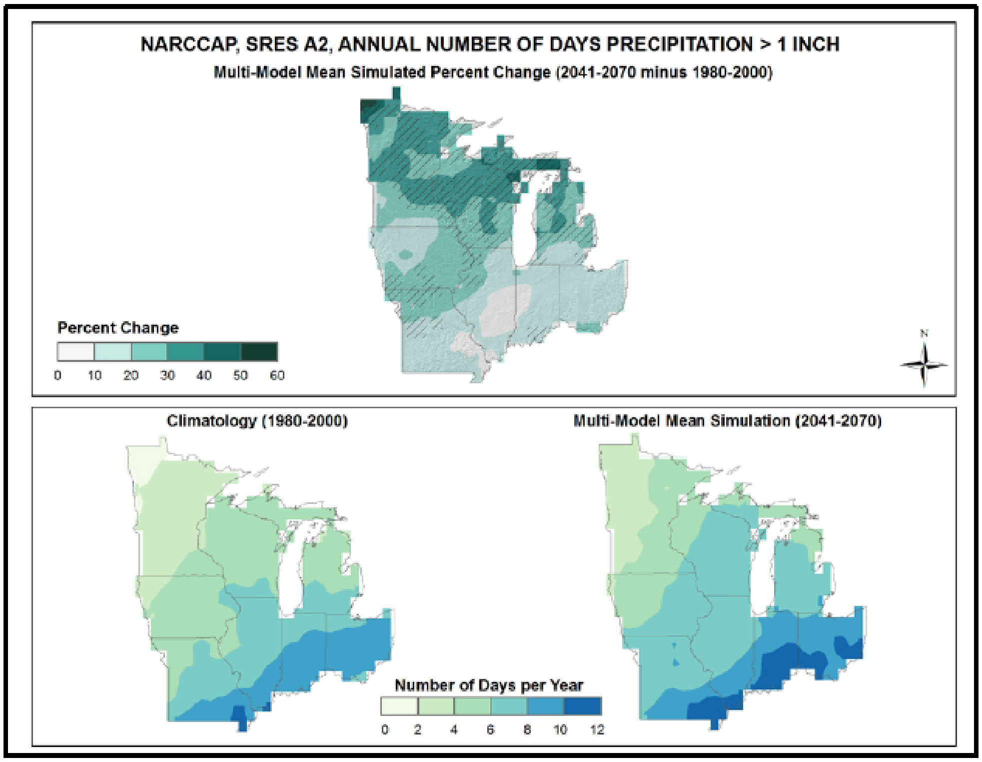

Figure 3.18. (Top) Similar to Figure 3.17, but for simulated differences in the annual number of days with precipitation >1 in. from the NARCCAP projections for the mid-century. Color and crosshatching have the same meaning as Figure 3.17. (Bottom) Climatological mean for the present (left) and future (right). (Source: Kunkel et al. 2013b)

The changes in extreme precipitation also can be summarized by depicting the changes in the 20-year return value of daily precipitation (Figure 3.19). The 20-year return value was calculated based on statistically downscaled data obtained by the Localized Constructed Analogs method (Pierce et al. 2014) applied to the CMIP5 global climate model (GCM) outputs. The Localized Constructed Analogs method assumes that meteorological processes produce cyclostationary statistical relationships between large-scale and finer-scale values of a climatological field. By finding the day with observed values from fine-scale gridded observation data, and best matching the GCM simulation in the wider region and in the local neighborhood around a model grid point, the GCM value is downscaled to $^{1}/_{16}$-degree resolution using the historical analog, scaled to match the amplitude of the model day being downscaled. The 20-year return values from the Localized Constructed Analogs data show increases everywhere in the United States in both the lower (RCP4.5) and higher (RCP8.5) emissions scenarios. Changes between 10 and 20 percent are found over the Midwest, depending on the period and emissions scenarios.

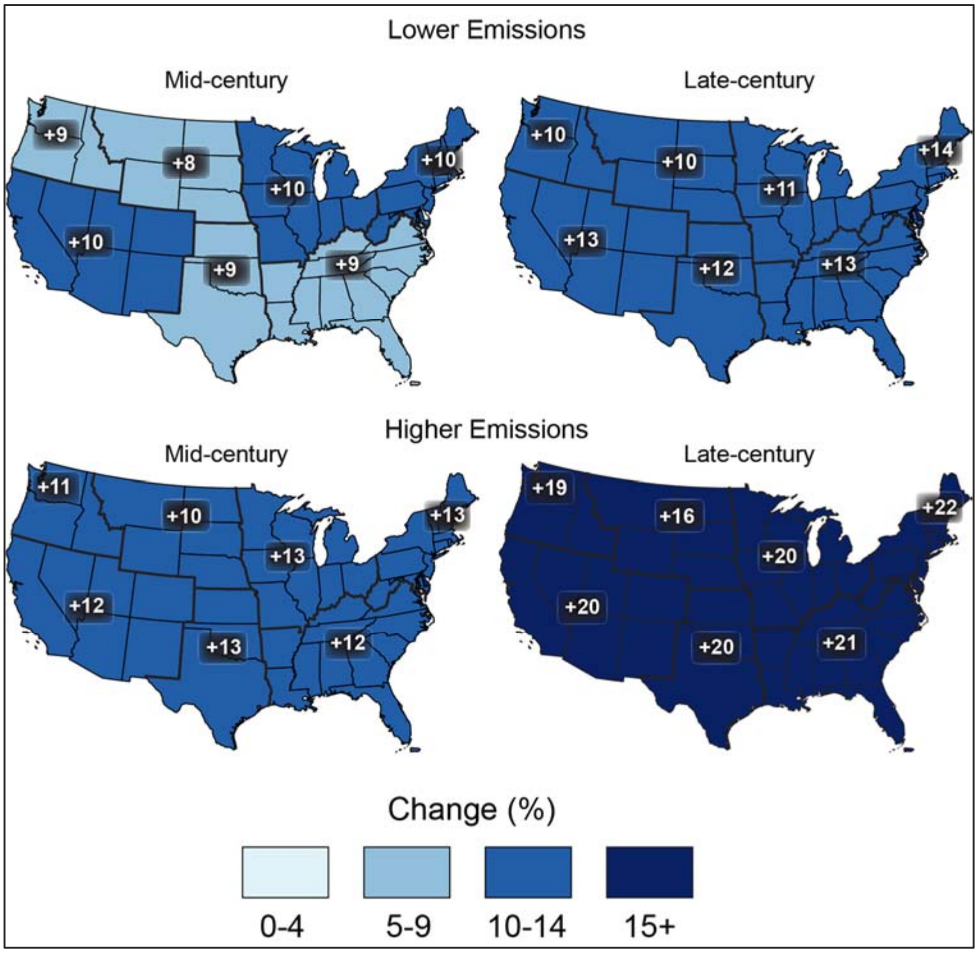

Figure 3.19. Projected change in the 20-year return period amount for daily precipitation for mid- and late-21st century for RCP4.5 and RCP8.5 emissions scenarios using Localized Constructed Analog downscaled data. (Source: Easterling et al. 2017)

As part of the 2017/2018 Indiana Climate Change Impacts Assessment, Byun and Hamlet (2018) analyzed projected changes in temperature and precipitation for the Midwest and Great Lakes Regions, which covers part of the United States and Canada around the Great Lakes, as shown in Figure 3.20. Their analysis includes several steps: (1) evaluate the performance of 31 GCMs from CMIP5 based on the normalized center root mean square errors comparing the model historical simulations of temperature and precipitation with observations; (2) select a subset of 10 GCMs from the 31 GCMs with good performance in reproducing the observations and capture the range of projected changes represented by the 31 GCMs; (3) apply a hybrid delta statistical downscaling method (Hamlet et al. 2013; Tohver et al. 2014) to the 10 GCMs to produce daily time series of temperature and precipitation for the historical (1950–2005) and three future 30-year time windows centering on the 2020s (2011–2040), 2050s, (2041–2070), and 2080s (2071–2100). The hybrid delta method is similar to the BCSD method (Wood et al. 2004), except after quantile mapping between the monthly mean GCM simulations and observations, an additional step of temporal sequencing and daily disaggregation is performed. This additional step generates daily time series for future periods, combining the temporal variability of the fine-scale observations with the monthly statistics from each future period. Last, extreme statistics are analyzed by fitting Generalized Extreme Value probability distributions to ranked extreme events such as the maximum daily peak temperature and precipitation for a given year or season to calculate extreme events with 10-, 50-, and 100-year return intervals for the 90th, 98th, and 99th percentiles, respectively.

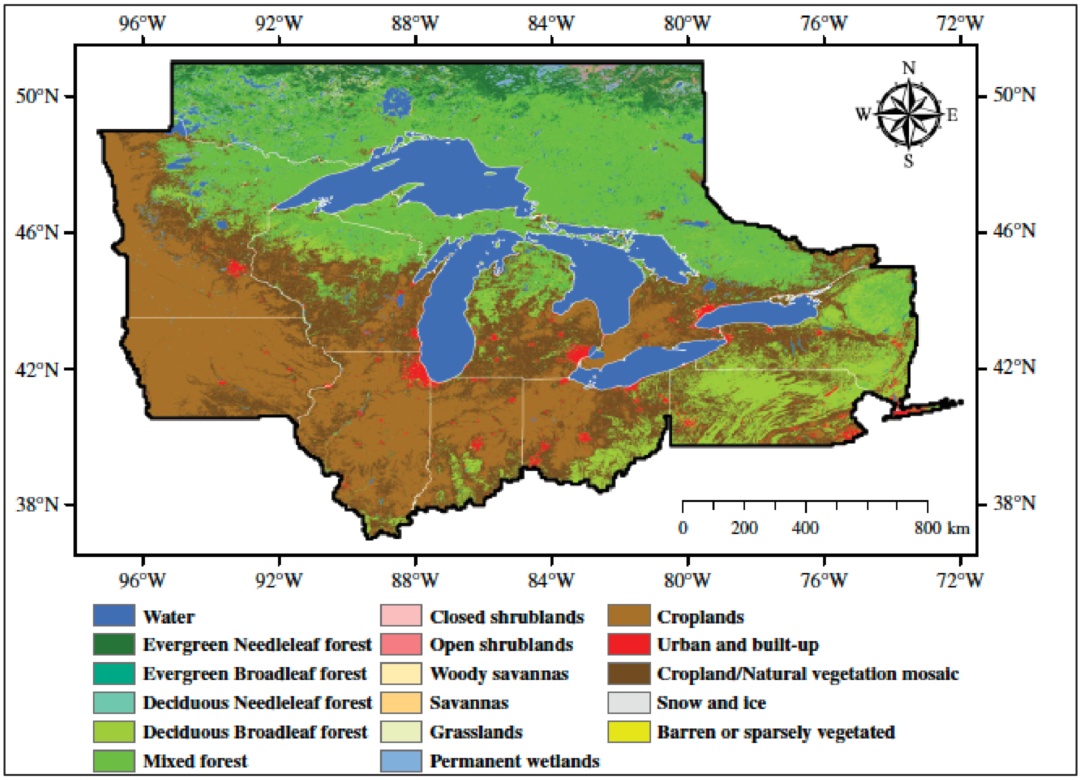

Figure 3.20. Study area in the Midwest and Great Lakes region shown with remotely sensed land cover provided by MODIS at 500 m resolution. Meteorological data are processed at 1/16-degree resolution within this domain. (Source: Byun and Hamlet 2018)

The regional mean temperature and precipitation changes from the downscaled scenarios of 10 GCMs are comparable to those of the 31 GCMs, showing increases in precipitation in three seasons and decreases in summer. Figure 3.21 shows the spatial distribution of precipitation changes downscaled to $^{1}/_{16}$-degree resolution for summer and winter, highlighting the contrasting dry and wet trends, respectively, and the larger changes over time. Changes in extreme events are analyzed by comparing the historical and future daily peak values based on their rank positions (Figure 3.22). For summer, future peak values of precipitation are lower than the historical peak values based on the ensemble mean (red dots), but uncertainty is large because different GCM projections lie above and below the one-to-one line. For winter, all GCMs projected increases in peak values above the historical peak values. The ensemble mean changes are -6.65 percent for summer and +32.75 percent for winter. Future daily peak temperature values are higher than the historical peak temperature values for all models and both summer and winter. For winter in the 2080s under the RCP8.5 scenario, the historical 100-year extreme temperature is projected to become a 2-year event, and the historical 100-year daily precipitation event will become approximately a 10-year event. Because of warmer temperatures, the ratio of snow-to-total precipitation decreases substantially by 10–20 percent in 2080 in the RCP8.5 scenario. Combined with the increase in daily peak precipitation, the chance of flooding will likely increase, as discussed further in Chapter 5.

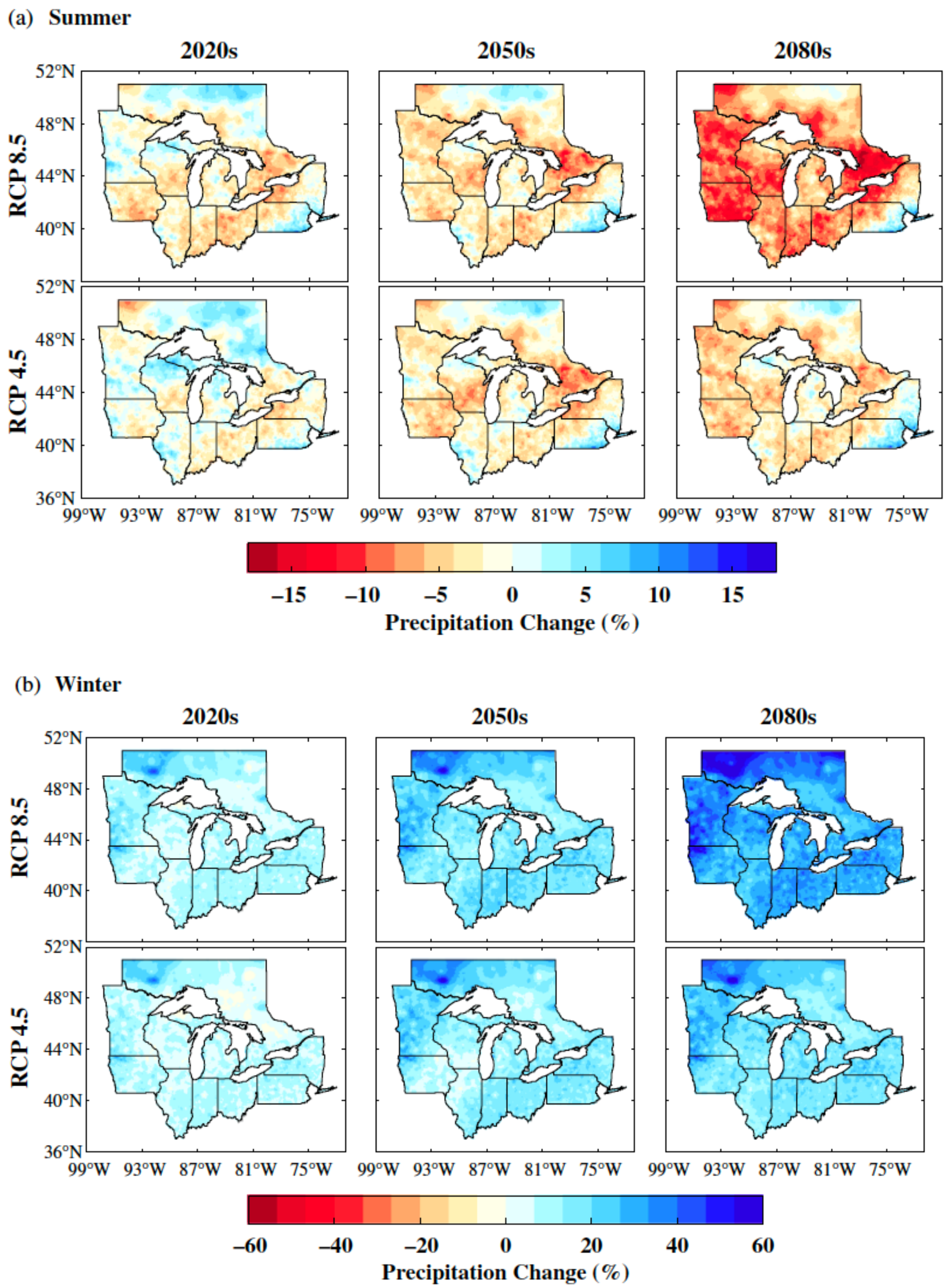

Figure 3.21. Spatial variability of projected ensemble mean precipitation change (percent) for (a) summer (June-July-August) and (b) winter (December-January-February) based on RCP4.5 (bottom row) and RCP8.5 (top row) for 2020s (left), 2050s (middle), and 2080s (right) relative to the historical baseline period of 1971–2000. (Source: Byun and Hamlet 2018)

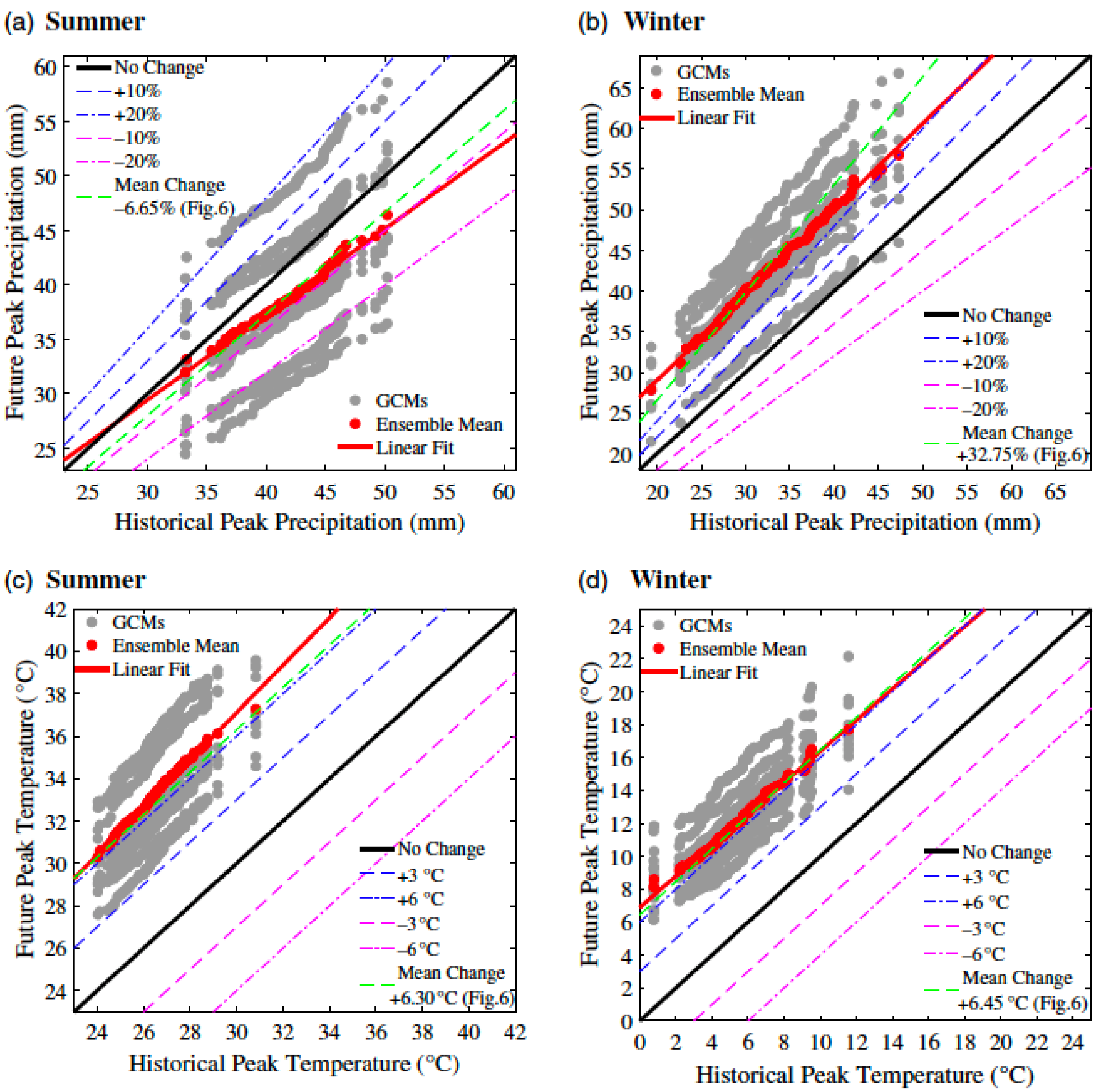

Figure 3.22. Scatter plots of spatially averaged historical and future daily peak events for 10 2080s RCP8.5 scenarios: precipitation (mm) for (a) summer and (b) winter and temperature (ºC) for (c) summer and (d) winter seasons. Each set of 10 x-y pairs (hist-future) is plotted based on rank position in the historical and future distribution. (Source: Byun and Hamlet 2018)

Projecting changes in warm season precipitation for the central and midwestern United States is particularly challenging. During summer, convection frequently develops in the Rocky Mountains in the late afternoon. As the convective disturbance propagates eastward with the mean flow, it organizes into MCSs that produce abundant precipitation during evening and early morning hours in the Great Plains and Midwest Regions. Hence, MCSs contribute about 40–70 percent of warm season precipitation east of the Rocky Mountains (Fritsch et al. 1986). Most climate models are not able to reproduce the observed nocturnal rainfall maximum and mean rainfall in the Great Plains and Midwest Region. This suggests that climate models are unable to simulate MCSs and the associated heavy precipitation.

Lin et al. (2017) found that the dry biases in the CMIP5 multimodel mean summer rainfall over the central United States are mainly associated with the lack of intense rainfall in the simulations (Figure 3.23).

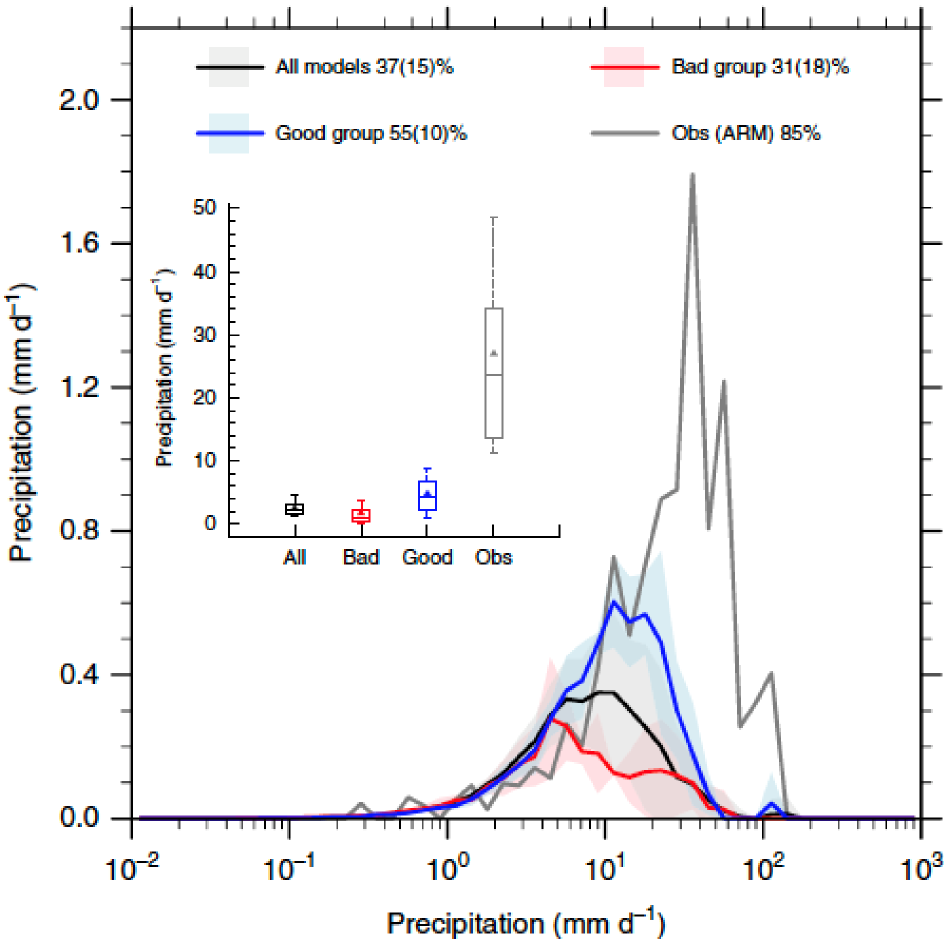

Figure 3.23. Distribution of daily precipitation for all models, good group, bad group, as well as that observed by Atmospheric Radiation Measurement Program during 1996–2005 at the Southern Great Plains site. The inset plot is the boxplot of daily precipitation. The boxes indicate the 25th, 50th, and 75th percentiles and the whiskers indicate the 10th and 90th percentiles, respectively. Solid triangles stand for the mean values. (Source: Lin et al. 2017)

The dry biases reduce soil moisture and evapotranspiration, leading to warm biases of 3°C in the upper Midwest Region (Figure 3.24). Models with larger warm biases also projected larger warming in the future (Figure 3.25). Using this linear relationship, Lin et al. (2017) constrained the projected warming and its uncertainty in the CMIP5 multimodel ensemble, which reduces the warming by 0.7°C. This temperature correction also was used to bias correct the projected precipitation changes based on the linear relationship between the temperature and precipitation biases. With the bias correction, instead of a drying in the summer as projected by the CMIP5 models (also seen in Figure 3.17 from the NARCCAP projections and Figure 3.21 from Byun and Hamlet [2018]), there is a negligible increase in precipitation in the future.

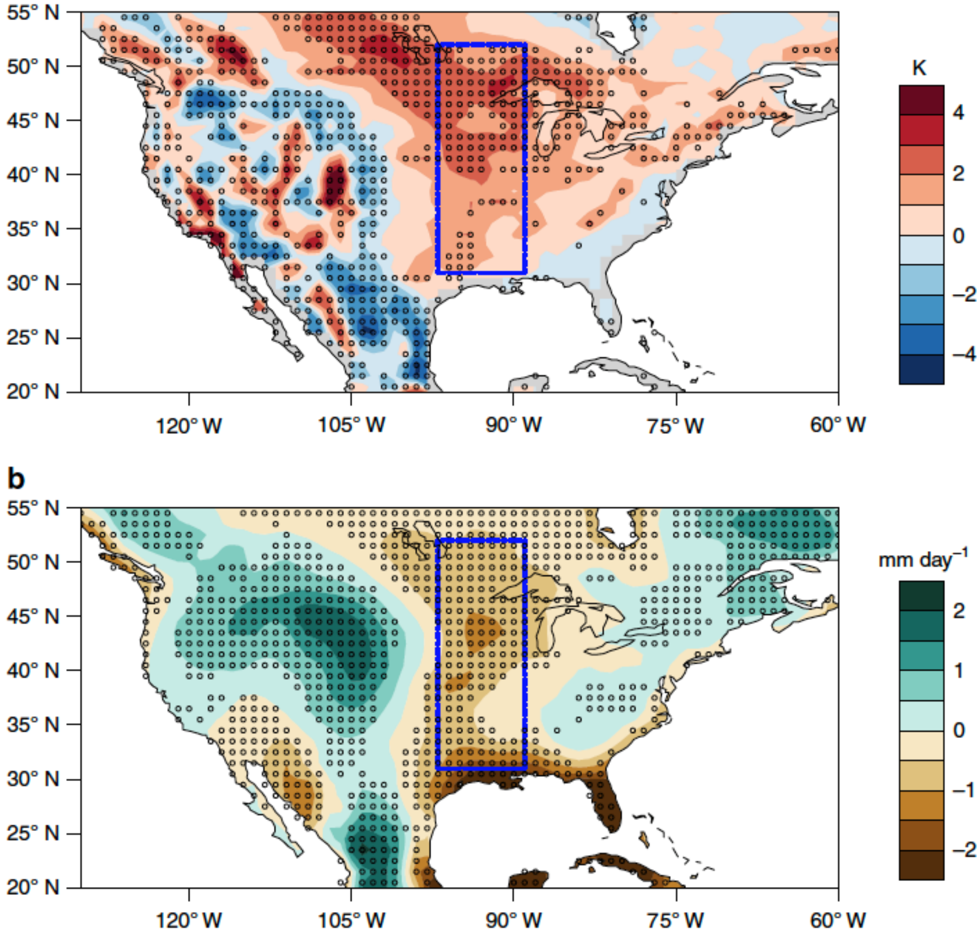

Figure 3.24. (a) Multimodel mean temperature biases and (b) precipitation biases in summer during 1979–2005 from 19 CMIP5 historical simulations. Regions where at least two-thirds of the models agree on the sign of the difference are marked with black circles. The blue rectangle (31-52 °N, 262-271 °E) indicates the central United States (Source: Lin et al. 2017)

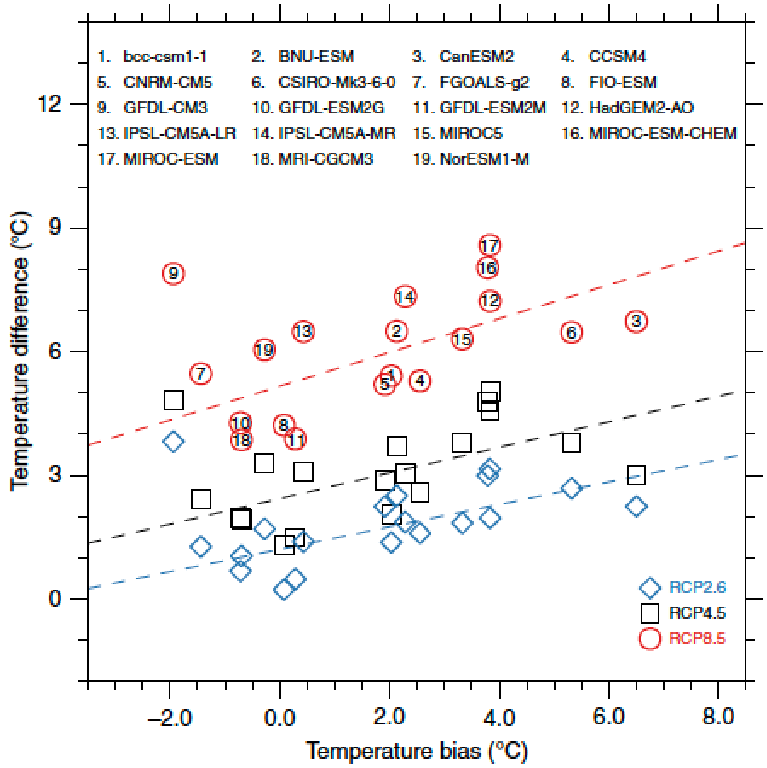

Figure 3.25. The relationships between temperature changes (2080–2099) relative to (1981–2000) and temperature bias for the three RCP scenarios. RCP2.6, RCP4.5, and RCP8.5 are represented by blue, black, and red symbols. Dashed lines indicate the linear fit to each scenario excluding model 9. Circled numbers represent the corresponding models. (Source: Lin et al. 2017)

The findings of Lin et al. (2017) highlight the importance of correctly modeling the processes responsible for producing precipitation and the subsequent land-atmosphere interactions that connect temperature and precipitation and their projected changes in the future. By explicitly resolving deep convection rather than relying on cumulus parameterizations used in global and regional climate models, convection-permitting modeling is a promising approach for addressing the ubiquitous warm and dry biases in GCMs. Recent advances have been made in dynamical downscaling using regional climate models at grid spacings much beyond the 50 km used in NARCCAP. For example, Prein et al. (2017a) performed a convection-permitting simulation over the contiguous United States at 4 km grid spacing with convection parameterization turned off. The regional model was driven by large-scale circulation from a global reanalysis for 2000–2013. Using a precipitation object-tracking method, they identified MCSs in the simulation and observations and found that the model is able to reproduce the observed MCS statistics in spring, including size, propagation speed, total precipitation volume, and maximum hourly precipitation within observational uncertainties (Figure 3.26). However, the simulation has a notable negative bias during late summer, which was attributed to the weak synoptic forcing, so correct representation of local-scale processes, such as soil-atmosphere interactions, regional-scale wind systems, and mixing in the planetary boundary layer, are essential. Hence, even though convection-permitting modeling generally improves the simulation of MCSs, improving the modeling of land-atmosphere interactions, boundary layer turbulence, and cloud microphysical processes also is important under conditions of weak synoptic forcing (which occurs often in late summer). The ability to represent MCSs has important implications for projecting not only changes in mean precipitation, as discussed above, but also severe storms, as discussed in Chapter 4.

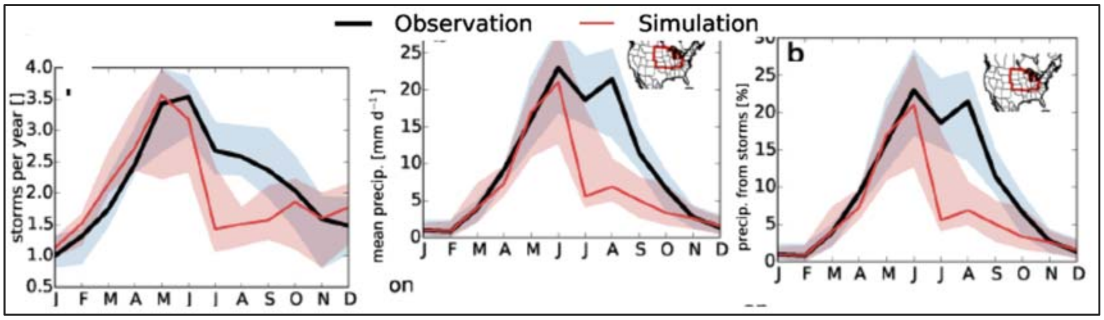

Figure 3.26. The monthly mean annual cycle of the numbers of MCSs (left), mean MCS precipitation (middle), and percentage of precipitation from tracked MCSs relative to regional total monthly precipitation (right) for the Midwest Region. The shadings show the interquartile range of the interannual variability. Black lines and blue shading correspond to the observations, while red lines and pink shading show simulated results. (Adapted from Prein et al. 2017a)

Following Prein et al. (2017a), Prein et al. (2017b) performed another simulation, called the pseudo-global warming (PGW) experiment, using the same model configuration as the convection-permitting simulation shown in Figure 3.26. In the PGW experiment, the model was driven by large-scale circulation that included monthly mean perturbations corresponding to the ensemble mean climate change signals (i.e., climatological monthly mean difference between 2071–2100 and 1976–2005) determined from the CMIP5 multimodel ensemble for the RCP8.5 scenario. The perturbations were added to the large-scale circulation of the global reanalysis for 2000–2013. Comparing the PGW and the control simulations, winter mean and extreme precipitation increase almost everywhere in the United States. During summer, the Midwest Region exhibits a reduction in mean and moderate (97.5 percent) hourly precipitation, but extreme (99.95th percentile) hourly precipitation shows small increases (Figure 3.27).

It is useful to contrast the projections of precipitation changes in spring versus summer in the Midwest Region. Although MCSs contribute importantly to the total precipitation in the region in both spring and summer, the projection of enhanced precipitation during spring is more robust across models while the projection of drying in summer has larger uncertainty. Two reasons may contribute to the spring versus summer difference. First, MCSs that develop in spring are more associated with frontal systems, while MCSs that develop in summer tend to occur under weaker synoptic conditions, so other processes such as land-atmosphere interactions and boundary layer processes may be equally, if not more, important for modeling summer MCSs in the regions. This has been discussed above following the argument of Prein et al. (2017a), which can also be used to explain the model disagreement in the projections because model representations of land-atmosphere interactions and boundary layer processes are known to have large uncertainties. Second, the springtime increase in precipitation is supported by the strengthening of the Great Plains low-level jet that supplies more moisture to the central and Midwest Regions (Cook et al. 2008). The spring low-level jet response to warming is a robust feature found across the models. In contrast, the low-level jet is not enhanced as much during summer. The seasonally-dependent response of the Great Plains low-level jet is associated with the seasonally dependent response of the North Atlantic subtropical high to warming. The latter is associated with the seasonal delay in tropical precipitation found robustly across the CMIP5 models (Song et al. 2018a). As the subtropical high is strengthened more in spring than in summer, the Great Plains low-level jet is strengthened more in spring than summer and the enhanced moisture transport results in larger increase in precipitation in the northern Plains and Midwest in spring relative to summer (Figure 3.28). Hence, lacking a dominant response of the subtropical high and low-level jet, the CMIP5 models projected summer drying, with larger disagreements among models. These findings point to the need for more research to understand and constrain model projections of summer precipitation changes in the Midwest Region.

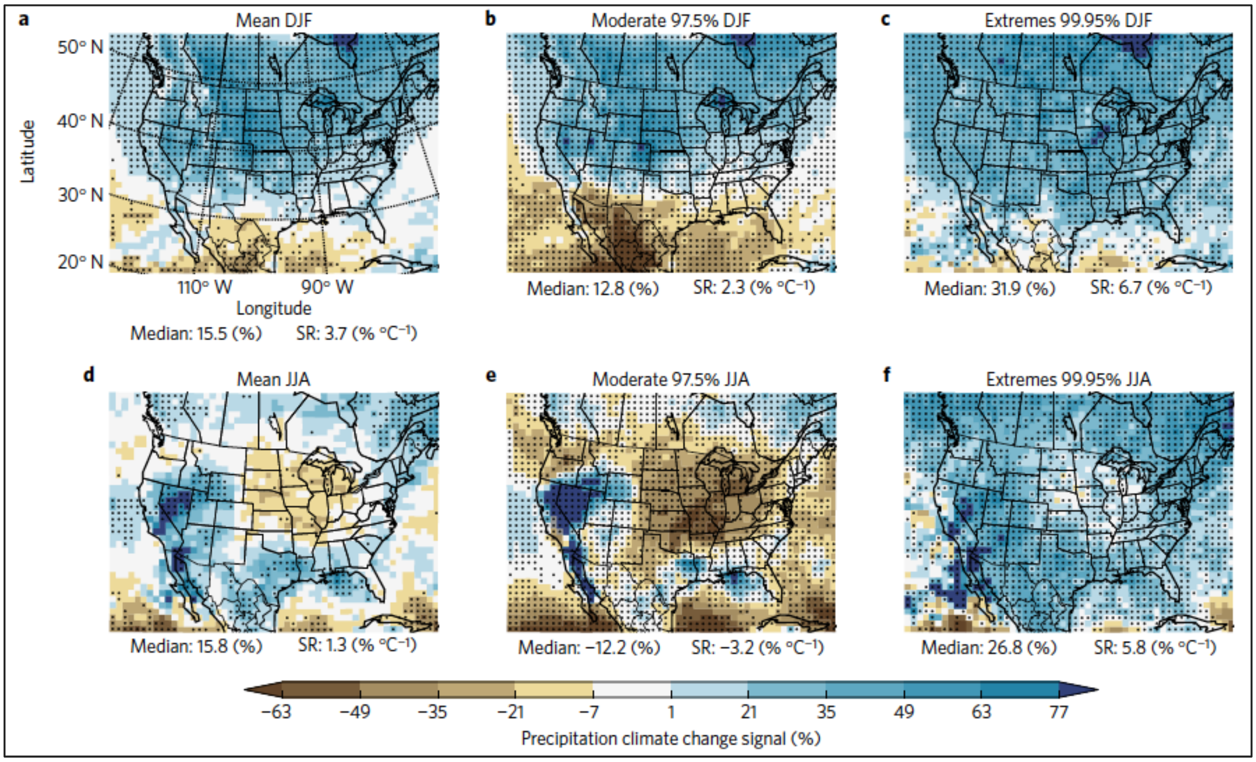

Figure 3.27. Relative changes in mean (a, d), moderate 97.5 percent (b, e), and extreme 99.95 percent (c, f) hourly precipitation for winter (DJF) (upper panels) and summer (JJA) (lower panels) comparing the PGW and control simulations (i.e., PGW minus control). Dots highlight regions with significant changes. The relative changes correspond to the climate change signals calculated based on the difference between (2071–2100) and (1976–2005) from the multimodel CMIP5 mean for RCP8.5 used in the PGW method. (Source: Prein et al. 2017b)

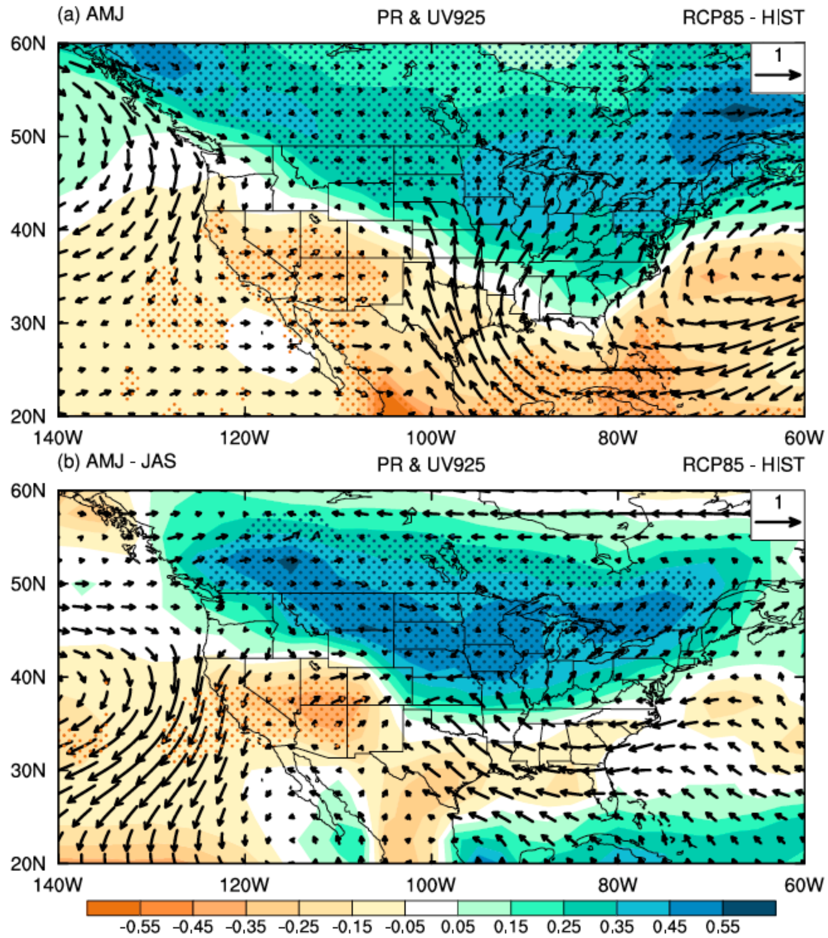

Figure 3.28. Changes of the 925-hPa wind (vector; unit: m/s) and precipitation (shading; unit: mm/day) during (a) April-May-June and (b) April-May-June minus JAS for the ensemble mean difference between the CMIP5 RCP8.5 (2056-2099) and HIST (1962-2055) simulations. Stippling indicates that at least 70% of the models agree on the sign of the difference. AMJ = April–June; JAS = July–September; RCP8.5 = Representative Concentration Pathway 8.5; HIST = historical. (Source: Song et al. 2018b)

4.0 Severe Storms in the Midwest Region

This chapter summarizes the observed and projected changes in severe storms in the Midwest Region. As discussed in Chapter 3, MCSs contribute to about 60 percent of warm season precipitation in the Great Plains and Midwest Regions (Figure 4.1).

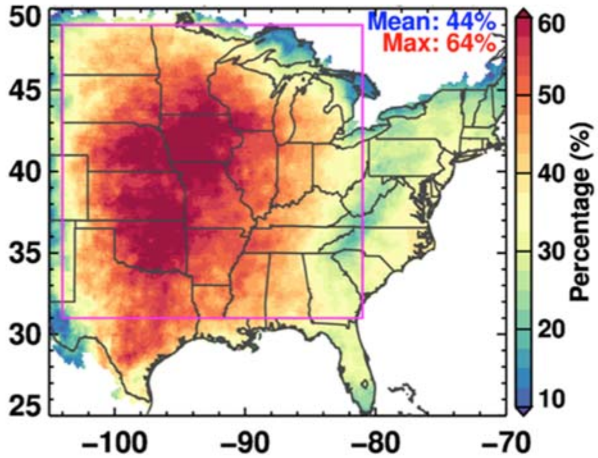

Figure 4.1. Percentage of precipitation produced by MCSs during the warm season (April–August) based on 10-year climatology. (Source: Feng et al. 2016)

Schumacher and Johnson (2006) examined extreme rainfall events during 1999–2003 using a rain gauge network east of the Rocky Mountains and found that most extreme rainfall events occurred during July and more than half were associated with MCSs. More recently, Stevenson and Schumacher (2014) extended the study of Schumacher and Johnson (2006) by using 10 years (2002–2011) of data from a gridded multisensory precipitation analysis (known as the National Centers for Environmental Prediction stage-IV precipitation analysis) that combines radar-estimated rainfall and rain gauge data to provide better coverage over the United States. Focusing on events at 50- and 100-year return periods, they found that over half of the 100-year, 24-hour events were a result of MCSs, and synoptic and tropical systems were responsible for nearly one-third and one-tenth, respectively (Figure 4.2). The top 10 events from the 100-year, 24-hour threshold in the central and eastern United States include two events in the Midwest Region, both associated with MCSs, producing 152.4 to 351.3 mm of precipitation on August 19, 2007, and 152.8 to 344.9 mm of precipitation on September 15, 2004. As noted in Chapter 3, flooding in the Midwest in 2008 is also associated with heavy precipitation produced by MCSs and mesoscale convective complexes (MCC). The latter is a very intense form of an MCS, identifiable in infrared satellite imagery as having a large, cold cloud top roughly circular in shape (Maddox 1980).

Besides producing heavy precipitation and floods, some MCSs also are associated with severe weather. For example, a squall line is a common type of MCS that is characterized by intense convective cells arranged in a line followed by a zone of stratiform precipitation. Squall-line MCSs are marked by a sequence of events including a sudden windshift, followed by a short duration of heavy rain or hail and a longer period of quasi-steady lighter stratiform rain. While a squall line passes over quickly, a supercell, another type of MCS, is long-lived and highly organized by a rotating updraft. Most large and intense tornadoes come from supercells. Because MCSs occur frequently in the Midwest, understanding past and future changes in MCSs is important for understanding changes in severe storms in the Midwest.

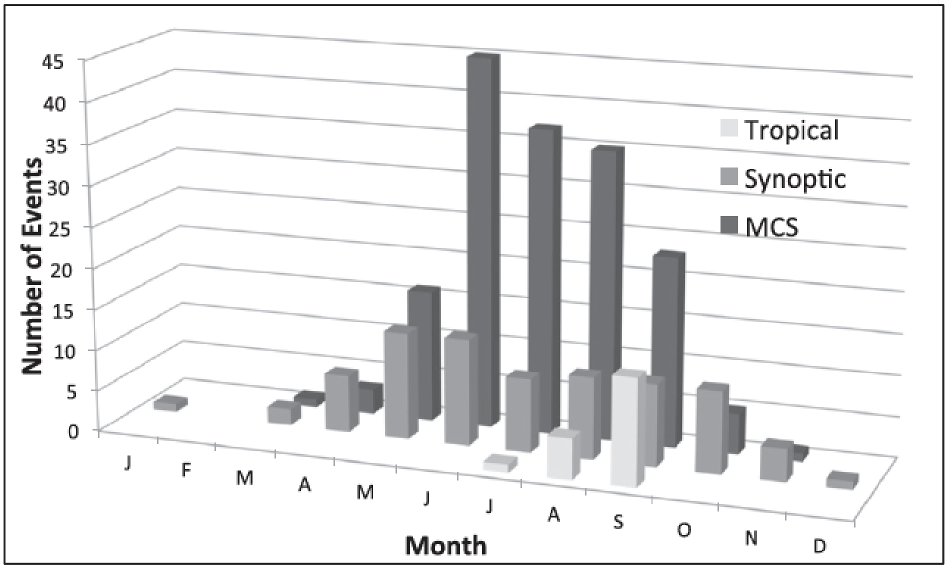

Figure 4.2. The 100-year, 24-hour monthly distribution of system type for 2002–2011 events. (Source: Stevenson and Schumacher 2014)

4.1 Changes in Mesoscale Convective Systems

4.1.1 Observed Changes

- The precipitation frequency and lifetime of MCSs in the north-central United States, including the Midwest Region, increased by 11 percent per decade and 4 percent per decade, respectively, during April–June in the 1979–2014 period.
- The 95th percentile exceedance frequency and 95th percentile rain-rate of MCS precipitation increased by 2–10 percent per decade and 1–2 percent per decade, respectively, over the Midwest Region in the 1979–2014 period.
- Changes in MCSs are associated with larger warming over land relative to the adjacent ocean, which creates a sea-level pressure anomaly that enhances moisture transport by the low-level jet to the Great Plains and supports more frequent and longer-lived MCSs.

Using precipitation data from rain gauges, Kunkel et al. (2013a) evaluated the changes in the 20-year return value of daily precipitation in the United States. They found spatially coherent and statistically significant positive trends in the central United States during the 1948–2010 period (Figure 4.3). Because over half of the 100-year, 24-hour extreme precipitation events are associated with MCSs (Stevenson and Schumacher 2014), it could be inferred that the frequency or intensity of MCSs has increased in the past, but quantitative evaluation is important to establish historical trends. Kunkel et al. (2012) performed the first study to attribute changes in extreme precipitation to different meteorological causes. From 935 Cooperative Observer stations, they identified daily extreme precipitation events that exceeded a threshold for a 1-in-5-year occurrence for the period of 1908–2009. Based primarily on analysis of surface pressure and temperature, each event was assigned a meteorological cause, categorized as extratropical cyclone near a front (FRT), extratropical cyclone near center of low pressure, tropical cyclone (TC), MCS, air mass (isolated) convection, North American monsoon, and upslope flow.

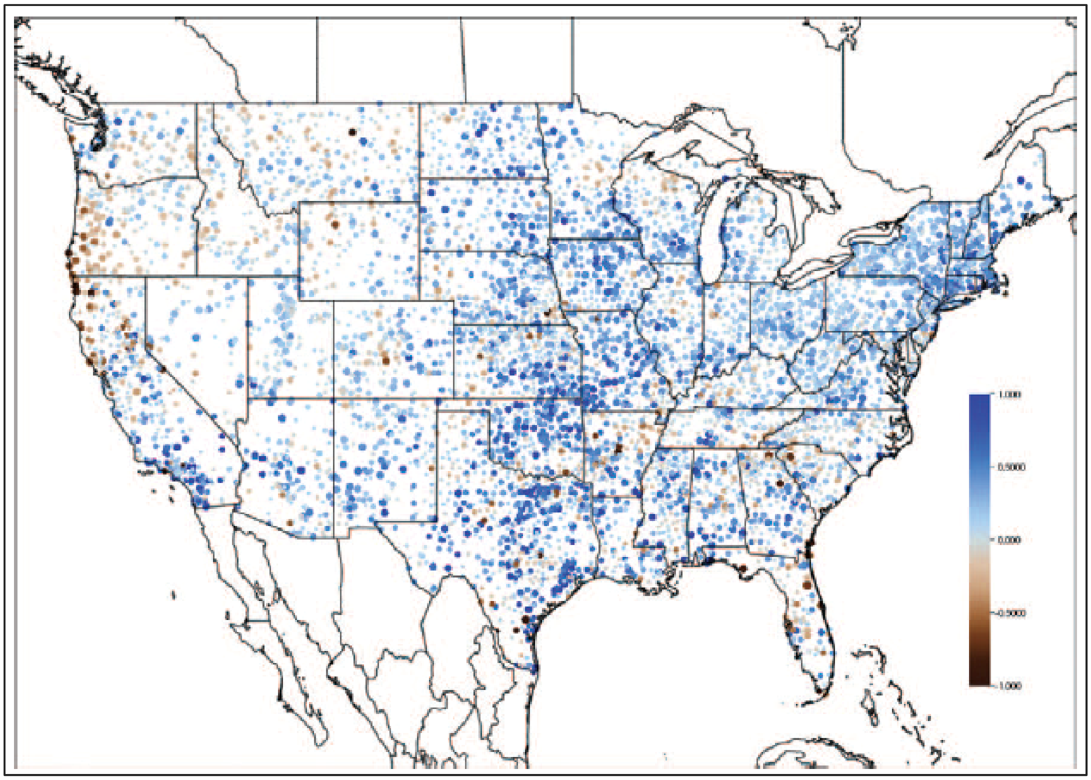

Figure 4.3. Changes in the observed 20-year return value of the daily accumulated precipitation (in.) during the 1948–2010. The color scale ranges from -1.0 in. to 1.0 in. in 0.5-in. intervals. Only locations for which data from at least two-thirds of the days in the 1948–2010 period were recorded are included in this analysis. The change in the return value at each station is shown by a circle whose relative size portrays its statistical significance: the large circles indicate the z score (estimated change in the return value divided by its standard error) is greater than two in magnitude; medium circles indicate the z score is between one and two in magnitude; and the small circles indicate the z score is less than one in magnitude. (Source: Kunkel et al. 2013a)

Figure 4.4 shows the classification of meteorological causes of extreme precipitation in the United States. from Kunkel et al. (2012). In the east north-central and central regions that encompass the Midwest Region, they attributed a majority (78–82 percent) of extreme precipitation events to FTR and 6–8 percent of extreme precipitation events to MCSs. Based on this classification, they found statistically significant increasing trends in extratropical cyclone near center of low and FRT for the east north-central region and FRT and TC for the central region, but no statistically significant trends in MCS in either region. Note, however, that this study attributed less than 10 percent of extreme precipitation events to MCSs in the Midwest Region, which is in stark contrast to the findings of Schumacher and Johnson (2006) and Stevenson and Schumacher (2014). Notably, it is difficult to separate between frontal systems and MCSs because many MCSs are initiated along frontal boundaries, although they frequently move away as intensification occurs. Kunkel et al. (2012) remarked that "… an event was often classified as an MCS if no other category was appropriate." Hence, it is likely that extreme precipitation events attributed to MCSs are underestimated and MCS changes may have been combined with changes in FRT.

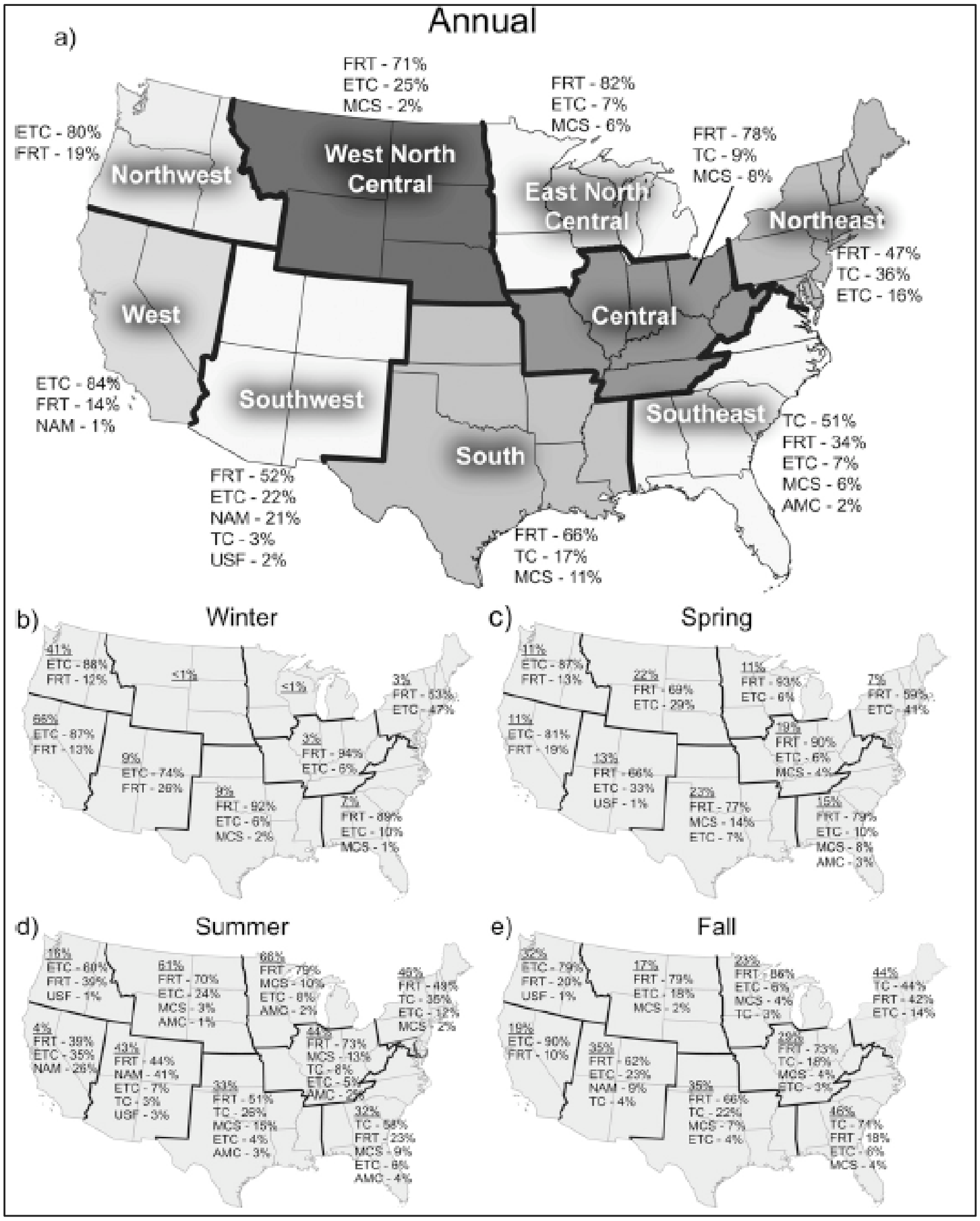

Figure 4.4. Maps of regional and seasonal contributions of major extreme event causes for (a) annual, (b) winter (December–February ([DJF]), (c) spring (March–May [MAM]), (d) summer (June–August [JJA]), and (e) autumn (September–November [SON]). In the seasonal maps, the underlined values are the percentages of total events occurring in that season; the values next to the causes are the percentages of total seasonal number of events. (Source: Kunkel et al. 2012)

The lack of satellite data in the early period limits the explicit identification of MCSs by Kunkel et al. (2012), who examined long-term trends over the 1908–2009 period. Focusing on the shorter 1979–2014 period, Feng et al. (2016) used the gridded hourly precipitation data from the North American Land Data Assimilation System (NLDAS) derived from a combination of rain gauge data and radar data and the NCDC hourly rain gauge data to investigate changes in MCSs in the central United States. Using satellite infrared brightness temperature data, they tracked MCSs using a commonly adopted satellite algorithm and developed a precipitation feature algorithm that is verified against the MCSs identified and tracked by the satellite algorithm. Applying the precipitation feature algorithm to the NLDAS data, they developed an MCS database for the 1979–2014 period and evaluated the changes in MCS characteristics over the past 35 years. They found an increasing trend in precipitation produced by MCSs in the northern Great Plains and Midwest Regions during the past 35 years (Figure 4.5).

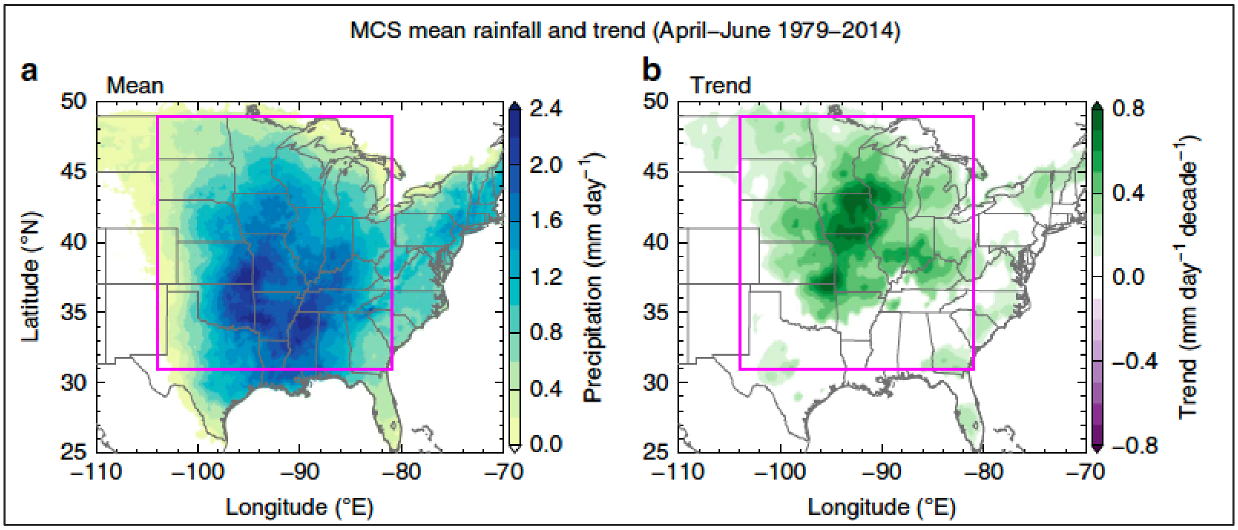

Figure 4.5. MCS (a) mean total rainfall and (b) total rainfall trend from 1979 to 2014. Total rainfall shown is the accumulated MCS rainfall during April–June divided by the total number of days (91). Only trends with statistical significance above 95 percent using a two-tailed Student's t-test are shown. Data within the magenta boxes are used to calculate the trends in Figure 4.6. (Source: Feng et al. 2016)

Separating all precipitation events into MCS and non-MCS events, Feng et al. (2016) quantified the long-term trends in MCS and non-MCS precipitation, MCS lifetime, and MCS and non-MCS precipitation frequency. They identified an increase in MCS precipitation frequency of 11 percent per decade and an increase in MCS lifetime of 4 percent per decade, which contribute to the increase in MCSs and total precipitation, despite a reduction in non-MCS precipitation. Using the NCDC hourly precipitation data and the MCS database, they also found an increasing trend of 2 to 10 percent per decade in 95th percentile exceedance frequency and an increasing trend of 1 to 2 percent per decade in 95th percentile rain rate for MCS precipitation over the Midwest Region (Figure 4.6). Compositing the large-scale circulation of MCS events, Feng et al. (2016) attributed the increase in MCS mean and extreme precipitation to the larger warming over land relative to the adjacent ocean in the past decades. This enhanced land-sea temperature gradient has resulted in an anomalous sea-level pressure gradient between the U.S. continent and the western Atlantic that promotes a stronger low-level jet transporting more moisture from the Gulf of Mexico to the Great Plains. Enhanced moisture supports more frequent and longer-lasting MCSs that increase MCS mean and extreme precipitation.

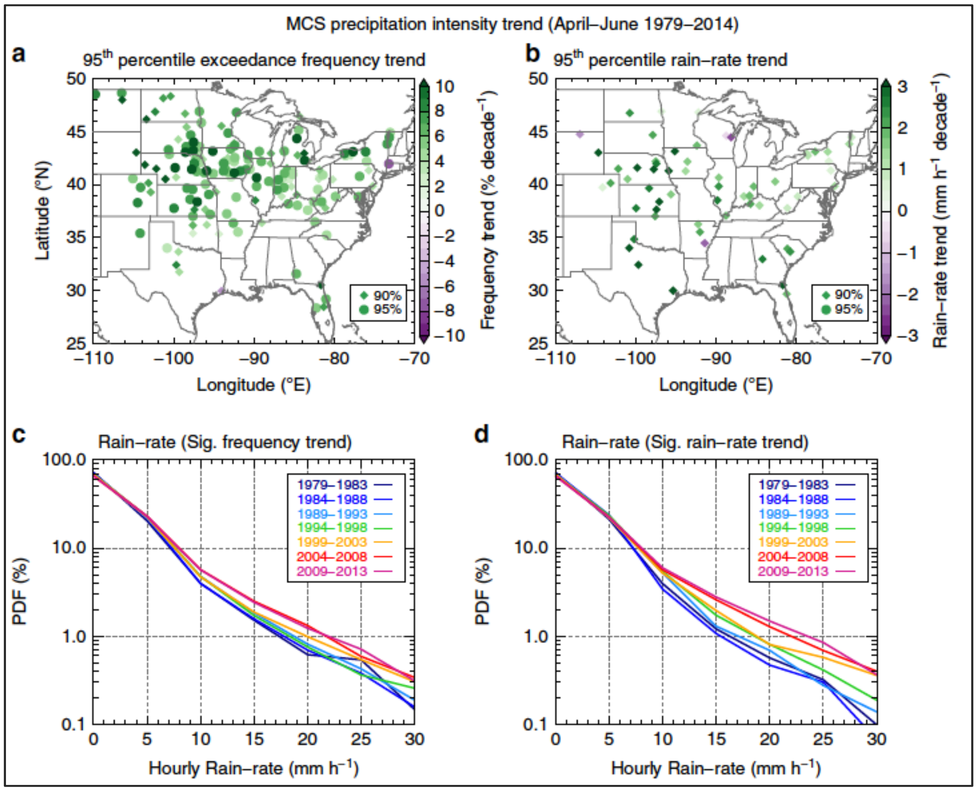

Figure 4.6. Trends in MCS (a) exceedance frequency of the 95th percentile hourly rain rate, (b) the actual 95th percentile hourly rain rate, (c) PDF of hourly rain rates from stations with a significant (Sig.) exceedance frequency trend, and (d) PDF of hourly rain rates from stations with a significant rain-rate trend. The trends are obtained using individual hourly rain gauge data (see the text for more details). Circle and diamond symbols in a and b show trends that are statistically significant at 95 percent and 90 percent with a two-tailed Student's t-test, respectively. PDFs in c and d are constructed using data from all stations that exhibited 90 percent statistically significant trends. (Source: Feng et al. 2016)

4.1.2 Projected Future Changes

- Climate models that explicitly resolved deep convection are more skillful in capturing MCSs than models that parameterized deep convection.
- MCS precipitation is projected to be more intense and covers larger areas in a warmer climate compared to the present.
- Projected changes in MCS precipitation are consistent with enhanced convective available potential energy and stronger updraft driven by a stronger low-level jet that transports more moisture into the central and Midwest Regions in a warmer climate.

Because MCSs are typically not simulated in global and regional climate models that rely on cumulus parameterizations to represent deep convection, the climate change literature does not include explicit analysis of how MCSs may change in the future in response to warming. Two exceptions are discussed in this report: 1) a study by Prein et al. (2017b) using continental-scale convection-permitting simulations produced by a regional climate model and 2) a study by Kooperman et al. (2014) using global climate simulations with a two-dimensional cloud-resolving model embedded within each global model grid cell, known as superparameterization or multiscale modeling framework (MMF). Both regional convection-permitting modeling and global modeling with MMF make use of high-resolution modeling to explicitly resolve deep convection. Analysis of these simulations shows that both approaches are able to capture MCSs much better than coarser resolution simulations that rely on deep convection parameterizations (Prein et al. 2017a; Pritchard et al. 2011; Kooperman et al. 2013).

Prein et al. (2017c) used their continental-scale convection-permitting simulations (Prein et al. 2017b) to perform analysis specifically focused on MCS changes in the simulations. Using the same precipitation object-tracking method described by Prein et al. (2017a), Prein et al. (2017c) identified MCSs in the control and PGW simulations and composited all the MCSs for the current and future climate. Figure 4.7 shows the precipitation associated with the composited MCSs for the present and future. With warmer temperature and increased moisture, the future storm composite shows more intense and larger spatial coverage of MCS precipitation compared to the present climate. Near the center of the storm, the model projected a 30 percent increase in precipitation from ~80 mm h^{-1} to over 100 mm h^{-1}. The largest percentage increase in precipitation of ~70 percent occurs at a radial distance of ~30 km from the center of the storm.

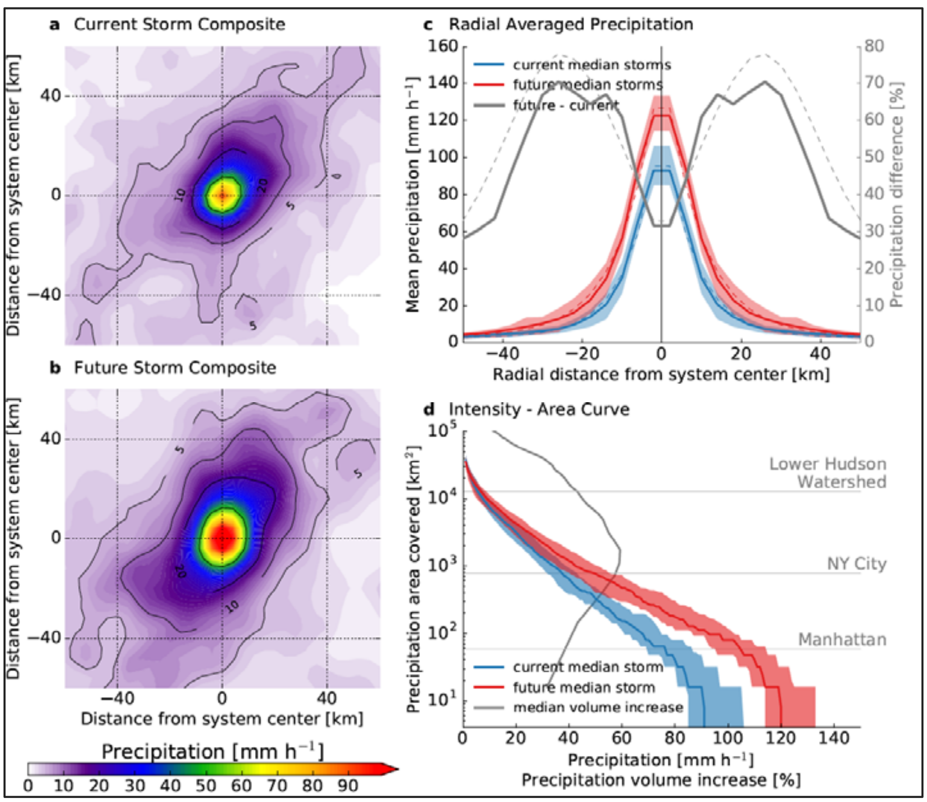

Figure 4.7. Hourly MCS precipitation averages at the time of Pmax (maximum hourly precipitation) in the current (a) and future (b) climates composited according to the location of Pmax. (c) Mean rain rates at different radial distances from the location of Pmax for current (blue) and future (red) MCSs. Median relative differences are shown in gray and correspond to the secondary y axis. Dashed lines show fitted exponential functions. (d) Intensity-area curves that show the area covered by certain precipitation rates. The gray line shows relative changes in the precipitation volume relative to spatial scales. In (c) and (d), the shaded areas correspond to the interquartile range of the 40 MCSs. (Source: Prein et al. 2017c)

The changes in MCS storm size and precipitation are associated with, on average, a 1.8 km higher cloud top that is 3.8°C colder than the storms in the current climate. These changes in the cloud macrophysics are a response to the 10°C warmer equivalent potential temperature in the boundary layer combined with a higher tropopause that increase convective available potential energy (CAPE), despite also having larger absolute values of convective inhibition (CIN) of the inflow air (Figure 4.8). The storms in the future are marked by stronger updrafts that produce more graupel and hail in the core of the MCSs above the freezing level. Melting of the frozen hydrometeors in the warm cloud layer increases the precipitation rate because raindrops fall faster than ice and snow. Prein et al. (2017b) noted that wind shear changes are small and have only minor effects on the changes in the dynamics of MCSs. The increase in CAPE and storm size with warming is consistent with previous studies of changes in severe storm environments (Trapp et al. 2007) and lightning with warming (Romps et al. 2014).

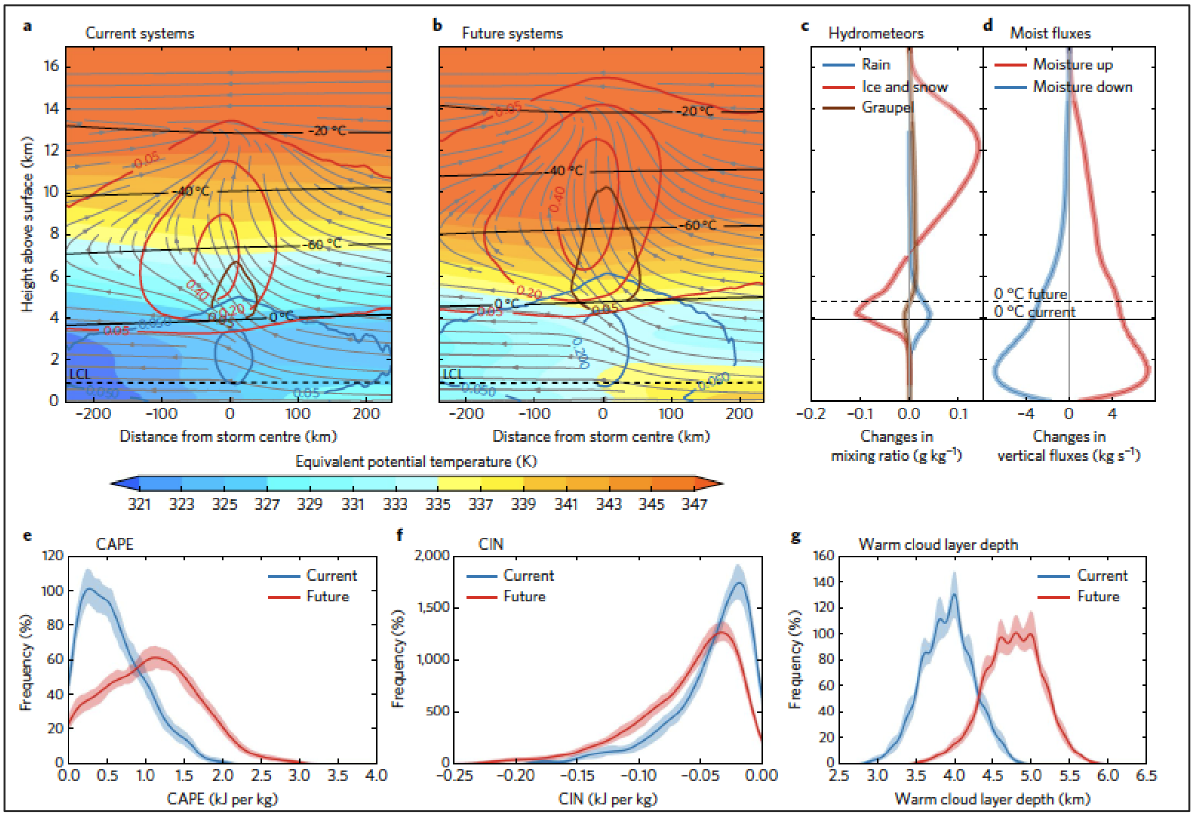

Figure 4.8. (a,b) Average cross section of the equivalent potential temperature (filled contour), hydrometeor mixing ratios (blue, brown, and red contours show rain and cloud, graupel and snow, and ice-mixing ratios, respectively), and wind field (streamlines) relative to the MCS movement for 807 current (a) and 1207 future hourly time slices of mid-Atlantic MCSs (b). Black solid lines show isothermals and the black dashed line shows the lifting condensation level (that is, the cloud base). (c,d) Average changes (future minus current) in hydrometeor mixing ratios (c) and vertical moisture flux (d) (upward/downward fluxes are shown as red/blue lines) at different heights above surface. Thick lines show significant changes (alpha is 0.01) according to 100 bootstrap samples. (e,f) PDFs of CAPE (e), CIN (f), and warm cloud layer depth (g) for current (blue) and future (red) MCSs. Shaded areas show the 1–99 percentile range of 100 bootstrap samples. Changes in CAPE and CIN are calculated in the MCS inflow region. (Source: Prein et al. 2017c)

Kooperman et al. (2014) performed simulations using the Community Atmosphere Model with superparameterization (SPCAM) for the control pre-industrial (PI) conditions and 4 × CO_2 (carbon dioxide) conditions by prescribing sea surface temperature and sea ice from a fully coupled Community Earth System Model PI simulation and a 4 × CO_2 simulation. A similar set of simulations also were performed using the Community Atmosphere Model (CAM) without MMF and driven by the same sea surface temperature and sea ice boundary conditions for the PI and 4 × CO_2 conditions. Comparing the PI and 4 x CO_2 simulations from SPCAM and CAM, Kooperman et al. (2014) found large differences between the two sets of simulations in the 99th percentile precipitation rate response to 4 × CO_2. Most notably, during the warm season, CAM simulated a reduction of 99th percentile precipitation across the central United States and over the Great Lakes, but SPCAM simulated an opposite response (i.e., an increase in 99th percentile precipitation for the same region) (Figure 4.9).

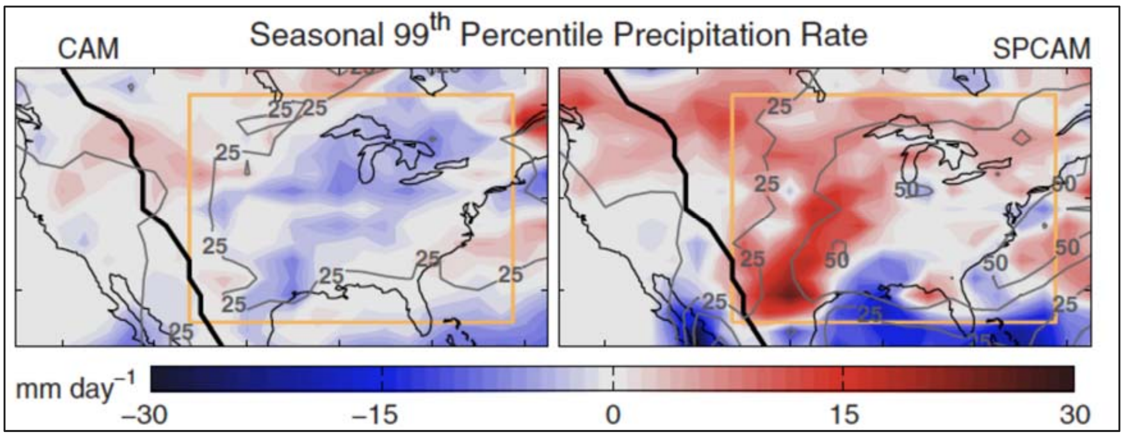

Figure 4.9. A 5-year seasonal May–August PI (contours) and the difference between 4 x CO_2 and PI (colors) 99th (PI intervals of 12.5 mm d^{-1}) percentile precipitation rates from CAM (left) and SPCAM (right) three-hourly output. The black line shows the Rocky Mountain ridgeline. (Source: Kooperman et al. 2014)

Using an MCS index, Kooperman et al. (2014) analyzed the MCSs in the CAM and SPCAM PI and 4 × CO_2 simulations. The MCS index is defined based on the longwave cloud forcing (i.e., the impact of clouds on the top-of-atmosphere longwave radiation, which is large and positive for high clouds because they emit longwave radiation at the cold temperatures of the high cloud tops, thereby reducing the outgoing longwave radiation and warming the Earth). Kooperman et al. (2014) used three criteria: the forcing has to (1) exist for a minimum number of hours and exceed a certain amplitude, (2) propagate eastward spanning at least 70 percent of the domain (the orange box in Figure 4.9), and (3) occur between 6 P.M. and 3 A.M. local time. These criteria ensure that the cloud features resemble the properties of MCSs in terms of their cloud height, diurnal timing, and propagation. Figure 4.10 shows that SPCAM captures MCS events much more prominently than CAM, as indicated by the propagating tracks shown using phase diagrams and the starting and ending locations of the MCS events in the phase space (a–d). Comparing the composite of MCSs in the PI and 4 × CO_2 SPCAM simulations (e–i), MCSs in the warmer climate have a larger spatial coverage and produce more precipitation than the PI control. These changes are consistent with the intensification of the low-level jet and anomalous moisture transport that amplify MCS activity. In contrast, the CAM simulations showed reduced rain occurring entirely during the afternoon in 4 × CO_2 relative to PI, but the strong afternoon rain in the CAM simulations is a significant modeling error; observed rainfall in the region occurs mostly in the evening and early morning.

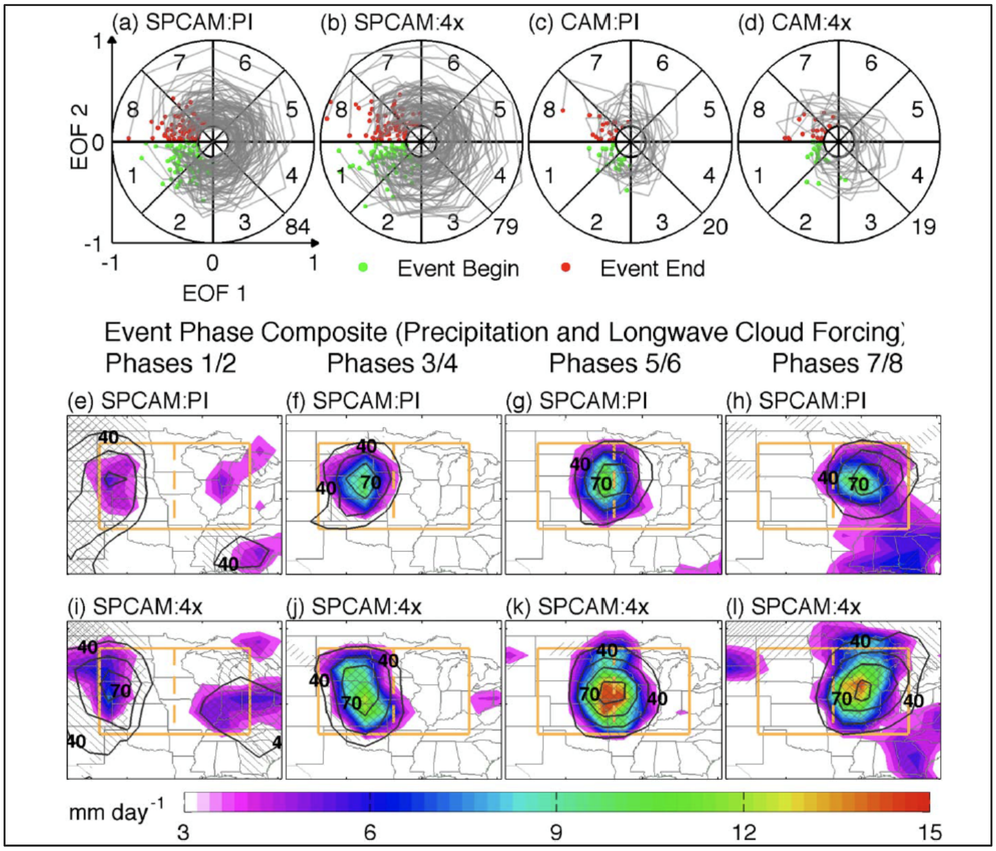

Figure 4.10. Phase diagram of empirical orthogonal function principle component time series 1 and 2 tracing MCS events for (a and b) SPCAM and (c and d) CAM for the PI (a, c) and 4 × CO_2 (b, d) simulations, and composite event phase average of precipitation (colors) and longwave cloud forcing (contours with intervals of 15 W m^{-2}) for phases (e and i) 1 and 2, (f and j) 3 and 4, (g and k) 5 and 6, and (h and l) 7 and 8 in SPCAM (e–h) PI and (i–l) 4 x CO_2 simulations. The right/45° (left/-45°) slashes indicate that precipitation (longwave cloud forcing) is significant at 95 percent confidence interval. (Source: Kooperman et al. 2014)

Overall, by using models that explicitly resolve deep convection, Prein et al. (2017b) and Kooperman et al. (2014) consistently projected increases in spatial coverage and precipitation amount and intensity produced by MCSs in a warmer climate. They attributed the changes to enhanced moisture that increases CAPE and vertical updraft. Furthermore, simulations with parameterized versus resolved deep convection projected very different changes in precipitation, demonstrating the significance of representing intense rainfall in the models. Although not explicitly investigating MCSs, Kendon et al. (2017) reviewed studies using simulations with parameterized and resolved deep convection and came to similar conclusions that resolving deep convection is important for modeling rainfall intensity and duration, short-duration rainfall extremes, and severe convective wind gusts.

4.2 Observed and Projected Changes in Severe Weather

4.2.1 Observed Changes

- In the Midwest, tornadoes occur most frequently in Illinois and Indiana between April and June by month and between 1 P.M. and 10 P.M. by time of day.
- Extreme outbreaks (i.e., outbreaks with 12 or more tornadoes that are rated F1 and greater) have increased between 1954 and 2015 and are possibly associated with the Atlantic Multidecadal Oscillation that influences the vertical wind shear.
- A spatial redistribution of tornado counts with a reduction in Tornado Alley and an increase in Dixie Alley has been noted.

The Midwest Region is within the "Tornado Alley" of the central United States where tornadoes are most frequent. Figure 4.11 shows the touchdown points and tracks for all Fujita scale (F)[1] or Enhanced Fujita scale (EF)[2] level 3, 4, and 5 tornadoes between 1950 and 2016 displayed by the Tornado Track Tool.[3]

Tornadoes of F/EF 3–5 can produce 3-sec gust wind speeds from 136 mph to over 200 mph, leading to severe damage. In the Midwest, F/EF 3–5 tornadoes occur most frequently in Illinois and Indiana (Figure 4.11) between April and June by month and between 1 P.M. and 10 P.M. (Figure 4.12), although tornadoes can occur in other months and any hours. In northern Illinois and northwest Indiana, F/EF 3–5 tornadoes make up 6.5 percent of all tornadoes (Figure 4.13).

Of the 10 deadliest documented tornado events in the United States,[4] five affected the midwestern states including the top-ranked EF-5 event on March 18, 1925, that affected Missouri, Illinois, and Indiana; the third-ranked EF-4 event on May 27, 1896, that affected Missouri and Illinois; the seventh-ranked EF-5 event on May 22, 2011, that affected Missouri; the ninth-ranked EF-5 event on June 12, 1899, that affected Wisconsin; and the tenth-ranked EF-5 event on June 8, 1953, that affected Michigan.

Long-term trends in tornadoes are not uniform across the United States and depend on the metrics. As noted in the second-year report, Tippett et al. (2016) found an increasing frequency of U.S. tornado outbreaks, defined as sequences of six or more tornadoes rated F1 and greater on the Fujita scale or rated EF1 and greater on the Enhanced Fujita scale. Using the Generalized Pareto approach to model the extreme outbreaks (i.e., outbreaks with 12 or more tornadoes that are rated F1 and greater), they found a higher increasing rate for outbreaks that are more extreme. When conducting a study to determine what environmental factors contribute to the tornado outbreak trend, Tippett et al. (2016) found that the observed increased frequency of tornado outbreaks could be part of the multidecadal variability associated with the Atlantic Multidecadal Oscillation (AMO) that influences vertical wind shear, rather than as a consequence of warming that increases CAPE. In addition to the increasing number of tornadoes per outbreak, another study by Tippett (2012) identified an increasing extent of the season for tornado activity, and an earlier calendar-day start of the season of high activity.

[1] The Fujita scale categorizes the intensity of a tornado based on damage to structures, vegetation, etc.
[2] The Enhanced Fujita scale categorizes the intensity of a tornado based on based on its wind speed and related damage to structures, vegetation, etc.
[3] http://mrcc.isws.illinois.edu/gismaps/cntytorn.htm# accessible from the Midwestern Regional Climate Center.
[4] https://www.ncdc.noaa.gov/climate-information/extreme-events/us-tornado-climatology/deadliest

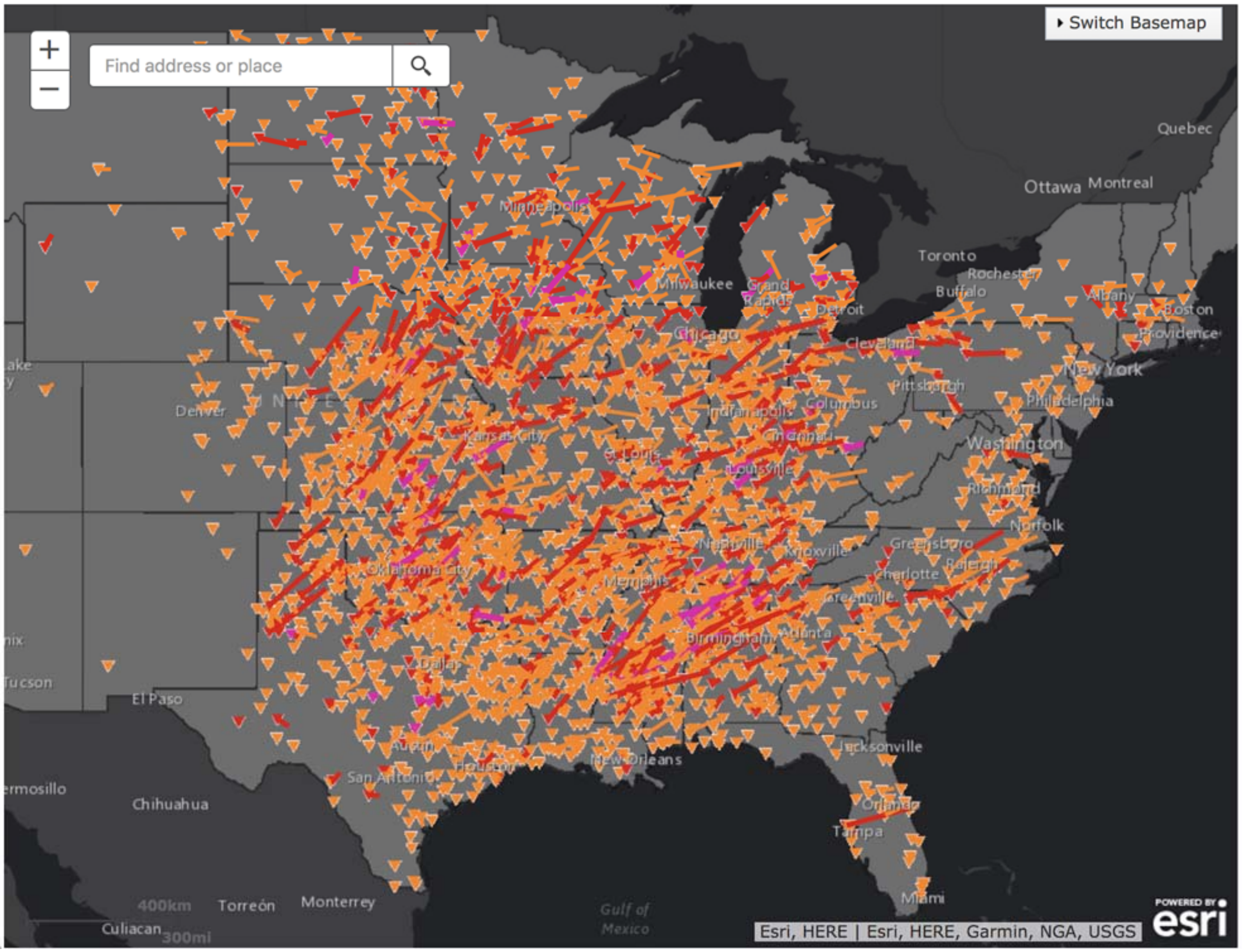

Figure 4.11. Touchdown points and tracks of all tornadoes of Fujita or Enhanced Fujita (F/EF) scale 3, 4, and 5 between 1950 and 2016 over the eastern United States from the Tornado Track Tool (Source: http://mrcc.isws.illinois.edu/gismaps/cntytorn.htm#).

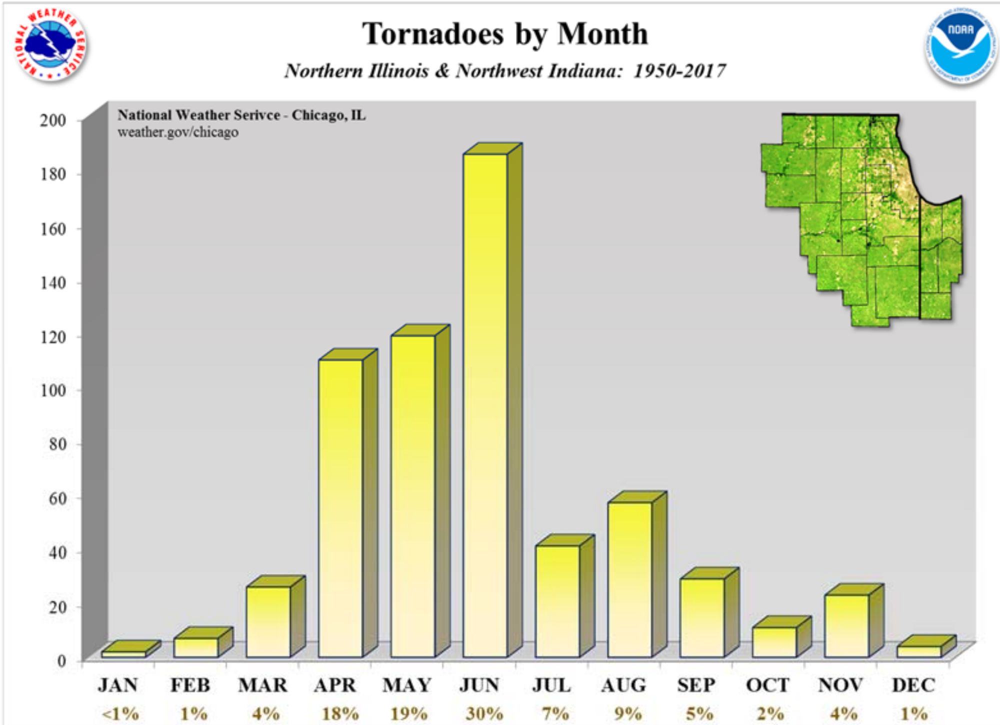

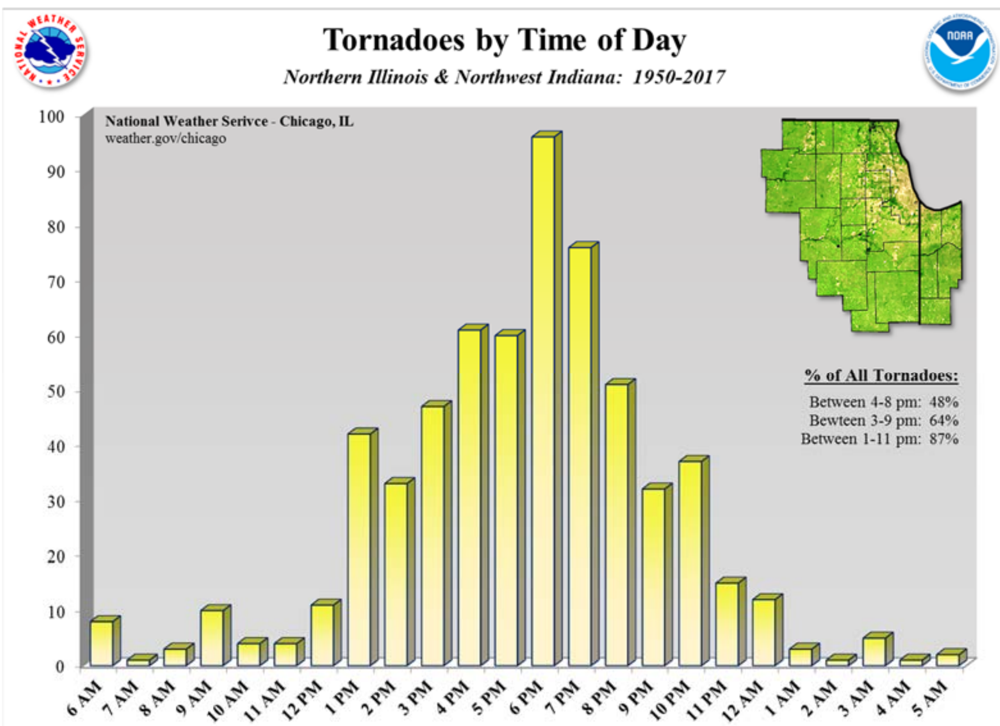

Figure 4.12. Tornado counts by month (upper) and by time of day (lower) for northern Illinois and northwest Indiana between 1950 and 2017. (Source: https://www.weather.gov/lot/tornadoclimatology)

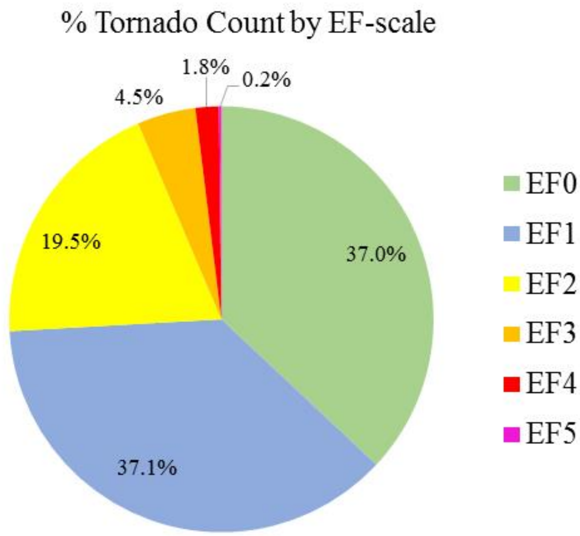

Figure 4.13. Percentage of tornado count by EF-scale for northern Illinois and northwest Indiana between 1950 and 2014. (Source: https://www.weather.gov/lot/tornadoclimatology)

Also discussed in the second-year report, Agee et al. (2016) analyzed tornado counts and days in the past 50 years and noted a spatial redistribution of the tornado counts and days for (E)F1to E(F5) tornado events on the Enhanced Fujita scale comparing the later and earlier 25-year periods. More specifically, they found significant decreases in annual tornado activity in the Tornado Alley centered over Oklahoma and the emergence of a new maximum center of tornado activity centered over Tennessee or "Dixie Alley." As shown in Figure 4.14, reductions in tornado activity are also notable in Illinois and Indiana for the more intense tornadoes (F/EF 2 and above). However, Agee et al. (2016) did not analyze and attribute the observed tornado changes to changes in the environment so it is not clear if the changes have a meteorological origin, because other changes in the environment such as wildfire aerosols (e.g., Saide et al. 2015) and urbanization (e.g., Niyogi et al. 2011) have also been linked to changes in severe storm initialization, intensity, and spatial distribution. More research is needed to document and understand different aspects of changes in tornado activities in the United States in general and the Midwest Region in particular.

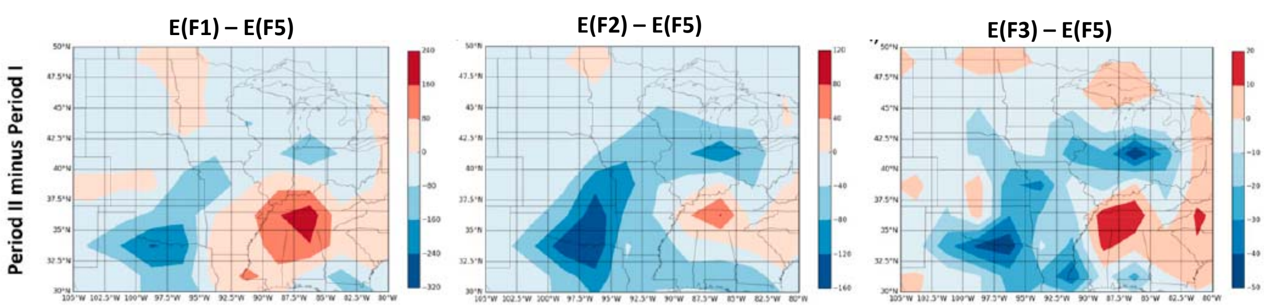

Figure 4.14. Tornado counts (left) (E)F1–(E)F5, (center) (E)F2–(E)F5, and (right) (E)F3–(E)F5 for the difference between Period II (1984–2013) and Period I (1954–1983). (Source: Agee et al. 2016)

4.2.2 Projected Changes

- Driven mainly by increases in moisture in a warmer climate, a severe convective thunderstorm environment is projected to increase during the warm season east of the Rocky Mountains, including the Midwest Region, despite differences in regional patterns from different models.
- Simulations that explicitly resolve severe thunderstorms suggest that the environmental proxy based on CAPE and vertical wind shear can efficiently explain 81 percent of the storms in the simulations.
- Changes in storm initiation due to changes in convective inhibition and frequency of extratropical cyclones could reduce the probability of severe storms conditional on favorable large-scale environment.

As discussed in the Year 1 and Year 2 reports, projecting changes in severe weather is generally addressed through analysis of severe weather environments, because climate models are not capable of simulating severe weather explicitly due to their coarse resolution. Two quantitative measures of local thunderstorm environments are CAPE and vertical wind shear. CAPE measures the vertically integrated buoyant energy available to the storm or the theoretical maximum updraft speed that supports large hailstones and rain rates, leading to more intense downdrafts and outflow winds (Trapp et al. 2007). Vertical wind shear, defined as the magnitude of the vector difference between the horizontal wind at 6 km above the ground and the wind at the lowest model level, promotes storm-scale rotation around a vertical axis and helps sustain a deep updraft in the presence of a precipitation-driven downdraft and outflow. Based on the Clausius-Clapeyron relationship, a warmer climate increases moisture in the atmosphere, which increases CAPE. On the other hand, a weaker meridional temperature gradient due to polar amplification generally reduces the vertical wind shear through the thermal wind relationship.

Previous studies projecting future changes in severe weather analyzed the changes in CAPE and vertical wind shear simulated by GCMs to determine the changes in severe weather environments favorable for severe storms. Figure 4.15 summarizes the results from a few such studies using global and regional climate models (Trapp et al. 2007; Diffenbaugh et al. 2013; Seely and Romps 2015).

These studies compared the changes in severe weather environments for spring and summer comparing the last two to three decades of the 21st century with that of the 20th century over the United States. Despite differences in the spatial patterns and magnitudes of change, increases in CAPE in the future due to warming generally outweigh the reductions in vertical wind shear, resulting in more favorable severe storm environments in the warm season, particularly in coastal areas where increases in moisture, hence CAPE, are projected to be more significant. Seely and Romps (2015) noted that the future severity of thunderstorms is closely tied to low-level humidification so achieving some level of consensus among climate model projections of low-level humidification processes is important for projecting changes in severe thunderstorms. They also noted several important sources of uncertainty:

- Equal weight is assigned to CAPE and vertical wind shear in determining “favorable” severe weather environment, although there is some observational evidence that wind shear may be more important than CAPE in determining the severity of storms.
- It is not clear whether the probability of severe thunderstorms depends mainly on whether storm environments exceed a certain threshold or by how much the environments exceed the threshold.
- The fraction of severe-thunderstorm environments developing into actual storms is assumed to be constant in time but this is not well justified.

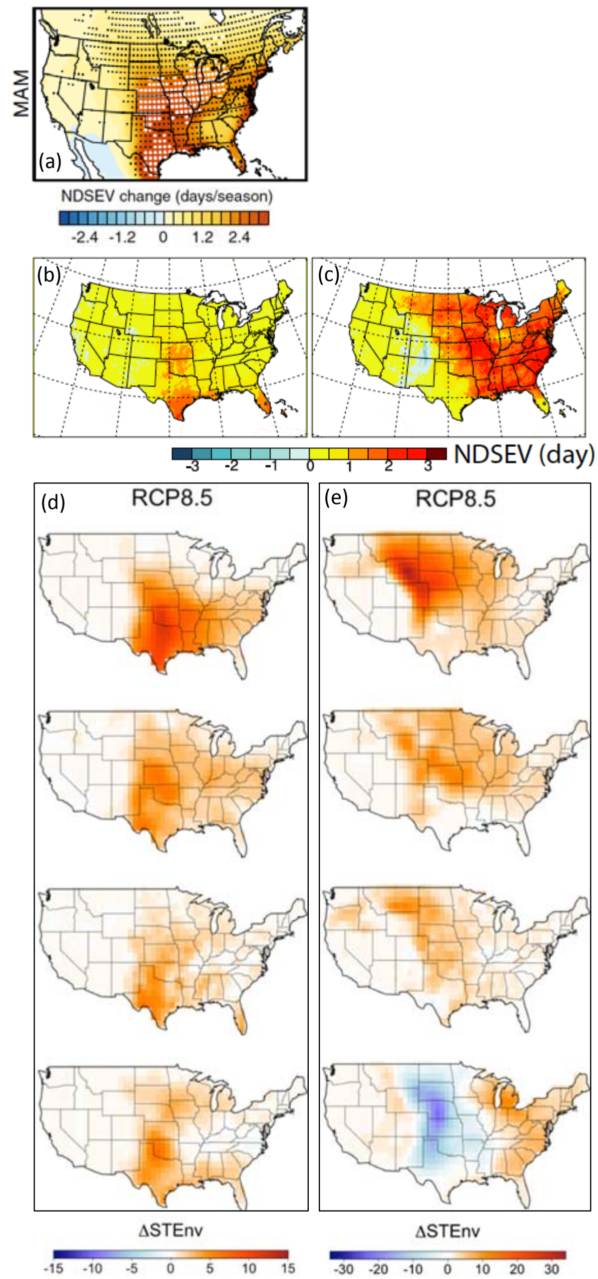

Figure 4.15. Summary of projections of changes in severe weather environments for spring (left: March-April-May) and summer (right: June-July-August) reported in three studies. (a) Changes in number of days with spring severe-thunderstorm environment (NDSEV) comparing 2070–2099 with 1970–1999 from CMIP5 models in the RCP8.5 scenario (Diffenbaugh et al. 2013). Black (gray) dots identify areas where the ensemble signal exceeds one (two) standard deviations of the ensemble noise. (b,c) Difference in severe-thunderstorm environment days (NDSEV) for spring (left) and summer (right) comparing 1962–1989 and 2072–2099 based on the A2 high-emission scenario based on downscaled regional climate simulations at 25 km grid spacing driven by a GCM (Trapp et al. 2007). (d,e) Changes (percent) in severe-thunderstorm environment (ΔSTEnv) during spring (left) and summer (right) from four GCMs in the CMIP5 archive for RCP8.5 comparing 1996–2005 with 2079–2088. (Source: Seely and Romps 2015)

Hence, there is a need for research to find was to reduce these sources of uncertainty for projecting future changes in severe storms.

One approach to addressing the above uncertainties is to use high-resolution models that explicitly simulate convective storms to evaluate how well environmental factors such as CAPE and vertical wind shear explain the variance of severe storms. Gensini and Mote (2015) performed simulations using the Weather Research and Forecasting (WRF) model at 4 km grid spacing over the United States east of the Rocky Mountains and using boundary conditions from a single GCM for the present (1980–1990) and future (2080–2090). WRF simulations were performed only for three months (March–May) of each year. A model-based proxy is used to identify tornadoes in the simulations. The proxy is based on hourly thresholds of updraft helicity and simulated composite radar reflectivity factor as described by Kain et al. (2008). The radar reflectivity factor value is determined by the drop-size distribution of precipitation, which is proportional to the radar reflectivity if the precipitation particles are spheres small compared with the radar wavelength. Specifically, a synthetic hazardous convective weather (HCW) event occurs when an hourly WRF grid cell contains updraft helicity values ≥60 $m^2 s^{-2}$ juxtaposed with radar reflectivity factor values ≥40 dBZ. These synthetic HCW events, aggregated to a 50 km grid and summed over the historical (1980–1990) period, are evaluated against observed HCW reports after bias correction is applied, as in Gensini and Mote (2014).

Figure 4.16 shows the difference between the future and present synthetic severe weather reports derived from the WRF simulations. It shows statistically significant changes in the central and eastern United States, including the southern boundary of the midwestern region. More locations in the central and eastern United States are marked by increases than decreases. Also, importantly, Gensini and Mote (2015) found that the product of CAPE and vertical wind shear exceeding 20,000 explains 81 percent of the variability of the HCW reports over the historical and future periods (Figure 4.17), lending some support to the finding that environmental analysis using severe weather environments defined by the product of CAPE and vertical wind shear is an efficient predictor of HCW occurrence across the regions east of the Rocky Mountains.

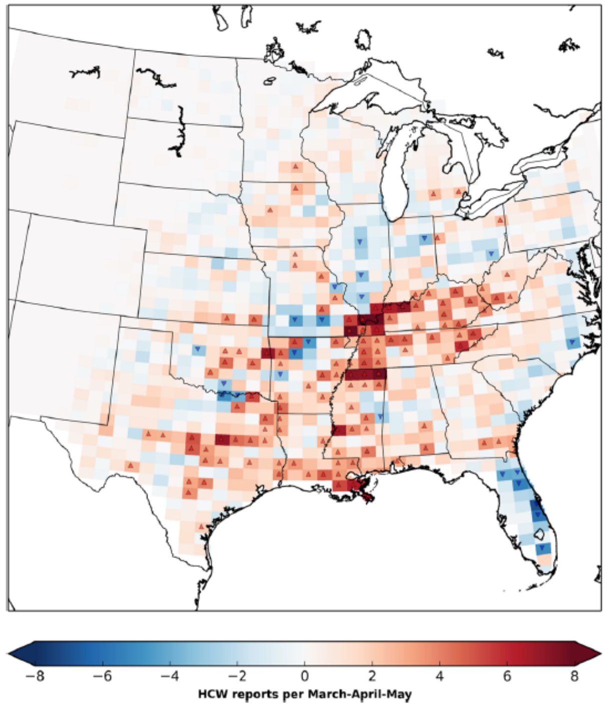

Figure 4.16. Average difference between 2080–2090 and 1980–1990 modeled severe weather reports. Red (blue) grid cells indicate a positive (negative) change in the average number of modeled reports per season. Triangles indicate the statistical significance at the 95 percent confidence level. (Source: Gensini and Mote 2015)

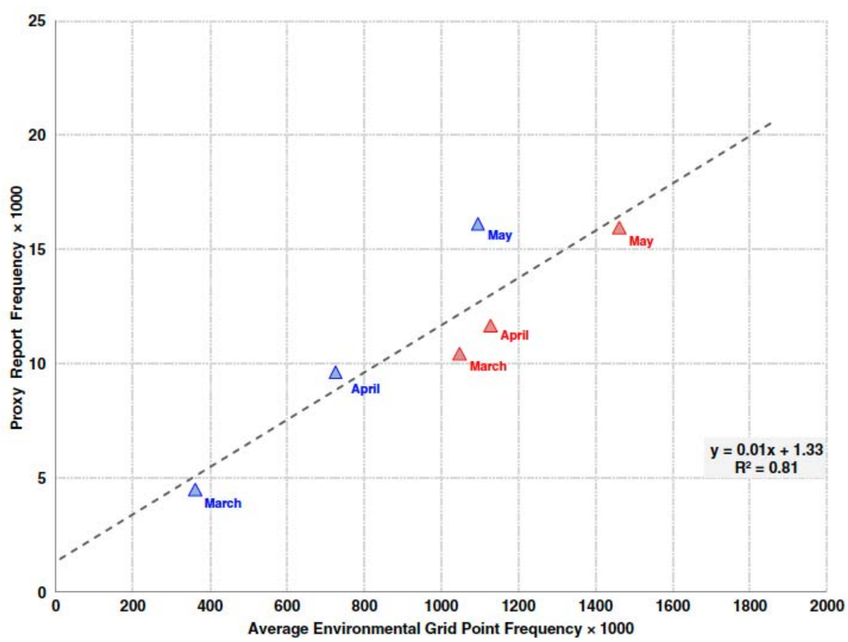

Figure 4.17. Linear correlation between average grid point frequency with CAPE × ~0–6 km vertical wind shear ≥20,000 and average synthetic report frequency by month. Blue triangles correspond to the period 1980–1990, while red triangles correspond to the period 2080–2090. The least-squares regression equation and coefficient of determination are displayed in the gray box. (Source: Gensini and Mote 2015)

Using the WRF model, Hoogewind et al. (2017) also dynamically downscaled simulations from a single GCM (the Geophysical Fluid Dynamics Laboratory [GFDL] GCM) to investigate future changes in HCW. Although their approach is similar to Gensini and Mote (2015) using WRF at 4 km grid spacing, the approach used by Hoogewind et al. (2017) includes several notable differences in that (1) their simulations cover 30 years for the present (1971–2000) and 30 years for the future (2017–2100), while Gensini and Mote (2015) only covered March–May for 10 years of the present and 10 years of the future; (2) their model domain covers the entire contiguous United States, while Gensini and Mote (2015) only performed simulations over the eastern United States; and (3) Hoogewind et al. (2017) reinitialized their simulations daily to keep the WRF large-scale circulation closer to the GCM large-scale circulation, while the simulations of Gensini and Mote (2015) are continuous simulations for March to May initialized only at the beginning of March each year.

Using upward vertical velocity exceeding 22 m s^{-1} as a proxy for HCW occurrence (or synthetic HCW), Hoogewind et al. (2017) compared the changes (i.e., future minus present) simulated by the WRF model with the changes in NDSEVs determined from the GCM simulations. They found an increase in both the frequency and intensity of HCW from the WRF simulations, particularly during spring and summer. Results from both the WRF simulations and GFDL simulations showed a lengthening of the HCW season by more than a month. However, NDSEV determined from the GFDL simulations show larger percentage change in the future relative to the present compared to the percentage change in HCW days determined from the WRF simulations (Figure 4.18). Furthermore, although Hoogewind et al. (2017) found that the NDSEV explains over 80 percent of the variance of synthetic HCW, which is consistent with the finding of Gensini and Mote (2015), the slope of the linear regression line of the synthetic HCW days against NDSEV differs between the historical and future periods (Figure 4.19). The spatial patterns of NDSEV changes from GFDL and synthetic HCW changes from WRF are shown in Figure 4.20 for each season. The changes in NDSEV are larger than the changes in HCW in all seasons, but the differences are particularly large in spring and summer.

To understand the differences between the changes in NDSEV and the synthetic HCW, Hoogewind et al. (2017) calculated the environmental bias (ratio of NDSEV to HCW) and the conditional probability of a synthetic HCW day given the occurrence of NDSEV. They found that the environmental bias increases throughout the entire annual cycle, but most significantly over the months of May to September, suggesting that NDSEV overestimates synthetic HCW during the warm season. For the conditional probability, they found that the occurrence of NDSEV in the future is more likely to produce synthetic HCW in December-January-February, March-April-May, and September-October-November, but the opposite is true during June-July-August. For a large corridor of the central United States, the conditional probability of a synthetic HCW day given NDSEV decreases significantly. This suggests that processes (CIN and parcel lifting) that promote or inhibit initiation of convection may be modulated in the future climate. Hoogewind et al. (2017) noted that the changes in CIN alone are unlikely to be the primary contributor to the changes in storm initiation. Noting that Chang (2013) found a 24.5 percent reduction in extratropical cyclone frequency in June-July-August in the GFDL-projected future climate relative to the historical climate, Hoogewind et al. (2017) suggested that reduced forced ascent due to the reduced extratropical cyclone frequency may play an important role in reducing the likelihood of synthetic HCW days conditional on the occurrence of NDSEV. These findings drive the need to further investigate how the realization of HCW from favorable NDSEV may change in the future due to changes in storm initiation.

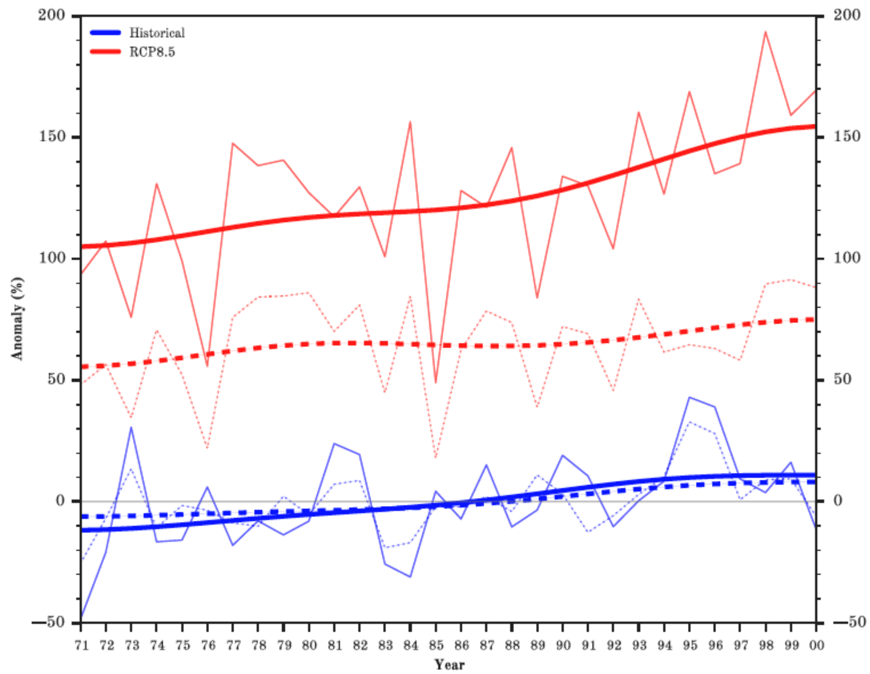

Figure 4.18. Time series of annual regional anomaly over land points in the contiguous United States east of 105 °W in NDSEV from GFDL (solid line) and synthetic HCW days from WRF (dashed line). The historical (1971–2000) values are shown in blue and the future RCP8.5 (2071–2100) values are shown in red. The thick lines represent data smoothed with a Gaussian filter (σ = 5 years). (Source: Hoogewind et al. 2017)

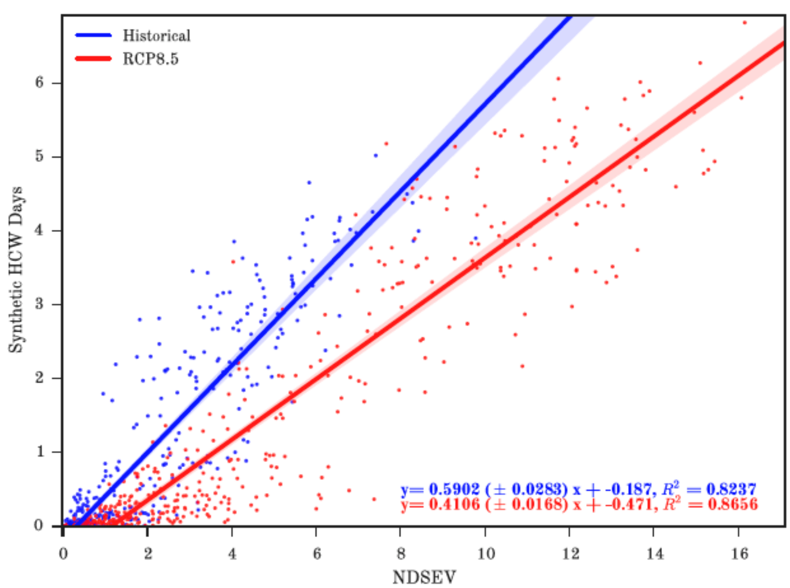

Figure 4.19. Linear association between regional monthly mean NDSEV from GFDL and synthetic HCW days from WRF for all land points over the contiguous United States east of 105°W. Monthly mean values were computed for each of the 30 years of the historical (1971–2000; blue) and future (RCP8.5, 2071–2100; red) periods, and bootstrapped 95 percent confidence intervals are shaded. The least square regression equation (and 95 percent confidence intervals for the slope) and coefficients of determination are displayed in the bottom-right corner. (Source: Hoogewind et al. 2017)

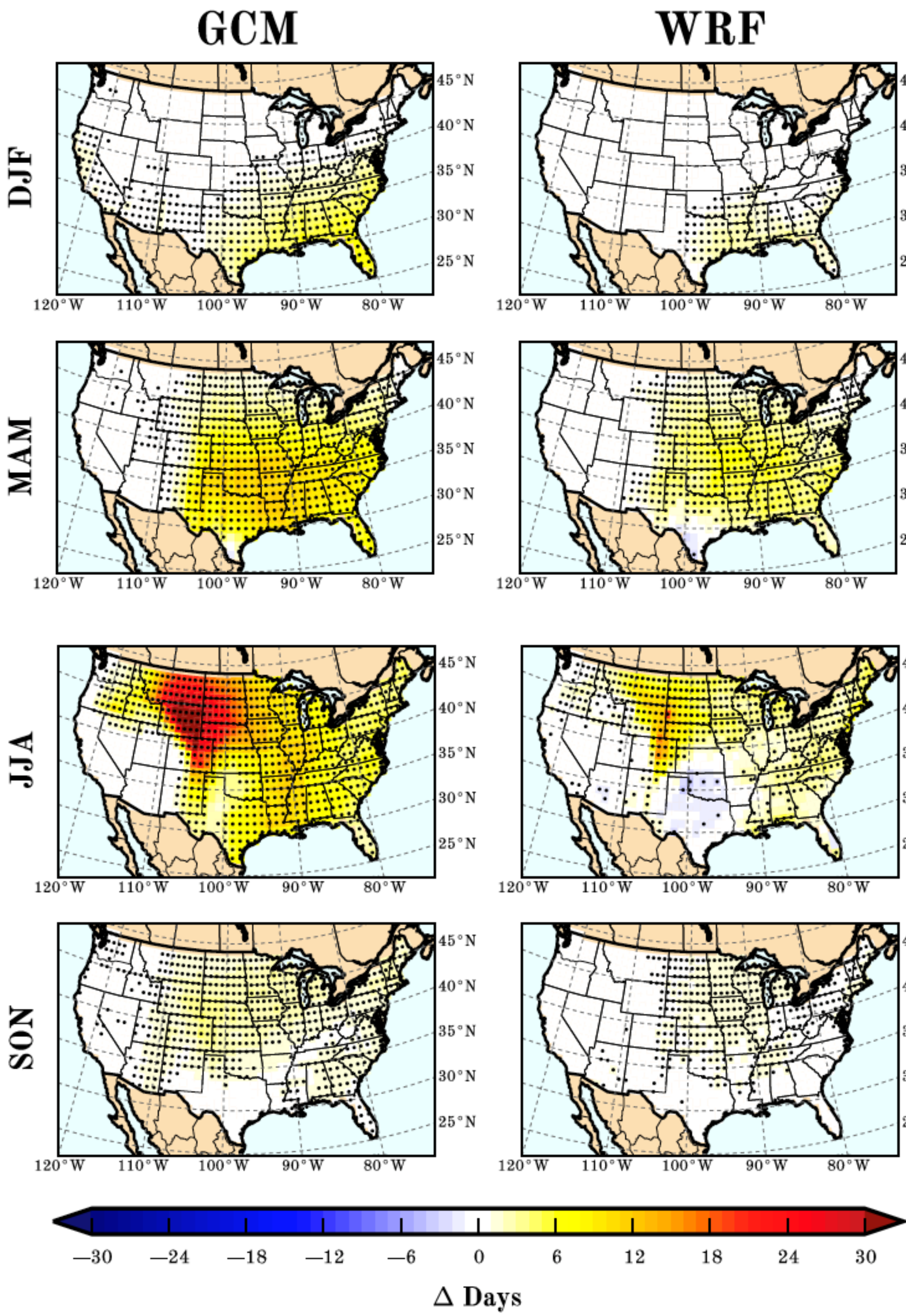

Figure 4.20. Mean seasonal response in NDSEV from GFDL GCM, and synthetic HCW days from WRF in the future (2071–2100) relative to the historical (1971–2000) period. Stippling indicates where the distribution of seasonal means between the two periods are statistically significantly different from one another at the 95 percent confidence level using the Mann-Whitney U test. (Source: Hoogewind et al. 2017)

5.0 Great Lakes Water Levels

This chapter summarizes current conditions, observed trends, and projected changes in Great Lakes water levels. Information from NCA3 (Pryor et al. 2014), NCA4 CSSR (USGCRP 2017), and peer-reviewed literature is the basis for the summary. Note that assessment of observed trends and projected changes is challenging because of uncertainties in estimating components of the overall water budget of the lakes.

The Great Lakes drainage basin is approximately 295,000 mi^2 in area, 59 percent of which lies in the United States and 41 percent in Canada (Figure 5.1). Approximately 52 percent of the basin is forested, 35 percent is agricultural, 7 percent is urban or suburban, and 6 percent is used for other purposes. Lake Superior is located at the upstream end of the basin and discharges into Lake Huron via St. Mary's River (USGS 2007, see Figure 5.1). Lake Michigan and Lake Huron are hydraulically connected at the Straits of Mackinac and therefore are usually treated as a single water body in hydrologic analyses. Lake Huron is connected to Lake Erie via the St. Clair River, Lake St. Clair, and the Detroit River. Lake Erie discharges into the Niagara River that further connects to Lake Ontario. Lake Ontario discharges to the Saint Lawrence River.

Figure 5.1. Drainage area contributing to the Great Lakes. (Source: USGS 2007)

5.1 Observation and Characterization of Great Lakes

Great Lakes water levels are monitored and analyzed by binational cooperative efforts of U.S. and Canadian federal agencies (see Figure 5.2). National Oceanic and Atmospheric Administration National Ocean Service Center for Operational Oceanographic Products and Services water-level monitoring stations (blue circles in Figure 5.2) on the Great Lakes record a 3-minute average water level every 6 minutes. The water-level data are archived as hourly, daily, and monthly averages. The Canadian Department of Fisheries and Oceans Hydrographic Service also operates water-level stations (green circles in Figure 5.2).

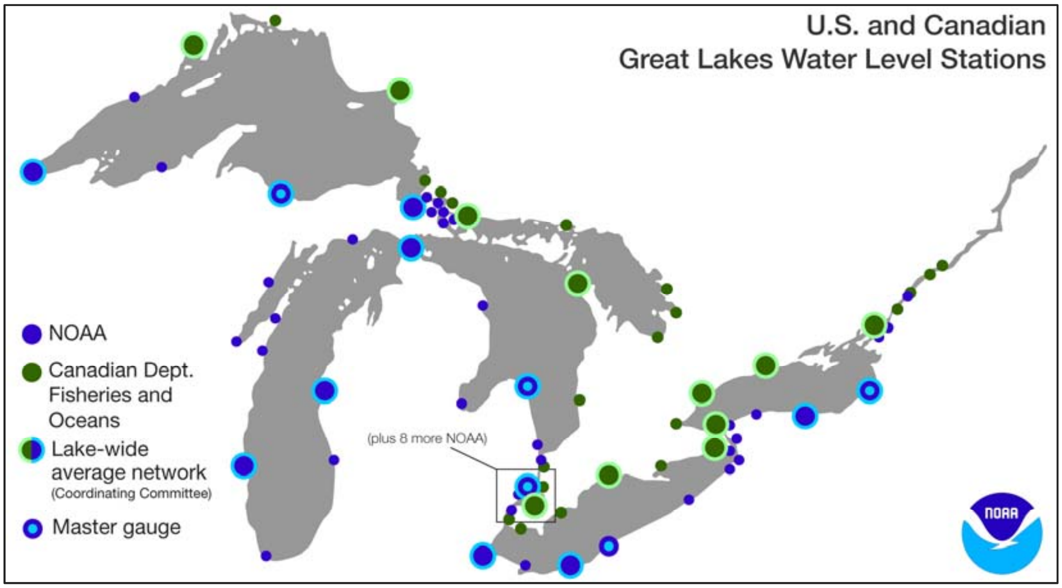

Figure 5.2. Great Lakes water-level monitoring network. (Source: NOAA Great Lakes Environmental Research Laboratory, https://www.glerl.noaa.gov/data/wlevels/#monitoringNetwork)

The Coordinating Committee on Great Lakes Basic Hydraulic and Hydrologic Data is an international advisory group of U.S. and Canadian government agencies established in 1953. The committee is currently supported by the U.S. Army Corps of Engineers (USACE), Environment and Climate Change Canada, NOAA, Fisheries and Oceans Canada, USGS, and Natural Resources Canada.[1] The committee has four subcommittees—Hydrology, Hydraulics, Vertical Control-Water Levels, and Regulation and Routing Model.[2] The committee coordinates on (1) methods for measuring discharges, computing streamflows, measuring water levels; updating the International Great Lakes Datum; maintaining databases of binational discharge measurements, managing diversions in the Great Lakes System, and measuring lake water levels and (2) various hydrologic, hydraulic, regulation, routing, and gravity models. The committee is also responsible for coordinating compilation, use, and dissemination of hydrology, hydraulics, and vertical control data for the Great Lakes. The first vertical datum for the Great Lakes, the International Great Lakes Datum (IGLD), was established in 1955 and was subsequently updated in 1985. The IGLD is periodically updated to account for variable motion of the Earth's crust including that from glacial isostatic adjustment. The committee is currently in the process of developing the next IGLD, which is expected to be completed in 2020 (CCGL 2017).

[1] The composition of the committee is described at http://www.greatlakescc.org/wp36/home/about_us/composition-and-approach/.

[2] More details about the subcommittees and their activities are described at http://www.greatlakescc.org/wp36/home/subcommittees/.

The Great Lakes Commission (GLC) was established in 1955 by the five-state (Illinois, Indiana, Michigan, Minnesota, and Wisconsin) compact that was consented to by the U.S. Congress in 1968 (Public Law 90-419, July 24, 1968). New York, Ohio, and Pennsylvania joined the compact later. Canadian provinces Ontario and Quebec are associate members. The GLC works with its member U.S. states and associate-member Canadian provinces "…to address issues of common concern, develop shared solutions and collectively advance an agenda to protect and enhance the region's economic prosperity and environmental health" (GLC 2019). GLC has a strategic plan that lays out its statement of visions, mission goals, objectives, and strategic actions (GLC 2017).

The NOAA Great Lakes Environmental Research Laboratory (GLERL) has been developing and maintaining the GLERL monthly hydrometeorological database (GLM-HMD), a historical time series of North American Great Lakes basin-scale monthly hydrometeorological data (Hunter et al. 2015). Most of these data either represent or are directly related to the major components of the Great Lakes water budget. GLM-HMD data directly related to water budget includes overlake evaporation, overland and overlake precipitation, runoff, and both overlake and overland air temperature. GLM-HMD also includes wind speed, cloud cover, and other hydrometeorological variables indirectly related to the major components of the Great Lakes water budget. We note that ice-cover data and hydrometeorological variables at higher spatiotemporal resolutions are distributed separately through the NOAA Great Lakes Ice Atlas (Assel 2003; Wang et al. 2012) and the Great Lakes Coastal Forecasting System (Schwab and Bedford, 1994), respectively.

5.2 Observed Changes in Great Lakes Water Levels

- After remaining at or below long-term mean levels in the first decade of the 21st century, mean annual water levels for Lakes Superior and Michigan-Huron experienced a record 2-year rate of rise between January 2013 and December 2014.
- Mean annual water levels in the Great Lakes Superior and Michigan-Huron show a periodicity of approximately 13 years. Warm-season (April–September) changes in water levels are correlated with (1) large-scale atmospheric patterns (500 hPa geopotential height) extending across the north Pacific Ocean through northern North America and into the north Atlantic Ocean and (2) sea-level pressure anomalies near the Gulf of Alaska and southeastern coast of the United States.
- Reconstructed prehistorical lake levels show a quasi-periodic behavior in Lake Michigan-Huron water level of 160±40 years with a shorter 32 ±6 year fluctuation superimposed on it.

Figure 5.3 shows the monthly Great Lakes water levels from 1918 through 2018. Mean annual water levels for the five Great Lakes are shown in Figure 5.4.

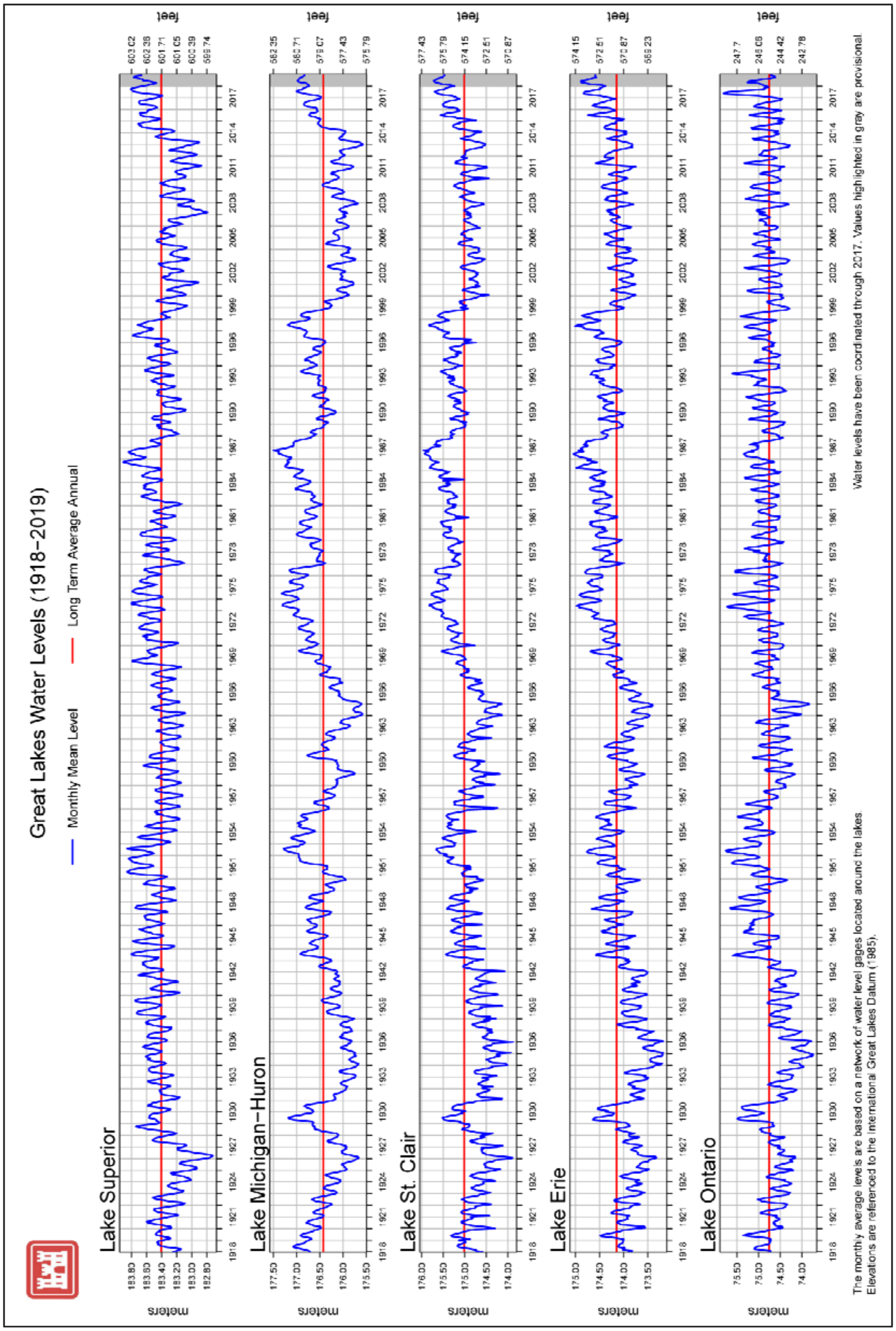

Figure 5.3. Great Lakes monthly average water level from 1918 through 2018. (Source: USACE Detroit District, available at http://lre-wm.usace.army.mil/ForecastData/GLBasinConditions/LTA-GLWL-Graph.pdf.)

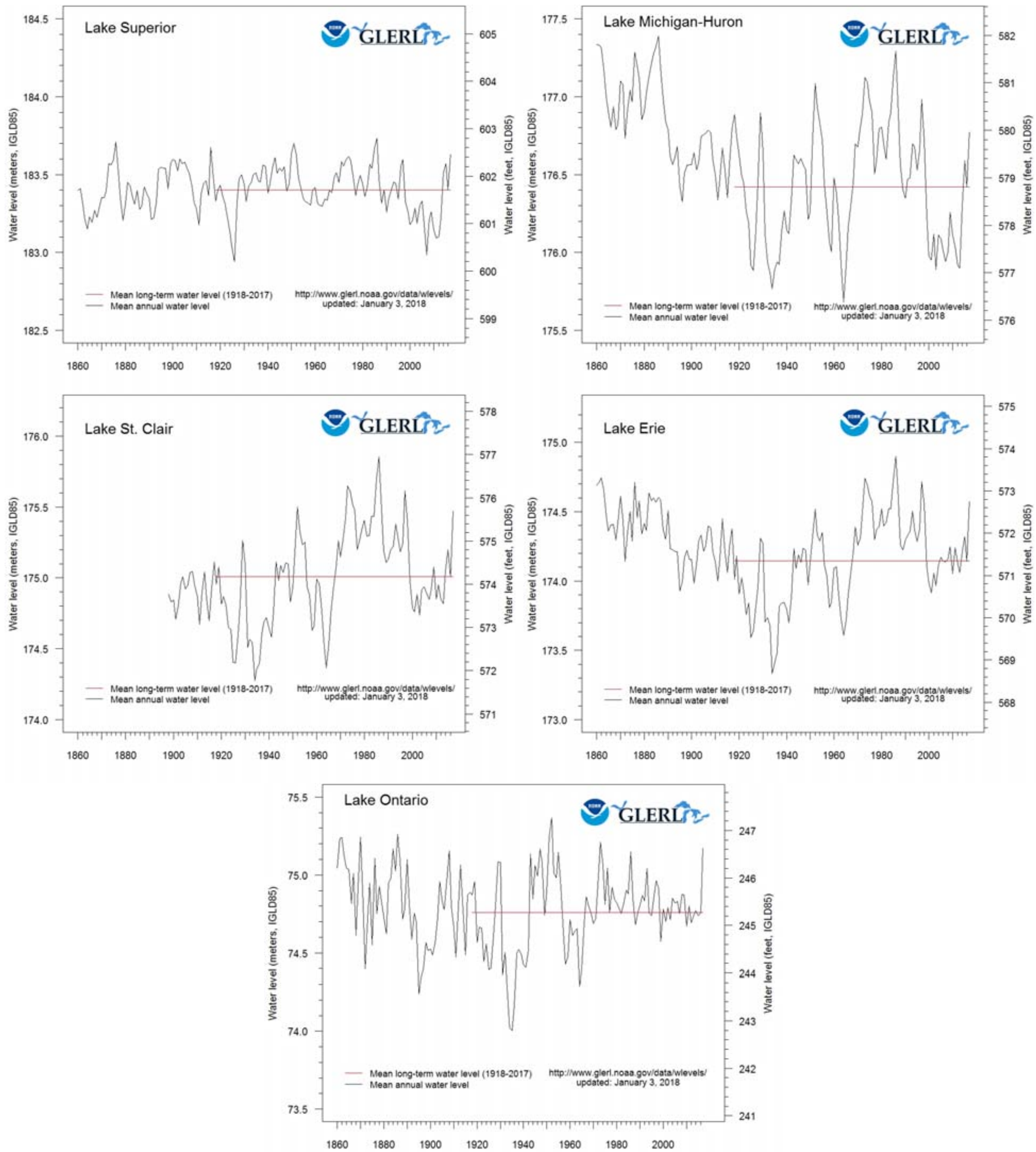

Figure 5.4. Mean annual water levels in the Great Lakes through 2017. (Source: NOAA Great Lakes Environmental Research Laboratory)

Water levels in Lakes Superior and Michigan-Huron seem to be recovering in the last few years after remaining at or below long-term mean levels in the first decade of the 21st century. Gronewold and Stow (2014) described the approximately 15-year period when water levels were persistently below average. The large decrease in water levels and rise in surface water temperatures in Lakes Superior and Minchigan-Huron during the late-1990s coincided with strong 1997–1998 El Niño events. The higher surface water temperatures persisted during the first decade of the 21st century, which combined with annual precipitation showing minimal changes, resulted in increased overlake evaporation, decreased ice cover, and sustained low-water levels. Gronewold et al. (2016) described the record rate-of-rise of water levels in Lakes Superior and Michigan-Huron during the 2-year period between January 2013 and December 2014. This water level rise coincided with an anomalous meridional upper air flow (the polar vortex), below-average regional air temperatures, and extensive ice covers. Gronewold et al. (2016) concluded that the Lake Superior water level rise in 2013 was caused by increased spring runoff and overlake precipitation, and the continued water level rise in 2014 was a response to reduced overlake evaporation. The 2013 water level rise in Lake Michigan-Huron resulted from increased spring runoff and persistent overlake precipitation. However, the water level rise in Lake Michigan-Huron in 2014 was caused by a rare combination of reduced evaporation, increased runoff and precipitation, and high inflow rates from Lake Superior via the St. Marys River.

Official 6-month Great Lakes water level forecasts are produced each month through a binational partnership between USACE Detroit District and Environment and Climate Change Canada. Figure 5.5 shows the USACE forecast published in February 2018 (USACE 2018). These monthly average water forecasts are based on computer simulations along with more than 100 years of data on past weather and water level conditions. The GLERL develops many of the simulation models used in the monthly water level forecasts. In addition, GLERL publishes a bi-annual (spring and fall) fact sheet that provides a discussion of observed and forecasted trends in Great Lakes water levels (e.g., NOAA GLERL 2018a). The USACE 6-month forecast for February 2018 stated that water levels in Lakes Superior, Michigan-Huron, and Erie would follow their typical seasonal trend at above-average levels (NOAA GLERL 2018b).

5.2.1 Hydrologic Characterization of the Great Lakes

5.2.1.1 Great Lakes Commission's "Toward a Water Resources Management Decision Support System for the Great Lakes Report"

In 2003, the GLC published a report containing research and findings for the *Toward a Water Resources Management Decision Support System for the Great Lakes* project (GLC 2003). Chapter 2 of that report contains a description of the hydrology of the Great Lakes System, which is complex and highly dynamic. Lake Superior basin lies at the upstream end with Lake Superior discharging into Lake Huron via the St. Marys River (Figure 5.1). Lake Michigan and Lake Huron are hydraulically connected via the Strait of Mackinac and Lake Huron is connected to Lake Erie by the St. Clair River, Lake St. Clair, and the Detroit River. Further downstream in the system, Lake Erie discharges to Lake Ontario via the Niagara River, Welland Canal, and the DeCew Falls power plant tailrace. Lake Ontario, the most downstream Great Lake, discharges to the Saint Lawrence River. Various control structures, locks, dams, hydroelectric facilities, canals, and diversion exist in the Great Lakes System.

The Great Lakes basin has highly variable climate due to its large extent and the effects of the lakes themselves on nearshore temperature and precipitation (GLC 2003). Mean January temperatures vary from -2°F (-19°C) in the north to 28°F (-2°C) in the south. Mean July temperatures range from 64°F (18°C) in the north to 74°F (2°C) in the south. Precipitation is relatively uniform across the year but shows variability from the west to the east; mean annual precipitation ranges from 28 in. (71 cm) north of Lake Superior in the west to 52 in. (132 cm) east of Lake Ontario. Snowfall varies greatly from 20 in. (51 cm) in the south to 140 in. (355 cm) in the downwind areas of Lakes Superior and Ontario, and can exceed 200 in. (508 cm) locally. In late fall and winter, low-pressure systems traveling northeast bring cold air over the much warmer Great Lakes waters, resulting in very high lake evaporation rates and subsequent local, lake-effect precipitation (NOAA 2019, Laird and Kristovich 2002, Liu and Moore 2004). The water balance components of the Great Lakes was subsequently described by USGS (USGS 2005).

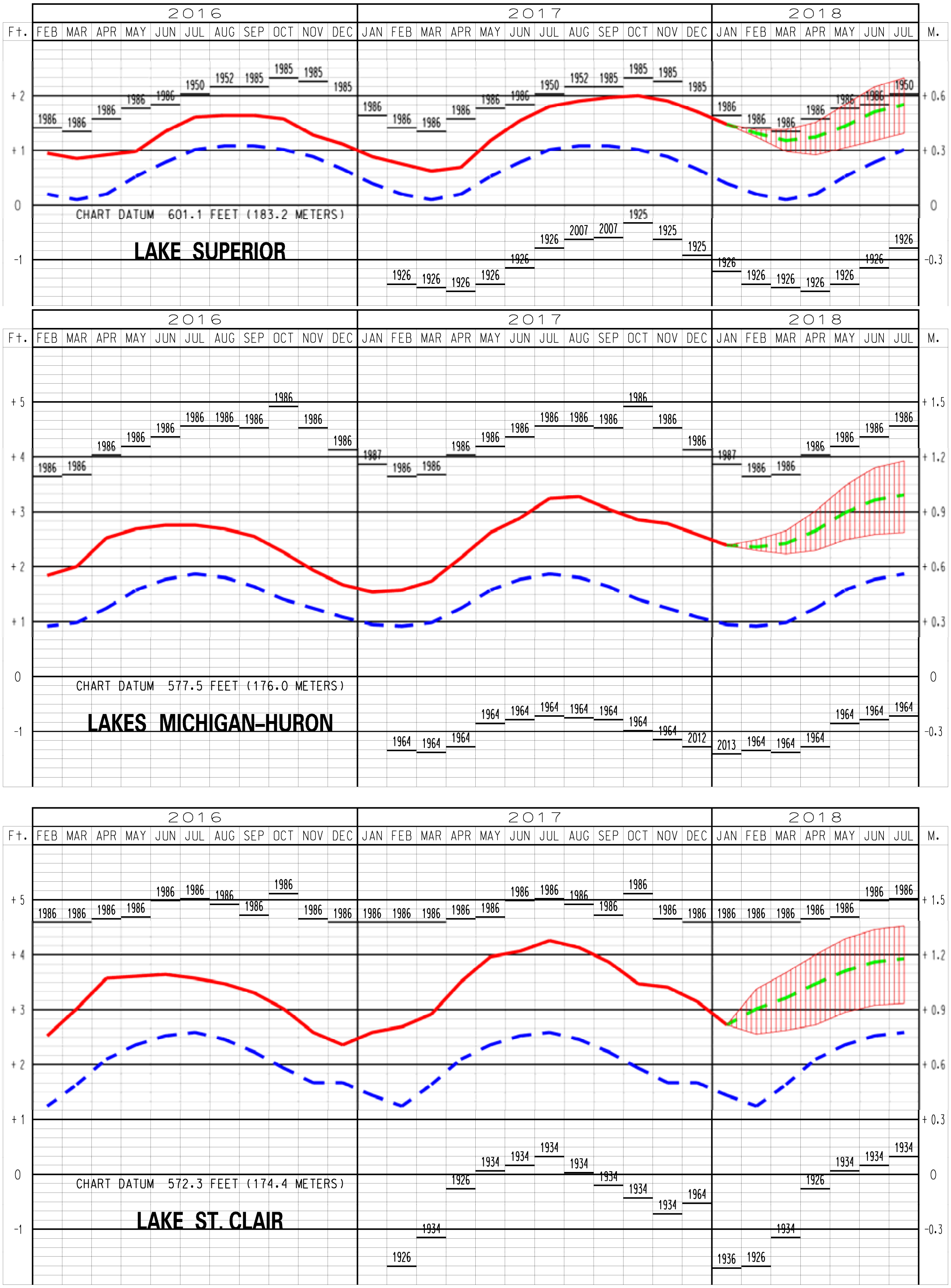

Figure 5.5. USACE Detroit District's Great Lakes water-level forecasts for February 2018

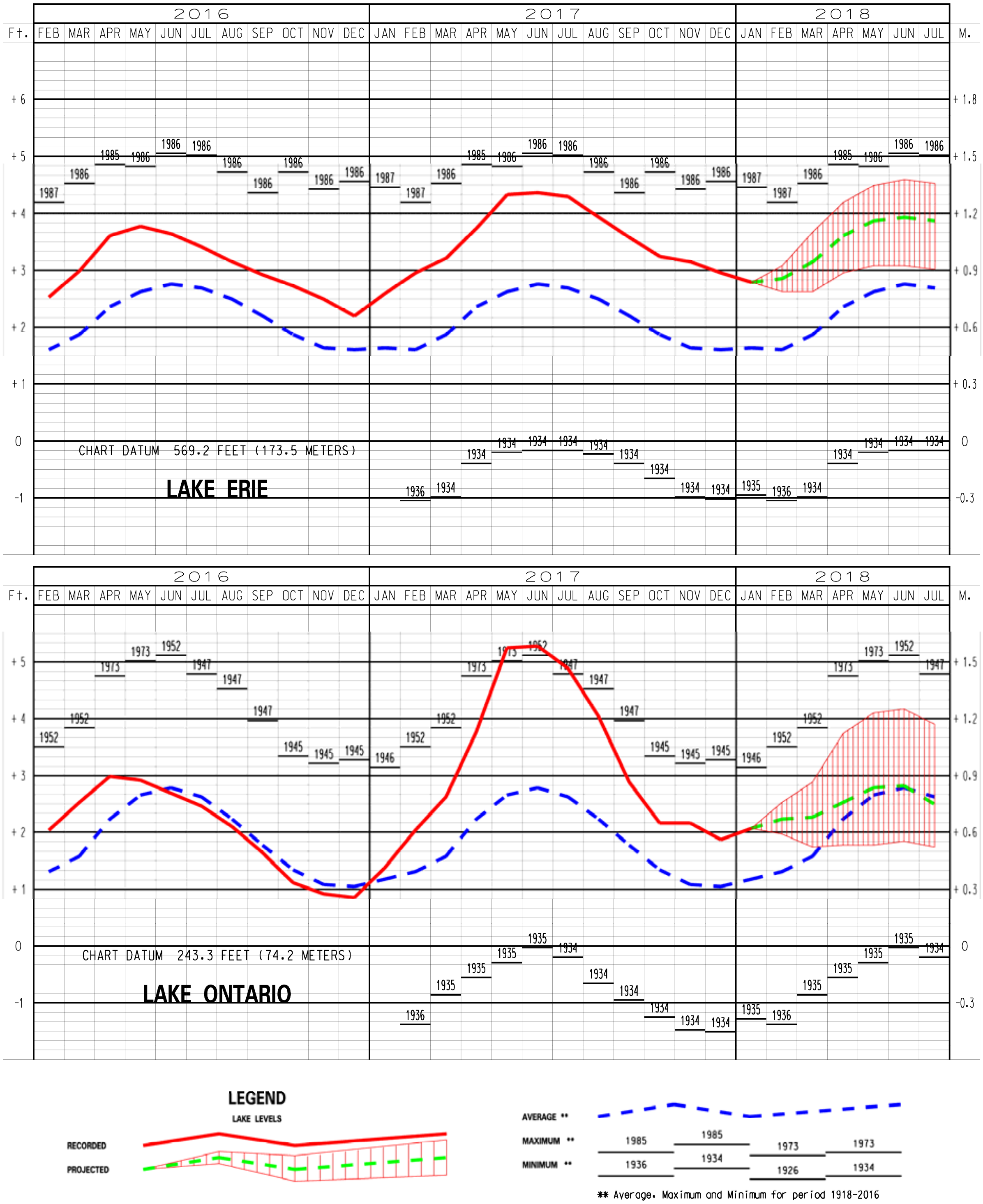

Figure 5.5 (cont.). USACE Detroit District’s Great Lakes water-level forecasts for February 2018

The water levels in the Great Lakes are affected by their storage capacities, isostatic rebound, overlake precipitation, runoff from their drainage basins, evaporation from the lake surfaces, inflow from upstream lakes, outflow through outlet channels to downstream lakes, operating policies of control structures, and diversions (GLC 2003). Seasonal variations of the lake water levels reflect the annual hydrologic cycle with net basin supply[1] (NBS) being higher in spring and early summer and lower during the rest of the year. The lakes also exhibit short-term (durations of less than an hour to several days) water level fluctuations in response to set-up or set-down caused by winds or barometric pressure differences; these short-term changes in water levels can temporarily influence outflows from the lakes. During winter, flow in outlet channels can be influenced by ice formation, particularly in St. Clair and Detroit Rivers. In the Niagara and Saint Lawrence Rivers, ice booms help stabilize ice cover. Water levels in the Great Lakes are affected by isostatic rebound, the gradual rising of the Earth's crust from removal of the weight of glaciers that covered the region during the last ice age. The rate of isostatic rebound is variable throughout the region.

5.2.1.2 Great Lakes Water Balance and Reconstructed Water Levels

The USGS Scientific Investigations Report 2004-5100 described the water balance components of the Great Lakes (USGS 2005). USGS included overlake precipitation, runoff, inflowing groundwater seepage, inflowing diversions, and inflow from connecting channels as components of inflow into the lakes. Evaporation, outflow through connecting channels, outbound diversions, and consumptive use comprise components of outflow from the lakes. Connecting channels are rivers that flow between the lakes and eventually to the Atlantic Ocean. Using the compiled data sources in USGS Water Resources Investigations Report 2002-4296 and NOAA Technical Report TM-083 and analyses conducted as part of the Water Resources Management Decision Support System for the Great Lakes, USGS described the water balance components for the Great Lakes (Figure 5.6).

USGS also identified potential sources of uncertainties in each component of water balance of the Great Lakes (USGS 2005). Average uncertainties in monthly estimates of individual components ranged from 1.5 to 45 percent. The uncertainties were described in the context of estimating NBSs, which is conceptually described as the net quantity of water entering a lake. USGS estimated uncertainties associated with using two methods—the component method and the residual method—to quantify NBSs for the lakes. They concluded that the residual method produced NBS estimates with the least uncertainty for Lake Superior and Lake Michigan-Huron whereas the component method produced NBSs with least uncertainty for Lake Erie and Lake Ontario. USGS identified four gaps related to reliable estimation of Great Lakes' water balance: (1) lack of overlake weather monitoring that leads to inaccuracies in overlake precipitation and evaporation estimation, (2) need for improvements in wintertime streamflow measurements in connecting channels, (3) need for improvements in ungauged basin runoff, and (4) need for improvements in interbasin diversions accounting to better inform their impacts on water balance.

[1] Net basin supply is defined (IUGLSB 2012) as the net amount of water inflow into a lake resulting from precipitation falling on the lake, runoff from surrounding drainage into the lake, and evaporation loss from the lake. It does not include inflow from an upstream lake or inflow or outflow from diversions. NBS formulation is based on the water balance of a lake over a specified time period.

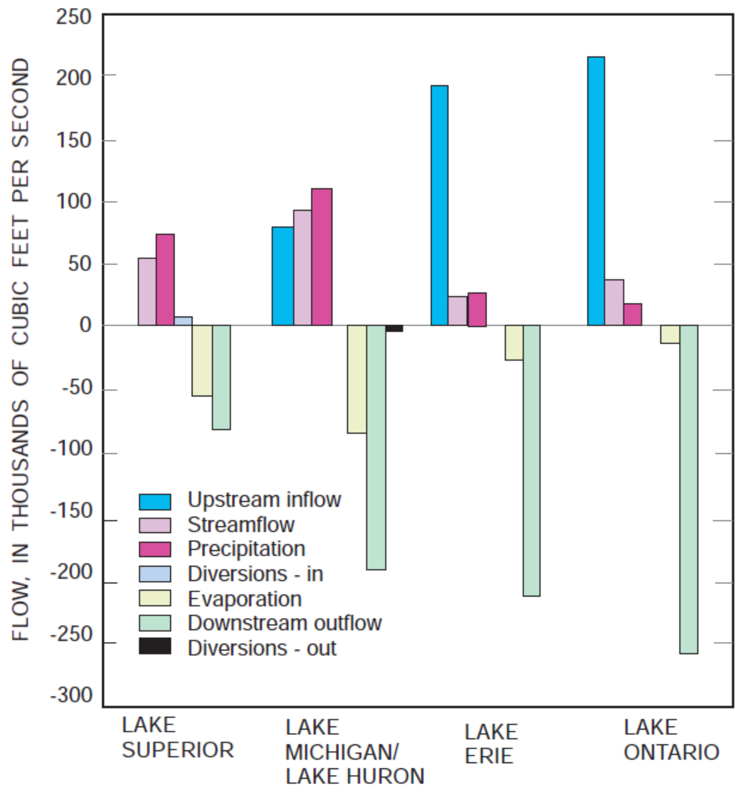

Figure 5.6. Water balance components of the Great Lakes as described by the USGS Scientific Information Report 2004-5100 (USGS 2005).

USGS Circular 1311 (USGS 2007) stated that groundwater inflow and consumptive uses are a very small portion of the total flows for the Great Lakes (Figure 5.6). Streamflow comprises a large protion of each lake's inflow (47 percent for Lake Michigan-Huron to 68 percent for Lake Ontario) and varies across the lakes depending on their respective contributing areas. Precipitation comprises the other large portion of inflow to the lakes. Connecting channel flows and evaporation comprise large portions of outflows from the lakes whereas diversions are only a small portion. The USGS Circular presented reconstructed (i.e., pre-historical) water levels of Lake Michigan-Huron (Figure 5.7). Pre-historical water levels were inferred from coastal features and associated sedimentary deposits. These features included wave-cut terraces, mainland-attached beaches, barrier beaches, spits, dunes, and deltas. Deposits examined included riverine, palustrine, and lacustrine sediments. Based on the reconstructed water levels for Lake Michigan-Huron, USGS concluded that three major high water level phases occurred on the lake—from 2300 to 3300, from 1100 to 2000, and from 0 to 800 years ago (from 1950). USGS estimated a quasi-periodic behavior in Lake Michigan-Huron water level of 160 ±40 years with a shorter 32 ±6 year fluctuation superimposed on it.

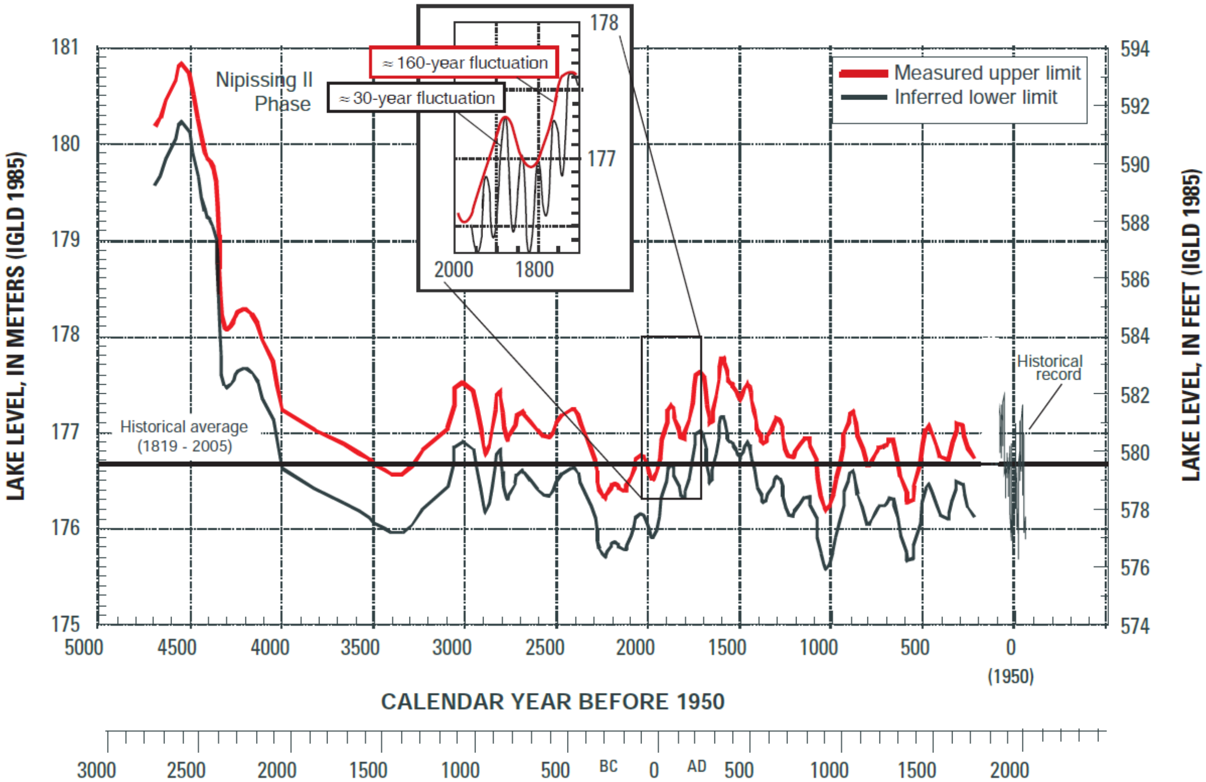

Figure 5.7. Pre-historical water levels for Lakes Michigan-Huron. The red line represents water levels interpreted from beach-ridge studies and the black line represents an inferred lower limit using the range of historical measurements. (Source: USGS 2007)

5.2.1.3 Great Lakes Water Supply Forecasting Project

Gronewold et al. (2017) described the development of a new version of a suite of hydrologic and hydraulic models that are used to forecast Niagara and Saint Lawrence River flows over both short (hours to days) and longer (multiple months to years) durations. The processes that influence the flow system in the Great Lakes were generally divided into two categories: (1) meteorological and hydrologic processes (overlake precipitation, overlake evaporation, and tributary runoff) that control water supply within each lake's basin and (2) hydraulic conditions and regulation that control the flow through the connecting channels (St. Marys, St. Clair, Detroit, Niagara, and Saint Lawrence Rivers). The set of models used in the forecasting system encompasses the whole spatial domain of the Great Lakes basin and explicitly address the two categories of processes.

Meteorological and Hydrologic Process Models

Two sets of meteorological forcings are used in the forecasting system. The first set consists of 1950–2010 historical sequences of air temperature (minimum, average, and maximum), precipitation, wind speed, cloud cover, and dew point temperature. The second set consists of meteorological forcings derived from CMIP5. Gronewold et al. (2017) noted that the conventional way of using alternative historical meteorological sequences to generate seasonal forecasts essentially assumes a stationary climate. The CMIP5 sequences are used to overcome this limitation. The publicly available CMIP5 model output data usually do not include dew point temperature and cloud cover. Dew point temperatures were calculated using CMIP5 simulations of surface pressure and specific humidity. The hydrologic models were modified to use solar radiation (available in CMIP5 simulation) instead of cloud cover. Figure 5.8 shows how CMIP5 meteorological forcings are used in the water supply forecasting.

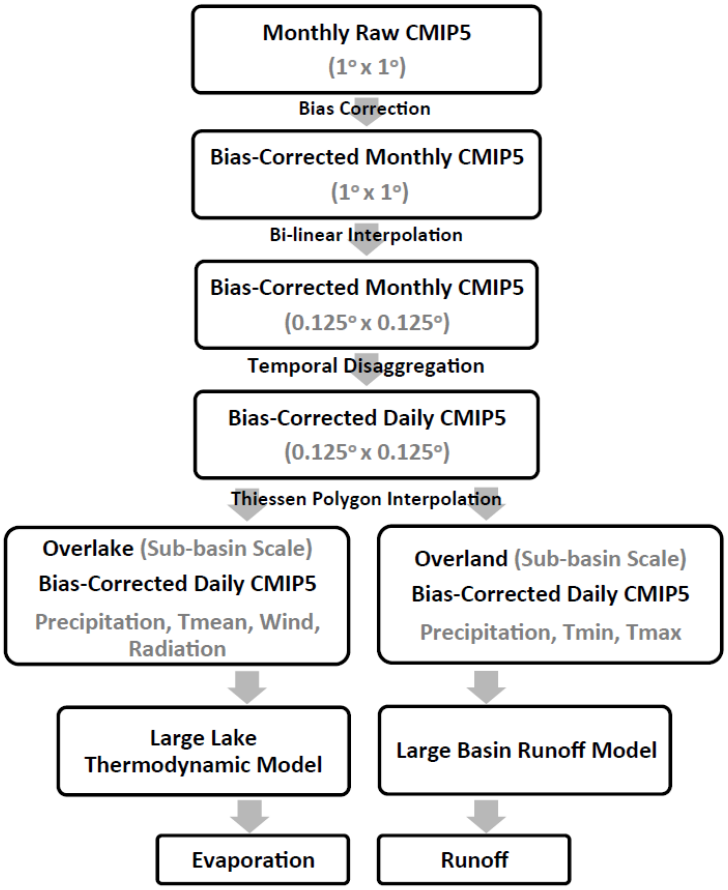

Figure 5.8. Bias correction and spatial and temporal disaggregation of CMIP5 meteorological forcings for use in the Great Lakes water supply forecasting. (Source: Gronewold et al. 2017)

Two models are used to simulate hydrology of the lakes' basins: (1) the large basin runoff model (LBRM) simulates the tributary inflow into each lake and (2) the large lake thermodynamic model (LLTM) simulates the overlake evaporation. The LBRM is a conceptual, lumped-parameter rainfall-runoff model that simulates daily, subbasin-scale lateral inflows into the lakes (Croley II 1983, Fry et al. 2014). Figure 5.9 shows the subbasins used by the LBRM.

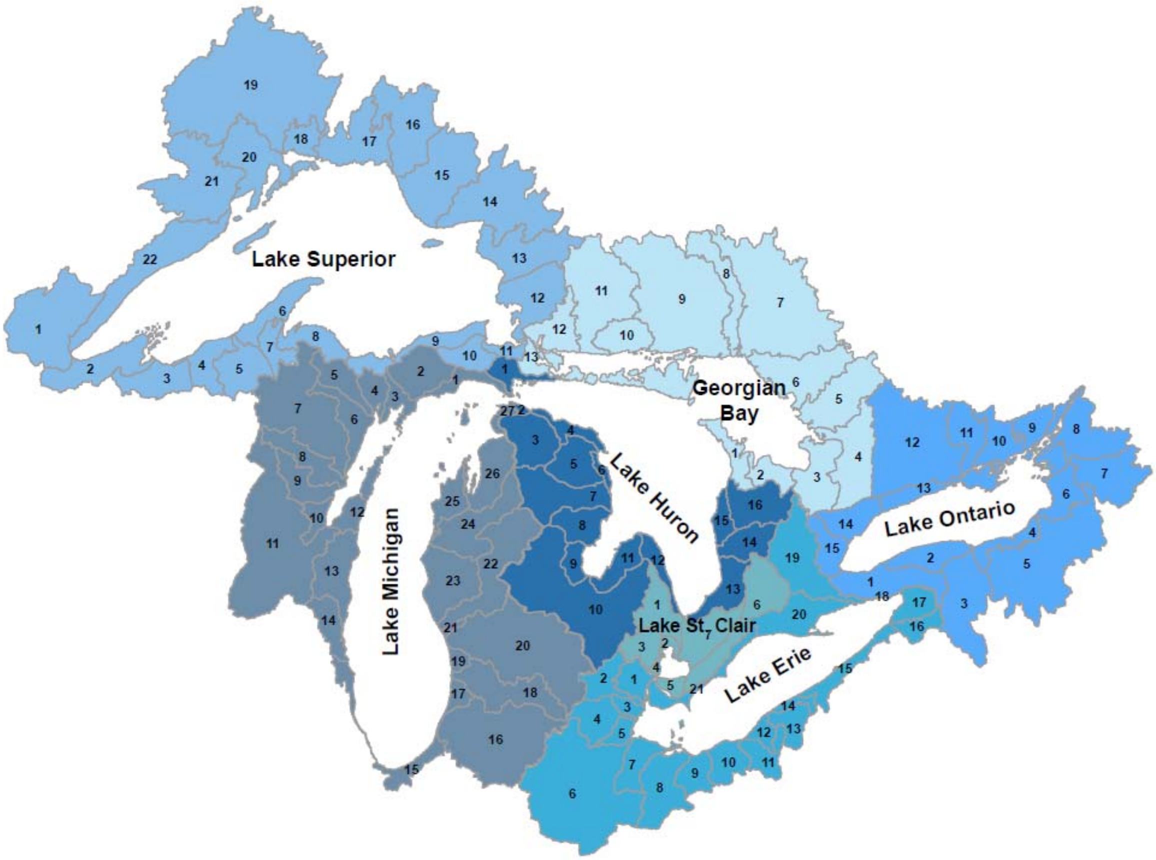

Figure 5.9. Subbasins draining into the Great Lakes used by Large Basin Runoff Model. (Source: Gronewold et al. 2017)

The LBRM has a tendency to overestimate evapotranspiration (Gronwold et al. 2017). To address this problem, Gronewold et al. (2017) developed a new version of the model, LBRMv2.0, by reformulating the evapotranspiration method and recalibrating the model. The original version of the model is referred to as LBRMv1.0. The LLTM, originally developed by Croley II (1989), and its parameters were subsequently updated in 2014. This version is referred to as LLTMv1.0 and is used with historical meteorological forcings. A second version of the model, LLTMv2.0, uses an alternative configuration to allow use of CMIP5 forcings.

Gronewold et al. (2017) used five different water supply forecasting systems shown in Table 5.1 that generate NBS ensembles for the lakes. While the four of the systems take meteorological inputs and propagate them through the two hydrologic models, the residual net basin supply system uses residual net basin supply[1] developed by the Coordinating Committee on Great Lakes Basic Hydraulic and Hydrologic Data. Because of challenges in maintaining the Great Lakes Advanced Hydrologic Prediction System (GL-AHPS), Gronewold et al. (2017) developed the new Great Lakes Seasonal Hydrologic Forecasting System (GLSHyFS). Three vesions of GLSHyFS are used as shown in Table 5.1.

[1] Residual NBS is calculated as the difference between change in lake water level and the net inflow into the lake via connecting channels. It is expressed as $NBS_r = \Delta Z - Q_i + Q_o$, where ΔZ is the monthly change in lake storage calculated as a change in lake water level and Q_i and Q_o are the monthly inflow and outflow through the upstream and downstream connecting channels, respectively, expressed in depth units over the surface of the lake.

Table 5.1. Great Lakes water supply forecasting systems and their components

Forecasting System Name	Meteorological Input	Hydrologic Models	
		Inflows	Evaporation
Great Lakes Advanced Hydrologic Prediction System (GL-AHPS)	Climatology	LBRMv1.0	LLTMv1.0
Great Lakes Seasonal Hydrologic Forecasting System-1 (GLSHyFS-1)	Climatology	LBRMv1.0	LLTMv1.0
GLSHyFS-2	Climatology	LBRMv2.0	LLTMv1.0
GLSHyFS-3	CMIP5	LBRMv2.0	LLTMv2.0
Residual Net Basin Supply System	None	Historical NBS sequences	

Regulation and Routing Models

Gronewold et al. (2017) used two regulation and routing models: (1) the Coordinated Great Lakes Regulation and Routing Model (CGLRRM), developed in the 1990s and used for regulation and forecasting since the early 2000s and (2) the Lake Ontario Routing and Regulation Model. CGLRRM is used to route flows for Lakes Superior, Michigan-Huron, St. Clair, and Erie through the connecting channels and to estimate lake water levels. Currently, the Coordinating Committee is developing a replacement for CGLRRM (Gronewold et al. 2017). Environment and Climate Change Canada and USACE maintain a regulation and routing model that is used to route water supply and flows associated with Lake Ontario. The Lake Ontario Routing and Regulation Model also is being updated by the Coordinating Committee.

Ensemble Processing for Water Level Forecasts

The NBS ensembles generated by the water supply forecasting systems are run through the regulation and routing models using the Great Lakes Ensemble Regulation and Routing Forecasting System that results in an ensemble of water levels and outflows for each Great Lake. The forecasing system also can be supplied with user-specified weights to develop weighted probabilistic forecasts of water levels and outflows (Figure 5.10).

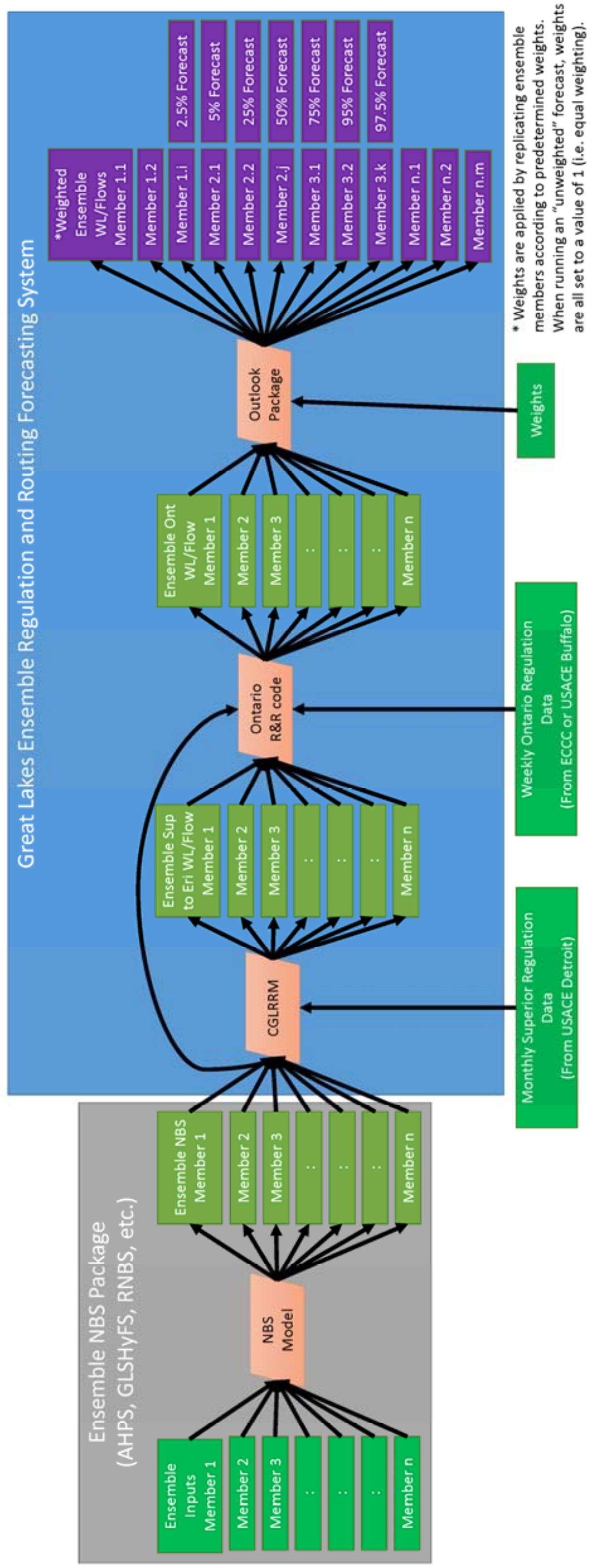

Figure 5.10. The Great Lakes Ensemble Regulation and Routing Forecasting System. (Source: Gronewold et al. 2017)

5.2.1.4 Large Lake Statistical Water Balance Model (L2SWBM) (Gronewold et al. 2016, Smith and Gronewold 2018)

To identify the causes behind the record rate-of-rise of water levels in Lakes Superior and Michigan-Huron, Gronewold et al. (2016) developed a Bayesian Markov chain Monte Carlo routine for inferring historical estimates of the Great Lakes' water budget components for the January 2005–December 2014 period. The monthly water budget for the two lakes were expressed using monthly overlake precipitation, overlake evaporation, tributary runoff, interbasin diversions, and outflows (via St. Marys River for Lake Superior and St. Clair River for Lakes Michigan-Huron). An area adjustment was used for inflow into Lakes Michigan-Huron via St. Marys River to account for the difference in surface area of the two lakes. Contributions to change in the lakes' storage caused by groundwater fluxes, thermal expansion, isostatic rebound, and consumptive use was deemed minor and collectively represented using an error term.

Monthly changes in storage were inferred from the beginning-of-month water level records maintained by USACE and Environment Canada through the Coordinating Committee. Monthly flows through the connecting channels (St. Marys and St. Clair Rivers) were taken from data maintained by the Coordinating Committee and from the international gauging stations maintained by USGS and Water Survey of Canada. Interbasin diversion data also was obtained from the Coordinating Committee. Two data sources were used for overlake precipitation, overlake evaporation, and tributary inflows: (1) the spatially and temporally extensive GLM-HM) and (2) temporally shorter (2005–2014) Canadian Meteorological Centre's GEM modeling system (the GEM tributary inflow estimates were not available for the time period of this study).

Using the 1950–2004 GLM-HMD data, prior probability distributions for overlake precipitation, overlake evaporation, interbasin diversion, lake outflows, and tributary inflows were estimated. Overlake precipitation was represented using a gamma prior probability distribution; interbasin diversion, lake outflow, and overlake evaporation were represented using normal prior distributions; and tributary inflow was represented using a lognormal prior probability distribution (Figure 5.11). Gronewold et al. (2016) updated the estimated monthly prior probability distributions of each water budget component using the 2005–2014 data from the two monthly data sources (GLM-HMD and GEM) and assuming normal likelihood functions for the water budget components. They used noninformative normal and gamma priors for the bias and precision (inverse of variance) terms in the likelihood functions. Five Monte Carlo chains were run until each converged. Figure 5.12 shows the posterior probability distributions of the water budget components obtained by Gronewold et al. (2016). Figure 5.13 shows the 2005–2014 monthly water budget components (top four panels) and the cumulative change in water level since January 2005 (bottom panel) for Lake Superior.

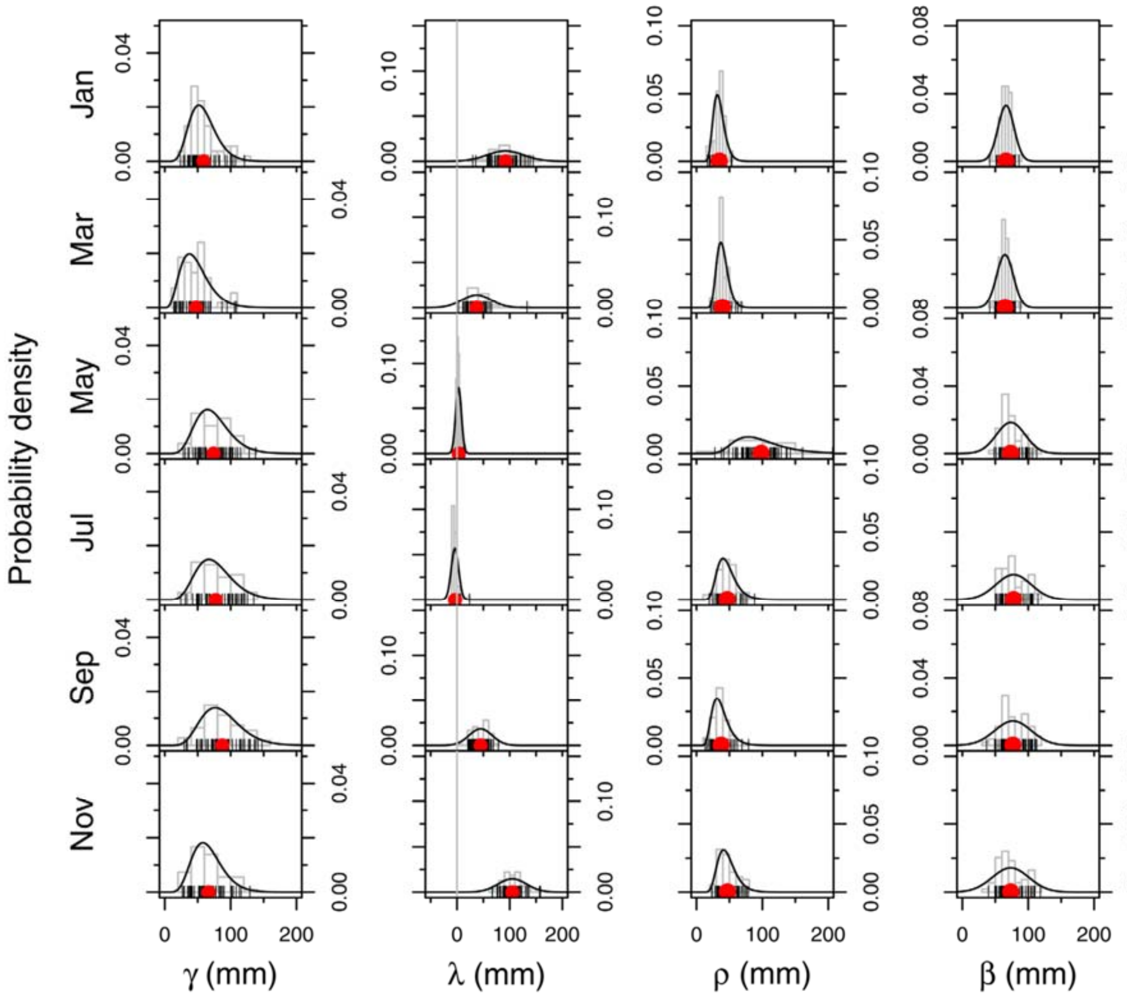

Figure 5.11. Prior PDFs for Lake Superior's monthly overlake precipitation (γ), overlake evaporation (λ), tributary inflow (ρ), and connecting channel outflow (β) based on 1950–2004 NOAA-GLERL Great Lakes hydrometeorological database. For clarity, only every other month starting in January is shown. Vertical tick marks and histograms represent the historical data, the red dots represent historical means, and the black curve represents the estimated prior probability distribution. (Source: Gronewold et al. 2016)

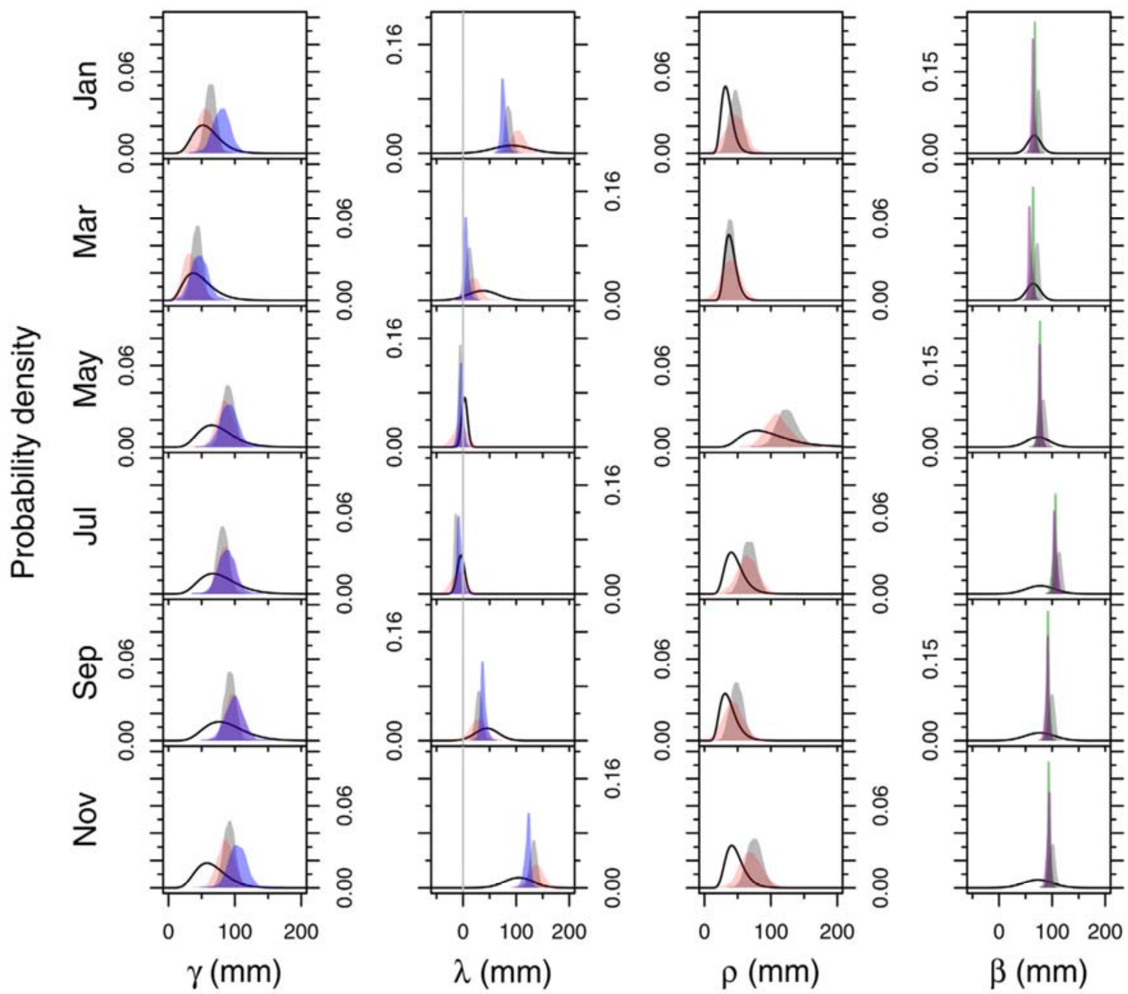

Figure 5.12. Posterior PDFs for Lake Superior's monthly overlake precipitation (γ), overlake evaporation (λ), tributary inflow (ρ), and connecting channel outflow (β). For clarity, only every other month starting in January is shown. The black line represents the prior probability distribution and the gray shaded curve represents the posterior probability distribution. Blue shaded curves for γ and λ represent the likelihood functions from the GEM dataset. Red shaded curves for γ, λ, and ρ represent the likelihood functions from the GLM-HMD dataset. The green and purple curves for β represent the likelihood functions from international gauging station estimates and the internationally coordinate estimates, respectively. Notice that the vertical scales have different ranges from those in Figure 5.11. (Source: Gronewold et al. 2016)

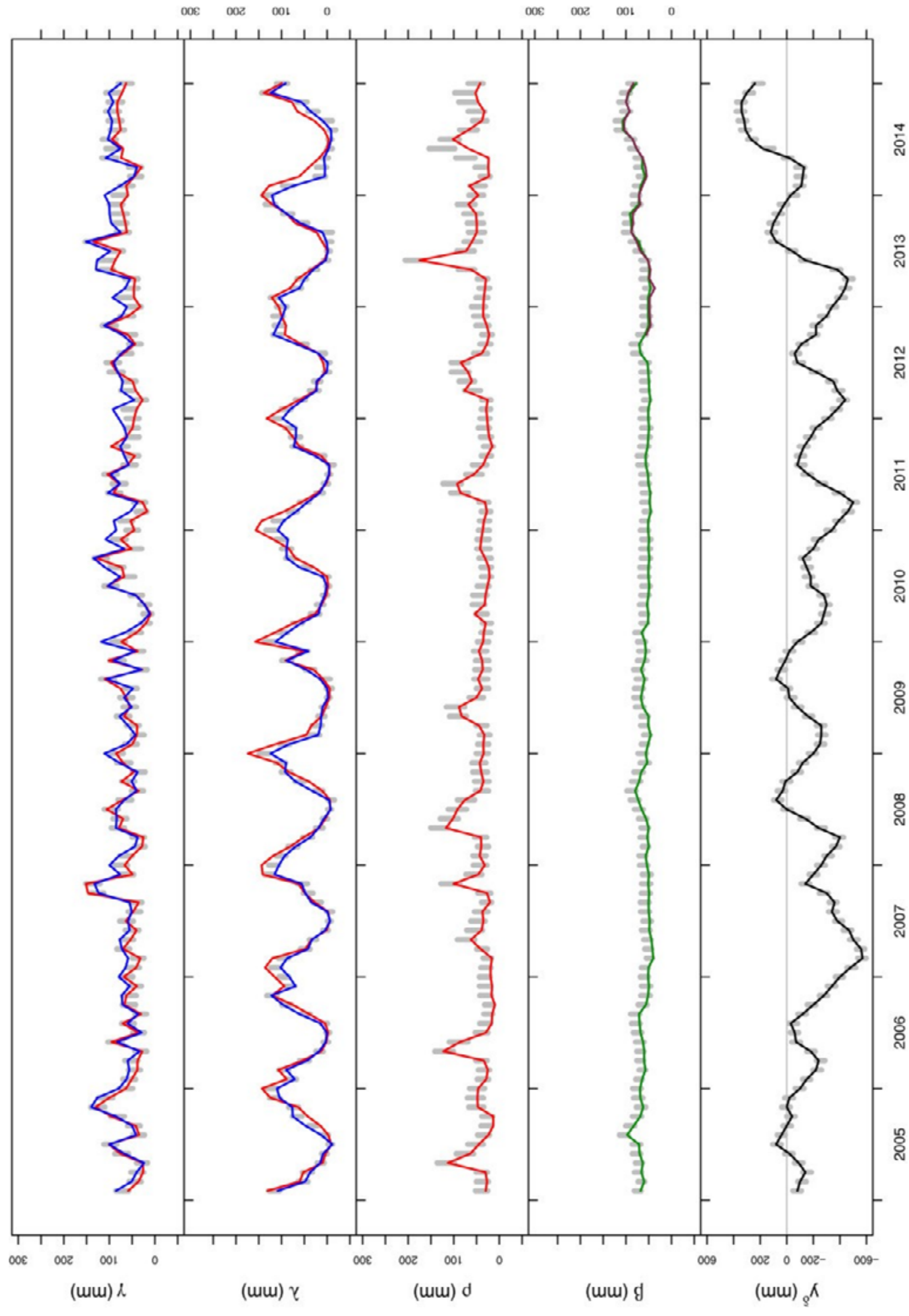

Figure 5.13. The 2005-2014 monthly water budget components (top four panels) and the cumulative change in water level since January 2005 (bottom panel) for Lake Superior. Blue and red lines represent estimates from the Global Environmental Multiscale Model (GEM) and GLM-HMD, respectively. The green and purple lines represent internationally coordinated outflow estimates and the international gauging stations estimates. The gray bars represent the 95 percent interval from the respective posterior probability distributions (top four panels) and the posterior predictive distribution for cumulative water level change (bottom panel). (Source: Gronewold et al. 2016)

Smith and Gronewold (2018) refer to the Bayesian water balance model described by Gronewold et al. (2016) as the prototype L2SWBM. Smith and Gronewold (2018) developed a framework for improving the prototype L2SWBM. The prototype L2SWBM had shown an unrealistic range of uncertainty in its inference of St. Clair River flows, which may have resulted from unresolved uncertainties in individual water balance components. Smith and Gronewold (2018) stated that their objective was to develop a framework for systematic evaluation and selection of alternative formulations of L2SWBM. In L2SWBM, water balance components (overlake precipitation, overlake evaporation, tributary inflow, connecting channel inflow and outflow, and diversions) are treated as random variables whose probability distributions are inferred using observed data—prior distributions were estimated using 1950–2004 data while the posterior distributions were estimated for the 2005–2014 time period.

Instead of the monthwise cumulative storage change with a fixed base month formulation of Gronewold et al. (2016), Smith and Gronewold (2018) adopted a formulation using a variable-length rolling period (multiple months). Three sets of models were considered: the first was the Gronewold et al. (2016) formulation and the other two were the rolling period formulations with period lengths of 1 and 12 months. Smith and Gronewold (2018) also considered three alternative structures for the model or process error term: the first was the same as that used by Gronewold et al. (2016), the second used a monthly-varying error term with fixed precision (fixed error model), and the third used a monthly-varying error term with variable precision (hierarchical error model). Prior probability distributions were estimated using historical (1950–2004) data—lognormal and gamma distributions were used for precipitation and tributary runoff, while normal distribution was used for evaporation, channel flow, and diversions. Likelihood functions for the water balance components were represented using normal distributions with explicit accounting of observation bias in the likelihood function. Expert opinion from regional water-management authorities was used to specify similar bias constructs for channel flow and diversion estimates. Altogether, Smith and Gronewold (2018) evaluated 26 variations of L2SWBMs: two of these variations used the water balance formulation of the prototype L2SWBM and the remaining 24 L2SWBMs differed in rolling window lengths (1 or 12 months), how they modeled process error (none, fixed, or hierarchical), how they modeled observation bias (fixed or hierarchical), and whether or not bias construct was used for channel flows and diversion. The models were evaluated using deviance information critera and Bayesian information criteria. Smith and Gronewold (2018) found that the 95-percent posterior predictive intervals for simulated storage changes did not adequately match the observed 12 and 60-month changes in lake storage when the 1-month rolling window L2SWBM was used. On the other hand, the 12-month rolling window L2SWBM was able to match the 12 and 60-month observed changes in lake storage very well and also the month-to-month changes in lake storage fairly well (Figure 5.14). The authors reasoned that models that used shorter rolling windows allow for more freedom in selecting water balance component values but the lack of information from other months causes a problem in matching water balance for longer durations. Based on how well and efficiently the models closed the water balance, the authors recommended two L2SWBMs, both using 12-month rolling windows, fixed observation bias terms, and a bias construct for channel flow and diversions; the difference between the two L2SWBMs was the representation of process error term—one using monthly-varying fixed-precision error term and the other assuming no process error term. The model that included a representation for the process error term performed slightly better in terms of monthly water balance simulations. The authors noted that incorporating expert opinion for bias in channel flows and diversions significantly reduced uncertainty in channel flow estimates without impacting the variability and bias in other components of the water balance. The authors also noted that extending L2SWBM to all Great Lakes or extending the model back in time to 1950 would require substantial effort.

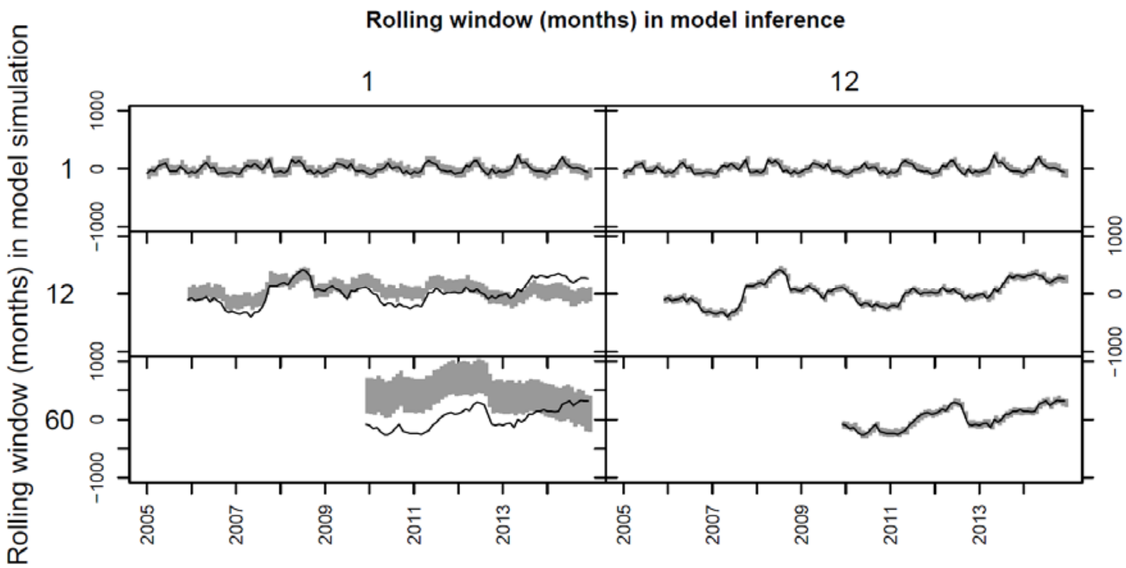

Figure 5.14. Comparison between observed and simulated Lake Superior changes in storage (mm) across 1, 12, and 60 months (panels arranged vertically) from models inferred using 1 and 12 month windows (panels arranged horizontally). (Source: Smith and Gronewold 2018)

5.2.1.5 Correlation between Great Lakes Superior and Michigan-Huron Water Levels and Levels in Seepage Lakes in Northern Highland Lake District of Wisconsin

The Northern Highland Lake District (NHLD) of Wisconsin, contains the northern Chippewa River and the upper Wisconsin River drainages which are adjacent to the Great Lakes drainage basin, but flow south and away from the Great Lakes. These drainages contain small lakes which have no inflowing or outflowing streams and have negligible surface runoff from their small contributing areas. Therefore, the hydrology of these lakes is controlled by groundwater fluxes. These lakes are called seepage lakes. Using measured seepage lake levels, precipitation, evaporation, and groundwater levels in the northern Chippewa and upper Wisconsin River drainages, Watras et al. (2014) correlated the fluctuations in the water levels in the seepage lakes to those of Great Lakes Superior and Michigan-Huron. They found a strong coherence between NHLD seepage lakes levels and those in the Great Lakes (Figure 5.15) (i.e., the fluctuations in water levels of both the NHLD seepage lakes and the Great Lakes follow remarkably similar patterns in time). Based on spectral analysis, Watras et al. (2014) concluded that annualized water level data show a periodicity of approximately 13 years. Using a water balance formulation, Watras et al. (2014) correlated change in stage in the NHLD seepage lakes to net precipitation (precipitation minus evaporation, P-E) and found that P-E accounted for 65 percent of the variability in change in stage and groundwater flux was a contributing factor. They also investigated the correlation between 1948–2010 April–September monthly NHLD seepage lake-level changes to 500 hPa geopotential height and sea-level pressure (the latter two obtained from a NCAR reanalysis data set). Figure 5.16 shows the correlation maps. Watras et al. (2014) noted that April–September changes in NHLD seepage lake levels are correlated with a large-scale atmospheric wave train (Figure 5.16, top panel) that extends from the north Pacific Ocean across North America into the North Atlantic Ocean. They also noted that the April–September changes in NHLD seepage lake levels are positively correlated with high-pressure anomalies near the Gulf of Alaska and near the southeast Atlantic coast of the United States. Based on the correlation between the NHLD seepage lake levels and the large-scale atmospheric circulation patterns, the authors suggested that these small isolated lakes may be useful indicators of future regional hydrologic change (Watras et al. 2014).

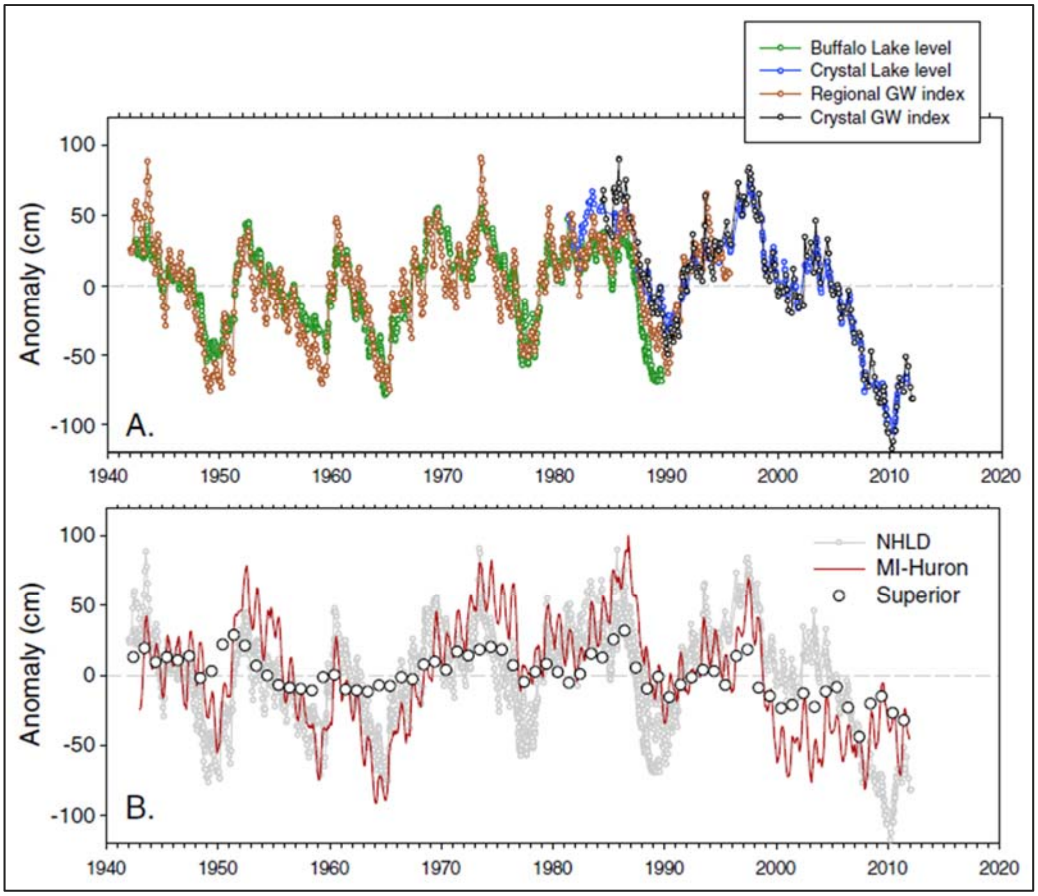

Figure 5.15. Anomalies in regional water levels for 1942–2011. Buffalo Lake is located in the upper Wisconsin River drainage and Crystal Lake is located in the northern Chippewa River drainage. The two drainages are adjacent to, but outside of, the Great Lakes drainage. NHLD stands for the Northern Highland Lake District of Wisconsin. Water table anomalies are labeled "GW index." (Source: Watras et al. 2014)

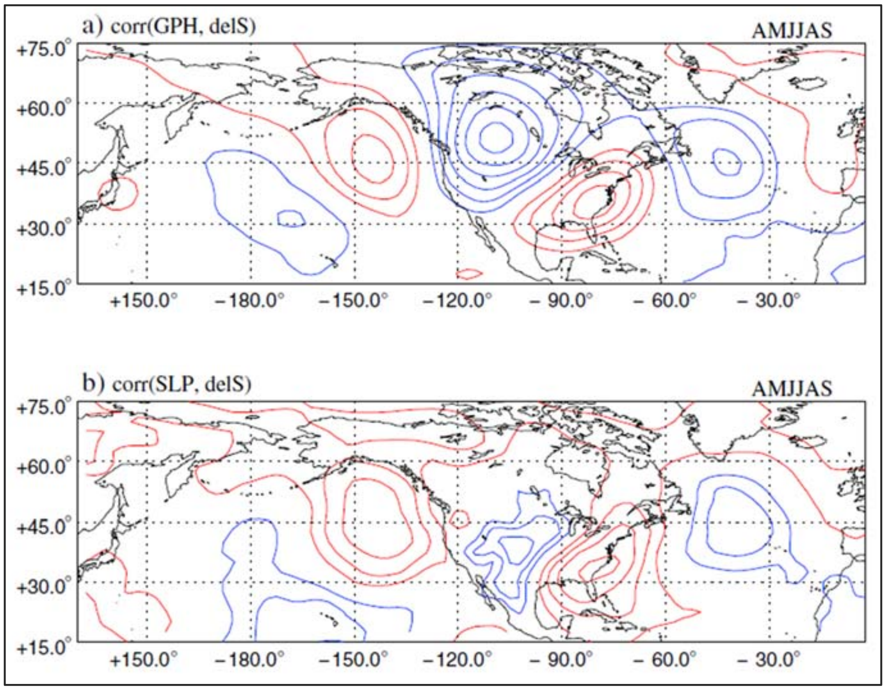

Figure 5.16. Correlation map for the April–September (denoted AMJJAS) change in lake levels (delS) and 500 hPa geopotential height, top panel) and sea-level pressure (bottom panel). Red contours indicate positive correlation values and blue contours indicate negative correlation values. The contour interval is 0.05 and the no-correlation contour is not shown. Correlation values above/below ±0.11 were determined to be significant at 99 percent confidence interval. (Source: Watras et al. 2014)

5.3 Projected Changes in Great Lakes Water Levels for the 21st Century

- Projected water levels in the Great Lakes range from a slight decrease to a slight increase. Projections show differences in seasonal cycle from observed historical patterns; however, this could be a result of incomplete hydrologic process representation in models.
- The Great Lakes water budget is a complex process. This is underlined by recent efforts to develop newer generation of both mechanistic models to improve hydrologic forecasting and statistical models to infer changes in lake levels using Bayesian approaches.

In 2007, to prevent and resolve potential disputes regarding use of the Great Lakes and rivers between the United States and Canada, the International Joint Commission, which was founded in 1909 under the Boundary Waters Treaty, directed a 5-year cooperative study—the International Upper Great Lakes Study (IUGLS)—to improve understanding of how the Great Lakes function, how water levels in the lakes are changing, and what potential management options may be available with changing water levels in the future (IUGLSB 2012). The study included all Great Lakes except for Lake Ontario (hence “Upper Great

Lakes" in the name). The final report of the study focused on (1) historical estimates of NBSs[1] in the Upper Great Lakes and (2) potential impacts of natural variations and anthropogenic climate change on future regulation of the Upper Great Lakes. The study used both indirect (the residual method) and direct, model-based (the component method) estimates of NBS. Models used in the component methods were the GLERL model, the Environment Canada's Modélisation Environnementale – Surface et Hydrologie (MESH) model coupled to the Global Environmental Multiscale atmospheric model, and the Coupled Hydrosphere Atmospheric Research Model (CHARM).

The study used the GLERL model to calculate NBS and lake levels for the current climate for the 1970–1999 period. To estimate future sequences (2005–2034, 2035–2064, and 2065–2094) of NBS, the study used 565 model runs from 23 GCMs. The study reported estimated future lake-level changes for Lake Michigan-Huron (Table 5.2). Because of the large bias corrections needed in projected precipitation to match current conditions, the study cautioned that the estimated future lake-level changes should be viewed as indicative rather than predictive.

Table 5.2. Estimated future lake -level changes (m) for Lakes Michigan-Huron Lake. (Source: IUGLSB 2012)

Year	5th	50th	95th
B1 Emission Scenario			
2020	-0.60	-0.18	0.28
2050	-0.79	-0.23	0.15
2080	-0.87	-0.25	0.31
A1B Emission Scenario			
2020	-0.55	-0.07	0.46
2050	-0.91	-0.24	0.40
2080	-1.43	-0.28	0.83
A2 Emission Scenario			
2020	-0.63	-0.18	0.20
2050	-0.94	-0.23	0.42
2080	-1.81	-0.41	0.88

Source: Angel and Kunkel (2010)

Because GCMs may not accurately capture surface-atmosphere feedbacks, the IUGLS also employed dynamical downscaling using the Canadian Regional Climate Model (CRCM) in two different approaches (IUGLSB 2012). The first approach was a multimodel, multi-member ensemble approach that used eight CRCM simulations driven by three different GCM boundary conditions. The second approach further downscaled one of the CRCM simulations using the Great Lakes CRCM developed for the study. The grid resolution was 45 km in the first approach and 22.5 km in the second approach. The study concluded that mean monthly NBSs for (1) Lake Superior in the future (2021–2050) will increase less than 1 percent compared to the historical period (1962–1990); (2) Lake Michigan-Huron will decrease by about 2 percent; and (3) Lake Erie will decrease by about 8 percent (Table 5.3). IUGLS also reported that for all lakes, increases in monthly standard deviations of NBS are larger, ranging from 7 percent (Lake Erie) to 22 percent (Lake Superior).

[1] Net basin supply is defined (IUGLSB 2012) as the net amount of water inflow into a lake resulting from precipitation falling on the lake, runoff from surrounding drainage into the lake, and evaporation loss from the lake. Net basin supply does not include inflow from an upstream lake or inflow or outflow from diversions. NBS formulation is based on the water balance of a lake over a specified time period.

Table 5.3. Comparison between mean (standard deviation) monthly NBS for a historical period and a future period. (Source: IUGLSB 2012)

NBS	Observed = GL-CRCM 1962-1990	GL-CRCM 2021-2050	Change
Superior	67.9 (70.5)	68.3 (86.3)	0.4 (15.8)
Michigan – Huron	74.8 (69.7)	73.2 (79.2)	-1.6 (9.5)
Erie	82.7 (106.6)	74.9 (113.8)	-7.8 (7.2)

(1962-1990, and 2021 – 2050) (mm over lake)

IUGLS also used CHARM to estimate NBS for historical (1964–2000) and future (2043–2070) periods, driven by observed CO_2 concentrations during the former and the A2 emission scenario for the latter period (IUGLSB 2012). CHARM is a regional climate model that includes full interaction between the land surface and the atmosphere and simulated runoff on a 40 km grid. The CHARM NBS results are shown in Figure 5.17. IUGLS reported that the CHARM simulations showed an increase in NBS during late spring and early summer for Lakes Superior and Michigan-Huron. In Lakes Michigan-Huron, St. Clair, and Erie, NBS also increases in December and January. NBS decreases in fall in Lake Superior.

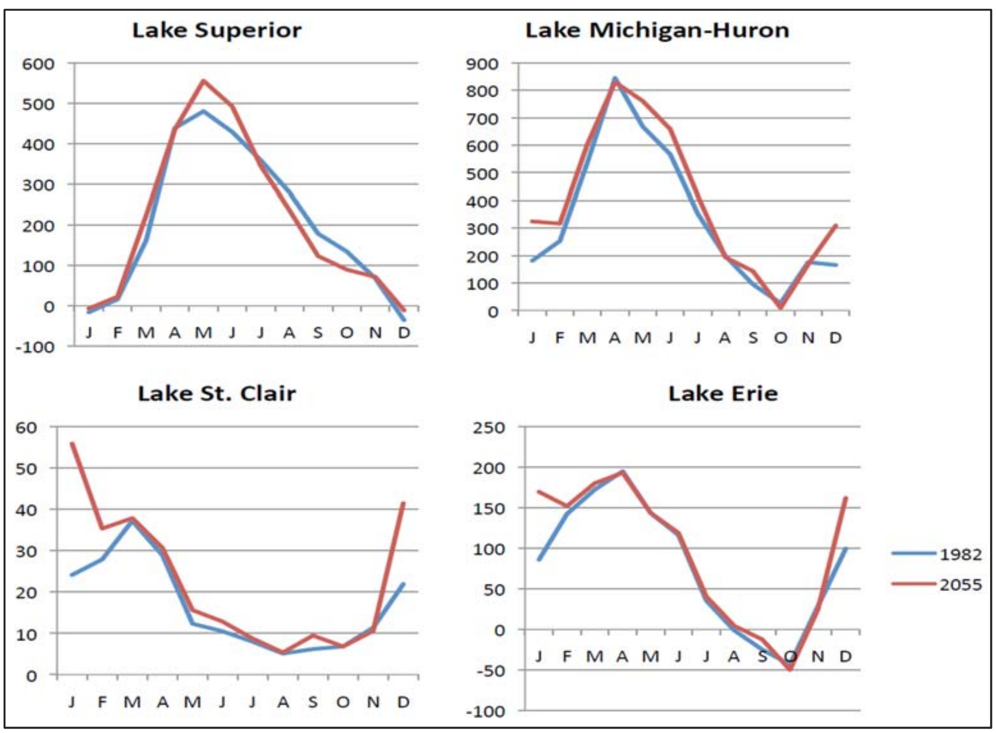

Figure 5.17. Climatological NBS (× 10 m^3/s) simulated by CHARM for a historical (1964–2000, "1982") and future (2043–2070, "2055") periods. (Source: Lofgren and Hunter 2011)

The study concluded that:

- The dynamics of the Great Lakes hydrologic system are only partially understood.
- Despite improved estimates of runoff and precipitation, the lakes' water balance still exhibits significant uncertainty.
- Incorporation of GCM simulations are difficult to reconcile with historical data, and incorporation of GCM outputs into water balance introduced more uncertainty.
- Lake evaporation is increasing and is likely to continue increasing in the future because of increasing surface water temperature and wind speed and decreasing ice cover.

To address some of the issues identified by IUGLS, the Great Lakes Runoff Intercomparison Project was formed as a binational collaboration to assess predictions of basin-scale runoff to Great Lakes from a variety of hydrologic models. The first phase of the project focused on Lake Michigan (Fry et al. 2014) and the second phase on Lake Ontario (Gaborit et al. 2017). Fry et al. (2014) evaluated five different models in a total of seven configurations. These models ranged from empirical to lumped conceptual and spatially distributed models. Some of the models were calibrated with historical discharge data, while three models' existing calibrations were deemed sufficient. Validation of the models relied on measured discharge at 20 locations during 2004–2008. Model skill was evaluated using Nash-Sutcliff efficiency, percent bias, and Spearman rank correlation measures. Fry et al. (2014) concluded that:

- Few models are adaptable for Great Lakes basin-wide water budget modeling.
- Model skills vary for simulating discharges at specific locations; however, when aggregated at the basin scale, model skills improved.
- Relatively simple, empirical models showed good model skills for simulating monthly runoff to Lake Michigan.

Gaborit et al. (2017) compared two lumped models (the modèle du Génie Rural à 4 paramètres Journalier, GR4J, and the LBRM) for their ability to simulate daily runoff from the Lake Ontario drainage basin. GR4J simulates daily runoff continuously and has four free parameters. GR4J was coupled with CémaNeige snow model (that has two free parameters) for the study. LBRM also simulates daily runoff continuously and has nine free parameters. As implemented for the study, the two models had 6 and 10 free parameters, respectively. A 4.5-year calibration period was used followed by a 2-year validation period. Two different precipitation data sets—the Global Historical Climatology Network – Daily and the Canadian Precipitation Analysis (CaPA)—were used for four model combinations (two models driven using the two different precipitation data sets). The authors reported that GR4J, input with the Global Historical Climatology Network data set, resulted in the best performance. The model was able to perform well both in unregulated and regulated drainages. Gaborit et al. (2017) noted that GR4J is suitable for both spatially distributed and basin-scale estimation of runoff to Lake Ontario.

MacKay and Seglenieks (2013) used a downscaled GCM simulation with a regional climate model, bias-corrected the simulated NBS, and used the bias-corrected NBS in a river routing/lake storage model. They used Environment Canada's GCM run performed at 3.75-degree resolution with the observed emission scenario for the historical period (1961–2000) and the Special Report on Emissions Scenarios (SRES) A2 emission scenario for the future period (2001–2100). Dynamical downscaling was performed using the CRCM with a grid resolution of approximately 45 km. A simple lake model was in the CRCM but no streamflow routing was included. A second downscaling was performed using the CRCM at 22.5 km resolution (called the Great Lakes Regional Climate Model, GLRCM), driven by the 45 km CRCM run. Streamflow routing was performed using a storage-discharge power function calibrated to observed monthly flow, uncoupled from the GLRCM. Great Lake levels were computed using GLERL's

CGLRRM that incorporates Lake Superior regulation rules. For computing NBS for the future period, MacKay and Seglenieks (2013) assumed that regulation rules and streamflow routing characteristics remain unchanged. GLRCM-simulated NBS greatly underestimated the historical NBS and therefore was unsuitable for driving the CGLRRM without bias correction. The GLRCM-simulated NBS was bias-corrected by rescaling the simulated monthly NBS to match the mean and standard deviation to those of the observed monthly NBS. The authors concluded that the bias-corrected simulations only grossly captured the observed mean seasonal cycle for all Great Lakes. The greatest decreases in NBS for all lakes occurred during late summer and early fall (Figure 5.18). Lake Superior exhibited an amplified seasonal cycle.

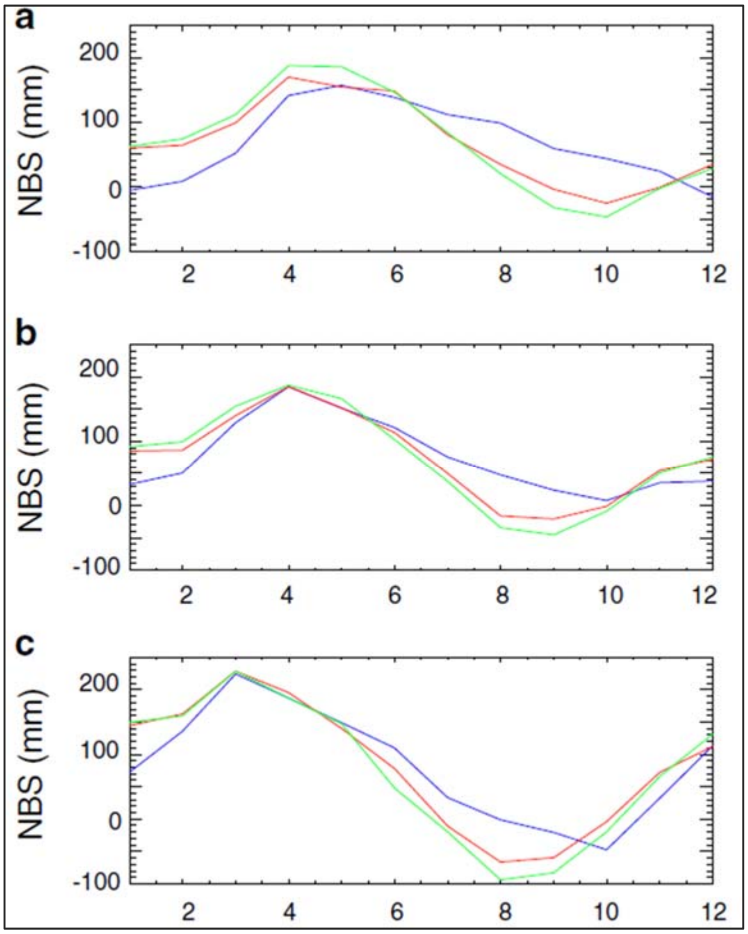

Figure 5.18. Observed (blue), 1962–1990 (historical period) GLRCM-simulated (red), and 2021–2050 (future period) GLRCM-simulated mean seasonal NBS cycle (green) for (a) Lake Superior, (b) Lakes Michigan-Huron, and (c) Lake Erie. (Source: MacKay and Seglenieks 2013)

The bias-corrected GLRCM-simulated NBS was used to drive the CGLRRM (MacKay and Seglenieks 2013). Simulated lake levels showed a slight positive bias, 2 and 7 cm, for Lakes Michigan-Huron and Erie, respectively. Future levels for all Great Lakes showed reductions in mean, ranging from 3 cm for Lake Superior to 6 cm for Lake Erie. The simulated mean seasonal cycle for lake levels is shown in Figure 5.19. Lake Superior showed a 2–3 month too-early drop to minimum lake levels, consistent with simulations of NBS. The seasonal cycle for lake levels was also amplified, as was the case with NBS; the increase in mean difference between annual maximum and annual minimum for the lake levels was about 7 cm for Lake Superior and about 4 cm for Lakes Michigan-Huron and Erie (MacKay and Seglenieks 2013).

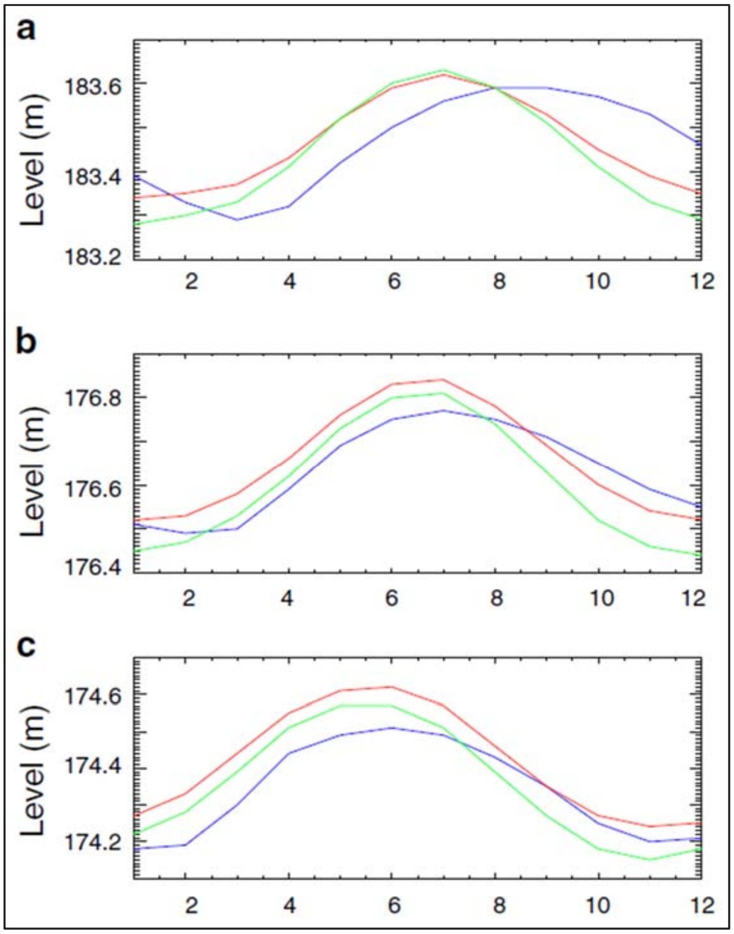

Figure 5.19. Observed (blue) 1962–1990 (historical period) GLRCM-simulated (red), and 2021–2050 (future period) GLRCM-simulated mean lake-level cycle (green) for (a) Lake Superior, (b) Lakes Michigan-Huron, and (c) Lake Erie. (Source: MacKay and Seglenieks 2013)

Notaro et al. (2015) dynamically downscaled RCP8.5 scenario outputs of two CMIP5 GCMs (the Model for Interdisciplinary Research on Climate, version 5 [MIROC5] and the Centre National de Recherches Météorologiques Coupled Global Climate Model, version 5 [CNRM-CM5]) using a high-resolution RCM (the Abdus Salam International Centre for Theoretical Physics Regional Climate Model, version 4 [RegCM4]). RegCM4 was coupled to a one-dimensional lake energy-balance model to account for vertical heat transfer within the water column by eddy diffusion and convective mixing; however, the lake model considers neither horizontal heat transfer within the lake nor the heat transfer between the lake bottom and the lake waters. The RegCM4 downscaling runs were carried out using a 25 km grid covering most of the continental United States and southern Canada. Notaro et al. (2015) used CGLRRM driven by the RegCM4-estimated NBS to estimate water levels in the Great Lakes. RegCM4 simulations were compared to GLERL's estimates of overlake precipitation, lake evaporation, and total NBS (Figure 5.20). The authors concluded that the seasonal cycle and total overlake precipitation was well simulated (Figure 5.20). Runoff was underestimated in winter; the authors noted that lack of explicit representation of groundwater, baseflow, and rivers may have been the cause. Simulated seasonal evaporation was out-of-phase by two to three months but the annual mean was reasonable. The authors noted that deficiencies in simulated lake surface temperatures, particularly the large summertime biases, may be partly responsible for the greater-than-estimated summertime lake evaporation. The downscaled simulations captured the April peak in NBS; however, the annual NBS was about 13 percent less than estimated. The authors pointed to insufficient annual runoff as the cause for the underestimated NBS.

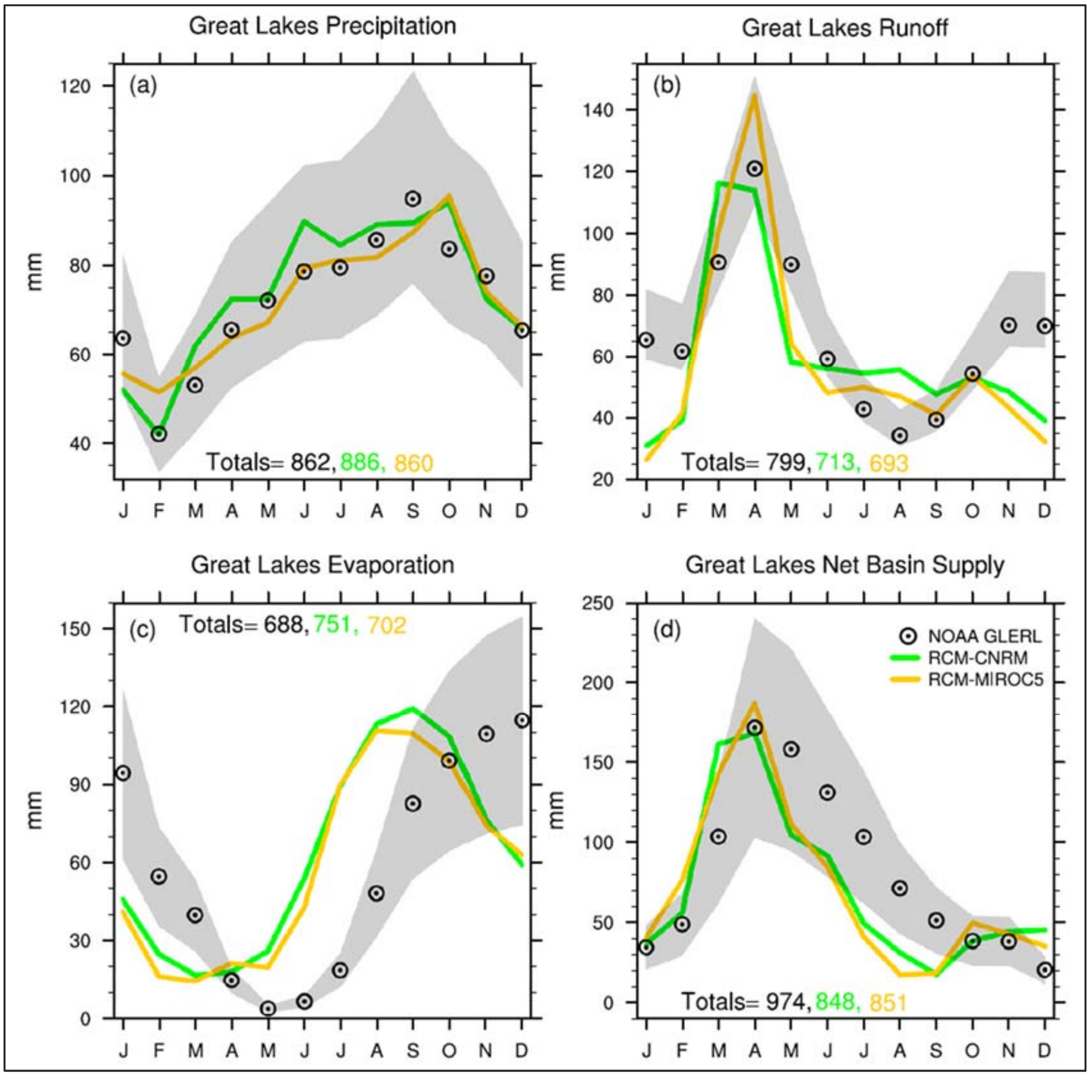

Figure 5.20. Comparison of mean seasonal cycle of (a) overlake precipitation, (b) runoff, (c) lake evaporation, and (d) NBS. The dotted circles are GLERL's estimates of the quantities and the shaded area represents the uncertainties in the data estimated by DeMarchi et al. (2010). RCM-CNRM denotes the RegCM4 downscaling of the CNRM-CM5 simulation and RCM-MIROC5 denotes the RegCM4 downscaling of the MIROC5 simulation (1980–1999). (Source: Notaro et al. 2015)

Projected changes in NBS to the Great Lakes for two future time periods, 2040–2059 and 2080–2099, compared to the historical time period of 1980–1999 are shown in Figure 5.21.

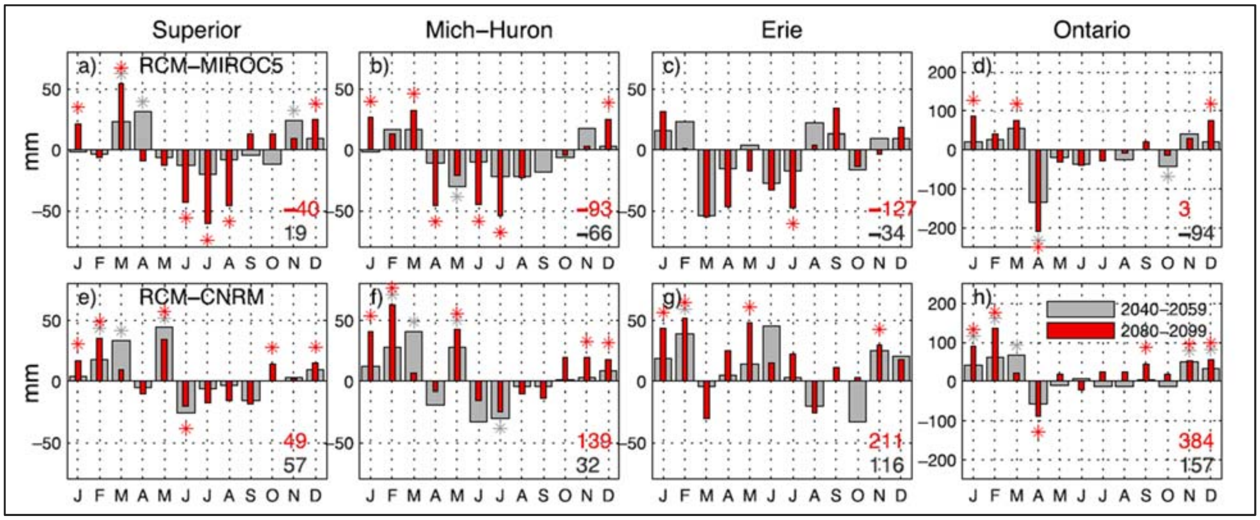

Figure 5.21. Changes in the seasonal cycle of NBS for two future time periods, 2040–2059 (gray) and 2080–2099 (red), compared to the historical time period 1980–1999. The top and bottom panels show the results from RegCM4-downscling of MIROC5 and CNRMC5 RCP8.5 simulations, respectively. The asterisks indicate significant changes ($p < 0.1$) and the numbers indicate total annual changes for the two time periods. (Source: Notaro et al. 2015)

For the mid-21st century period, 2040–2059, RegCM4 downscaling of MIROC5 RCP8.5 simulation showed declines in the annual mean level for all lakes except Lake Superior. For the late-21st-century period, 2080–2099, RegCM4 downscaling of MIROC5 RCP8.5 simulation showed larger declines for Lakes Michigan-Huron and Erie, and reversals of changes for Lakes Superior and Ontario, with Lake Superior declining 40 mm and Lake Ontatio rising 3 mm. For both future periods, RegCM4 downscaling of CNRM-CM5 RCP8.5 scenario shows increases in NBS for all lakes.

The water levels of the Great Lakes estimated using RegCM4 downscalings of the two GCMs' RCP8.5 scenarios showed increases (Figure 5.22). The seasonal cycle seems to be mostly preserved except for Lake Superior in the RegCM4 downscaling of the MIROC5 RCP8.5 scenario. In the RegCM4 downscaling of the MIROC5 scenario, the annual water level in the Great Lakes declined from 24 mm for Lake Superior to 132 mm for Lakes Michigan-Huron. For the late-21st century, the declines increased, from 97 mm for Lake Superior to 296 mm for Lakes Michigan-Huron (Figure 5.23). In the RegCM4 downscaling of the MIROC5 scenario, the largest declines in water levels for Lakes Superior, Michigan-Huron, and Erie occurred in late summer to autumn, autumn, and summer, respectively (Notaro et al. 2015, Figure 5.23).

In the RegCM4 downscaling of CNRMC5 scenario, annual water-level changes in the Great Lakes for the mid-21st century period ranged from a 75 mm increase for Lake Superior to a 180 mm increase for Lakes Michigan-Huron (Notaro et al. 2015, Figure 5.23). For the late-21st century, annual water-level increases in the Great Lakes ranged from 134 mm for Lake Superior to 420 mm for Lakes Michigan-Huron. In the RegCM4 downscaling of the CNRMC5 scenario, the largest increases in water levels for Lakes Superior and Michigan-Huron occurred in spring, and that for Lake Erie in summer (Notaro et al. 2015, Figure 5.23).

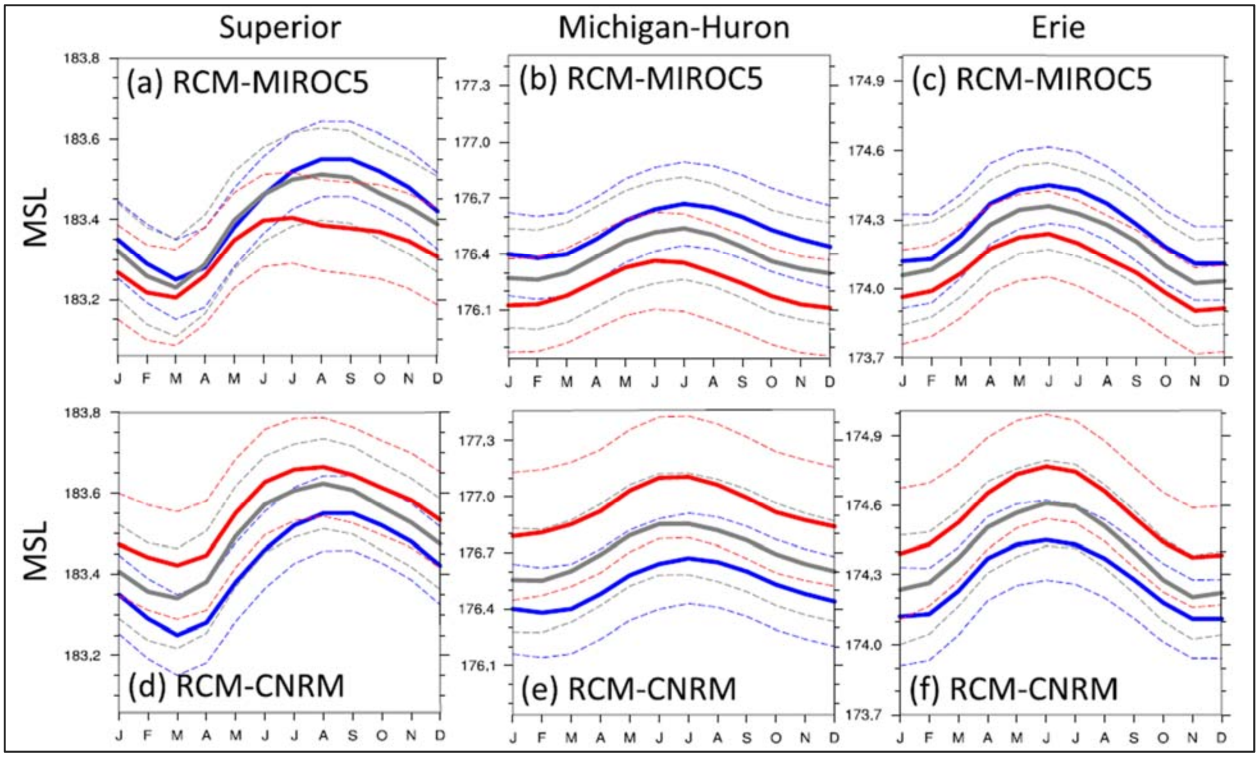

Figure 5.22. Mean seasonal cycle of water levels (m above sea level) from RegCM4 downscaling of MIROC5 and CNRMC5 RCP8.5 scenarios. The blue line indicates historical NBS estimates for 1948–2006, gray line indicates the mid-21st century (2040–2059) projections, and the red line indicates the late-21st century (2080-2099) projections. The dashed lines indicate the ±1 standard deviation in water levels for the respective periods. (Source: Notaro et al. 2015)

Notaro et al. (2015) noted that the RegCM4 downscalings of both CNRMC5 and MIROC5 showed increases in temperature and precipitation in the future. However, the projected warming was greater in the MIROC5 simulation and the projected increase in precipitation was greater in the CNRMC5 simulation. The relative changes in temperature and precipitation resulted in a net decrease of NBS in the MIROC5 simulation because greater lake evaporation caused by greater warming was not sufficiently offset by an increase in precipitation and subsequent runoff. In the CNRMC5 simulation, the greater increase in precipitation exceeded the relatively smaller increase in evaporation under a smaller increase in temperatures, causing NBS to increase substantially. The differences in the projected NBS between the two downscaled scenarios explain the difference between the projected water-level differences.

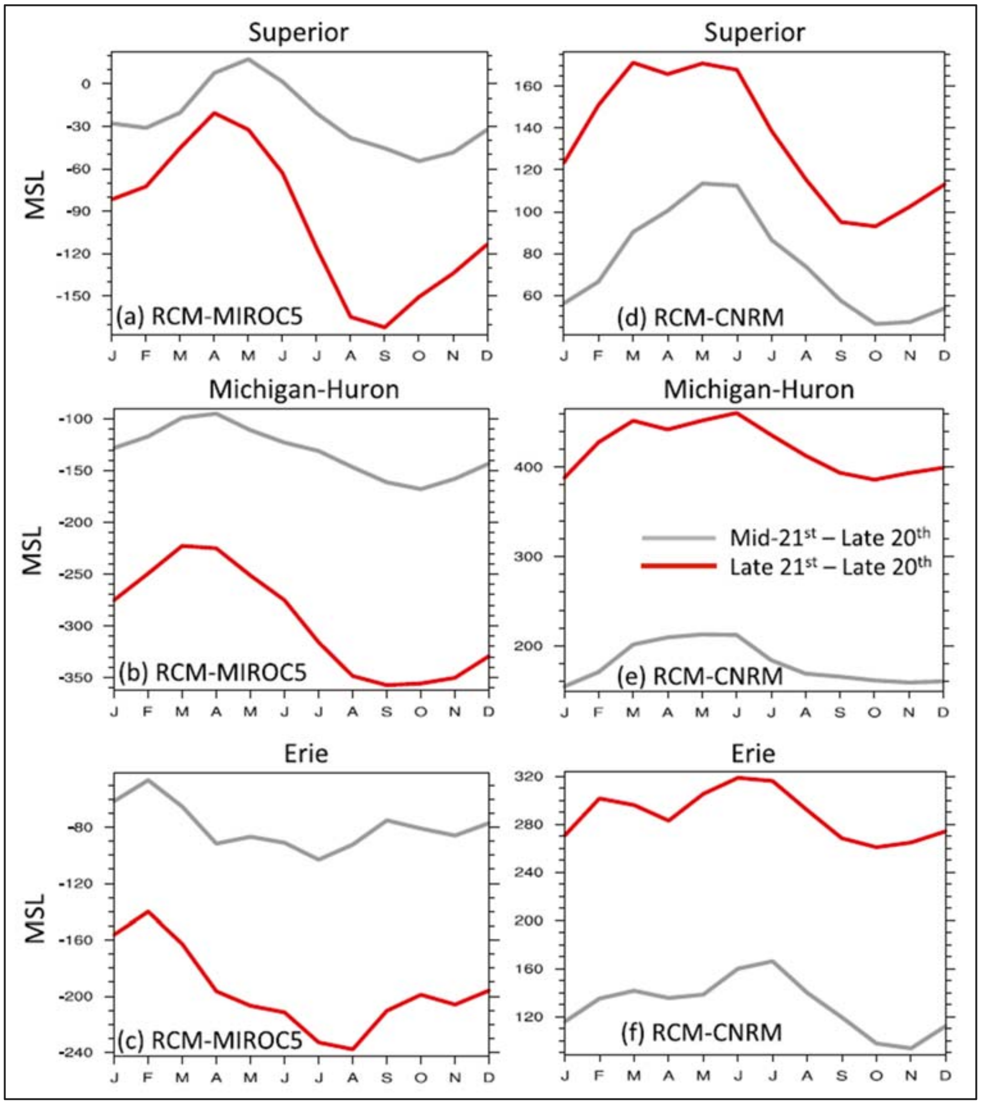

Figure 5.23. Projected changes in water levels (mm) in the Great Lakes from RegCM4 downscalings of MIROC5 (left panels) and CNRMC5 (right panels) RCP 8.5 scenarios. (Source: Notaro et al. 2015)

Lofgren et al. (2011) and Lofgren and Rouhana (2016) investigated the evapotranspiration component of the LBRM, employed by several studies that predict declines in projected NBS for the Great Lakes with a consequent decline in projected water levels. Lofgren et al. (2011) noted that evapotranspiration, both under moisture-unlimited conditions (i.e., potential evapotranspiration) and that under moisture-limited conditions (i.e., actual evapotranspiration) should be constrained by the net available radiative energy near the land surface. However, because observations of radiative energy terms are usually not available, alternative formulations to estimate potential evapotranspiration have been developed that use air temperature as a proxy; LBRM uses one such formulation. The air temperature-based formulations of potential evapotranspiration usually do not explicitly enforce radiative energy conservation. Lofgren et al. (2011) compared the predictions of changes in evapotranspiration predicted by a GCM to those by LBRM driven by that GCM's output. They found that the monthly latent heat flux differences, except for December, between the 2081–2100 and 1981–2000 periods were predicted to be larger in the LBRM simulation than those in the GCM itself. They found the discrepancy to add nearly 200 mm/yr evapotranspiration in the LBRM simulation with a corresponding decrease in NBS. They modified the way GCM output was used to drive LBRM to make it more consistent with the surface energy budget predicted by the GCM. In this formulation, they used a net radiation ratio in addition to a previously used temperature adjustment and precipitation ratio. They reported that the modified approach to driving LBRM resulted in smaller increases in evapotranspiration with corresponding increases in NBS and reductions in the lake-level drop previously simulated.

Lofgren and Rouhana (2016) focused on assessing whether the LBRM method greatly overestimates potential evapotranspiration in future scenarios compared to historical scenarios. In addition to the traditional temperature adjustment approach used with LBRM for future scenarios where potential evapotranspiration is not constrained by available net surface radiative energy, they used three additional formulations: (1) the energy adjustment method from Lofgren et al. (2011), (2) a modified energy adjustment method with additional adjustment for change in air temperature, and (3) a method based on the Clausius-Clapeyron relation where potential evapotranspiration from the historical base case is adjusted for change in the water vapor holding capacity of the atmosphere. To estimate NBS, Lofgren and Rouhana (2016) used LBRM with overlake precipitation for the historical base case adjusted by ratios of GCM-predicted precipitation and evaporation from the lakes calculated using the large lakes thermodynamics model. The LBRM was run for each of the four methods—temperature adjustment (TA), energy adjustment (EA), modified energy adjustment (PT), and the Clausius-Clapeyron relation adjustment (CC). The four estimates of NBS were used in the CGLRRM to estimate water levels in the Great Lakes. Lofgren and Rouhana (2016) used 1986–2005 as the historical period, 2056–2075 as the mid-21st century period, and 2081–2100 as the late-21st century period. They used a total of 64 LBRM/CGLRRM runs (two simulated time periods from 32 realizations of eight GCMs). Their results for Lakes Superior and Michigan-Huron are shown in Figure 5.24 and Figure 5.25.

In the Lake Superior basin, the ratios of potential evapotranspiration for future and historical time periods for the EA, PT, and CC methods were clustered near 1.0 with a few values less than 1.0 and a maximum of 1.72. In contrast, the ratios for the TA method had a median of 5.05 and a maximum of 565.4 (Figure 5.24a). Because the LBRM formulation for evapotranspiration links potential evapotranspiration to incoming solar radiation, Lofgrenand Rouhana (2016) noted that the TA method results for the ratio of potential evapotranspiration for future and historical time periods seemed unreasonable (an equivalent increase in incoming solar radiation by the same ratio). The actual evapotranspiration, being limited by the amount of available moisture, compared more reasonably among the methods; however, the median value of increase in evapotranspiration in the future compared to the historical period was larger than the top whiskers for the other three methods (Figure 5.24b). Changes in runoff were similar to those in actual evapotranspiration (Figure 5.24c). While the boxes for the three methods other than the TA method show an increase in runoff in the future, the box for the TA method shows a reduction in runoff. NBS and water levels in Lake Superior are generally similar to those of runoff (Figure 5.24d and e). In the TA method, most simulations show declines in future lake levels (the entire box is below zero). For the other three methods, while the median changes in lake levels are also negative (future lake-level declines), they are much less severe than those for the TA method (the PT method had a median of 1 cm decline). For all of the methods other than the TA method, the 75th percentile values of change in lake levels were positive, indicating a significant probability that lake levels could rise.

The comparisons for Lakes Michigan-Huron were similar to those for Lake Superior (Figure 5.25). Lofgren and Rouhana (2016) concluded that LBRM's reliance on air temperature as the predictor of potential evaporation resulted in significant overestimation of future evapotranspiration and led to underestimation of water levels in the Great Lakes. They suggested that future estimation of the Great Lakes' water budget should use hydrologic models based on consistent formulations of surface energy budgets and appropriate downscaling of GCM predictions.

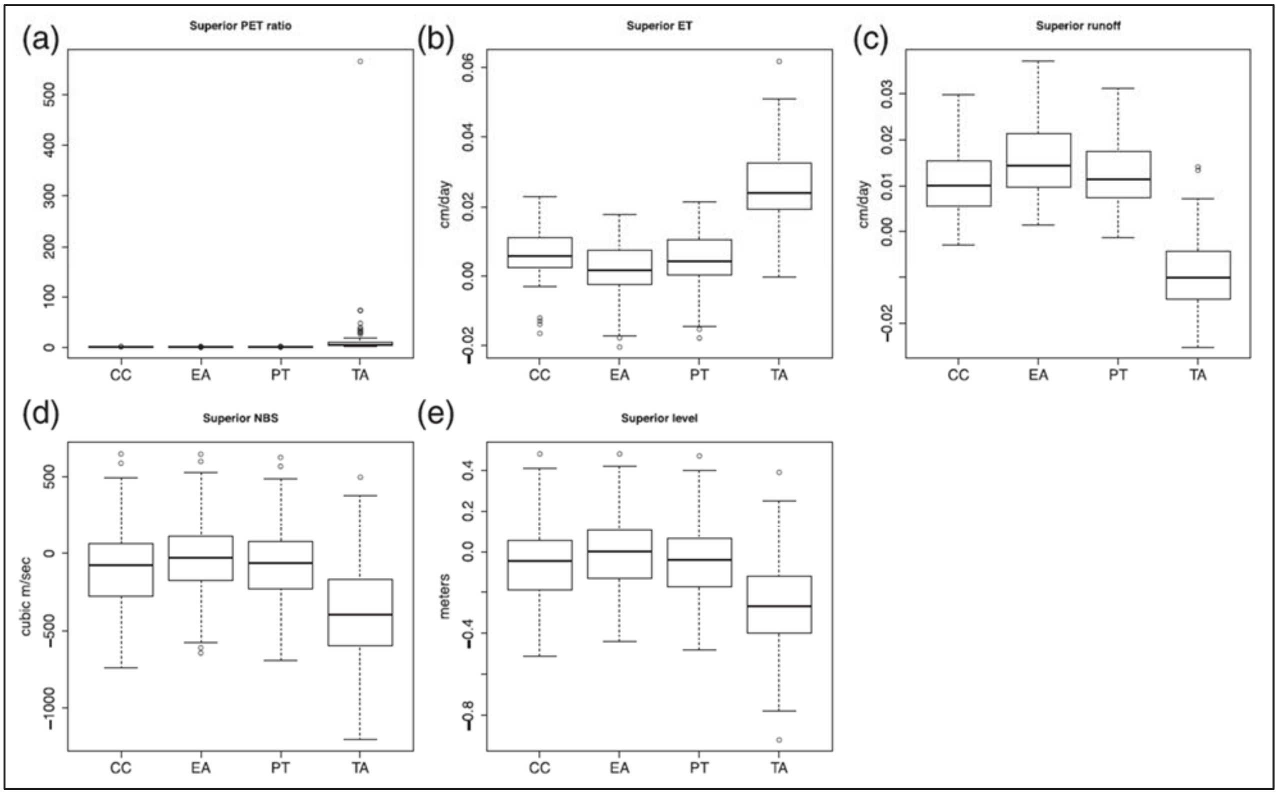

Figure 5.24. Comparison of the four adjustment methods for Lake Superior basin: (a) ratio of potential evapotranspiration for future and historical time periods, (b) difference in evapotranspiration (future minus historical), (c) difference in runoff (future minus historical), (d) difference in NBS (future minus historical), and (e) difference in water level (future minus historical). All 64 model runs were used to create the box plots. The horizontal line within the box indicates the median, the box spans 25 through 75 percentile, the whiskers denote points farthest, both above and below, from the boxes that are within 1.5 times the box height. Data points outside the whiskers are shown by circles. (Source: Lofgren and Rouhana 2016)

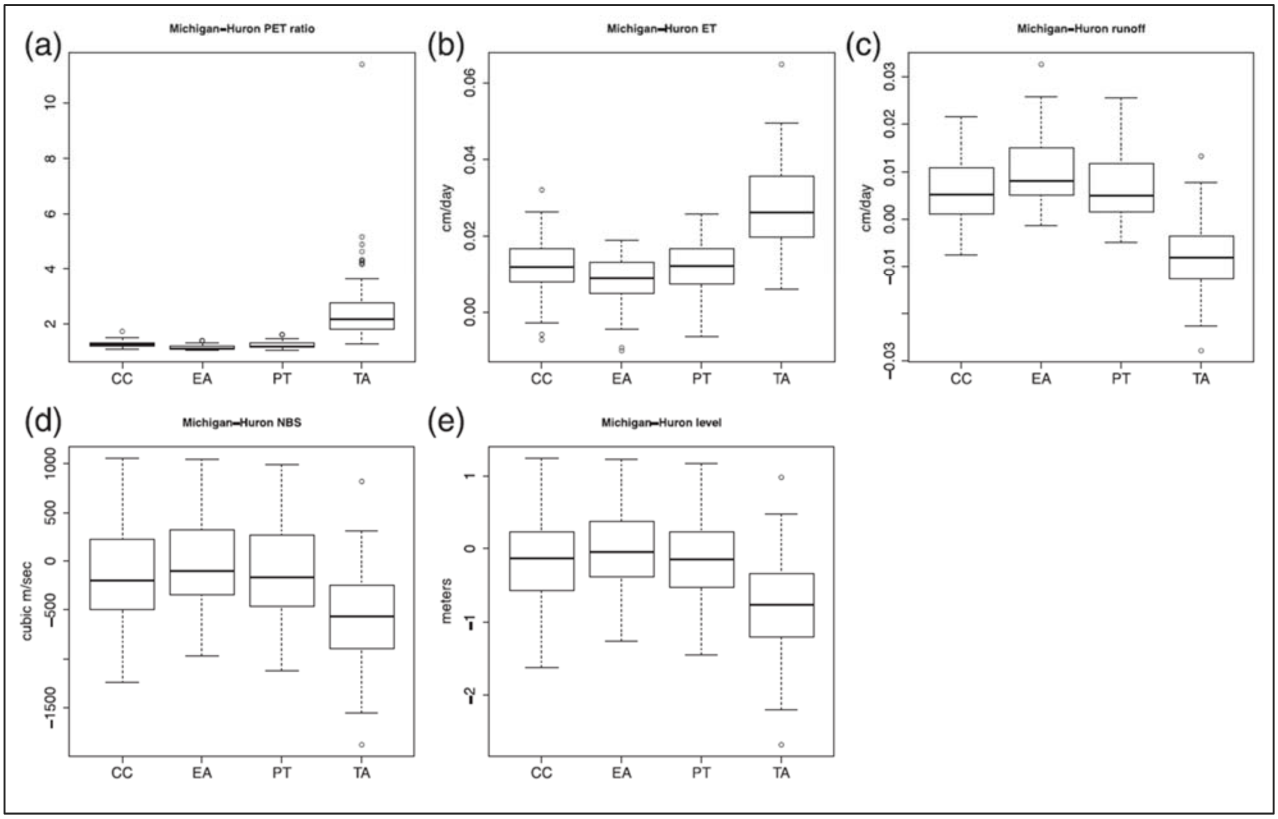

Figure 5.25. Same as Figure 5.24 but for the Lakes Michigan-Huron basin. (Source: Lofgren and Rouhana 2016)

6.0 Hydrologic Impacts of Climate Change in the Midwestern United States

This chapter describes the hydrological impacts of climate change in the Midwest Region. The focus is on two metrics—floods and low flows, resulting from precipitation and/or snowmelt events under climate change scenarios. Because both of these metrics are manifestations of runoff from precipitation and/or snowmelt, conditions other than just precipitation and snowmelt are also important to consider. For example, precipitation or snowmelt events that are similar in magnitude can differ in the amount of runoff from the drainage area because of differences in antecedent soil-moisture conditions or differences in the degree of imperviousness. The duration of the precipitation event is also important (e.g., a stalled storm system producing a low-intensity but longer-duration precipitation event can result in significantly greater flood magnitude compared to a higher-intensity shorter-duration storm for the same antecedent and physiographic conditions). Other factors that affect runoff include land use and cover and water management. Some of these hydrometeorologic parameters are not directly addressed in the National Climate Assessments.

6.1 Historical Flood Events

Floods in the Midwest Region can be produced by several mechanisms. These mechanisms include locally heavy precipitation (e.g., thunderstorms and MCCs), slow-moving extratropical cyclones during the cool season, remnants of tropical cyclones during summer and fall, late spring rainfall on snowpack, and occasional large releases from upstream dams. Some recent floods are briefly described below. The reason these recent flood events are highlighted is that they resulted from unusual combinations of hydrometeorological conditions and exceeded the previously recorded historical maximums. In general, the climate research community has not focused on evaluating trends and impacts of meteorological (and by extension, flooding) events of exceedance probabilities that are of interest to the NRC in a PFHA for permitting and licensing. Current climate models have significantly larger uncertainties for events whose exceedance probabilities approach those of interest to the NRC. The following events highlight some unusual combinations of hydrometeorological conditions that open a potential avenue to identifying similarly unusual combinations in climate simulations and how their frequencies are affected under various climate scenarios. This information could inform the NRC of combinations of hydrometeorological conditions relevant to PFHA.

6.1.1 2008 Midwest Floods

The USGS study area included all of the Midwest Region and the states of North Dakota, South Dakota, Nebraska, Kansas, Oklahoma, Arkansas, Tennessee, and Kentucky (USGS 2010). Record precipitation occurring on saturated soils in the Midwest resulted in flooding from January–July and in September 2008. During the preceding late fall and early winter, streamflows in the region were normal to above normal in the area affected by flooding. During the 2007–2008 winter, snowfall was above average in the northern half of the region, leading to large snowpacks. Snowmelt contributed to subsequent flooding because it resulted in saturated soils.

In May and June 2008, widespread flooding occurred in the Midwest (Budikova et al. 2010). A strong Great Plains low-level jet brought moist air into the region. A low-pressure system over the central-western United States enhanced the movement of moisture from the Gulf of Mexico into the Midwest Region. Further, the North Atlantic Oscillation was in a strong negative phase that promoted influx of moist Gulf air into the U.S. interior accompanied by unseasonably high precipitation. Six-month precipitation totals (January–June 2008) were the maximum recorded at 106 midwest locations (USGS 2010). Budikova et al. (2010) analyzed the regional hydroclimatic conditions that led to the 2008 floods. Their study area did not include Michigan and Ohio (Figure 6.1). They concluded that five factors contributed to the unique nature of the 2008 floods:

1. In the 10 months leading up to the 2008 floods, rainfall totals were above normal; precipitation was 150 percent above normal during four of those months. The above-normal precipitation combined with cooler-than-normal winter and early-spring temperatures limited evapotranspiration and resulted in wet antecedent conditions.
2. During May and June 2008, total precipitation was more than twice the expected amount on vast areas of the region (Figure 6.1).
3. During May and June 2008, the region experienced two to six times the expected number of short-term (1-day), moderate-magnitude (1-in.) rainfall events.
4. Widespread precipitation occurred on May 21 and June 13. Several high-precipitation events that occurred in early June 2008 were linked to MCCs and MCSs. More than 100 stations received precipitation exceeding 4 in. in a 7-day period and 6 stations received rainfall exceeding 10 in. in a 7-day period.
5. Regional convection cells that formed along a stationary front produced regional rainstorms.

Record peak streamflows were observed at 147 USGS gauges during 2008 (USGS 2010). During May and June 2008, recorded streamflows at 19 of the gauges had estimated annual exceedance probabilities of 0.002 or lower. Of these 19 gauges, 18 were located in the Midwest Region.

On June 9, 2008, the peak discharge in White River near Newberry, Indiana, as measured at USGS gauge 03360500 was 138,000 cfs with a stage of 28.6 ft above the gauge datum; both streamflow parameters were historical maximums (Figure 6.2). On June 13, the peak discharge in Cedar River at Cedar Rapids, Iowa, as measured at the USGS gauge 05464500 was 140,000 cfs with a stage of 31.1 ft above the gauge datum; both streamflow parameters were historical maximums (Figure 6.3). On June 21, 2008, the peak discharge in Rock River near Afton, Wisconsin, was 16,700 cfs, the historical maximum (Figure 6.4). These floods occurred over a wide area and at different times, depending on when the corresponding drainage basins received abnormal precipitation. Figure 6.5 shows the widespread nature of the accumulated precipitation over the Midwest from May 21 through June 14, 2008.

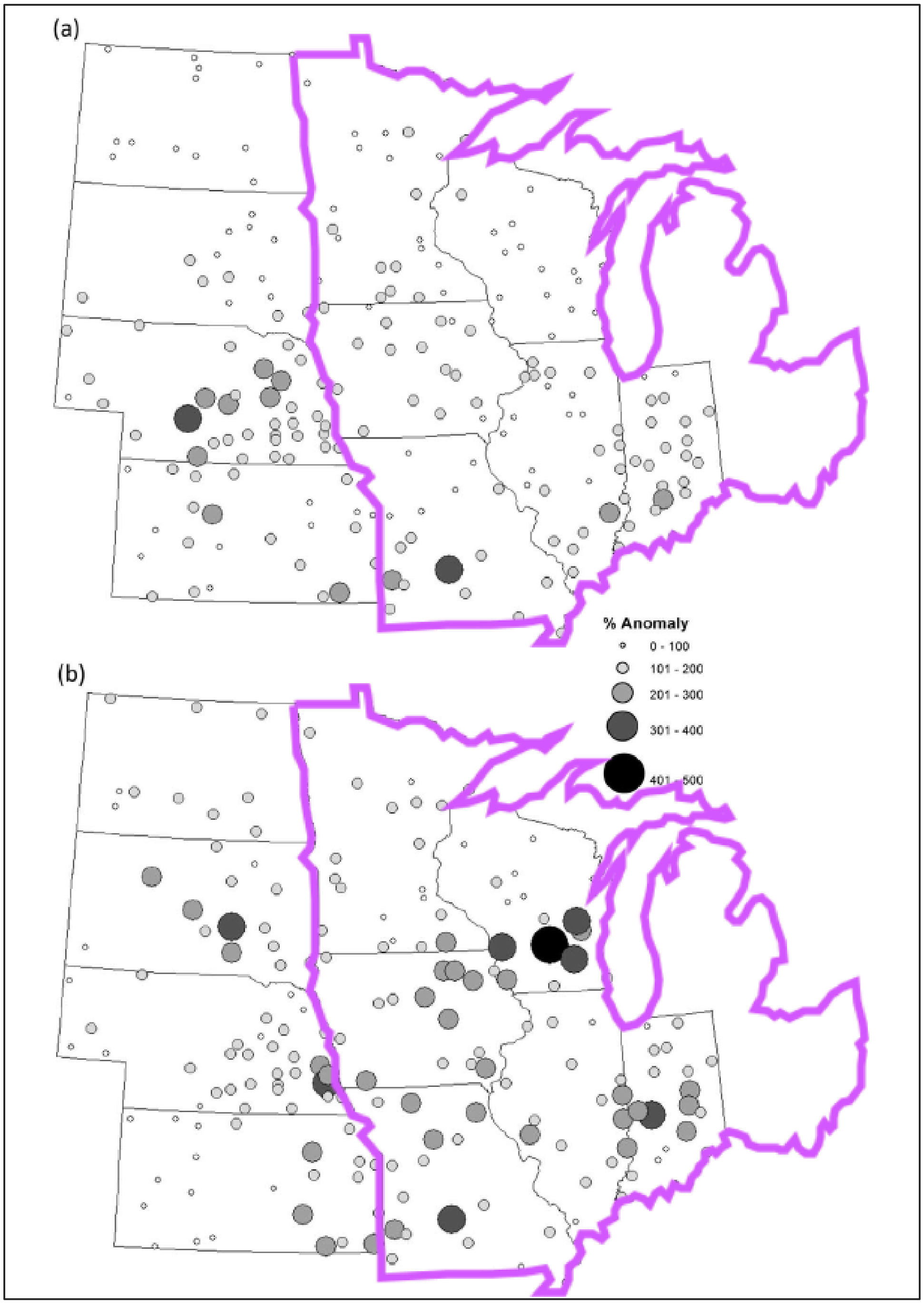

Figure 6.1. Monthly total precipitation anomaly at indicated locations in the Midwest during (a) May 2008 and (b) June 2008 compared to the 1971–2000 normals. (Source: Budikova et al. 2010)

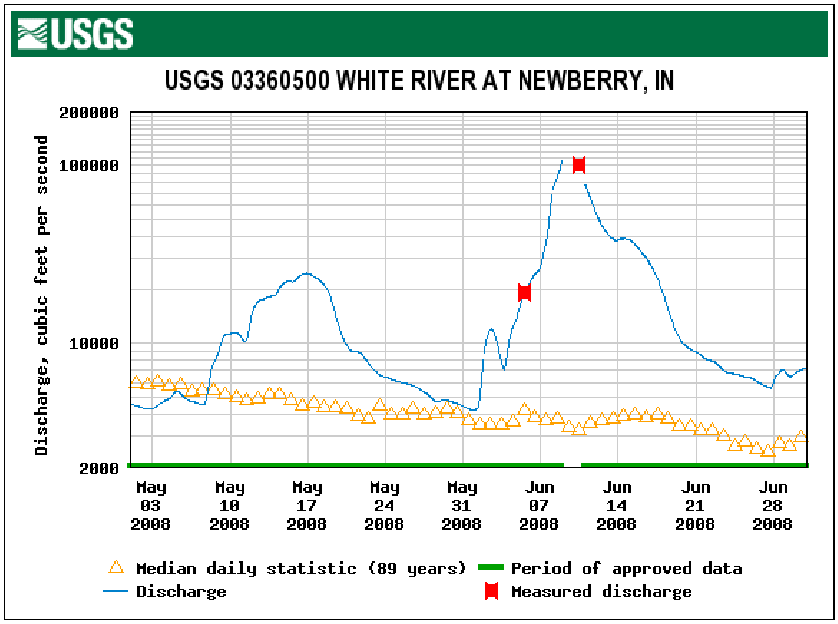

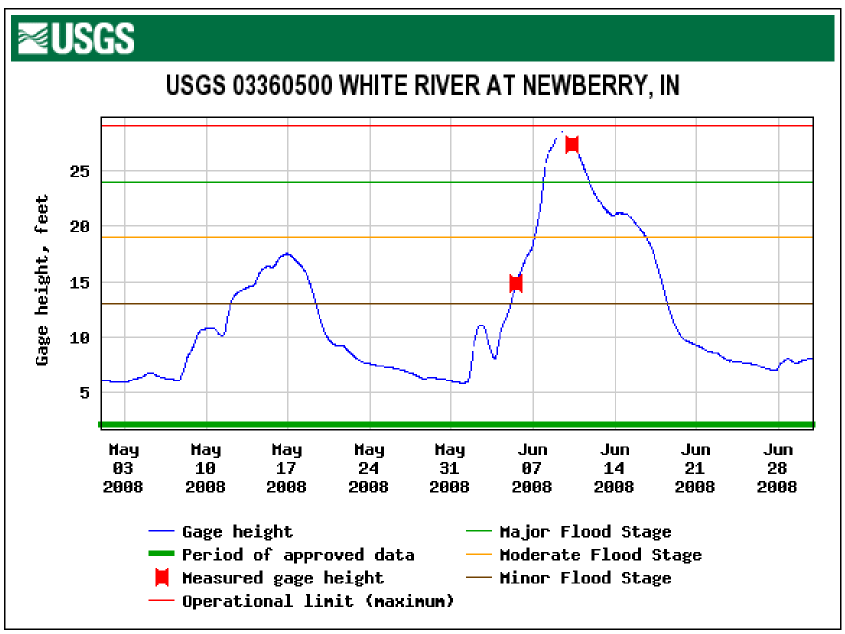

Figure 6.2. White River discharge (cfs, top panel) and stage (ft above gauge datum) during May and June 2008 at the USGS gauge. Peak discharge on June 9 was 138,000 cfs and the peak stage was 28.6 ft, both historical records. (Source: USGS National Water Information System)

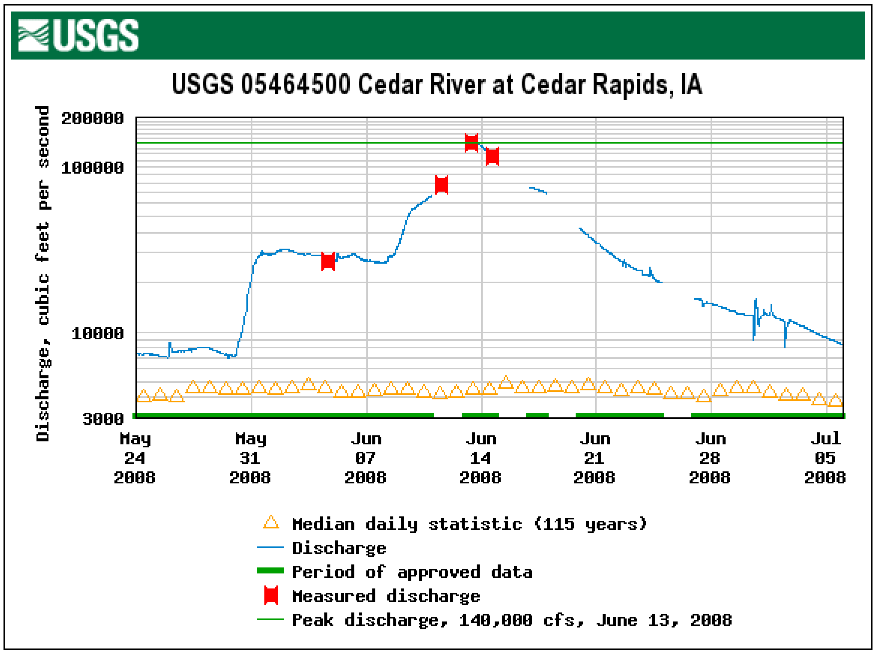

Figure 6.3. Cedar River discharge (cfs) during late May through early July 2008. Peak discharge on June 13 was 140,000 cfs, the historical record. (Source: USGS National Water Information System)

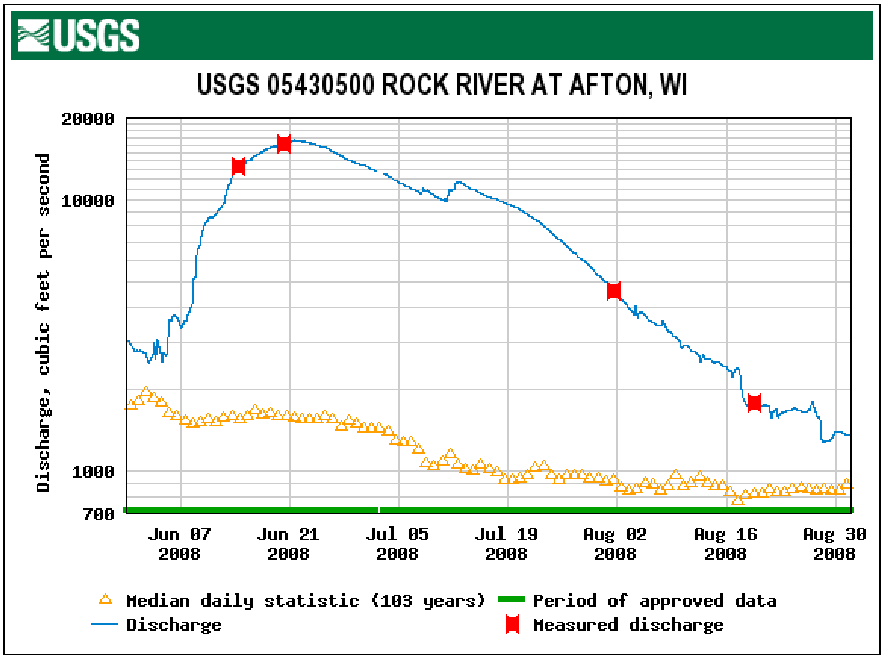

Figure 6.4. Rock River discharge (cfs) during June–August 2008 at the USGS gauge. Peak discharge on June 21 was 16,700 cfs, the historical record. (Source: USGS National Water Information System)

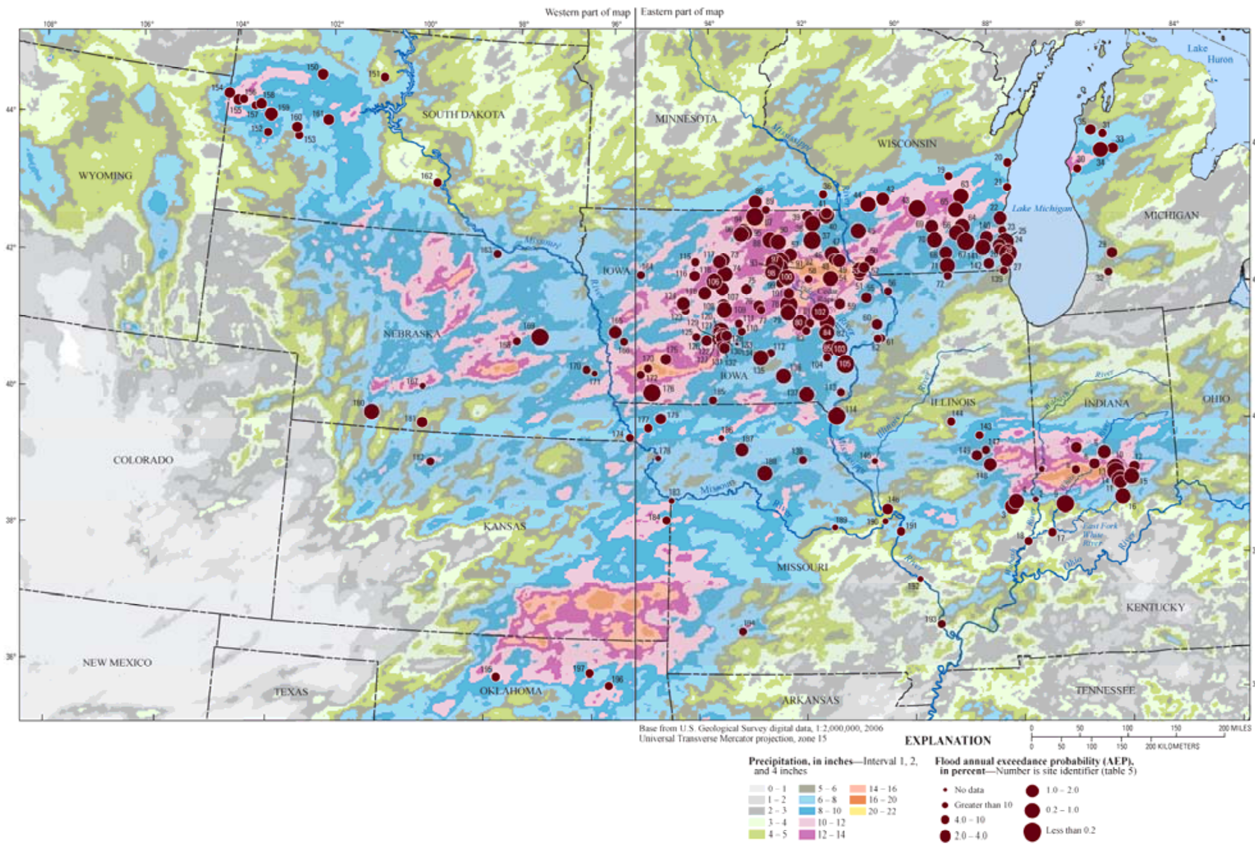

Figure 6.5. Accumulated precipitation over the Midwest from May 21 through June 14, 2008. The filled circles show the streamgauges where peak discharges corresponded to an annual exceedance probability of less than 0.1. The largest circles represent gauges where peak streamflow had estimated annual exceedance probabilities of 0.002 or less. (Source: USGS 2010)

6.1.2 2010 Southern Minnesota Floods

The Minnesota Department of Natural Resources Climate Office defines rainfall events in which the precipitation depth exceeds 6 in. over 1000 mi^2 and the precipitation depth at the core of the event exceeds 8 in. as “mega-rain” events (MNDNR 2018). Heavy rainfall during September 22–24, 2010, on wet antecedent conditions caused widespread flooding across southern Minnesota (Ellison et al. 2011) and was classified as a mega-rain event (Figure 6.6). Rainfall totals during summer were exceptionally high as a result of a wet June and heavy rainfall in August. The Minnesota State Climatology Office estimated that summer rainfall totals in southern Minnesota were as high as 20 in., exceeding the historical average by more than 4 in. The State Climatology Office also estimated that the rainfall total in September 2011 was the greatest going back to 1891. Rainfall events during the September 22–24 period were caused by remnants of two tropical storms, Georgette in the eastern Pacific Ocean and Hurricane Karl in the Gulf of Mexico, moving northward in the presence of low-pressure systems in the central plains. The total rainfall from September 22–24 at six locations ranged from 5.75 to 10.68 in.; by comparison, the 100-year, 72-hour rainfall for southern Minnesota is estimated to be about 7 in. (Ellison et al. 2011, Figure 6.7). During September 20–22, five of the six locations shown in Figure 6.7 received total rainfall exceeding the corresponding 100-year, 72-hour depth (Table 6.1).

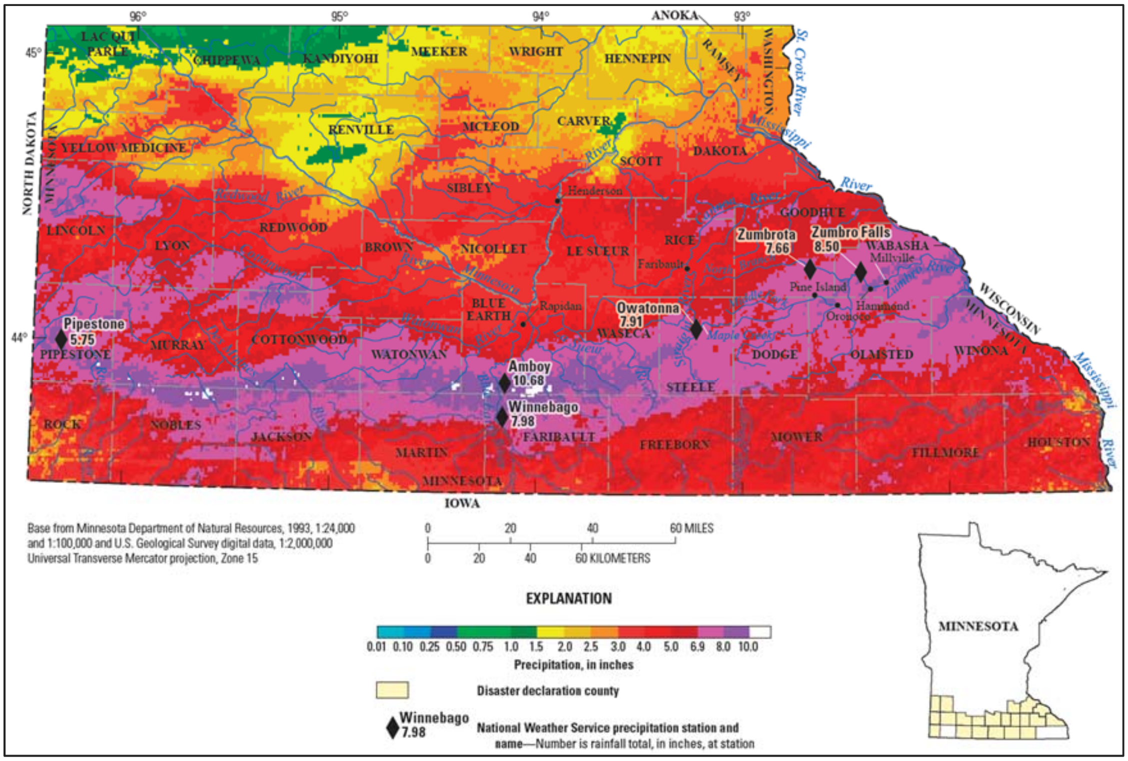

Figure 6.6. Rainfall totals during September 22–24, 2010 across southern Minnesota. (Source: Ellison et al. 2011)

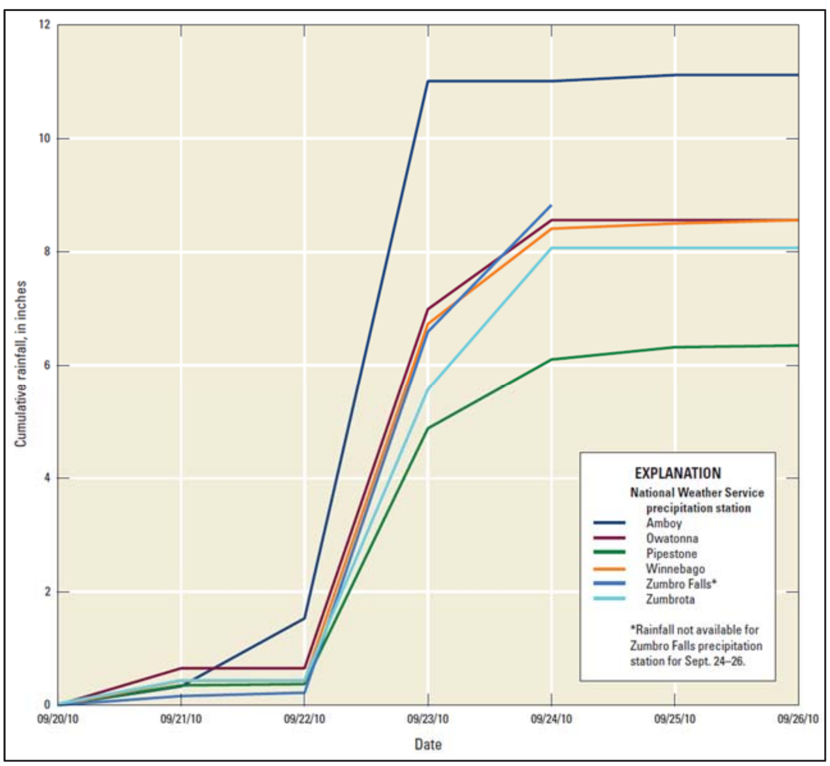

Figure 6.7. Cumulative daily rainfall during September 20–26, 2010 at selected National Weather Service stations. (Source: Ellison et al. 2011)

Table 6.1. Total rainfall during September 22–24, 2010 and corresponding 72-hour duration rainfall depth for selected annual exceedance probabilities. (Source: Ellison et al. 2011)

[Total rainfall from Minnesota Department of Natural Resources State Climate Office (2010c). Annual exceedance probabilities from Huff and Angel (1992). NWS, National Weather Service]

Station name (location shown in fig. 2)	County	NWS station identifier	Total rainfall (inches)	72-hour duration rainfall (inches) for selected annual exceedance probabilities[1]				
				0.20	0.10	0.04	0.02	0.01
Amboy, Minn.	Blue Earth	210157	10.68	4.06	4.77	5.67	6.43	7.08
Owatonna, Minn.	Steele	216287	7.91	4.06	4.77	5.67	6.43	7.08
Pipestone, Minn.	Pipestone	216565	5.75	3.96	4.57	5.50	5.93	7.13
Winnebago, Minn.	Faribault	219046	7.98	4.06	4.77	5.67	6.43	7.08
Zumbro Falls, Minn.	Wabasha	219231	8.50	4.35	4.97	5.74	6.30	6.83
Zumbrota, Minn.	Goodhue	219249	7.66	4.35	4.97	5.74	6.30	6.83

Ellison et al. (2011) reported that discharges between September 23 and October 2, 2010 at 12 streamgauges exceeded their previous historical maximums. Of these 12 streamgauges, 10 also exceeded their previously recorded maximum stage. The peak discharge at seven of these streamgauges had estimated annual exceedance probabilities of less than 0.002.

6.1.3 2011 Mississippi and Red River of the North Floods

The weather over the Midwest Region during December 2010 through July 2011 was influenced by a La Niña that usually results in cooler and wetter than normal conditions over the upper Mississippi River and Red River of the North (Red River) basins (USGS 2011b). During winter and spring of 2010–2011, the upper Mississippi and the Red River basins received above-normal precipitation as snowfall (Figure 6.8). During the eight months from December 2010 through July 2011, several states in the Midwest received above-normal precipitation (compared to the 1971–2000 normals), sometimes significantly exceeding respective normals (USGS 2011b). The number of months from December 2010 through July 2011 that received normal or above-normal precipitation for Illinois, Indiana, Iowa, Minnesota, Missouri, Ohio, and Wisconsin were four, five, five, seven, four, four, and six, for the respective states. In the upper Mississippi River basin, precipitation was variable spatially, but Minnesota recorded the third-wettest December, and January snowfall was 100 percent above normal from northeastern Minnesota through northern Iowa (USGS 2011b). In the Red River of the North basin, precipitation totals were much greater than normal during April through June 2011.

Stream discharges across the central United States, including nearly all of the Midwest Region, showed major flood peaks during 2011 (USGS 2011a, see Figure 6.9). Peak streamflow exceeded the historical maximum at 105 streamgauges in the Mississippi and the Red/Souris River basins. Annual runoff volumes exceeded historical maximums at 47 of 211 streamgauges in the Mississippi and the Red/Souris River basins (USGS 2011c). Flooding in the middle and lower Mississippi River basins started in February and March of 2011. Snowmelt-caused flooding in the Red River and upper Mississippi River basins occurred in late March and early April 2011. Another flood occurred in the Souris River basin, a part of the Red River basin, in June 2011. These floods were caused by various combinations of saturated soils, higher-than-normal antecedent streamflow, rapid melting of above-average snowpack, and large amounts of precipitation (USGS 2011c).

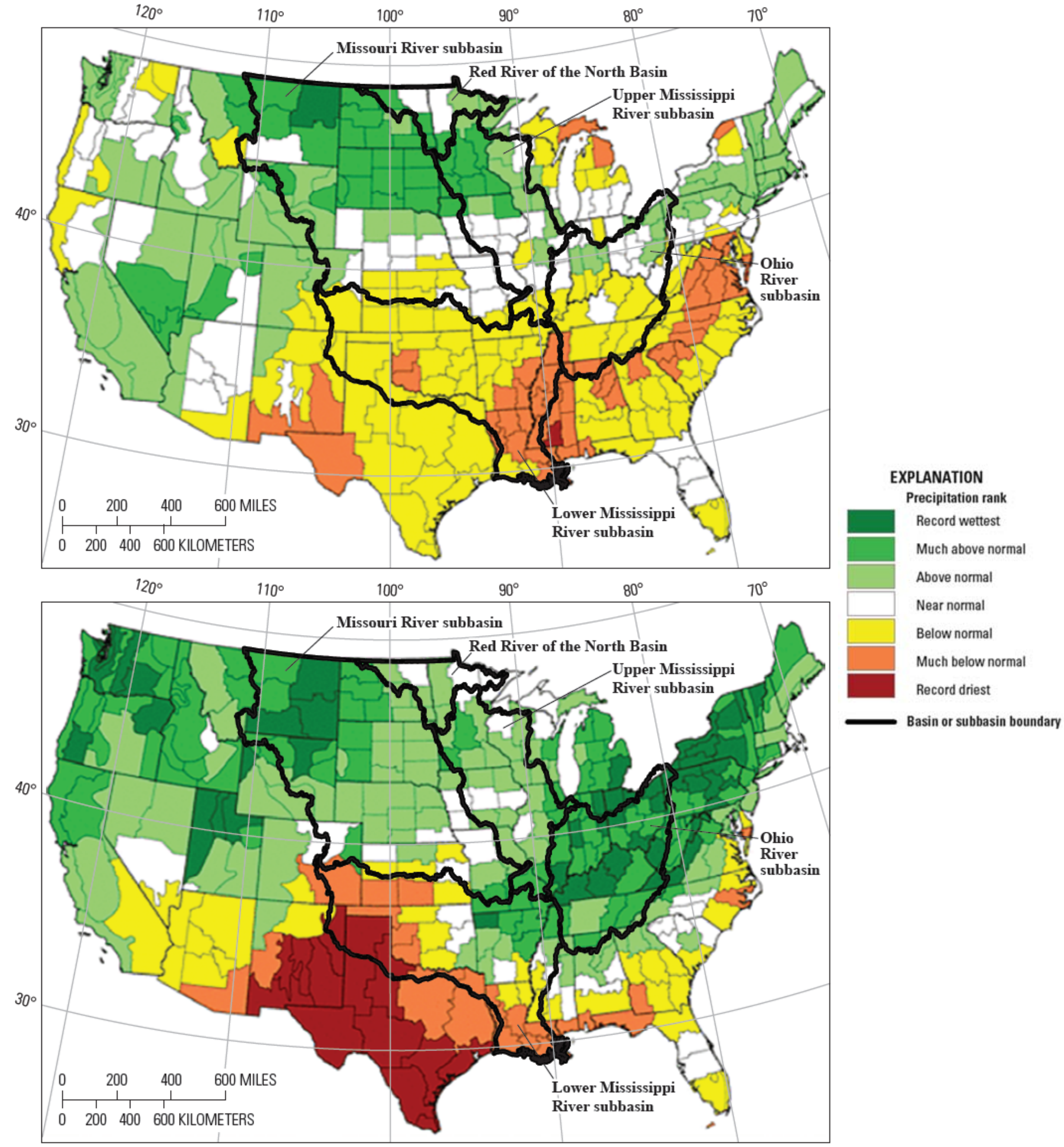

Figure 6.8. Precipitation during 2010-2011 winter (December 2010–February 2011, top panel) and spring (March–May 2011, bottom panel). (Source: USGS 2011b)

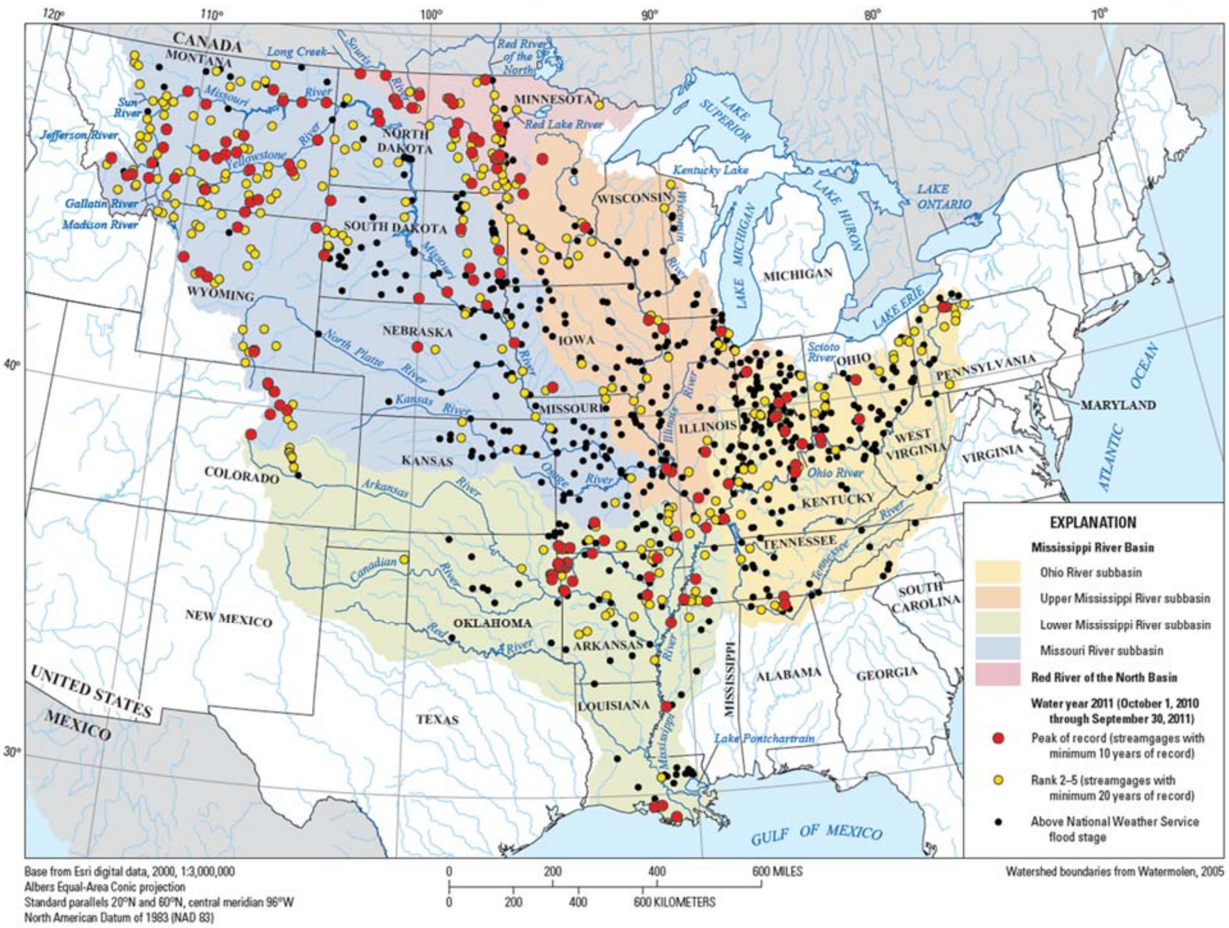

Figure 6.9. Major flood discharges during the 2011 floods. (Source: USGS 2011c)

USGS (2011c) estimated annual exceedance probabilities for 2011 peak discharges at 321 streamgauges and annual runoff volumes at 211 streamgauges located in the five river basins shown in Figure 6.10. In the Souris River basin, 6 of 11 streamgauges exceeded their previous maximum peak discharge by at least 100 percent. The annual exceedance probability for 2011 peak discharges at all of the six streamgauges was 0.01 or less. In the Souris River basin, at all seven of the analyzed streamgauges, annual runoff volume had estimated annual exceedance probabilities of less than 0.01. In the Red River of the North basin, estimated exceedance probabilities for annual runoff volumes were less than 0.002 at two streamgauges, between 0.002 and 0.01 at five streamgauges, and between 0.01 and 0.02 at four streamgauges. Figure 6.10 shows the estimated annual exceedance probabilities for the 2011 peak discharges. Figure 6.11 shows the estimated annual exceedance probabilities for the 2011 annual runoff volumes.

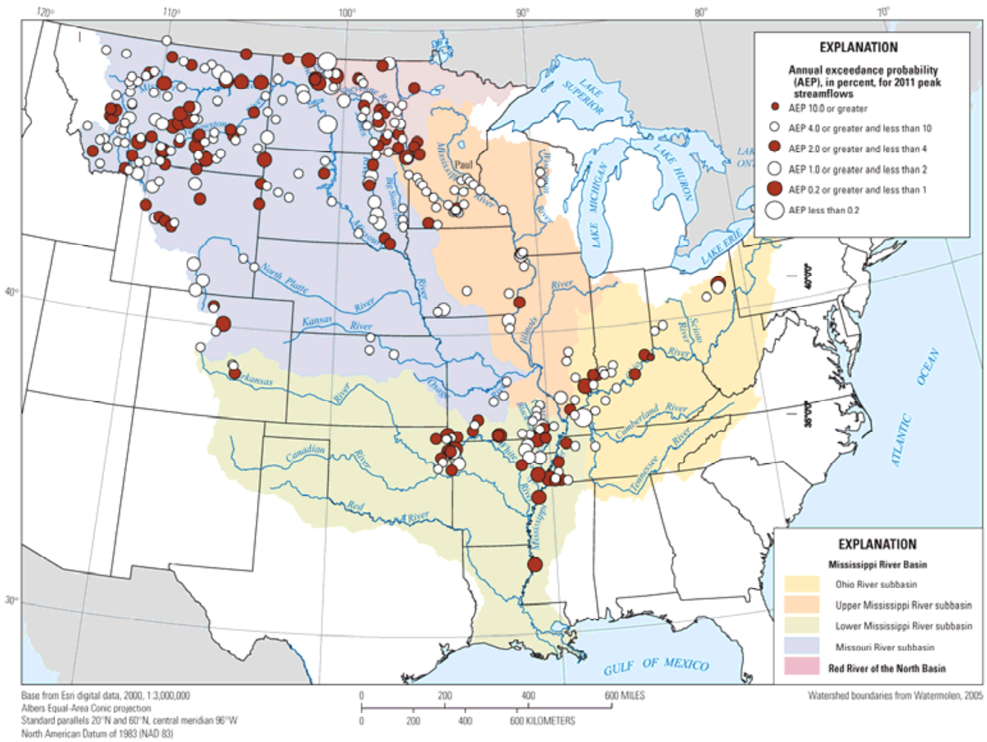

Figure 6.10. Estimated annual exceedance probabilities for the 2011 peak discharges. (Source: USGS 2011a)

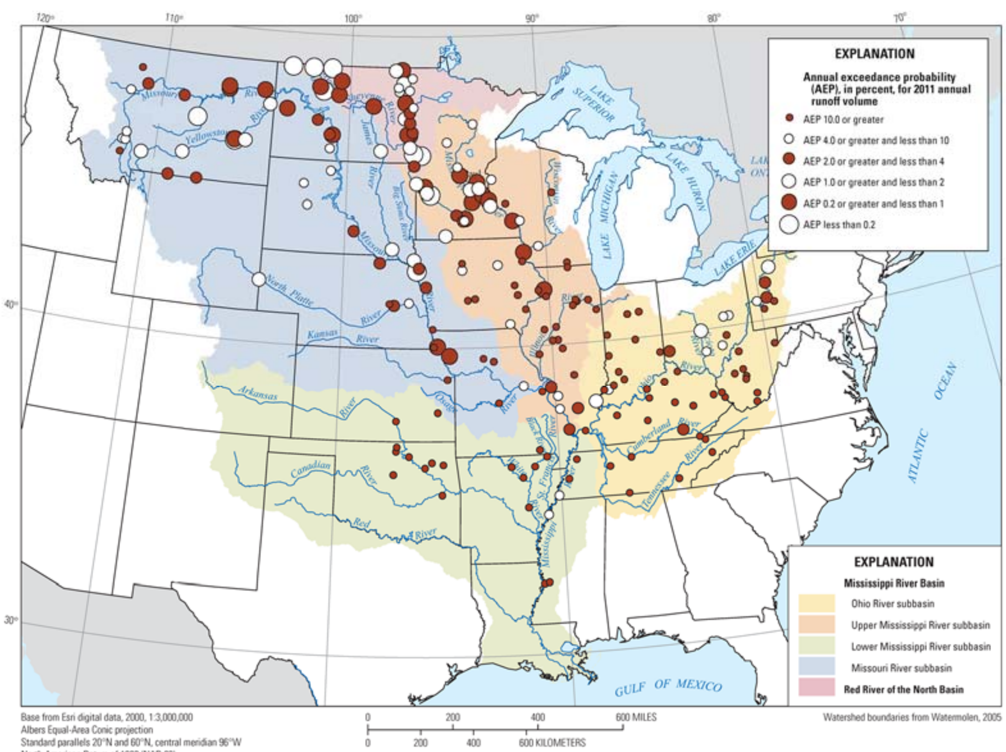

Figure 6.11. Estimated annual exceedance probabilities for the 2011 annual runoff volumes. (Source: USGS 2011a)

6.1.4 2017 Spring Floods

On the afternoon of April 28, 2017, a stationary front that extended from southeastern Missouri to the southwest across west-central Arkansas and south-central Oklahoma started moving north as a warm front (NWS 2018). Moisture from the Gulf of Mexico started moving northward up and over the warm front. A series of low-pressure systems moved northeast along the front producing thunderstorms that resulted in continuous heavy rainfall on April 29, 2017. Storm total rainfall ranged from 4 in. to over 10 in., and some places in south-central Missouri received up to 12 in. of rainfall (Figure 6.12 and Figure 6.13).

The heavy rainfall from the storm resulted in historical flooding in the Meramec and Gasconade Rivers. Meramec River near Steelville, Missouri, has a contributing area of 781 mi^2. The river exceeded its historical maximum stage and the historical peak discharge (Figure 6.14). On May 1, 2017, Meramec River near Sullivan, Missouri, which has a contributing area of 1475 mi^2, also exceeded its previous historical maximum stage and discharge (Figure 6.15). On May 2, 2017, Meramec River near Eureka, Missouri, which has a contributing area of 3788 mi^2, also exceeded its previous historical maximum stage and the corresponding discharge was the second greatest on record (Figure 6.16). On May 2, 2017, Gasconade River near Rich Fountain, Missouri, exceeded both its previous maximum stage and discharge (Figure 6.17).

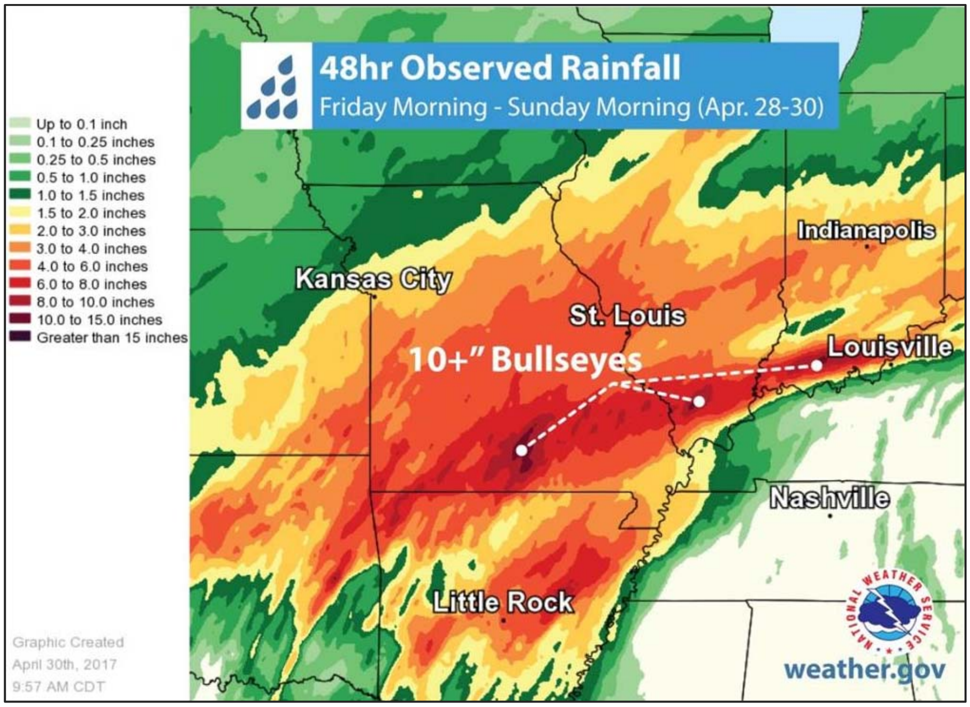

Figure 6.12. Regional 48-hour rainfall totals during the April 28–30, 2017 storm. (Source: National Weather Service)

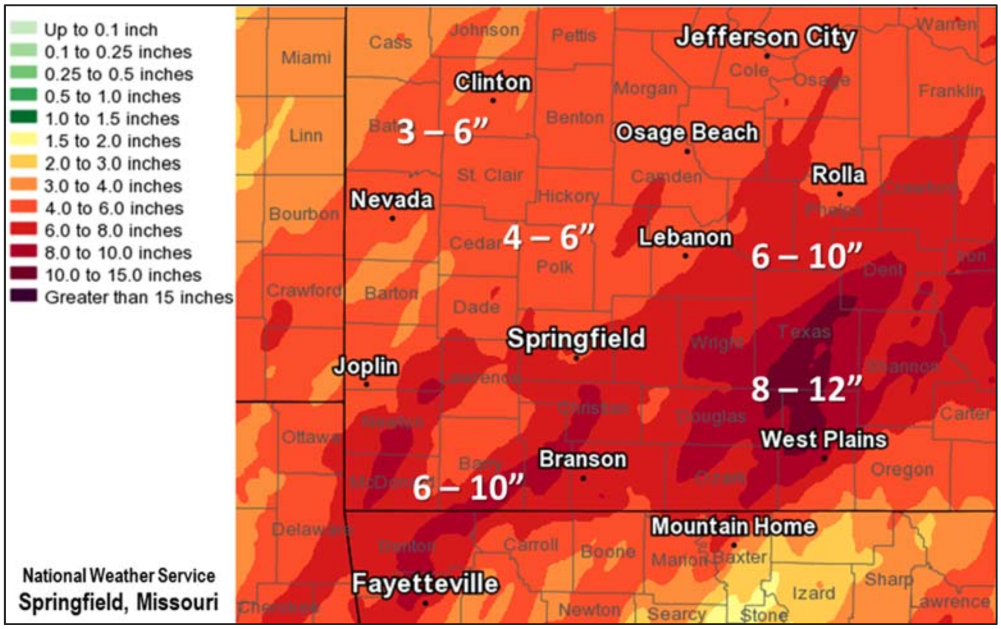

Figure 6.13. Accumulated rainfall over southern Missouri during the April 28–30, 2017 storm. (Source: National Weather Service)

6.2 Hydrologic Cycle, Streamflow, and Floods

NCA3 stated that the increasing trends of extreme rainfall events and flooding are expected to continue in the future (Pryor et al. 2014). Flooding in the Midwest Region occurs both as a result of spring rainfall and/or snowmelt and summer heavy rainfall (see Chapter 3). Runoff from these events is also affected by expanding urban areas and associated reductions in infiltration.

6.2.1 Observed Changes in Streamflow

Peterson et al. (2013) noted that long-term data (100 years) from midwest catchments that have experienced little or no land-use/water-management changes show increase in flooding in parts of the Midwest, especially over the last few decades and land management practices were noted as a potential contributing factor. The range trends in peak annual discharge over the Midwest was reported to be -10 to +15 percent per decade with some regional-scale similarity with total annual precipitation trends (Figure 6.18).

Mallakpour and Villarini (2015) analyzed daily streamflow in the central United States using 774 USGS streamgauges with 50 years (1962–2011) of record. They selected annual peak daily discharge from the record, and for the peaks-over-threshold method, they selected the threshold such that on average two flood events were selected per year. To detect abrupt changes in annual maximum flood discharges, they used the Lombard test (Lombard 1987). When abrupt changes were present in annual maximum discharge records, monotonic trends were detected using Mann-Kendall test for the most recent period. When abrupt changes were present, segmented regression was used for peaks-over-threshold flood count data. Accounting for abrupt changes affected the flood magnitude trends significantly; however, the flood frequency trends were relatively unaffected (Figure 6.19).

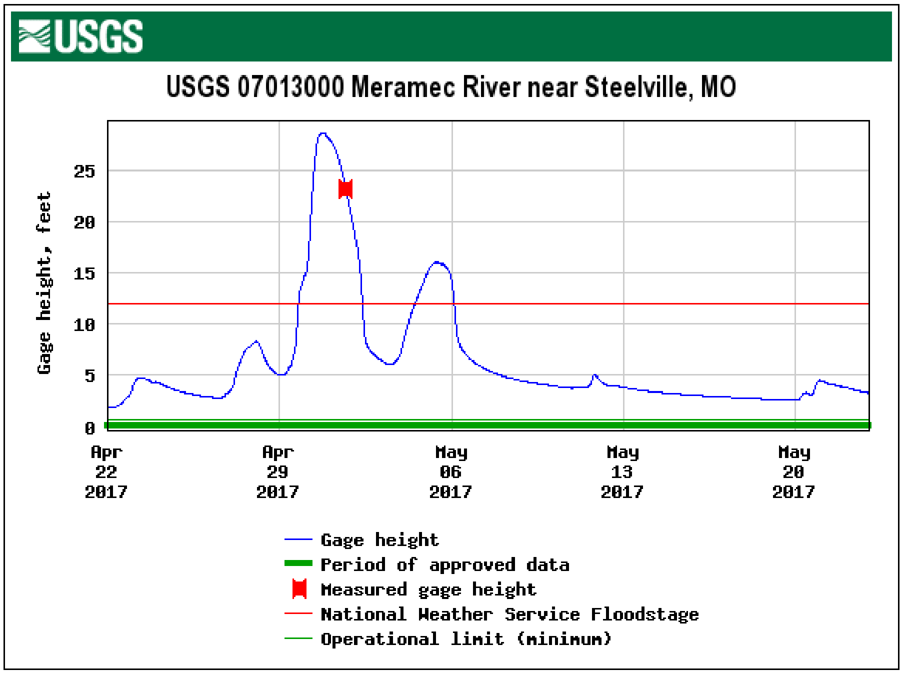

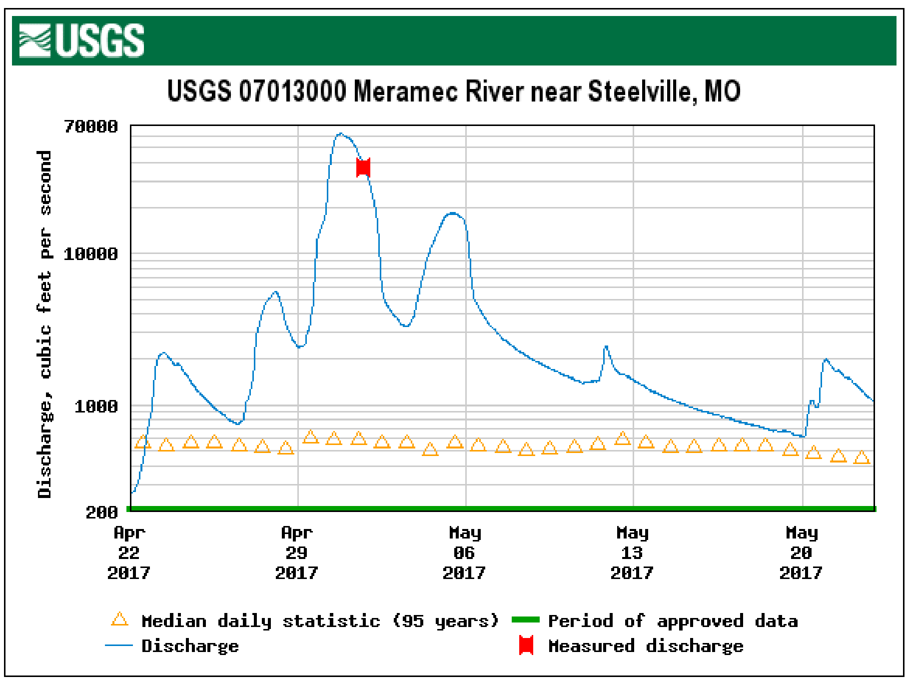

Figure 6.14. Stage (top panel) and discharge (bottom panel) hydrographs for Meramec River near Steelville, Missouri. The stage of 28.71 ft and discharge of 62,200 cfs, both historical maximums, were recorded on April 30, 2017. (Source: USGS National Water Information System)

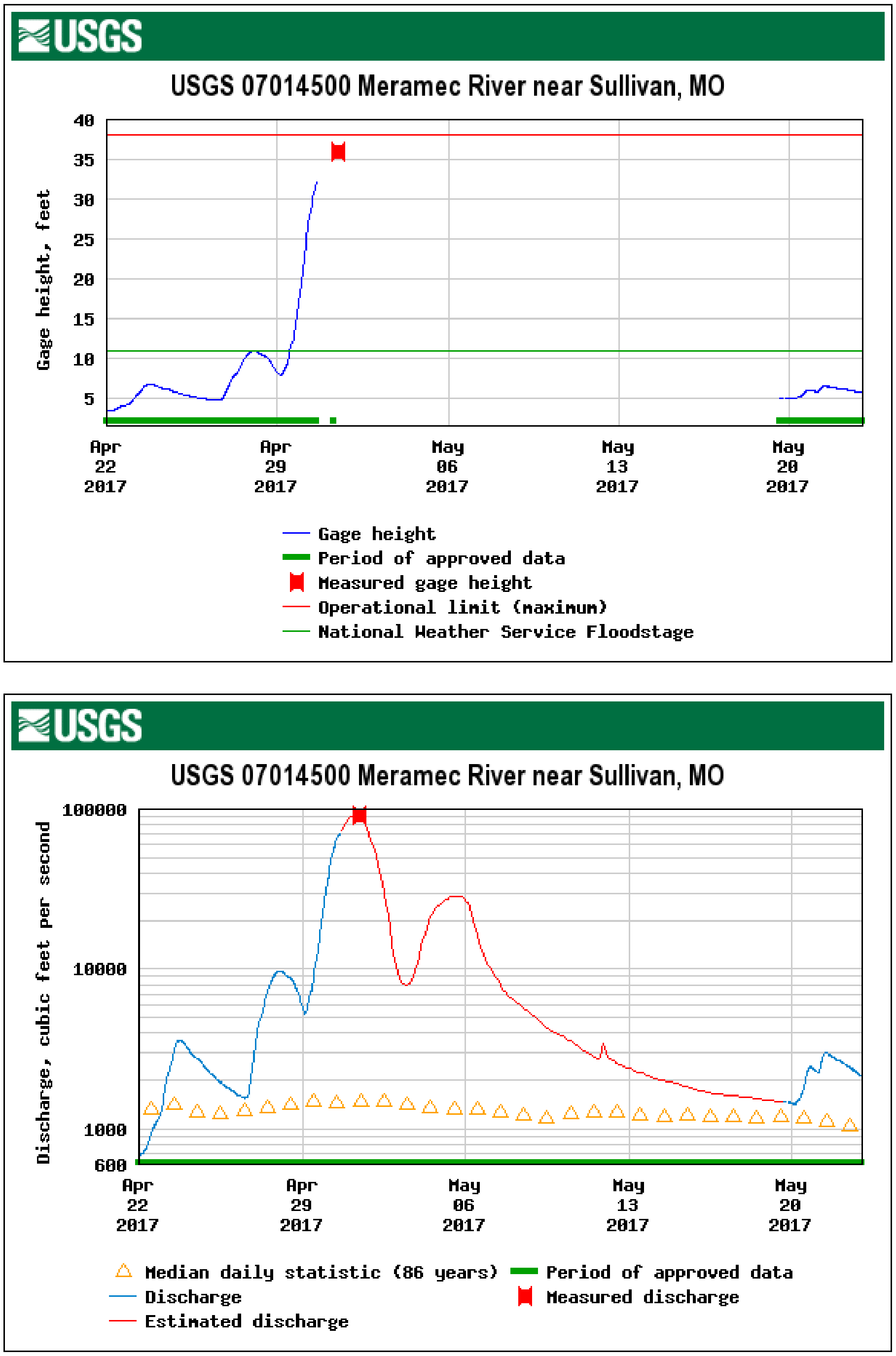

Figure 6.15. Stage (top panel) and discharge (bottom panel) hydrographs for Meramec River near Sullivan, Missouri. The stage of 36.38 ft and discharge of 95,300 cfs, both historical maximums, were recorded on May 1, 2017. (Source: USGS National Water Information System)

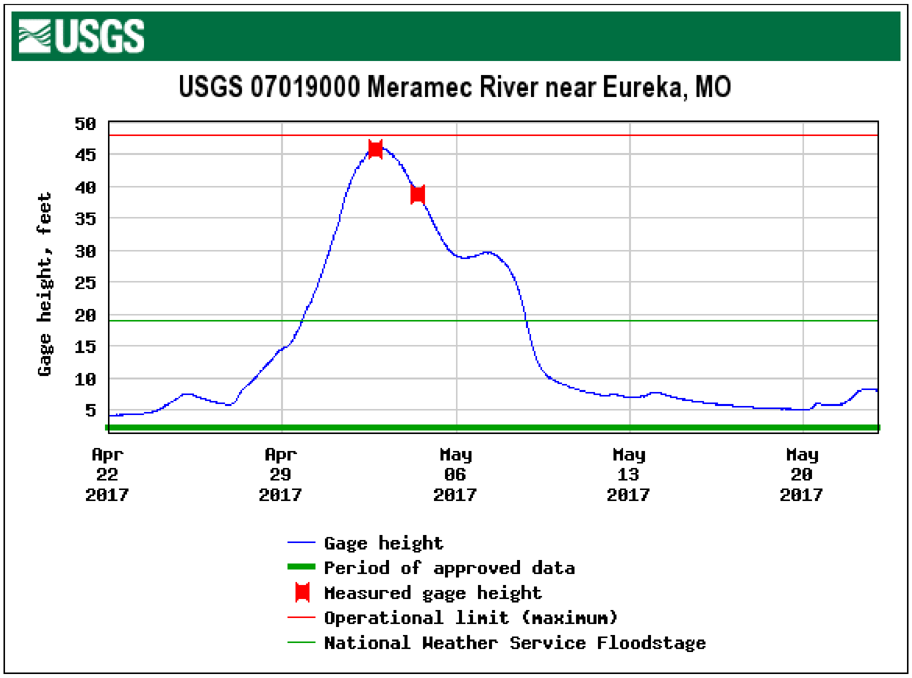

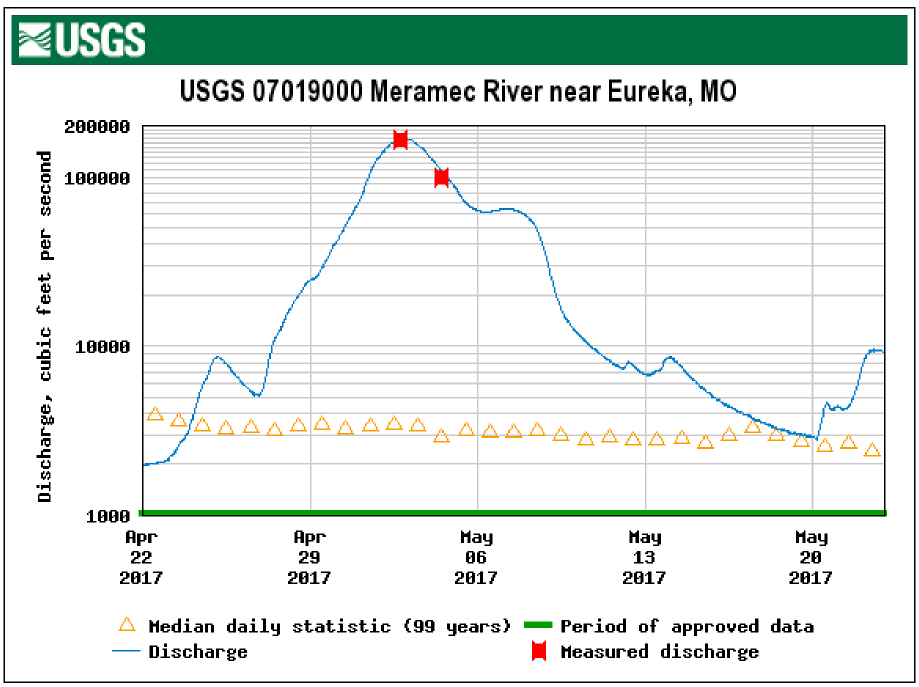

Figure 6.16. Stage (top panel) and discharge (bottom panel) hydrographs for Meramec River near Eureka, Missouri. Recorded on May 2, 2017, the stage of 46.11 ft was the historical maximum and the peak discharge of 169,000 cfs was the second greatest on record. (Source: USGS National Water Information System)

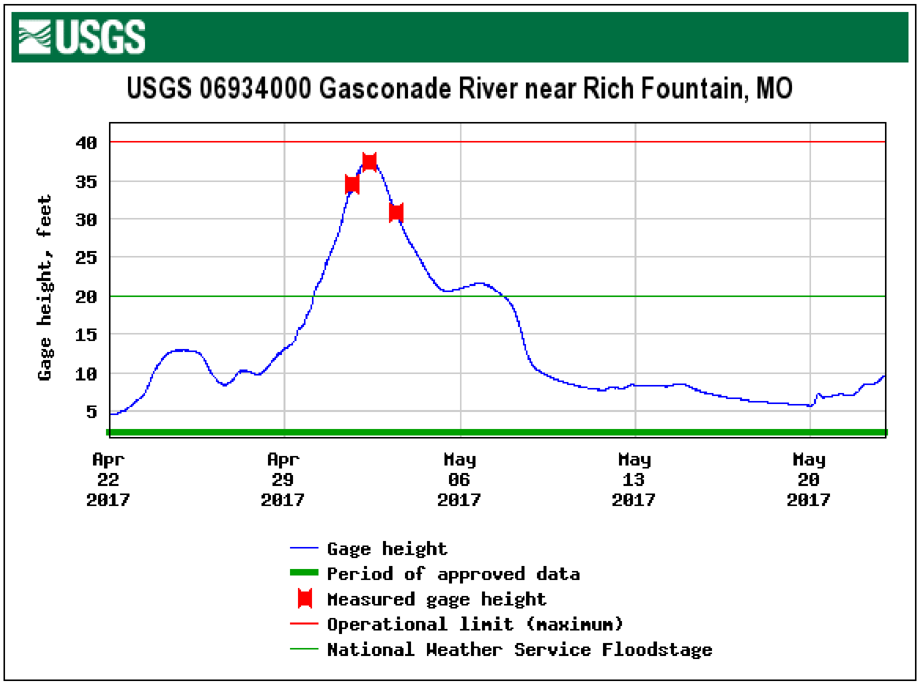

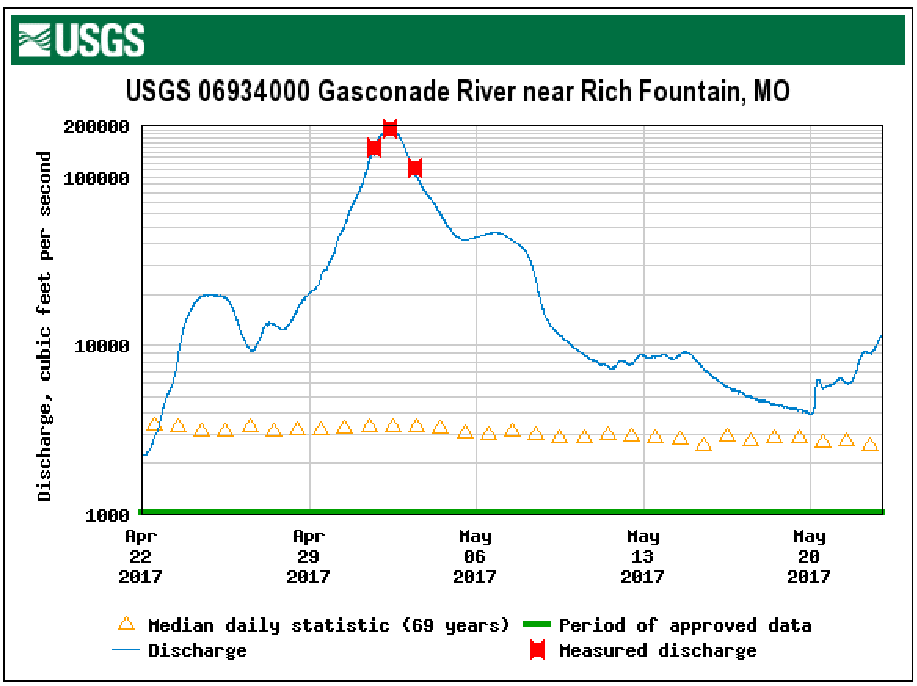

Figure 6.17. Stage (top panel) and discharge (bottom panel) hydrographs for Gasconade River near Rich Fountain, Missouri. The stage of 37.47 ft and discharge of 190,000 cfs, both historical maximums, were recorded on May 2, 2017. (Source: USGS National Water Information System)

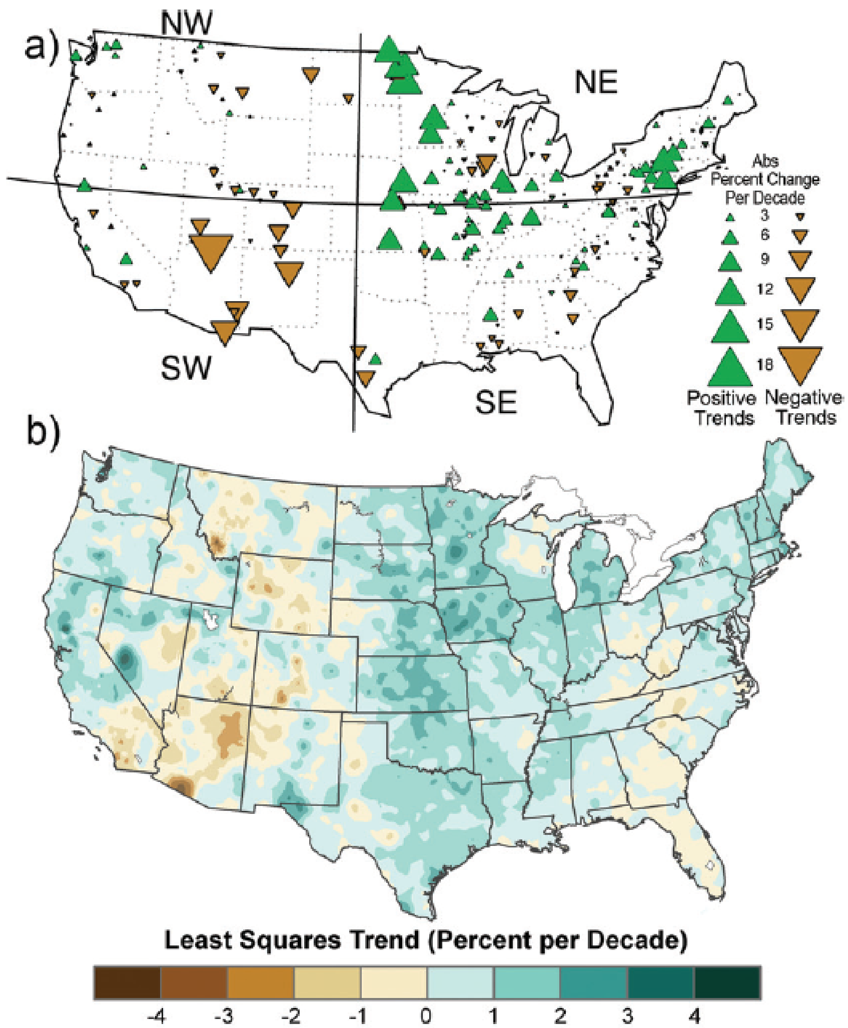

Figure 6.18. Trends in (a) annual flood magnitudes and (b) total annual precipitation. (Source: Peterson et al. 2013)

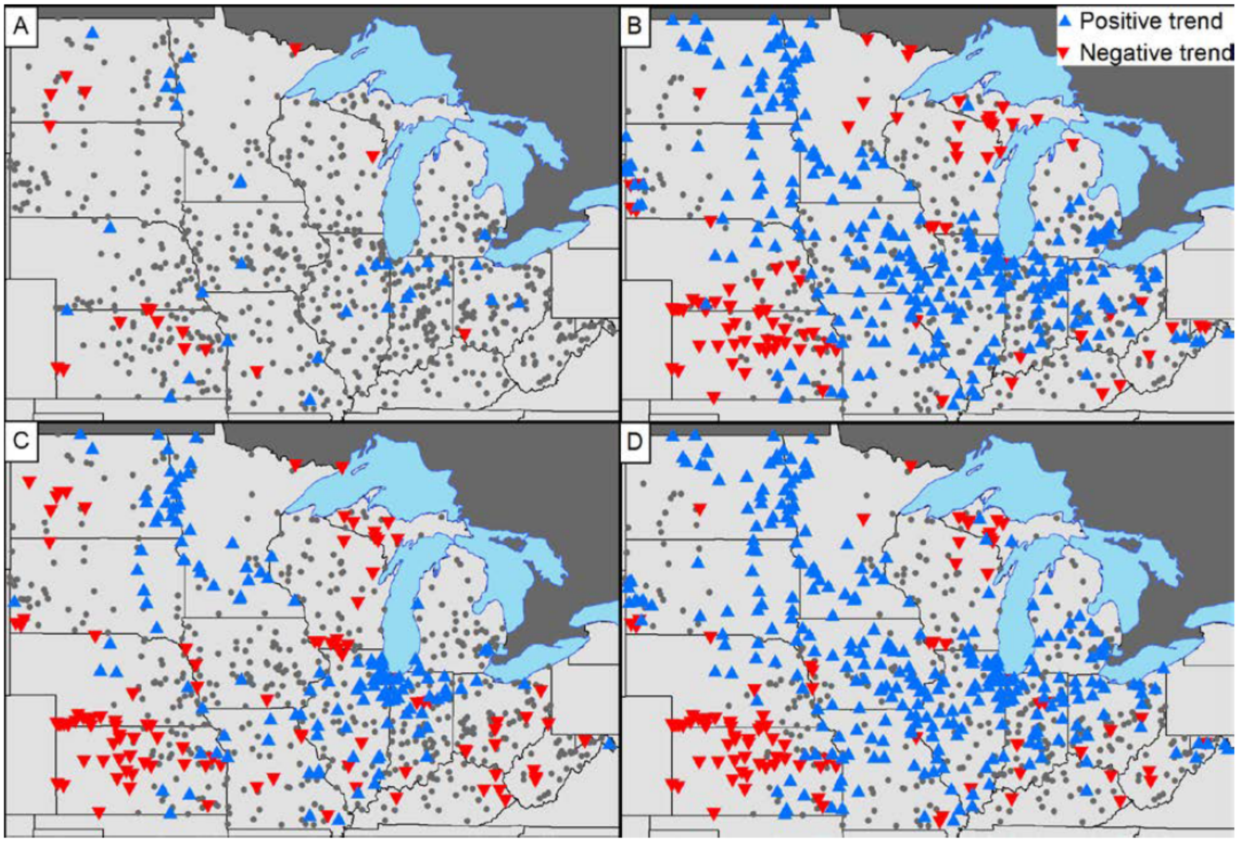

Figure 6.19. Trends in flood magnitudes (panels A and C) and frequency (B and D) accounting for (panels A and B) and not accounting for (panels C and D) abrupt changes. As shown, the spatial pattern of flood frequency trends is largely preserved when abrupt changes are considered; however, the spatial pattern of flood magnitude trends, while still evident, is largely suppressed. (Source: Mallakpour and Villarini 2015, supplemental information)

In their paper, Mallakpour and Villarini (2015) showed trends in flood magnitude and frequency (count of flood magnitude exceeding a threshold) without accounting for abrupt changes in the historical data. For this reason, the following description of flood magnitude trends should be interpreted allowing for the evidence in Figure 6.19. When they examined trends in annual maximum daily discharge magnitudes, no statistically significant trends were identified over much of the central U.S. (Figure 6.20a, top panel). Of the streamflow gauges analyzed, 20 percent showed statistically significant trends in flood magnitude and 13 percent showed an increasing trend in flood magnitude. However, when Mallakpour and Villarini (2015) analyzed the frequency of flood events using a peaks-over-threshold approach, 34 percent of the gauges showed an increasing trend and 9 percent showed a decreasing trend (Figure 6.20b, bottom panel).

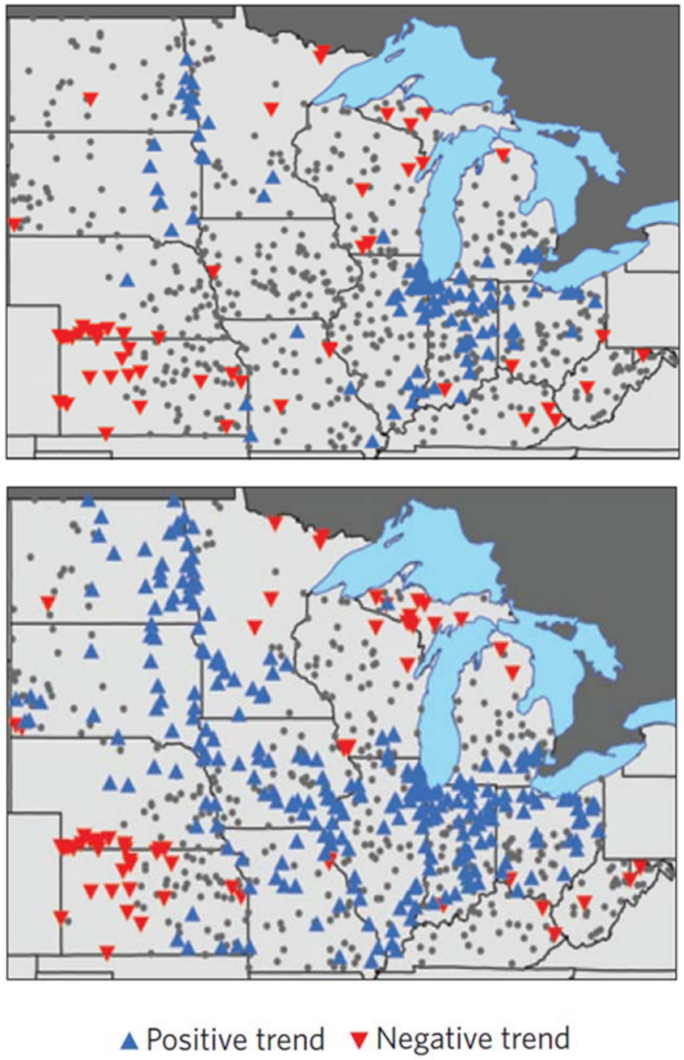

Figure 6.20. Trends in daily streamflow over the midwest: (a) top panel: trends in historical annual maximum daily discharge magnitudes, and (b) bottom panel: trends in historical frequency of flood events. (Source: Mallakpour and Villarini 2015, Figure 1)

Analyzing the seasonal trends for the period 1962–2011, Mallakpour and Villarini (2015) found that during spring and summer (the seasons where floods over most of the region occur), 6 and 30 percent of the gauges showed increasing trends in flood magnitude, respectively (Figure 6.21). Summer flood magnitude increases were mostly in the eastern part of the Midwest Region (Figure 6.21, bottom-left panel). Increases in flood frequency for spring and summer were reported to be similar to those at the annual scale; 18 and 28 percent, respectively, of the gauges showed statistically significant increases (Figure 6.21, right panels). Mallakpour and Villarini (2015) noted that changes in regional flooding behavior reflect the integrating effects of climate, stream dynamics, and watershed properties. To examine the underlying causes for detected changes in flooding over the region, Mallakpour and Villarini (2015) analyzed annual maximum daily rainfall and the number of days exceeding the 95th percentile of the rainfall distribution (Figure 6.22). Based on their analyses, Mallakpour and Villarini (2015) concluded that while there is limited evidence of significant changes in magnitude of peak floods, the frequency of flooding is increasing in the midwest. They attributed this change to both changes in seasonal rainfall and temperatures across the region.

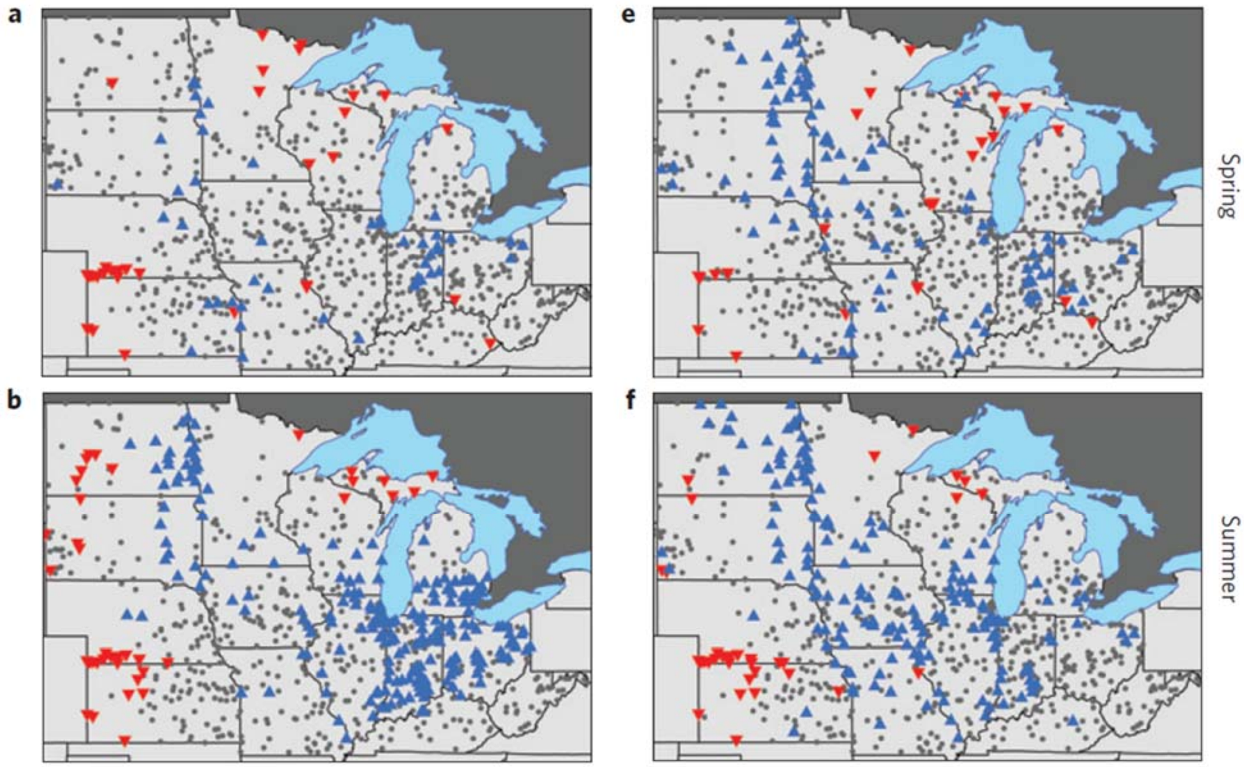

Figure 6.21. Spring and Summer trends in the seasonal flood magnitude (left panels) and frequency (right panels) for 1962–2011. (Source: Mallakpour and Villarini 2015, Figure 2)

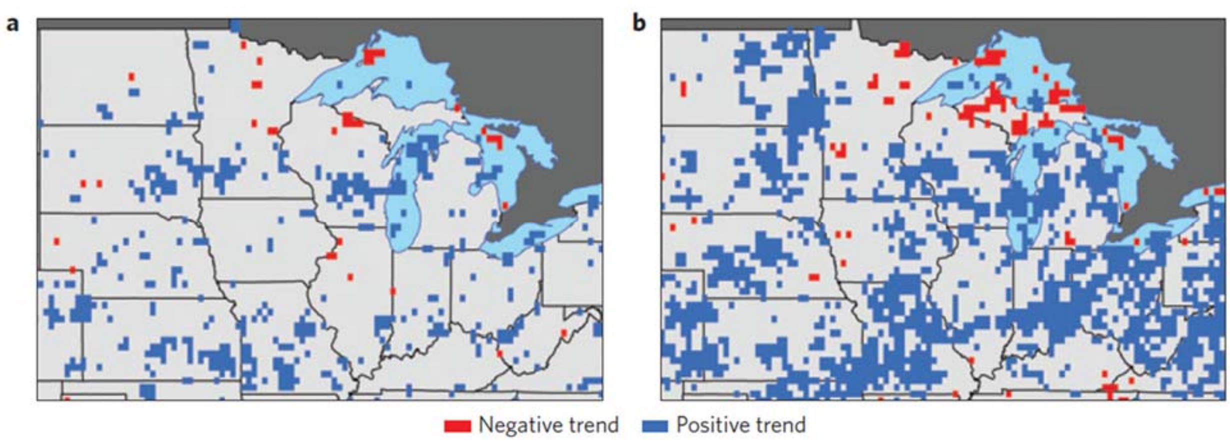

Figure 6.22. Trends in the magnitude of annual maximum daily rainfall (left panel) and number of days exceeding the 95th percentile of the rainfall distribution. (Source: Mallakpour and Villarini 2015, Figure 3)

Mallakpour and Villarini (2016) investigated whether five climate indices—the North Atlantic Oscillation (NAO), the Southern Oscillation Index (SOI), the Pacific Decadal Oscillation (PDO), the AMO, and the Pacific-North American pattern (PNA)—could describe the observed variability in flood frequencies over a central U.S. study area (same area as that used by Mallakpour and Villarini [2015]). They used daily streamflow records from 774 USGS gauges. They used NOAA Climate Prediction Center 0.25-degree gridded precipitation data based on daily observations. The analysis was conducted for four seasons—spring (March-April-May), summer (June-July-August), fall (September-October-November), and winter

(December-January-February). For NAO, the authors used a seasonally and geographically changing NAO index for 1948–2012 using the 2.5-degree monthly mean sea-level pressure reanalysis data set from National Centers for Environmental Prediction-National Center for Climate Research. The 1951–2012 SOI, the 1948–2012 PDO index, the 1948–2012 AMO index, and the 1950–2012 PNA index were obtained from the NOAA Climate Prediction Center.

Mallakpour and Villarini (2016) estimated the frequency of flood events using a peaks-over-threshold method with a threshold that, on average, identified two flood events per year. The precipitation threshold was set to 95th percentile of each grid cell's distribution. Using the streamflow and precipitation threshold, the authors counted the number of events exceeding the threshold for every season. The flood and extreme precipitation count data was correlated with the climate indicators using Poisson regression. The climate indices were assumed to influence the (seasonal) occurrence rate parameter of the Poisson distribution describing the number of occurrences of precipitation and flood events. The authors used multiple Poisson regression (a total of 31 different models) to find the optimal climate index or set of climate indices that describes the temporal variability of seasonal flood frequency for the 1951–2011 common period. The authors first selected a subset of all models for which the estimated coefficients relating the climate indices to the occurrence rate parameter were different from zero at the 10 percent significance level. Then the authors selected the final model, which has the smallest Akaike information criterion[1] value. Results from the final model are shown in Figure 6.23 through Figure 6.27. The authors noted that over the study area, floods showed statistically significant relationship with several climate indices as shown in Table 6.2.

Moreover, Mallakpour and Villarini (2016) reported that the geographical pattern of relationships between the climate indices and frequency of flooding appeared to be more important than the fraction of streamflow gauges showing statistically significant relationships. The region stretching from southern Minnesota to Missouri showed a positive relationship between PDO and frequency of flooding while a negative relationship exists for northern Minnesota, Wisconsin, and Michigan (Figure 6.23a). During summer, a region stretching from Ohio through Indiana, Illinois, and Iowa into southern Minnesota showed a positive relationship with PDO (Figure 6.23b). During fall, Wisconsin, southern Illinois, parts of Indiana and Ohio, and Missouri show floods positively related to PDO (Figure 6.23c).

[1] Akaike information criterion is an estimator of the relative quality of statistical models fit to a data set (Akaike 1974). The criterion is based on information content of statistical models; it balances the number of parameters used in a model with the corresponding goodness-of-fit.

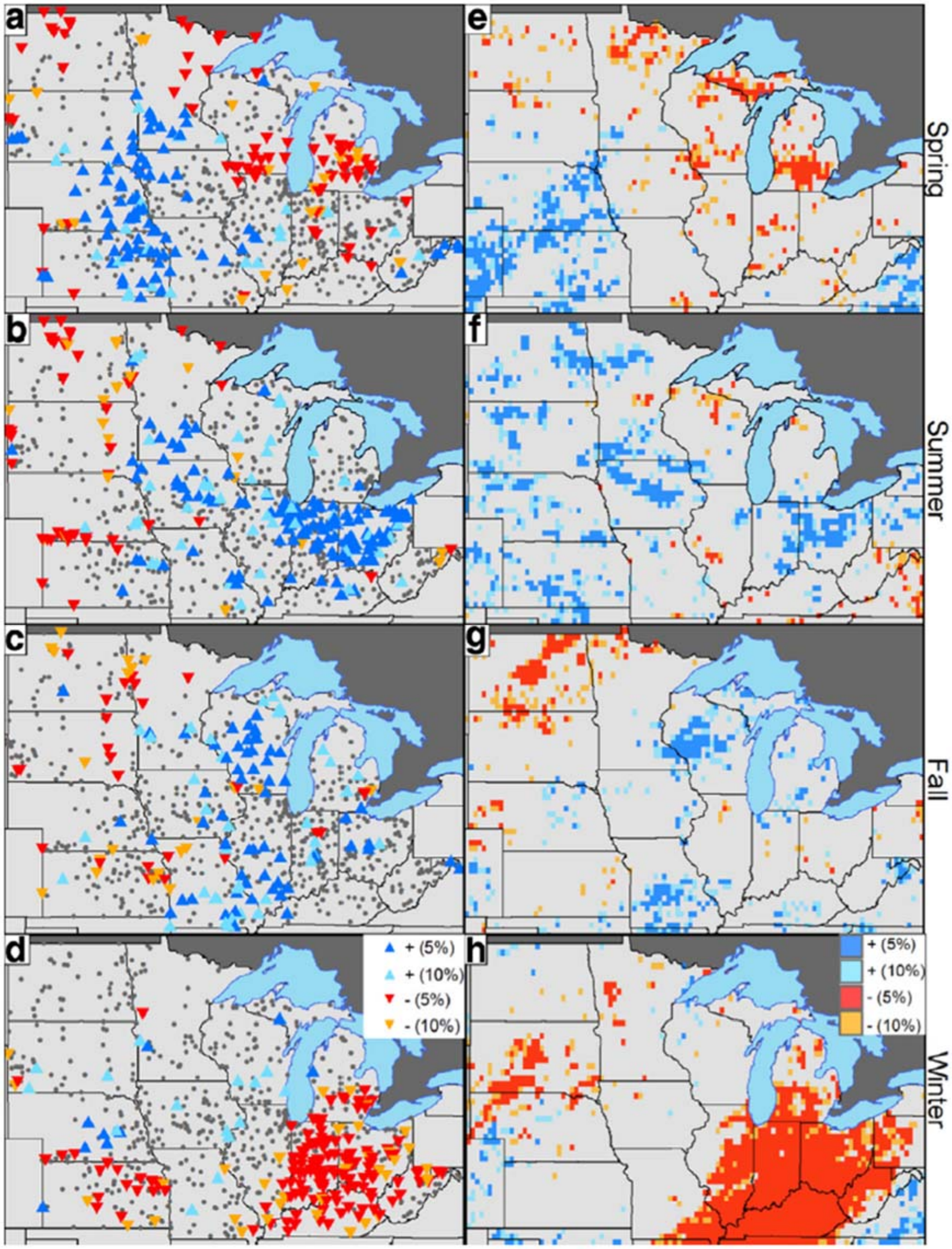

Figure 6.23. Relationship between PDO and seasonal frequencies of flooding (left panels) and precipitation exceeding the 95th percentile (right panels). Red and orange symbols indicate statistically significant negative relationship at the 5 and 10 percent significance levels. Dark and light blue symbols indicate positive relationship at the 5 and 10 percent significance levels. Gray dots are streamflow gauge locations where the relationship was not statistically significant. (Source: Mallakpour and Villarini 2016, Figure 2)

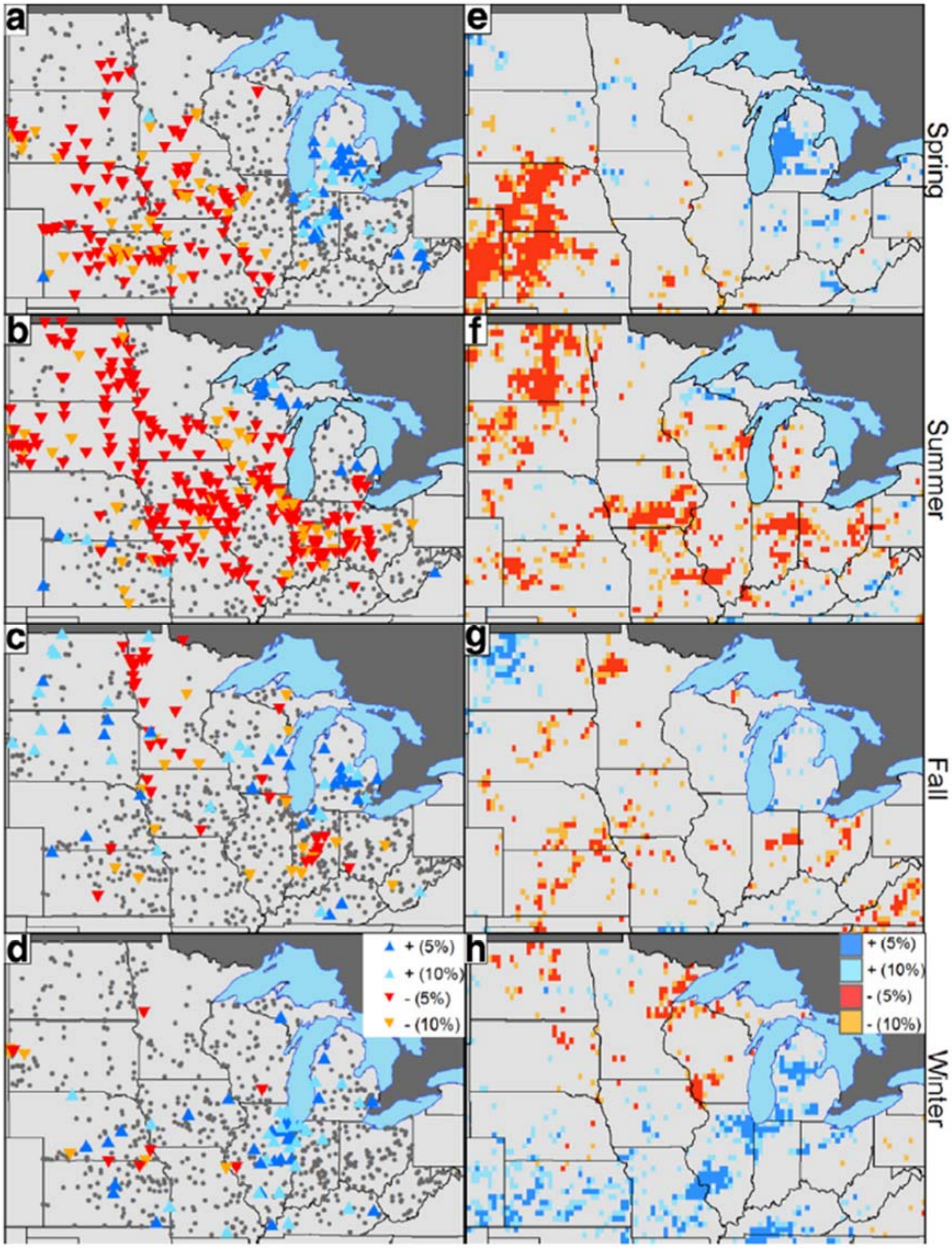

Figure 6.24. Relationship between NAO and seasonal frequencies of flooding (left panels) and precipitation exceeding the 95th percentile (right panels). Red and orange symbols indicate statistically significant negative relationship at the 5 and 10 percent significance levels. Dark and light blue symbols indicate positive relationship at the 5 and 10 percent significance levels. Gray dots are streamflow gauge locations where the relationships were not statistically significant. (Source: Mallakpour and Villarini 2016, Figure 3)

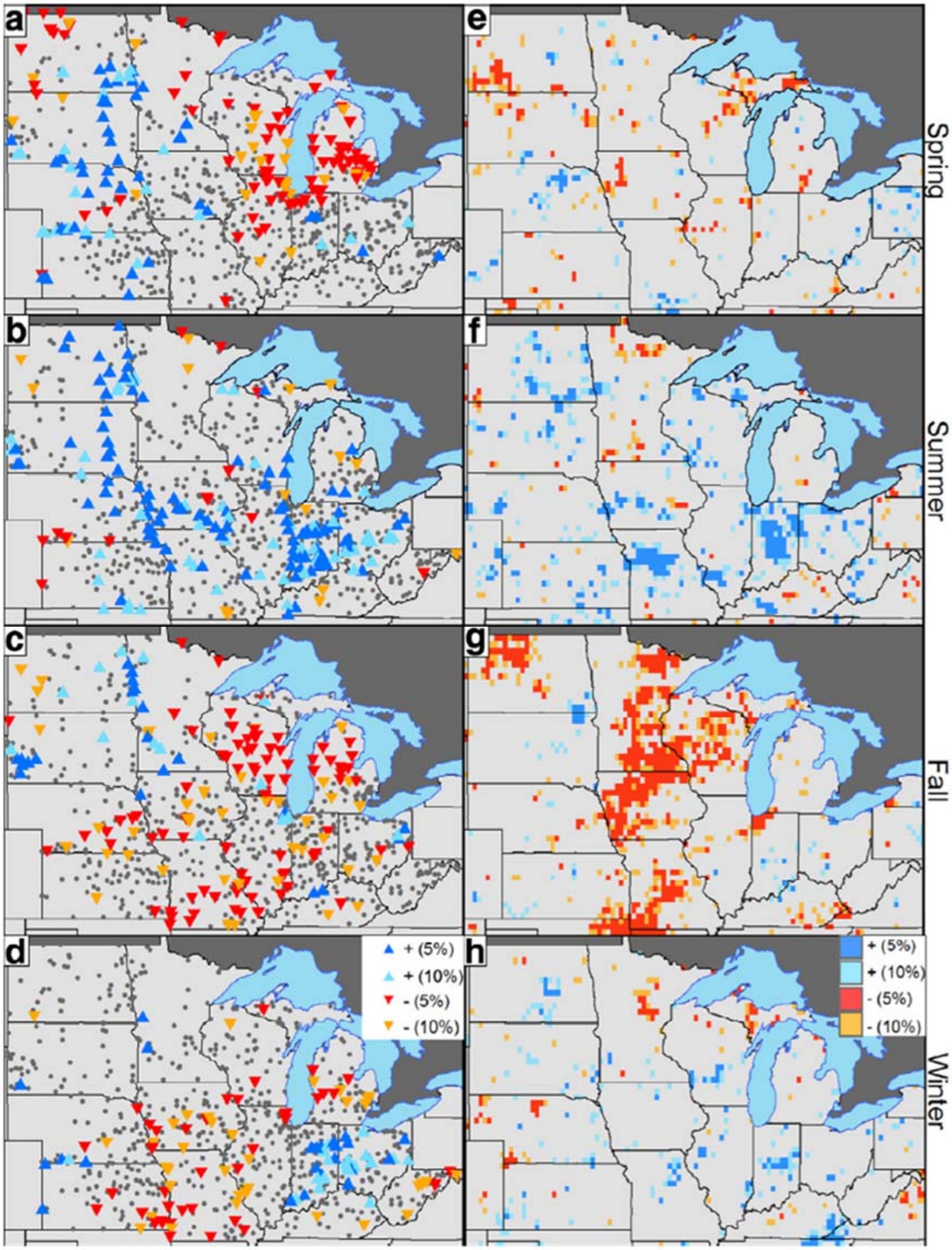

Figure 6.25. Relationship between AMO and seasonal frequencies of flooding (left panels) and precipitation exceeding the 95th percentile (right panels). Red and orange symbols indicate statistically significant negative relationships at the 5 and 10 percent significance levels. Dark and light blue symbols indicate positive relationships at the 5 and 10 percent significance levels. Gray dots are streamflow gauge locations where the relationships were not statistically significant. (Source: Mallakpour and Villarini 2016, Figure 4)

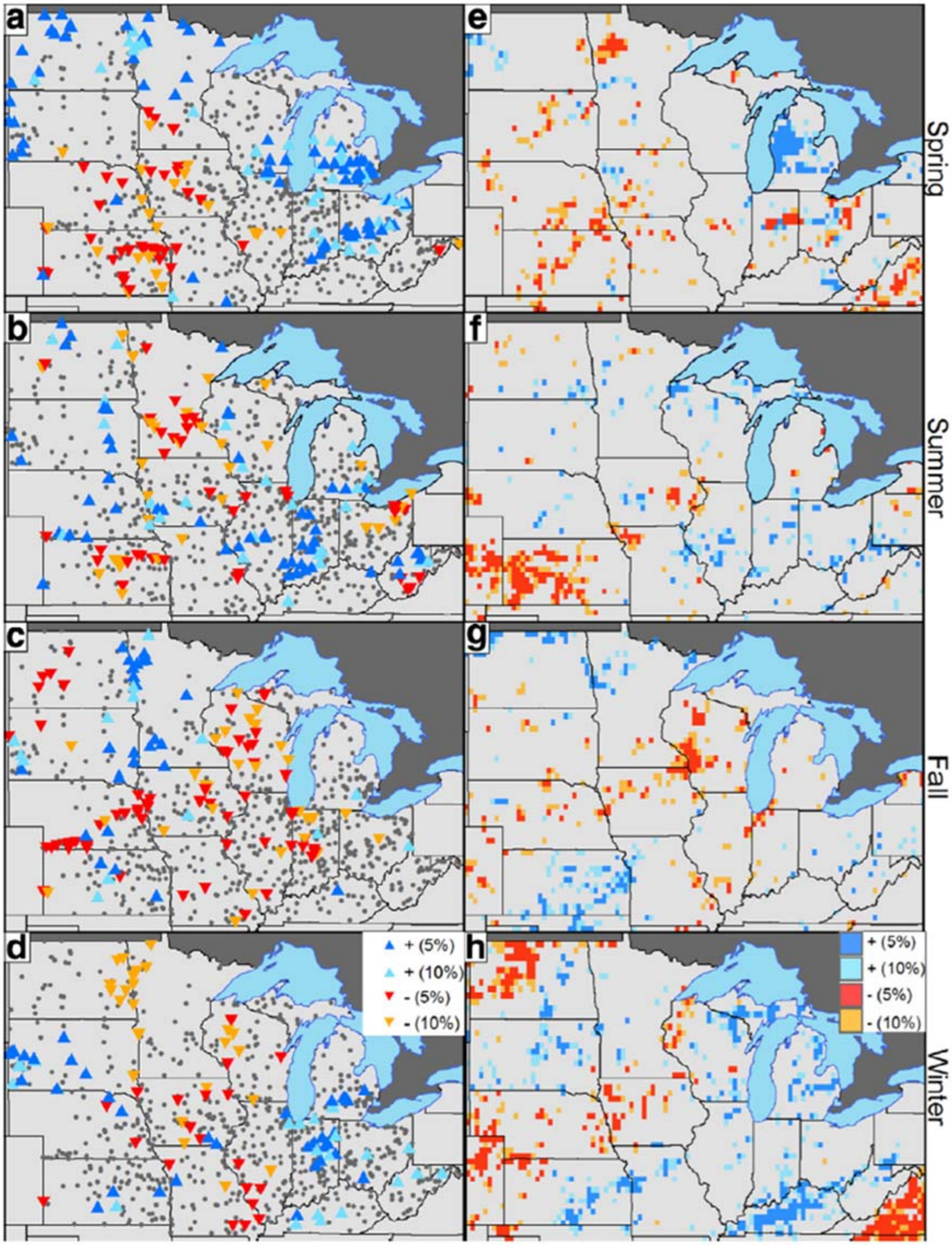

Figure 6.26. Relationship between SOI and seasonal frequencies of flooding (left panels) and precipitation exceeding the 95th percentile (right panels). Red and orange symbols indicate statistically significant negative relationships at the 5 and 10 percent significance levels. Dark and light blue symbols indicate positive relationships at the 5 and 10 percent significance levels. Gray dots are streamflow gauge locations where the relationships were not statistically significant. (Source: Mallakpour and Villarini 2016, Figure 5)

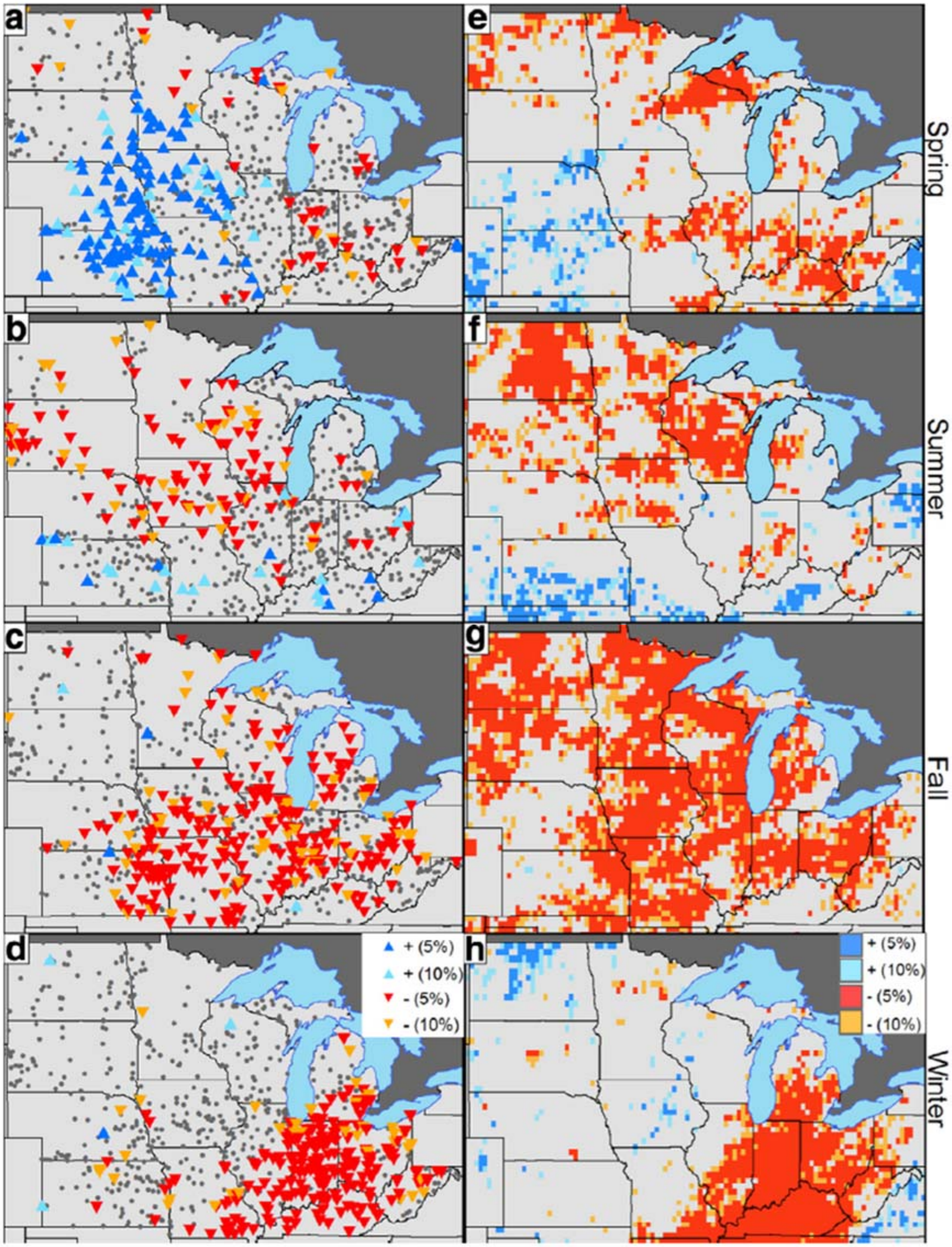

Figure 6.27. Relationship between PNA and seasonal frequencies of flooding (left panels) and precipitation exceeding the 95th percentile (right panels). Red and orange symbols indicate statistically significant negative relationships at the 5 and 10 percent significance levels. Dark and light blue symbols indicate positive relationships at the 5 and 10 percent significance levels. Gray dots are streamflow gauge locations where the relationships were not statistically significant. (Source: Mallakpour and Villarini 2016, Figure 6)

Table 6.2. Percentage of streamflow gauges with statistically significant relationships with the examined climate indices at 5 (10) percent significance.

Climate Indices	Winter	Spring	Summer	Fall
Pacific Decadal Oscillation	20 (27)	20 (27)	20 (30)	11 (19)
North Atlantic Oscillation	6 (10)	15 (25)	33 (40)	8 (15)
Atlantic Multidecadal Oscillation	8 (15)	16 (23)	15 (24)	13 (21)
Southern Oscillation Index	7 (13)	14 (22)	11 (19)	11 (18)
Pacific-North American Pattern	28 (36)	20 (27)	26 (33)	31 (42)

In winter, parts of southern Michigan, Ohio, and Indiana show negative relationships with PDO (Figure 6.23d). The authors also noted strong similarities in both the nature (positive or negative) of the relationships and in the spatial patterns of the relationships between precipitation and PDO (Figure 6.23e–h).

The spatial pattern of relationships between NAO and frequency of flooding in spring showed negative relationships west of Wisconsin and Illinois and positive relationships in Michigan and Indiana (Figure 6.24a). In summer, the relationship between NAO and frequency flooding is mostly negative all over the Midwest Region except for northern parts of Michigan (Figure 6.24b). Fall and winter only show a weak relationship between NAO and frequency of flooding (Figure 6.24c-d). The relationship between NAO and frequency of precipitation is generally similar to that of flooding, particularly for summer and winter (Figure 6.24e–h).

The spatial pattern of relationships between AMO and frequency of flooding in spring showed negative relationship in the northeast part of the Midwest Region and some positive relationships in the southwest part of the region (Figure 6.25a). In summer, most of the region showed positive relationships (Figure 6.25b). In fall, except for western Minnesota and southern Indiana, most of the Midwest Region showed negative relationships (Figure 6.25c). In winter, positive relationships occurred in Indiana, Ohio, and western Minnesota and negative relationships in the rest of the region (Figure 6.25d). The relationship between AMO and frequency of precipitation is generally similar to that of flooding (Figure 6.25e–h).

The spatial pattern of relationships between SOI and frequency of flooding in spring showed positive relationships stretching southeast from northern Minnesota to Indiana and Ohio and negative relationships in southern Minnesota, Iowa, and Missouri (Figure 6.26a) but the relationships were generally weak in all seasons. In summer, positive relationships occurred in Indiana, Wisconsin, and Iowa and positive relationships occurred in Minnesota, but no clear regional clustering occurred (Figure 6.26b). In fall, most of the Midwest Region, except for Minnesota, showed negative relationships (Figure 6.26c). In winter, eastern parts of the region (Indiana, Michigan, Ohio) showed positive relationships and the western parts (Minnesota, Wisconsin, Illinois, Iowa, and Missouri) showed mostly negative relationships (Figure 6.26d). The relationship between SOI and frequency of precipitation is generally similar to that of flooding (Figure 6.26e–h).

The spatial pattern of relationships between PNA and frequency of flooding was reported to be the most dominant (Mallakpour and Villarini 2016). A strong positive relationship exists during spring in the southwest parts of the Midwest Region (Figure 6.27a). In summer, almost the whole Midwest Region, except for southwest Missouri and Illinois, shows a strong negative relationship (Figure 6.27b). In fall, most of the region shows a strong negative relationship with PNA (Figure 6.27c). In winter, the southeastern parts of the Midwest Region shows a strong negative relationship with PNA (Figure 6.27d). The relationships between PNA and the frequency of precipitation (Figure 6.27e–h) are remarkably similar to those between PNA and flood frequency (Mallakpour and Villarini 2016).

To identify dominant climate indices for each season, Mallakpour and Villarini (2016) performed multiple Poisson regressions (Table 6.3). They reported that regression models that contained PNA as one of the covariates better described the variability in flood frequency during all seasons. The relationship during spring, depending on location, depended on at least one of the five climate indices. The relationship during summer depended on one or a subset of NAO, PDO, and PNA. During fall, the relationship was negative between PNA and frequency of flooding and positive between PDO and frequency of flooding. During fall, a strong negative relationship existed between PNA and frequency of flooding. The authors also performed a similar multiple Poisson regression for precipitation and reported that the relationships were similar to those for frequency of flooding, and PNA was the dominant climate mode across the Midwest Region for all seasons.

Table 6.3. Percentage of streamgauges with statistically significant (at 10 percent level) relationships with the five climate indices for the four seasons based on multiple Poisson regression. (Source: Mallakpour and Villarini 2016, Table 1)

Climate Index	Spring		Summer		Fall		Winter	
	Positive	Negative	Positive	Negative	Positive	Negative	Positive	Negative
PNA	19	7	5	27	1	45	1	36
PDO	8	8	28	5	21	5	8	3
NAO	5	16	4	25	9	7	8	4
AMO	9	15	13	5	5	7	5	8
SOI	16	2	16	7	6	10	6	7

Novotny and Stefan (2007) studied streamflow at 36 USGS streamgauges in Minnesota; 7 stations had continuous records over 90 years long, 11 had records between 70 and 90 years long, and 18 had records between 50 and 70 years long. Streamgauges reflecting heavily regulated flows were excluded. These streamgauges were in five river basins: those of Red River of the North (6 streamgauges), Rainy River (5 streamgauges), Mississippi River (11 streamgauges), Minnesota River (11 streamgauges), and tributaries of Lake Superior (2 stations). The authors estimated seven different statistics from daily streamflow: (1) mean annual flow, (2) maximum daily streamflow from snowmelt runoff (March–May), (3) maximum daily streamflow from rainfall runoff (June–November) (4) 7-day summer low flow (May–October), (5) 7-day winter low flow (November–April), (6) number of days with streamflow greater than mean plus one standard deviation (also called high flow days), and (7) number of days with streamflow greater than mean plus two standard deviations (also called extreme flow days). To compare statistics across river basins, the authors normalized the statistics using the streamgauge-specific, 1950–2002 means of the corresponding statistic. Basin averages for the statistics were computed by averaging the normalized statistics across all streamgauges in a basin.

Novotny and Stefan (2007) visually detected trends in the streamflow statistics by plotting 5-year moving averages. The authors concluded that trends over time varied among the examined river basins. In the Red River of the North basin, all seven streamflow statistics rise or fall at similar points in time (Figure 6.28). The streamflow statistics had low values during 1930s and 1940s (i.e., during the dust bowl). Streamflow rose and leveled off around the mean until 1985. Starting in the early to mid-1990s, all streamflow statistics increased to twice their means with a peak around 2000. In the Rainy River basin, no trends are apparent in any of the streamflow statistics. There were increases in 1950s and 1970s and a decline in the 1960s, but the recent values have been around the mean. In the Mississippi River basin, other than maximum daily streamflow from snowmelt runoff (labeled “Peak flow spring” in Figure 6.28), all streamflow statistics showed increases. The Minnesota River basin showed the largest changes. From the 1940s to the 1980s, all streamflow statistics were stable. In the mid-1980s, the statistics increased to twice the respective means and in the 1990s they increased to up to 3.5 times the respective means. In the 2000s, the streamflow statistics showed a return to around the respective means.

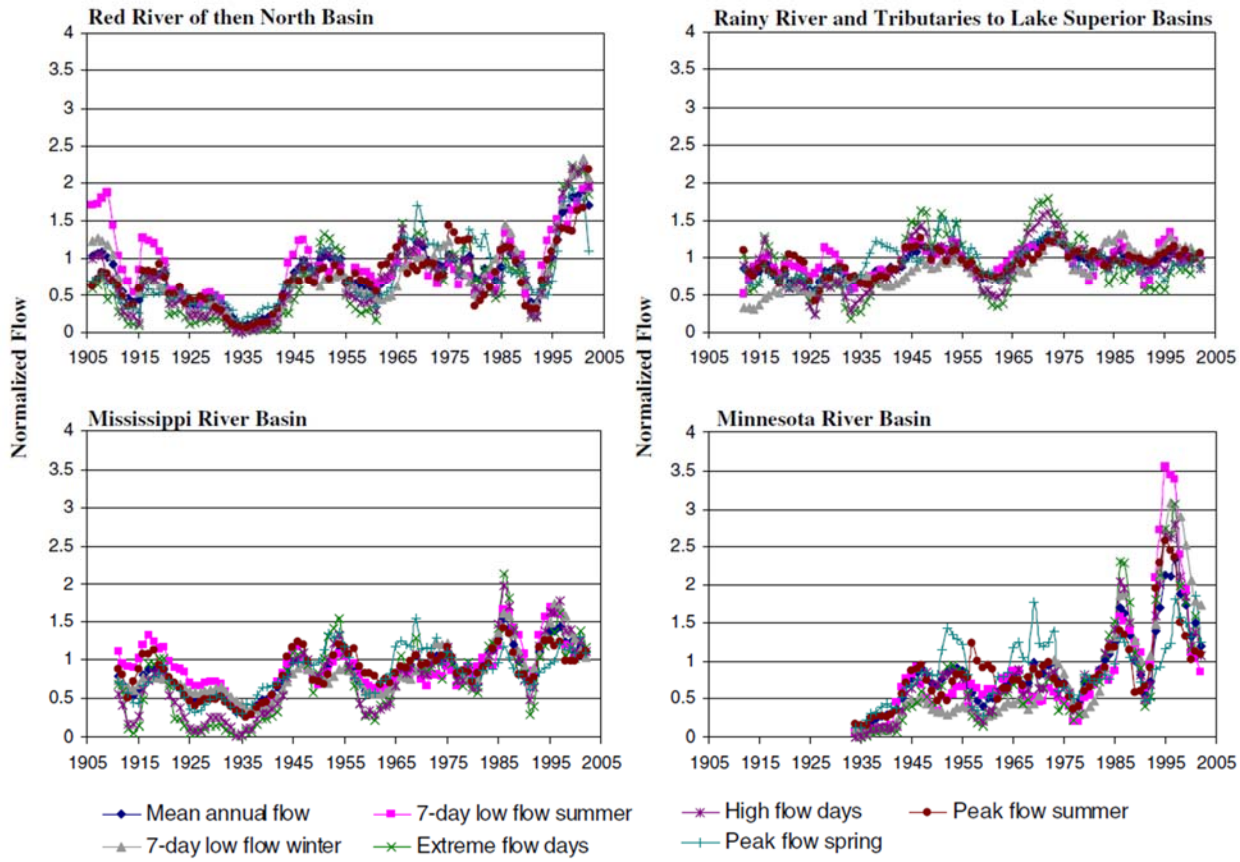

Figure 6.28. Five-year moving averages of the streamflow statistics for selected river basins in Minnesota. (Source: Novotny and Stefan 2007, Figure 2)

Novotny and Stefan (2007) performed the Mann-Kendall test for trends to the last 90, 70, 50, 30, 15, and 10 years of record ending in 2002. Data were available for 36 streamgauges for 50 years, 18 streamgauges for 70 years, and 7 streamgauges for 90 years. When trends were detected visually, a statistical trends analysis was performed and the Mann-Kendall test was used to determine their significance using the original data corrected for serial correlations. The authors found that the magnitude of trends was changing over time (the time period used in trend analysis, Table 6.4). Trends in more recent time periods appeared to be increasing and strengthening, except for the 1993–2002 period.

Table 6.4. Mean and standard deviation of trends in streamflow statistics in Minnesota. (Source: Novotny and Stefan 2007)

	1913–2002	1933–2002	1953–2002	1973–2002	1988–2002	1993–2002
Mean annual flow	**1 (0.3)**	**1 (0.6)**	**2 (0.5)**	**4 (0.5)**	**8 (4.3)**	−18 (14.3)
Peak flow (March–May)	**1 (0.3)**	**1 (0.6)**	**1 (0.3)**	2 (0.1)	6 (1.7)	10
Peak flow (June–November)	**1 (0.3)**	**1 (0.5)**	**1 (0.4)**	**3 (1.1)**	10 (6.2)	−25 (12.4)
7-Day low flow (November–April)	**1 (0.4)**	**2 (0.8)**	**2 (0.8)**	**4 (1.9)**	15 (6.0)	**−21 (13.0)**
7-Day low flow (May–October)	**1 (0.3)**	**1 (0.5)**	**1 (0.5)**	**3 (1.2)**	10 (4.9)	**−37 (15.0)**
High flow days	**1 (0.4)**	**2 (0.5)**	**2 (0.9)**	**4 (1.0)**	15 (3.9)	**−35 (5.7)**
Extreme flow days	**1 (0.4)**	**1 (0.8)**	**1 (0.8)**	3 (1.4)	12 (5.6)	−49 (8.3)

Values in bold have field significance at the 10% level.

To verify the apparent periodicity in the 5-year moving averages of the streamflow statistics, Novotny and Stefan (2007) calculated magnitudes and significance of trends in 25- and 10-year moving windows. Significant trends were then normalized using the 1950–2002 average for the streamflow statistic. The percent change in trend magnitudes was estimated relative to the 1950–2002 average (Figure 6.29). The authors noted that trends in all streamflow statistics show periodicity. The most noticeable change appeared in 7-day summer and winter low flows with pre-1994 changes between +6 and -6 percent per year. After 1994, the trends were as high as +12 percent per year.

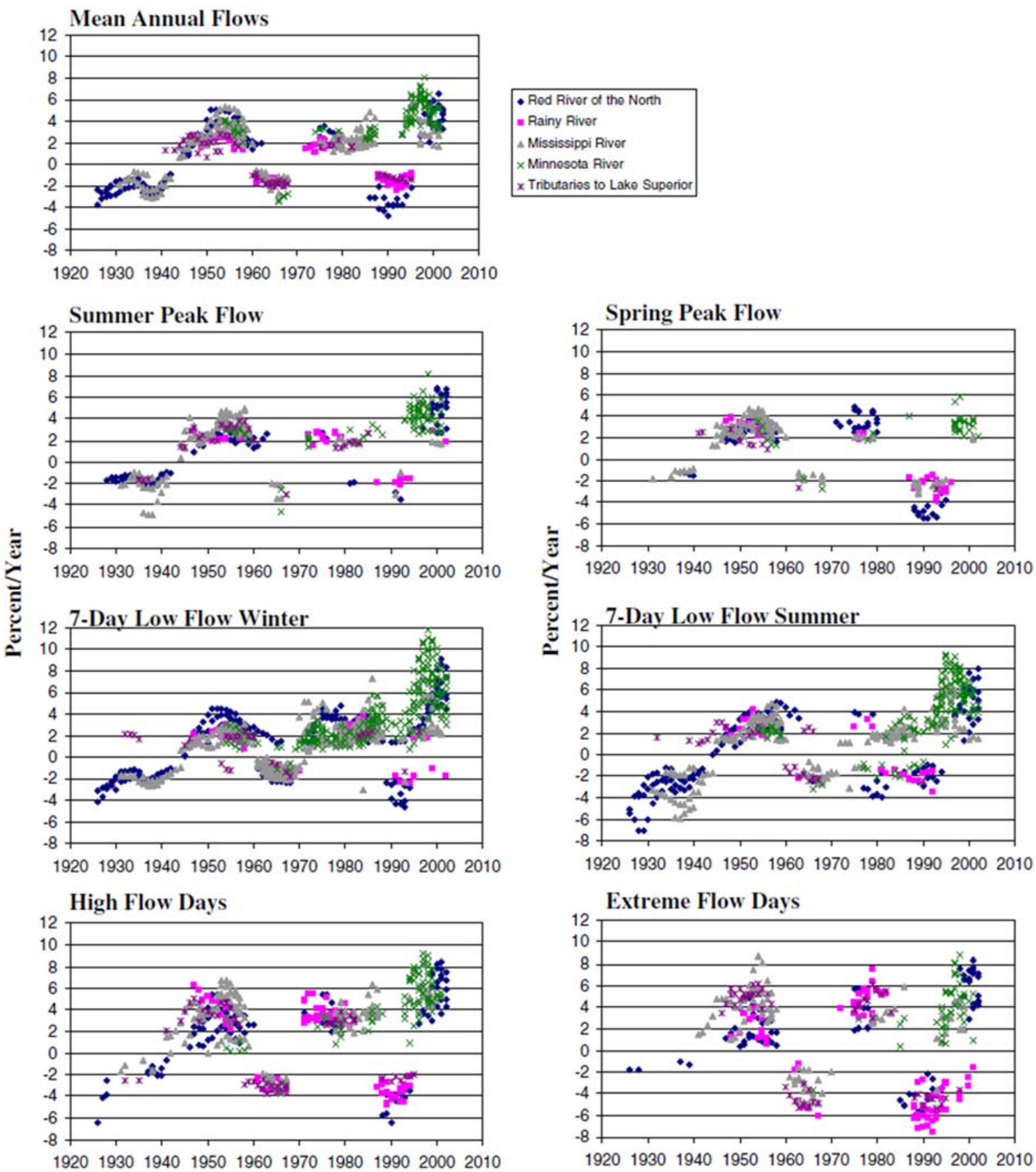

Figure 6.29. Significant percent change in streamflow statistics for 25-year moving window. (Source: Novotny and Stefan 2007, Figure 3)

Novotny and Stefan (2007) also examined total annual precipitation in nine climate divisions in Minnesota and concluded that precipitation showed trends similar to those of streamflow statistics. They concluded that (1) trends in the examined streamflow statistics in Minnesota were not monotonic but periodic, (2) streamflow changes were well correlated with changes in total annual precipitation, (3) snowmelt-induced floods did not change significantly, (4) rainfall-induced floods and the number of high flow days seemed to increase, possibly coinciding with increases in more frequent heavy rainfall events, and (5) 7-day low flows or baseflows seemed to increase.

6.2.2 Projected Changes in Streamflow

Choi et al. (2017) used statistically downscaled climate scenarios from nine GCMs and urban growth scenarios from a land-use simulation model to examine future streamflow characteristics in the 2330 km^2 (900 mi^2) Milwaukee River basin (Figure 6.30). The southern portion of the basin is heavily urban and the northern portion is dominated by agriculture.

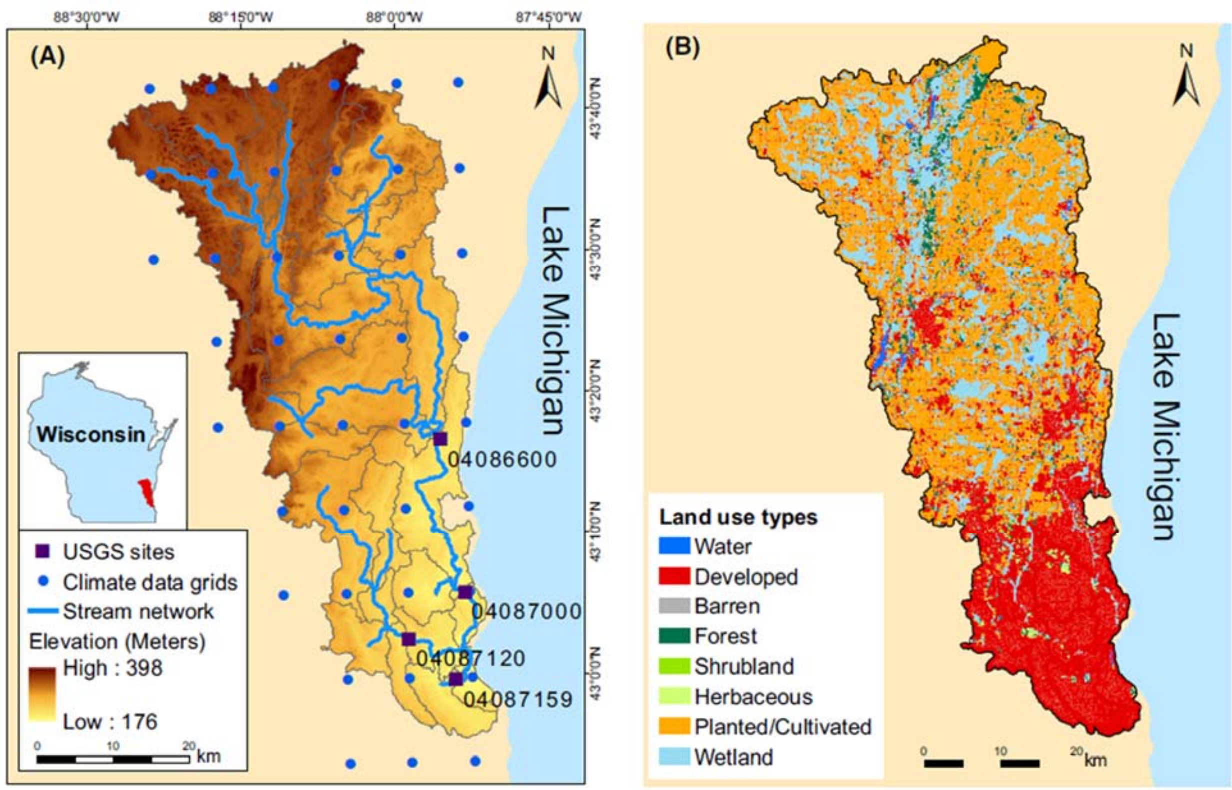

Figure 6.30. The Milwaukee River basin studied by Choi et al. (left panel). The land-use data were derived from the 2001 National Land Cover Database (right panel). (Source: Choi et al. 2017, Figure 1)

Choi et al. (2017) used the Hydrological Simulation Program-Fortran model, embedded within the U.S. Environmental Protection Agency's Better Assessment Science Integrating Point and Non-Point Sources (BASINS) version 4.1 software, to simulate streamflow in the Milwaukee River basin. The model was calibrated with measured 1986–1995 streamflow and was validated for the 1996–2005 period.

Goodness-of-fit was determined using the relative error (RE) and Nash-Sutcliffe efficiency[1] (NSE) measures. For the calibration period, with the exception of one site, the RE was less than 5 percent and NSE values ranged from 0.62 to 0.71 and were slightly lower for validation (Choi et al. 2017).

Choi et al. (2017) used climate scenarios derived from statistically downscaled outputs from nine GCMs that included both the latter part of the 20th century time period (1961–2000) and mid-21st century projections (2046–2065). The authors only used the SRES A1B scenario that lies in the middle of the six SRES scenarios. All of the nine downscaled GCM outputs matched the observed means and standard deviations of temperature and precipitation over the historical period. For the future time period, all GCMs showed increased temperatures, particularly in December and January. Precipitation for the future time period was also predicted to be higher with largest increases occurring in December and January.

Choi et al. (2017) used two cellular automata-based models to simulate land-use dynamics input by the 30 m resolution National Land Cover Database land-use data set. The probability of a grid cell converting to developed land was calculated based on a global probability of conversion to developed lands, a neighborhood effect, a constraint factor, and a random factor. The global probability of conversion to developed land was estimated using logistic regression based on driving factors including elevation, slope, and proximity to landscape, urban, and transportation features. The neighborhood effect was estimated by dividing the urban cell numbers within the neighborhood with the total cell numbers within the neighborhood. Constraints included grid cells that were occupied by water or had a slope exceeding 22.5 degrees. The model was calibrated using residential and commercial data for the 1990–2000 time period and the model was validated for the 2000–2005 time period. For 2050, the land-use dynamics model predicted an over 8 percent increase in developed lands and a 1 percent increase in barren lands. Vegetated and agricultural lands were projected to decrease. Choi et al. (2017) ran the Hydrological Simulation Program-Fortran model using land-use and climate scenarios, as shown in Table 6.5.

Table 6.5. Hydrologic modeling experiments perfomed by Choi et al. (Source: Choi et al. 2017, Table 3)

Modeling experiments	Acronym	Temperature and precipitation data	Land use data
Baseline	Baseline	Downscaled 1961–2000	2000
Land use change only	LUC	Downscaled 1961–2000	2050
Climate change only	CC	Downscaled 2046–2065	2000
Climate and land use changes	CLUC	Downscaled 2046–2065	2050

Choi et al. (2017) used three streamflow measures: mean streamflow, 7Q10 (90 percent exceedance probability lowest 7-day average streamflow), and 7Q2 (50 percent exceedance probability lowest 7-day average streamflow). Their results are shown in Figure 6.16. Land-use change only did not result in a significant change in mean streamflow (changes from baseline ranged from -1.2 to 0.0 percent). Under the climate-change-only case, changes in mean streamflow varied widely, from +18.3 to -29.5 percent. Mean streamflow decreased compared to the climate change case, when both climate change and land-use change were considered together (Table 6.6).

[1] Nash-Sutcliffe efficiency (NSE, Nash and Sutcliffe [1970]) is a common statistic used to measure the goodness-of-fit of statistical models in hydrology. It ranges from $-\infty$ to 1. A perfect match between predicted and observed values is represented by an NSE of 1. An NSE of 0 means that the model predictions are as good a predictor as the mean of the dataset. An NSE less than 0 indicates that the model's residual variance is larger than the variance of the observed data.

Table 6.6. Simulated mean streamflow for the entire simulation periods (m^3/s). (Source: Choi et al. 2017, Table 4)

Model	Baseline	LUC		CC		CLUC	
cccma_cgcm3_1	237.7	235.1	(−1.1)	239.4	(0.7)	236.7	(−0.4)
cnrm_cm3	224.4	224.4	(0.0)	262.0	(16.8)	260.2	(16.0)
csiro_mk3_0	236.5	235.1	(−0.6)	246.7	(4.3)	244.5	(3.4)
csiro_mk3_5	**256.4**	**255.2**	(−0.4)	205.4	(−19.9)	204.0	(−20.4)
gfdl_cm2_0	**220.0**	**218.0**	(−1.0)	**155.0**	(−29.5)	**155.3**	(−29.4)
giss_model_e_r	235.4	232.6	(−1.2)	**278.6**	(18.3)	**276.0**	(17.2)
miub_echo_g	229.1	227.9	(−0.5)	226.8	(−1.0)	224.4	(−2.0)
mpi_echam5	246.3	244.3	(−0.8)	244.0	(−0.9)	240.0	(−2.6)
mri_cgcm2_3_2a	244.4	243.7	(−0.3)	254.0	(3.9)	250.9	(2.7)

Percentage changes from Baseline are shown in parentheses. The largest and smallest flow values from each experiment are shown in bold

The changes in the low-flow measures, 7Q10 and 7Q2 are shown in Table 6.7. Compared to the baseline, land-use-only change in 7Q10 ranged from +1.5 to -11.5 percent. For the climate-change-only case, change in 7Q10 ranged from +41.9 to -71.2 percent. When both land-use and climate change were considered, change in 7Q10 ranged from +37.4 to -74.2 percent. Compared to the baseline, land-use-only change in 7Q2 ranged from +0.8 to -6.7 percent. For the climate-change-only case, change in 7Q2 ranged from +20.1 to -58.6 percent. When both land-use and climate change were considered, change in 7Q2 ranged from +17.6 to -60.2 percent. The authors concluded that (1) changes in land use only resulted in insignificant changes in streamflow, (2) low flows showed greater sensitivity to climate change than mean streamflow, (3) variability in streamflow increased with both land-use and climate change, and (4) uncertainty in streamflow simulated by GCM output scenarios was greater than the uncertainty in GCM outputs themselves.

Table 6.7. Simulated 7Q10 (top panel) and 7Q2 (bottom panel) for the hydrologic experiments conducted by Choi et al. (Source: Choi et al. 2017, Table 6)

Model	Baseline	LUC		CC		CLUC	
cccma_cgcm3_1	36.6	35.7	(−2.5)	34.0	(−7.0)	28.6	(−21.8)
cnrm_cm3	36.3	33.3	(−8.3)	37.0	(2.1)	34.8	(−3.9)
csiro_mk3_0	23.2	**20.6**	(−11.5)	29.7	(27.9)	29.2	(25.6)
csiro_mk3_5	**21.1**	21.4	(1.2)	**6.1**	(−71.2)	**5.4**	(−74.2)
gfdl_cm2_0	31.2	28.8	(−7.6)	10.3	(−67.1)	9.0	(−71.3)
giss_model_e_r	**44.4**	41.1	(−7.4)	**63.0**	(41.9)	**61.0**	(37.4)
miub_echo_g	44.3	**44.1**	(−0.6)	21.1	(−52.3)	18.4	(−58.4)
mpi_echam5	27.9	28.4	(1.5)	36.2	(29.6)	34.1	(22.2)
mri_cgcm2_3_2a	36.9	37.1	(0.4)	42.3	(14.5)	42.3	(14.5)

Model	Baseline	LUC		CC		CLUC	
cccma_cgcm3_1	71.7	66.9	(−6.7)	65.3	(−9.0)	61.1	(−14.7)
cnrm_cm3	75.8	75.5	(−0.4)	79.7	(5.2)	75.4	(−0.5)
csiro_mk3_0	**58.8**	**59.3**	(0.8)	58.4	(−0.8)	55.0	(−6.5)
csiro_mk3_5	70.8	69.6	(−1.7)	48.0	(−32.2)	47.1	(−33.4)
gfdl_cm2_0	69.0	68.6	(−0.5)	**28.6**	(−58.6)	**27.4**	(−60.2)
giss_model_e_r	78.3	76.4	(−2.3)	**94.0**	(20.1)	**92.0**	(17.6)
miub_echo_g	71.5	66.7	(−6.6)	51.2	(−28.4)	48.5	(−32.1)
mpi_echam5	75.5	74.5	(−1.3)	82.7	(9.6)	77.3	(2.5)
mri_cgcm2_3_2a	**78.9**	**77.5**	(−1.8)	86.6	(9.7)	81.2	(2.9)

Percentage changes from Baseline are shown in parentheses. The largest and smallest low flow values from each experiment are shown in bold

In 2015, USACE conducted a study to assess the impacts of climate change on flood frequency curves for the Red River of the North at Fargo, North Dakota (USACE 2015b). This report was prepared by the USACE St. Paul District for a pilot study conducted as part of USACE Responses to Climate Change Program. Instantaneous annual peak flood discharge record for Fargo, North Dakota, is considered non-stationary with a break in behavior in 1942 (USACE 2015b). The study used CMIP3 output statistically downscaled using the BCSD technique to $^{1}/_{8}$-degree grid resolution. Four time periods were used: the baseline period of 1950–1999 and future periods of 2011–2040, 2041–2070, and 2071–2100. For each of the future time periods, nine CMIP3 projections that encompass the variability of all 112 CMIP3 projections, were chosen in a tercile grid of future temperature and precipitation ratios (Figure 6.31). The CMIP3 projections for grid cells located in the subwatersheds of the Red River of the North upstream of the Fargo, North Dakota, streamflow gauge were used. The basin-averaged annual mean temperature and accumulated precipitation data sets are shown in Figure 6.32. USACE noted that CMIP3 data showed a steady increasing trend in winter (November through March) temperature and a small increasing trend in precipitation for the future time periods.

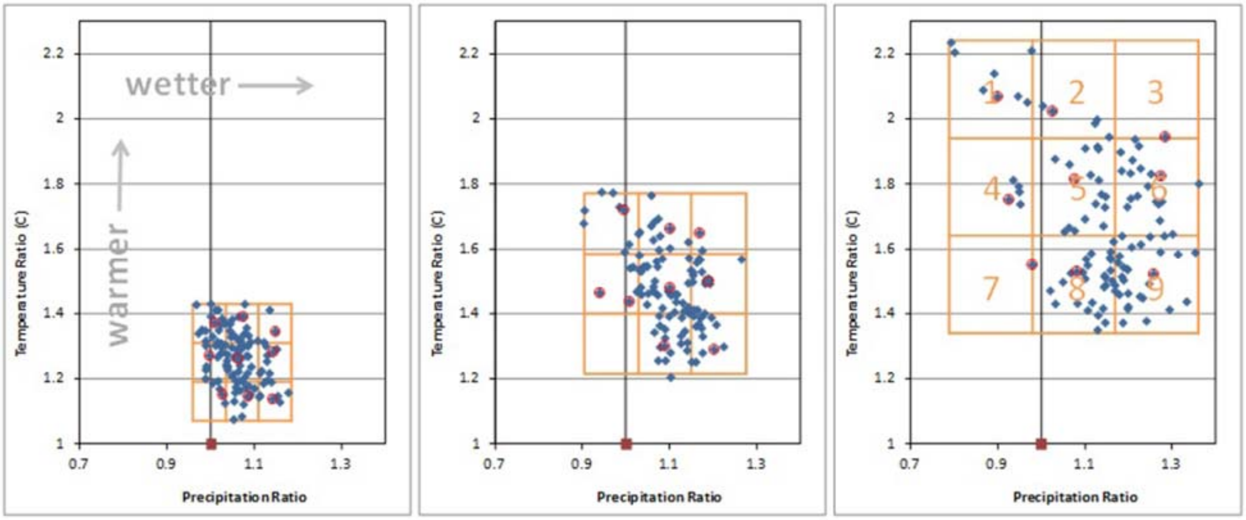

Figure 6.31. Selection of CMIP3 projections for the future time periods (left panel: 2011–2040, middle panel: 2041–2070, right panel: 2071–2100) using a tercile grid of temperature and precipitation ratio. (Source: USACE 2015b, Figure 6)

USACE (2015b) used the St. Paul District hydrologic models in the study that use an hourly timestep. Noting that running these models at hourly timesteps was not feasible because of the long time period, USACE reconfigured the hydrologic models to run at daily timesteps. The downscaled CMIP3 data consisted of mean monthly temperature and accumulated monthly precipitation. A weather-generation approach was used to generate daily temperature and precipitation from the downscaled CMIP3 monthly data. Historical data (1898–1999) were analyzed to identify eight categories for each month. The climate model output was processed to identify which category a month fell into and then a daily pattern for the category for that month was randomly chosen. For each climate model data set, 10 weather generations were made, which resulted in 90 daily data sets for each of the four time periods. To determine if the weather generations were reasonable in terms of predicting variations in peak discharge, the hydrologic models were run with 100 weather generations for the baseline, 1950–1999 period. USACE (2015b) determined that the weather generations of downscaled CMIP3 data resulted in a reasonable spread around the peak discharge frequency distribution based on observed data (Figure 6.33). USGS (2015b) noted that the daily variations of temperatures and precipitation for the same month can cause significantly different flood peak discharges.

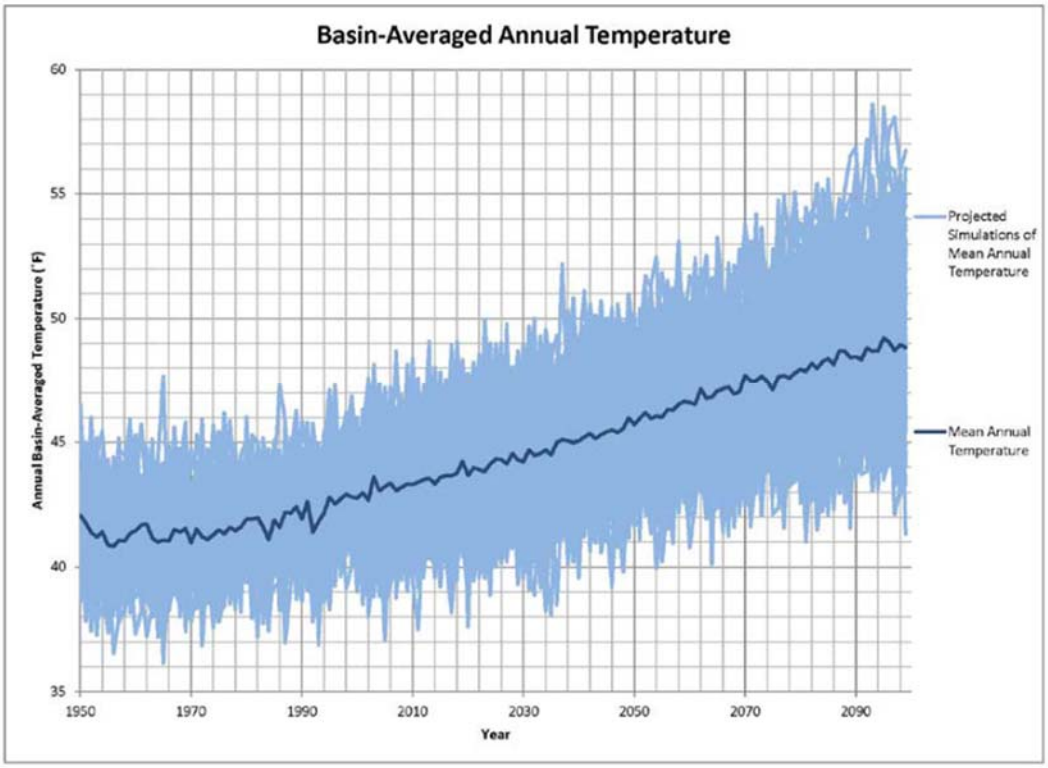

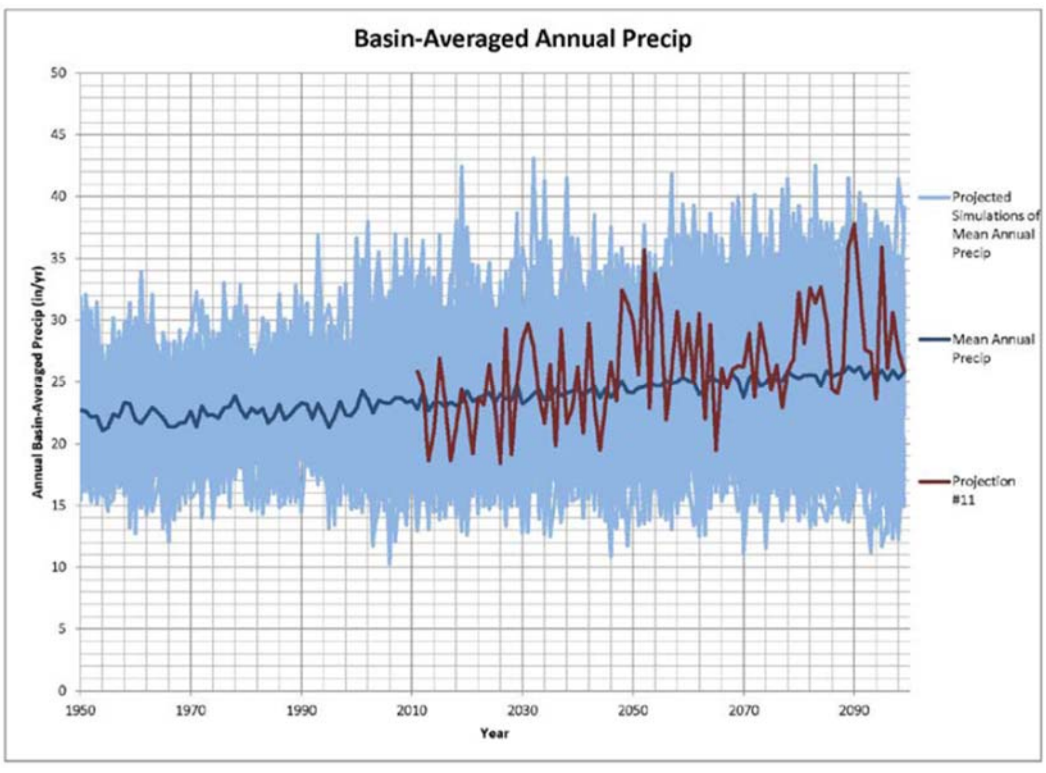

Figure 6.32. The basin-average annual temperature and precipitation from downscaled CMIP3 projections. Dark blue lines indicate the mean across CMIP3 projections. The dark red line shows one future precipitation projection. (Source: USACE 2015b, Figures 7 and 8)

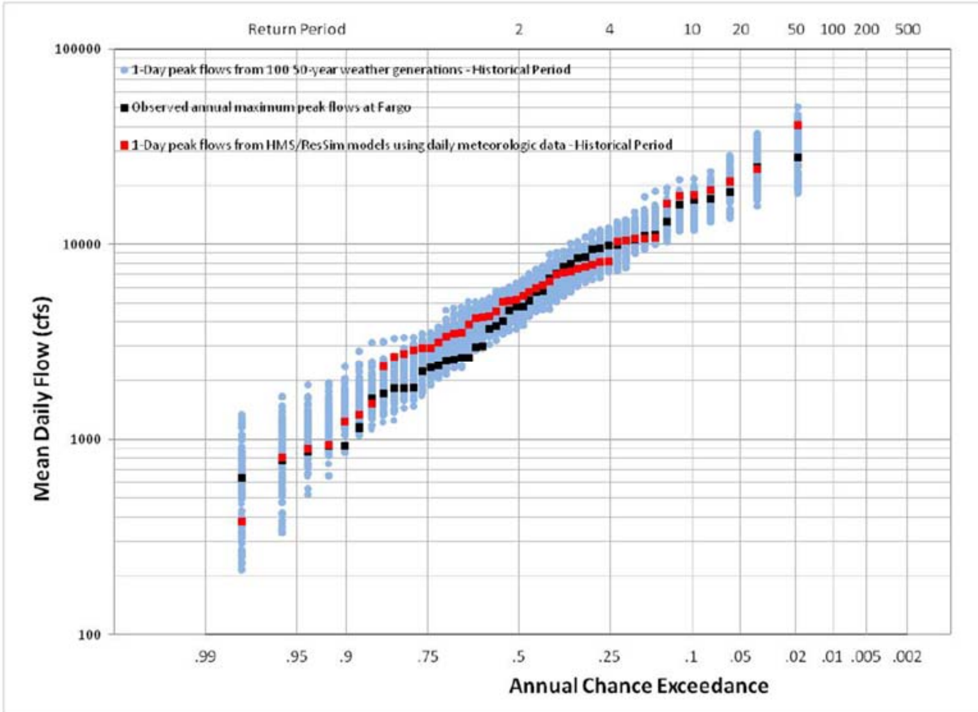

Figure 6.33. Comparison between observation-based peak discharge at various exceedance probabilities and the spread in predictions of peak discharges from daily weather-generation sequences of baseline period CMIP3 predictions. (Source: USACE 2015b, Figure 11)

USACE (2015b) used the Corps Watershed Management Study models that consists of Hydrologic Engineering Center-Hydrologic Modeling System (HEC-HMS), HEC-Reservoir System Simulation (ResSim; for reservoir operations and routing), HEC-River Analysis System (RAS), and HEC-Flood HEC-Impact Analysis (for consequence modeling). For this study, HEC-ResSim, rather than HEC-RAS, was used for channel routing. The models (HEC-HMS and HEC-ResSim) were calibrated, first using an hourly timestep for the 1997 and 2006 flood events, and were subsequently recalibrated using a daily timestep to match the frequency distribution of the flood peak discharges based on observed 1950–1999 data. For each of the time periods, 90 data sets (10 weather generations for each of the 9 climate models) were run in continuous simulation mode.

The impact of climate change on flood frequency curves were evaluated using two methods: (1) by pooling and sorting all annual peaks for each time period and (2) by fitting Log-Pearson Type III distributions to each of the 90 data sets in each time period and using the median of the 90 data sets in each time period. USACE (2015b) noted that the impacts shown by the two methods were similar. Bulletin 17B (USIAC 1982) guidance was used to remove outliers and regional skew adjustment was not used while fitting the Log-Pearson Type III distributions. The results are shown in Figure 6.34 through Figure 6.38 and Table 6.8.

USACE (2015b) concluded that peak flood discharge for all future time periods, compared to the baseline 1950−1999 period, showed increases for all exceedance probabilities. The greatest increase in peak discharge was for the 2011–2040 time period; it ranges from 20 to 35 percent greater than the baseline period. The increases in peak discharges for the later time periods, 2041–2070 and 2071–2100, were smaller than for the 2011–2040 time period. USACE (2015b) noted that this could be a result of the decrease in snow water equivalents after the 2011–2040 time period, possibly brought about by increasing temperatures that reduce accumulations of snow even though total precipitation is projected to increase.

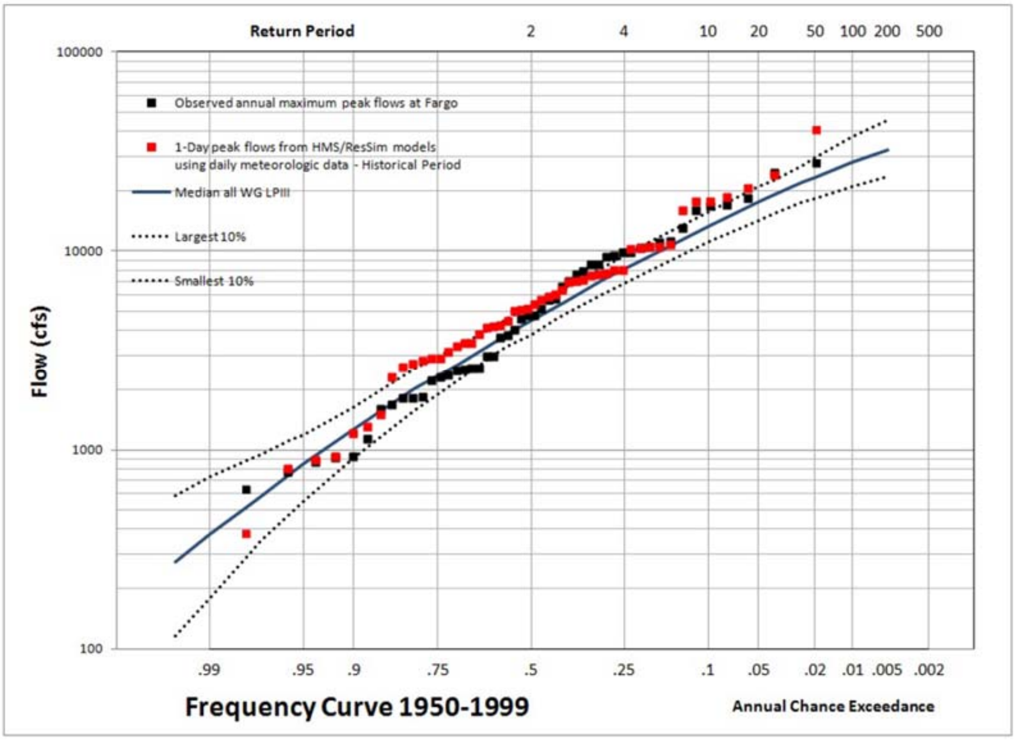

Figure 6.34. Comparison between flood frequency curves from observed and modeled data for the baseline period. (Source: USACE 2015b, Figure 15)

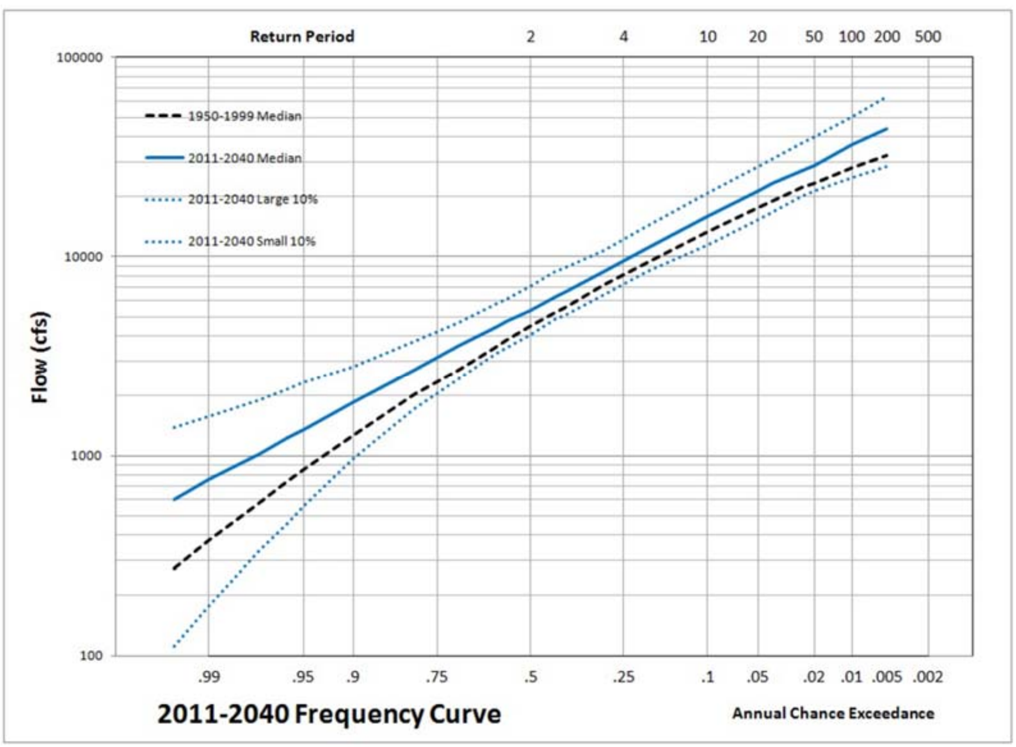

Figure 6.35. Comparison of 2011–2040 estimated flood frequency curve with the baseline. (Source: USACE 2015b, Figure 16)

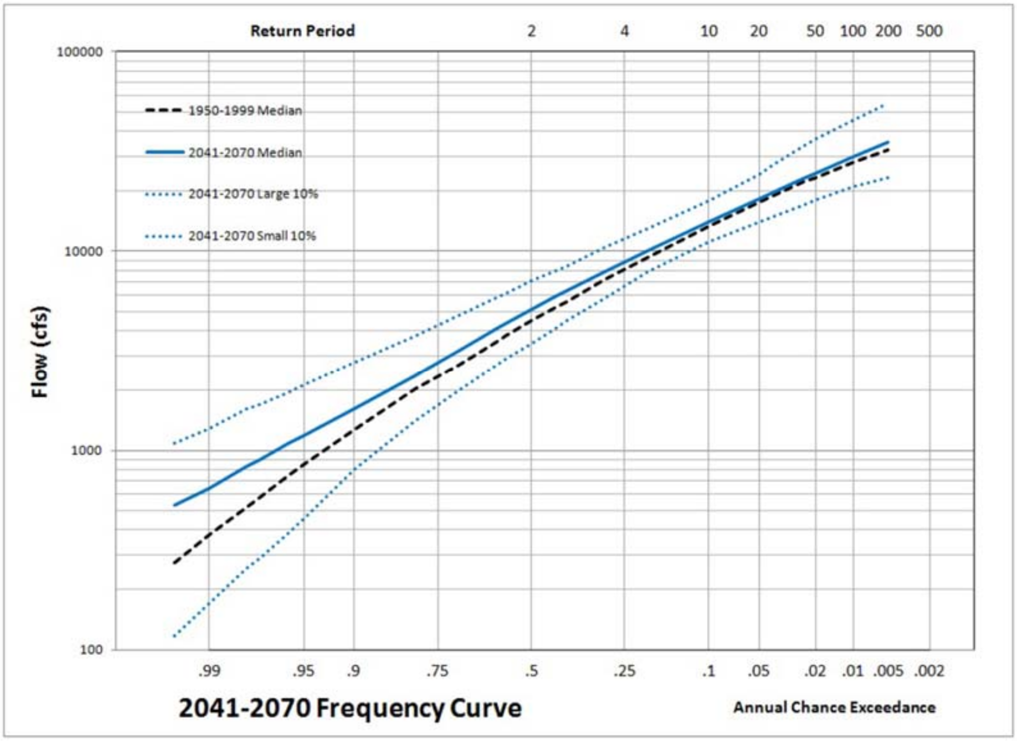

Figure 6.36. Comparison of 2041–2070 estimated flood frequency curve with the baseline. (Source: USACE 2015b, Figure 17)

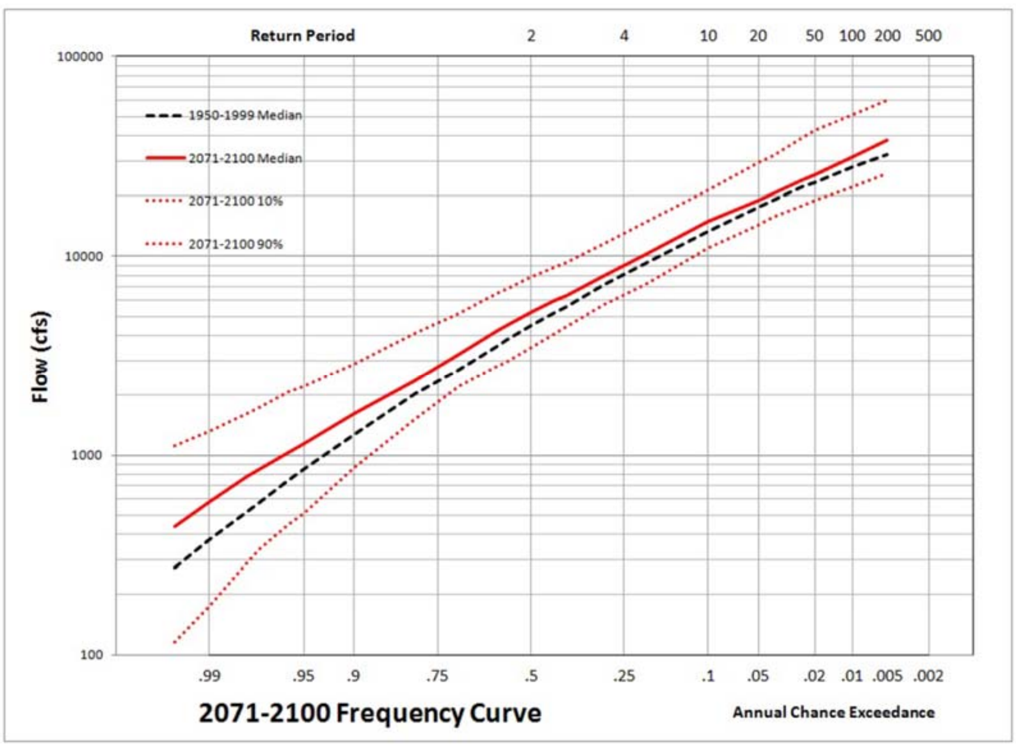

Figure 6.37. Comparison of 2071–2100 estimated flood frequency curve with the baseline. (Source: USACE 2015b, Figure 18)

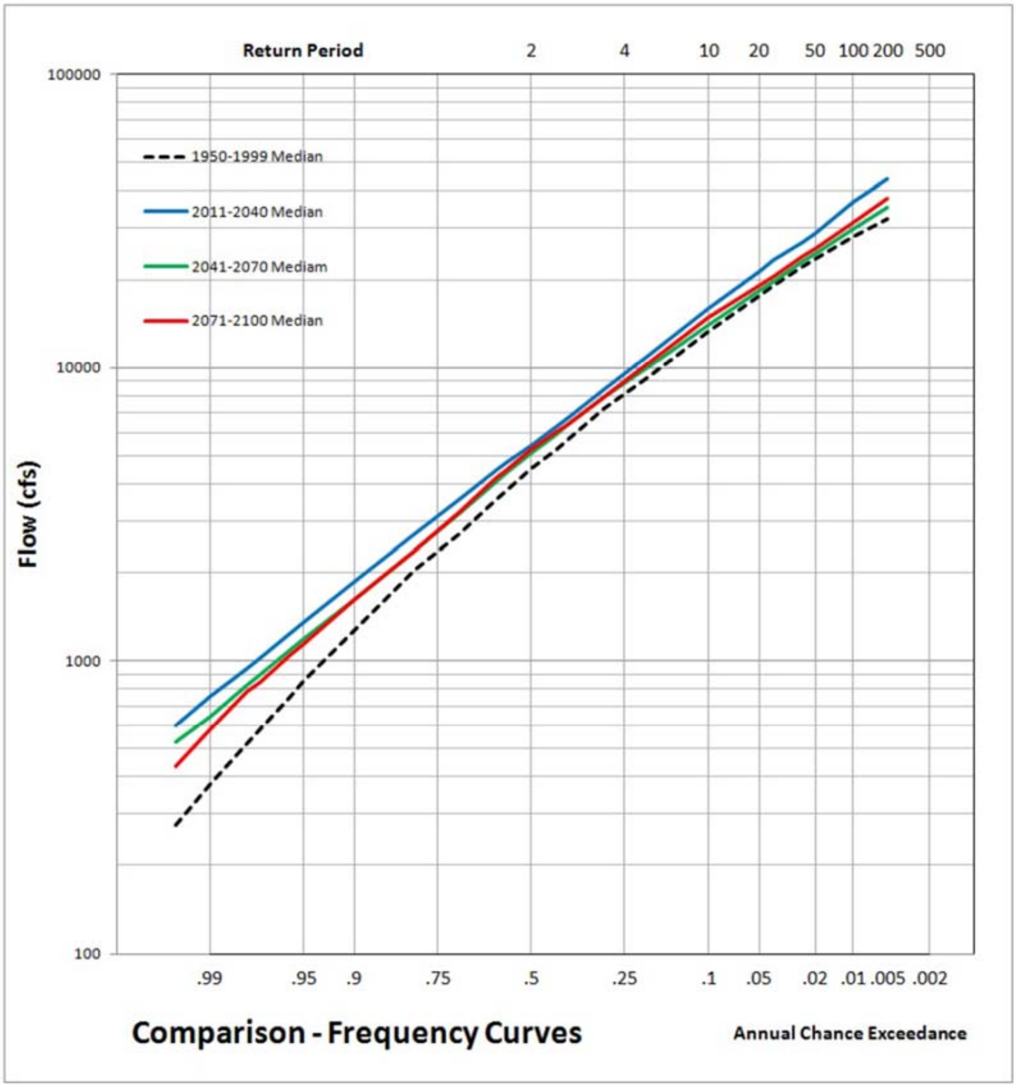

Figure 6.38. Comparison of flood frequency curves for the four time periods. (Source: USACE 2015b, Figure 19)

Table 6.8. Comparison of peak flood discharge at Fargo, North Dakota, for selected AEPs. (Source: USACE 2015b)

Annual Exceedance Probability	Return Period (yr)	Baseline, 1950-1999 (cfs)	2011-2040 Median (cfs, change from baseline)	2041-2070 Median (cfs, change from baseline)	2071-2100 Median (cfs, change from baseline)
0.5	2	4,500	5,400, 20%	5,100, 13%	5,200, 16%
0.1	10	13,300	16,000, 20%	14,000, 5%	14,900, 12%
0.02	50	23,500	28,900, 23%	24,500, 4%	25,600, 9%
0.01	100	28,000	36,800, 31%	29,700, 6%	31,300, 12%
0.005	200	32,400	43,800, 35%	35,400, 9%	37,900, 17%

6.3 Flooding in the Midwest – The NRC Context

- Increasing trends in rainfall events and flooding are expected to continue in the future.
- The frequency of flooding as indicated by number of flood magnitudes exceeding a specified threshold, rather than the flood magnitude, has been increasing in the Midwest Region.
- The spatial patterns of changes in the frequency of floods in the Midwest Region are related to one or more large-scale climate indices, particularly PNA.
- Locally in some river basins, discharges may be increasing for specified annual exceedance probabilities.

Many hydrometeorologic parameters that influence floods are not directly addressed in the NCAs. Some of the studies summarized above have attempted to investigate the impacts of climate change on runoff characteristics in the Midwest Region. Some of these studies used mean streamflow indicators (i.e., mean annual, seasonal, or monthly flows). Others have investigated the impacts of climate change on floods of annual exceedance probability of 0.005 and greater. Floods of interest to the NRC, particularly for safety analysis and review, include those that occur at significantly shorter timescales (hours to days) and almost always are in the tails of the distribution, away from the mean. Therefore, direct conclusions regarding shorter-duration, lower-frequency floods of interest to the NRC are difficult to draw. In addition, uncertainties arising from GCM differences, uncertainties in hydrologic models, uncertainties in socioeconomic responses, and uncertainties in water management can further complicate projections of flood risks.

Nevertheless, certain conclusions can be made that will give the NRC greater insights into flood analyses and their reviews. First, a site-specific analysis should be performed to assess the impacts of climate change on the behavior of floods. If frequency analyses are used, explicit accounting for non-stationarity in precipitation, land use, and/or flood data should be employed to ensure attribution of causative factors. A change in the mean behavior of floods can also reflect a change in the behavior in the tails. It is clear that the practical resolution of GCMs is going to remain incompatible for some time with the need for a local-to-regional-scale flood assessment. Therefore, further investigations, which may include exploring dynamical downscaling and nesting of hydrological models, are needed to couple the outputs of GCMs to hydrologic models.

Second, significant uncertainty in the predictions of hydrologic models (both aleatory and epistemic) will exist for the foreseeable future and can directly affect estimates of flood magnitudes under altered climate scenarios. A clear framework for enumerating and attributing the sources of these uncertainties, explicitly accounting for these uncertainties in flood estimation approaches, and propagating the uncertainties throughout flood analyses should be used. This framework will assist the NRC in investing resources to improve the parts of a flood assessment where uncertainties can be reduced given newer data sets and additional information. Given that climate change research, hydrologic understanding including newer data sets, and water-management practices are expected to continually evolve, a periodic refinement of site-specific flood assessments should be made.

Third, a site-specific assessment of flood protection and mitigation will be very useful from a safety perspective. It is noted that NRC current practice for permit and license application reviews relies on site-specific hydrologic engineering assessments that include both floods caused by multiple mechanisms relevant for the site and low-water issues. The site-specific flood assessment, including quantification of associated uncertainties, can facilitate clear articulation of risk faced by a plant and provide useful information for risk-informed licensing decisions.

6.4 Low Flows in the Midwest – The NRC Context

- Projected streamflow statistics related to mean annual and low-flow discharges appear to show periodic rather than monotonic increases.
- Urbanization and changing land use may result in changes in runoff. However, in river basins that are already significantly developed, climate change may influence streamflow to a greater degree than land-use change.

Many hydrometeorologic parameters that influence low flows are not directly addressed in the NCAs. Some of the studies summarized above have attempted to investigate the impacts of climate change on runoff characteristics in the Midwest Region. These studies used mean streamflow and low-flow indicators (i.e., mean annual, 7Q10, and/or 7Q2). These metrics are useful to the NRC in the review of water use and environmental impacts of plants. Additional low-flow metrics useful to the NRC include the persistence and frequency of low flows, both seasonally and in the context of multi-year low-flow events, and are not directly addressed in current studies.

Site-specific assessments may be needed to assess the characteristics of low-flow metrics under climate change scenarios. Some large-scale atmospheric patterns (e.g., PNA, NAO, and PDO) are related to low-flow events in the Midwest Region. Regional and local characteristics, including streamflow generation, urbanization and population growth, and water-management practices, would influence low flows at spatiotemporal scales of interest in NRC licensing reviews. Dynamically downscaled GCM outputs, nested climate and hydrologic modeling, and inclusion of water-management practices in low-flow assessments would be needed (see some examples above), with particular focus on seasonal to interannual persistence of low flows, to support NRC licensing.

As stated before, uncertainties in all aspects of climate hydrology assessments are expected to exist at significant levels for the foreseeable future. Given these uncertainties, decision-making would benefit from a framework for enumerating and attributing the sources of these uncertainties, explicitly accounting for these uncertainties in hydrologic estimation approaches and propagating the uncertainties throughout hydrologic analyses. This framework will assist the NRC in investing resources to improve the parts of low-flow assessment where uncertainties can be reduced given newer data sets and additional information. A periodic refinement of site-specific low-flow assessments can assist plants in mitigating the effects of sustained low-flow events on energy production and the environment.

6.5 Summary and Discussion

Studies of changes in observed floods over the last several decades in the Midwest Region show limited evidence of increase in peak flood discharge. However, changes in observed frequency of floods is increasing and shows spatial patterns within the Midwest Region and these patterns may be related to large-scale climate patterns. Within the last decade, unusual combinations of hydrometeorological conditions resulted in previously recorded historical maximums flood discharges.

The NCA has provided useful information about projected changes in precipitation, runoff, and soil moisture from climate models. To bridge between climate projections that are typically made at a grid resolution between 50 and 200 km and the hydrologic information needed to assess climate change impacts on water resources, some hydrologic modeling studies provide projections of hydrologic parameters such as streamflow, snowpack, and soil moisture. Overall, warming in the future can lead to changes in precipitation, runoff, and soil moisture in the Midwest Region. More specifically, increases in extreme precipitation have implications for floods and changes in temperature can affect snow water equivalent accumulation with subsequent effects on late-winter to early-spring streamflow timing. Besides warming, urbanization and land-use change could also affect the hydrologic characteristics through changes in both water demand and water supply. Simulations using downscaled CMIP3 projections of temperature and precipitation within a river basin showed that flood discharges across annual exceedance probabilities may be increasing with largest increases occurring in earlier periods of the 21st century. These studies have only been performed for limited regions or watersheds and do not quantify floods at annual exceedance probabilities of interest to the NRC. With CMIP5 simulations that contain larger number of climate model ensembles, future studies may provide increased confidence in flood discharge changes over the next century.

In general, the climate research community has not focused on evaluating trends and impacts of meteorological (and by extension, hydrologic) events of exceedance probabilities that are of interest to the NRC for permitting and licensing. The assessment of trends and impact at annual exceedance probablilities of interest to NRC also is limited by the fact that current climate models have significantly larger uncertainties for these events, therefore limiting the usefulness of predictions that may have large uncertainties. Moreover, uncertainties in climate model predictions are carried through and combined with uncertainties in hydrologic and hydraulic modeling approaches employed in hydrologic engineering assessments including PFHAs. Therefore, a consistent framework for enumerating, attributing, and incorporating these uncertainties, both in climate models and in hydrologic engineering assessments, should be used in site-specific PFHAs for permitting and licensing to clearly articulate the confidence associated with predictions at low annual exceedance probabilities.

7.0 Federal Climate Assessment and Modeling Activities

This section provides an overview of recent climate assessment and modeling activities, as well as guidance developed by federal agencies and interagency initiatives. This overview focuses on information with potiential relevance to NRC's mission.

7.1 U.S. Global Change Research Program

The USGCRP was established by Presidential Initiative in 1989 and mandated by Congress in the Global Change Research Act of 1990 (Pub.L. 101-606) to "… assist the Nation and the world to understand, assess, predict, and respond to human-induced and natural processes of global change." The act established a committee on Earth and Environmental Sciences, under the umbrella of the pre-existing Federal Coordinating Council for Science, Engineering, and Technology, to carry out functions relating to global change research, for the purpose of increasing the overall effectiveness and productivity of federal global change research efforts. The committee includes at least one representative from the National Science Foundation, National Aeronautics and Space Administration, NOAA, Environmental Protection Agency (EPA), Department of Energy, Department of Defense, Department of Interior, Department of Agriculture, Department of Transportation, Office of Management and Budget, Office of Science and Technology Policy, Council on Environmental Health Sciences of the National Institutes of Health, and such other agencies and departments of the United States as the President or the Chairman of the Council considers appropriate. The USGCRP performs its mandated functions primarily though working groups of this interagency committee. The USGCRP has a legal mandate to conduct a NCA every 4 years.[1] The third assessment, NCA3 (Melillo et al. 2014), released in May 2014, provides an important basis for this annual report focusing on climate change in the Midwest Region. NCA4 was released on November 23, 2018. An author of this report (Leung) served on a committee organized by the National Academies of Science, Engineering, and Medicine (NASEM 2018) to review a draft of the report. This NRC Climate Change Annual Report has also incorporated significant information from the CSSR (Volume 1 of NCA4; USGCRP 2017), which was developed to inform the fourth national assessment. More specifically the CSSR provides an update of the physical climate science presented in NCA3, including updated climate science findings and projections important to the authors of NCA4.

USGCRP's Interagency Group on Integrative Modeling has convened an annual U.S. Climate Modeling Summit since 2015, to improve the coordination and communication of national climate modeling goals and objectives. The fourth annual summit was convened on April 4–5, 2018.[2] The summit brought together representatives from the six U.S. "CMIP-class" climate model development centers and from operational climate-prediction programs. Specifically, two representatives—one lead and one additional delegate—from each of the following groups were invited to participate in the summit: GFDL (Climate Model/Earth System Model), Climate Forecast System, Goddard Institute for Space Studies (Model E), Goddard Earth Observing System (GEOS-5), Community Earth System Model, and Energy Exascale Earth System Model (E3SM). A workshop on "Land-Atmosphere Interactions and Extremes" was held on the first day of the summit. Land surface processes are increasingly being recognized as providing important information for weather and climate predictions, and the land surface represents an important intersection between human activities and the Earth system. The workshop provided a forum for discussions to prioritize research and development for the modeling centers. The subjects addressed included land-atmosphere interactions and extremes, hydrological extremes and coastal, land and human interactions.

[1] http://www.globalchange.gov/what-we-do/assessment

[2] https://climatemodeling.science.energy.gov/sites/default/files/IGIM_CMS_agenda%20_5916.pdf

7.2 Federal Climate Change and Water Working Group

The federal Climate Change and Water Working Group (CCAWWG) provides engineering and scientific collaborations in support of water management under a changing climate. Participating agencies include: U.S. Army Corps of Engineers (USACE), U.S. Bureau of Reclamation, NOAA, U.S. Geological Survey (USGS), EPA, Federal Emergency Mangement Agency, National Aeronautics and Space Administration (NASA), and U.S. Department of Agriculture. The working group's collaboration informs and coordinates with higher-level interagency activities such as the U.S. Global Change Research Program's Adaptation Science Interagency Working Group, Council of Environmental Quality's Climate Preparedness and Water Resources Work Group, the Office of Science and Technology Policy Committee on Environment and Natural Resources' Subcommittee on Water Availability and Quality, and the Advisory Committee on Water Information's Water Resources Adaptation to Climate Change Workgroup.

The USACE Civil Works Program recently published Engineering and Construction Bulletin (ECB) No. 2016-25, "Guidance for Incorporating Climate Change Impacts to Inland Hydrology in Civil Works Studies, Designs, and Projects" (USACE 2016). The ECB recognizes that in some geographical locations and for some impacts that are relevant to the USACE, climate change may be shifting, not only the climatological baseline, but also the natural variability about that baseline (USACE 2016). ECB 2016-25 noted that projections of climate change and impacts at local scales can be highly uncertain and proposed a qualitative assessment that may assist in future project modifications and consideration of alternatives (examples of the qualitative assessment were included). It also required the qualitative analysis to be performed for all hydrologic studies at inland watersheds at the time of its issuance. Figure 7.1 is the flow chart included in ECB No. 2016-25; it lays out the elements of the qualitative analysis.

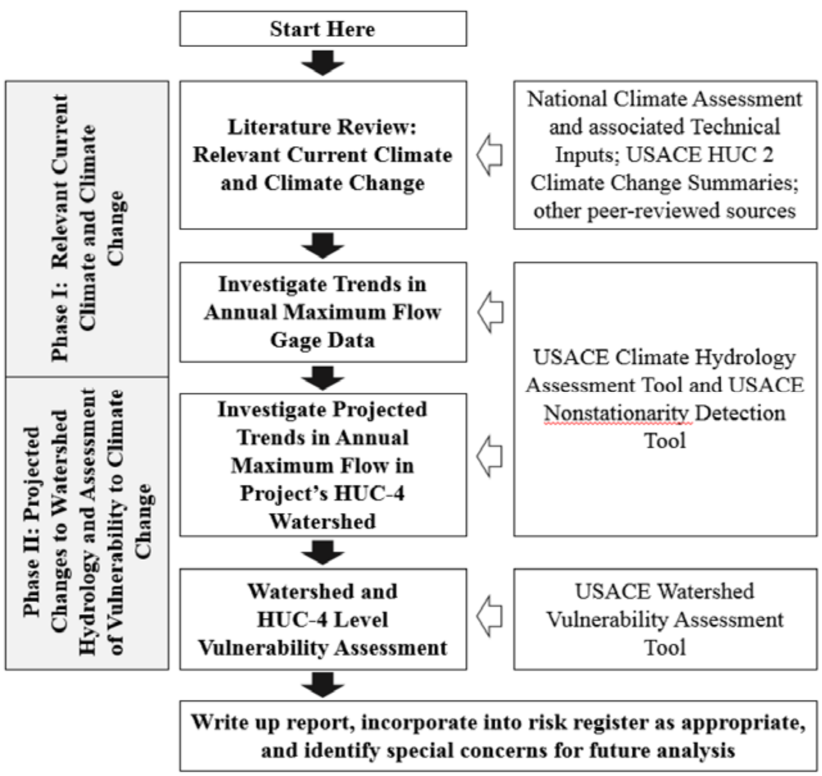

Figure 7.1. Flow chart for qualitative assessment of the impacts of climate change in hydrologic analyses (Source: USACE 2016)

USACE has also developed a web-based qualitative Climate Hydrology Assessment Tool available publicly at http://corpsclimate.us/ptcih.cfm. However, the ECB 2016-25 cautions that the climate hydrology output may be limited in precision, may not adequately represent watershed complexities including snowmelt and regulation, and may only be suitable for watershed-scale decisions. At the time of the publication of ECB No. 2016-25, USACE does not require qualitative assessment of climate change impacts on probable maximum flood because the exisiting body of research in this area is insufficient.

7.2.1 USACE Responses to Climate Change Program

USACE has also implemented a Responses to Climate Change Program to understand the potential impacts of climate change on natural and human-made systems (USACE 2017). As part of this program, USACE is preparing 21 regional climate syntheses. These regions are at the scale of a two-digit Hydrologic Unit Code (HUC) across the continental United States, Alaska, Hawaii, and Puerto Rico (Figure 7.2). USACE noted that outputs from climate models are coherent and useful at the scale of 2-digit HUCs and that confidence in climate model outputs declines for areas smaller than 4-digit HUCs. The regional syntheses summarize observed and projected climate and hydrological patterns as reported in national and regional reports and peer-reviewed literature. The syntheses for Regions 5, 10, and 11 were published in January 2015; that of Region 4 in April 2015; that of Region 9 in May 2015; and that of Region 7 in June 2015. The syntheses assess the vulnerability of each region to USACE business lines, including navigation, flood risk management, water supply, ecosystem restoration, hydropower, recreation, emergency management, regulatory mission, and military programs against several climate variables, including increased ambient temperatures, increased maximum temperatures, increased storm intensity and frequency, and sea-level rise.

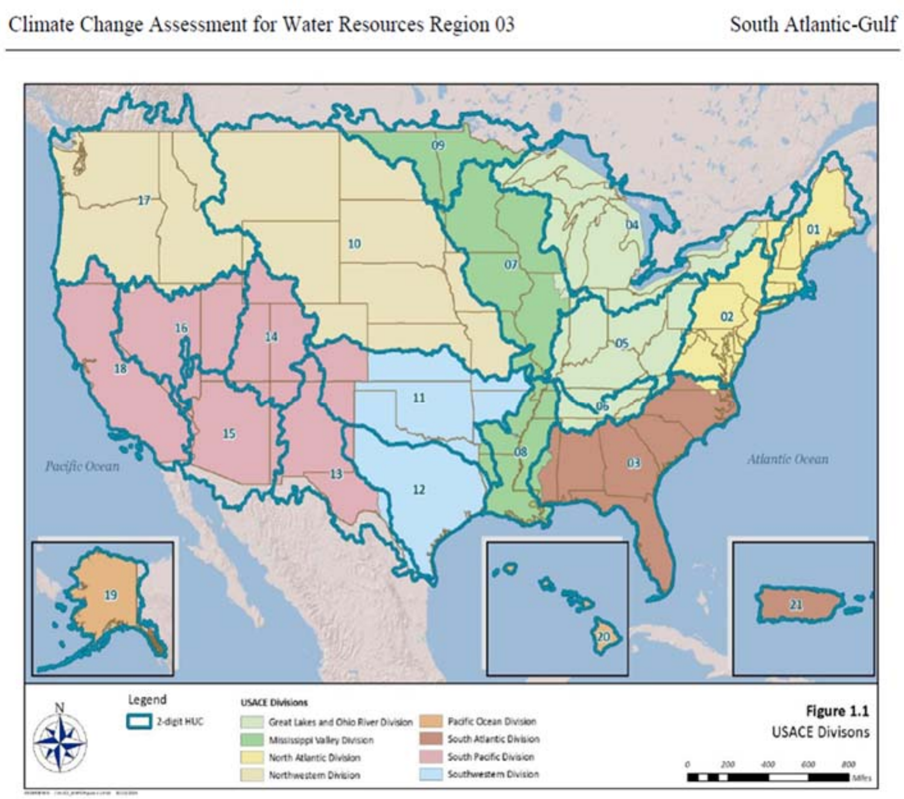

Figure 7.2. Regions used in the USACE Responses to Climate Change Program. The Midwest Region consists of parts of the USACE Regions 4, 5, 7, 9, 10, and 11 (Source: USACE 2015a)

7.2.1.1 Region 4

Based on information from a literature review, USACE concluded that observed temperatures in Region 4 show small increasing trends. Some studies point to seasonal differences with possible decreasing trends in fall or winter. The studies also point to increasing trend in average precipitation with seasonal and geographical variations. USACE noted that most studies showed that extreme precipitation events were becoming slightly larger and more frequent; they did not define the term "extreme." USACE also concluded that small increases in streamflow were found in some studies while others showed no significant changes.

For future climate projections, USACE noted the strong consensus that temperatures will increase over the next century with an increase in mean annual temperature ranging from 0–7□. The consensus also applies to more frequent, longer, and more intense heat waves. Projected precipitation variations are less certain—most studies project increases, some project decreases, and some project seasonal or geographial variability. Hydrologic projections contain significant uncertainty with some studies indicating increases and some indicating decreases in future streamflow. Great Lakes water levels are generally expected to decline although some modeling scenarios show an increase or no change.

7.2.1.2 Region 7

Based on information from a literature review, USACE concluded that observed temperatures in Region 7 show moderate increases in temperature (e.g., daily mean and minimum), precipitation, and streamflow (e.g., mean, low, and peak). Some of these observed changes are quantified to be statistically significant.

For future climate projections, USACE noted the strong consensus that temperatures will increase over the next century. The consensus also applies to increasing trends in future annual and extreme precipitation. There is no clear consensus on projections of streamflow with some studies indicating increases in future streamflows as a result of increasing precipitation and other studies indicating decreasing streamflows as a result of increased evapotranspiration. However, multiple studies indicate increases in winter and spring streamflows and a decrease in summer streamflows.

7.2.2 NOAA State Climate Summaries

The NOAA NCEI has released a set of state climate summaries containing information on historical climate variations and trends, future climate model projections of climate conditions, and past and future sea-level and coastal-flooding conditions. These state climate summaries build on information provided in the 2014 National Climate Assessment (NCA3) and contain three types of information: key messages, narrative summaries, and downloads. The downloads include state summaries, high-resolution figures suitable for report or presentations, and supplemental web graphics.

The description of historical climate conditions for each state are based on an analysis of core climate data (the data sources are described in the supplementary online material). However, to help understand, prioritize, and describe the importance and significance of different climate conditions, additional input was derived from climate experts in each state, some of whom are authors on these state climate summaries. In particular, input was sought from the NOAA Regional Climate Centers and from the State Climatologists. The historical climate conditions are meant to provide a perspective on what has been happening in each state and what types of extreme events have historically been noteworthy, to provide a context for assessment of future impacts.

The future climate scenarios are intended to provide an internally consistent set of climate conditions that can inform analyses of potential impacts of climate change. The scenarios are not intended as projections as there are no probabilities for their future realization attached. They simply represent an internally consistent climate picture under certain assumptions about the future pathway of greenhouse gas emissions. The future climate scenarios are based on well-established sources of information. No new climate model simulations or downscaled data sets were produced for use in these state climate summaries. State climate summaries (including the Midwest Region) can be found at https://statesummaries.ncics.org.

7.2.3 EPA Report on Climate Change Indicators in the United States

The EPA has released an externally peer-reviewed report describing a variety of climate change indicators in the United States as of 2016. The information provided gives a good national overview, with some regions highlighted for particular variables. The resources page lists other good sources of information. This report is available at https://www.epa.gov/sites/production/files/2016-08/documents/climate_indicators_2016.pdf.

7.3 (U.S.–Canada) International Joint Commission

In 1909, Canada and the United States signed the Boundary Waters Treaty, which authorizes the International Joint Commission (IJC) to regulate shared water issues, investigate transboundary issues, and recommend solutions related to the Great Lakes. The IJC establishes boards, task forces, and work groups to assist in carrying out its activities. For example, the Great Lakes Science Advisory Board provides scientific advice to the IJC and the Great Lakes Water Quality Board assists the IJC in identifying emerging issues and recommending solutions to complex water-quality challenges in the Great Lakes. As described in Chapter 5, the IJC directed the IUGLSB to improve understanding of how the Great Lakes function, how water levels in the lakes are changing, and what potential management options may be available relative to changing water levels in the future. In addition, NOAA's GLERL conducts research on the dynamic environment and ecosystems of the Great Lakes and its coastal regions.

8.0 References

Agee E, J Larson, S Childs, and A Marmo. 2016. "Spatial redistribution of U.S. tornado activity between 1954 and 2013." *Journal of Applied Meteorology and Climatology* 55:1681–1697. doi: 10.1175/JAMC-D-15-0342.1

Akaike H. 1974. "A new look at the statistical model identification." *IEEE Transactions on Automatic Control* 19 (6):716–723. doi:10.1109/TAC.1974.1100705

Barnes EA and L Polvani. 2013. "Response of the midlatitude jets, and of their variability, to increased greenhouse gases in the CMIP5 models." *Journal of Climate* 26:7117-7135. doi:10.1175/JCLI-D-12-00536.1

Boustead BEM, SD Hilberg, MD Shulski, and KG Hubbard. 2015. "The accumulated winter season severity index (AWSSI)." *Journal of Applied Meteorology and Climatology* 54:1693-1712 doi: 10.1175/JAMC-D-14-0217.1

Brohan P, JJ Kennedy, I Harris, SFB. Tett, and PD Jones. 2006. "Uncertainty estimates in regional and global observed temperature changes: A new data set from 1850." *Journal of Geophysical Research* 111:D12106

Budikova D, JSM Coleman, SA Strope, and A Austin. 2010. "Hydroclimatology of the 2008 Midwest floods." *Water Resources Research* 46:W12524. doi:10.1029/2010WR009206

Byun K and AF Hamlet. 2018. "Projected changes in future climate over the Midwest and Great Lakes region using downscaled CMIP5 ensembles." *International Journal of Climatology* doi: 10.1002/joc.5388.

CCGL (Coordinating Committee on Great Lakes). 2017." Updating the International Great Lakes Datum (IGLD). Vertical Control – Water Levels Subcommittee." http://www.greatlakescc.org/wp36/wp-content/uploads/2017/09/IGLD_Update_20170929_Exec_220dpi.pdf

Chang EKM. 2013. "CMIP5 projection of significant reduction in extratropical cyclone activity over North America." *Journal of Climate* 26:9903–9922. doi.org/10.1175/JCLI-D-13-00209.1

Chang EKM, Y Guo, and X Xia. 2012. "CMIP5 multimodel ensemble projection of storm track change under global warming." *Journal of Geophysical Research* 117:D23118. doi:10.1029/2012JD018578

Choi W, F Pan, and C Wu. 2017. "Impacts of climate change and urban growth on the streamflow of the Milwaukee River (Wisconsin, USA)." *Regional Environmental Change* 17:889-899.

Cook KH, EK Vizy, ZS Launer, and CM Patricola. 2008. "Springtime intensification of the Great Plains low-level jet and midwest precipitation in GCM simulations of the twenty-first century." *Journal of Climate* 21:6321-6340. http://dx.doi.org/10.1175/2008jcli2355.1

Croley II, TE. 1983. "Great Lake basins (USA-Canada) runoff modeling." *Journal of Hydrology* 64 (1):135-158.

DeMarchi C, Q Dai, ME Mello, and TS Hunter. 2010. "Uncertainty quantification in the net basin supply of Lake Erie and Lake Michigan." *Proc. SimHydro 2010: Hydraulic Modeling and Uncertainty*, Sophia-Antipolis, France, Société Hydrotechnique de France.

Diffenbaugh NS and M Ashfaq. 2010. “Intensification of hot extremes in the United States.” *Geophysical Research Letters* 37(15) doi: 10.1029/2010GL043888

Diffenbaugh NS, M Scherer, and RJ Trapp. 2013. “Robust increases in severe thunderstorm environments in response to greenhouse forcing.” *Proceedings of the National Academy of Science (USA)* 101:16,361–16,366. doi: 10.1073/pnas.1307758110

Easterling, DR, KE Kunkel, JR Arnold, T Knutson, AN LeGrande, LR Leung, RS Vose, DE Waliser, and MF Wehner. 2017. “Precipitation change in the United States.” In: *Climate Science Special Report: Fourth National Climate Assessment, Volume I*, Wuebbles, DJ, DW Fahey, KA Hibbard, DJ Dokken, BC Stewart, and TK Maycock (eds.). pp. 207-230, U.S. Global Change Research Program, Washington, D.C. doi: 10.7930/J0H993CC

Ellison CA, CA Sanocki, DL Lorenz, GB Mitton, and GA Kruse. 2011. Floods of September 2010 in Southern Minnesota, U.S. Geological Survey Scientific Investigations Report 2011-5045, 37 pp., *The 2011 Flood in the Mississippi and Tributaries Project*, USACE Mississippi River Commission. http://pubs.usgs.gov/sir/2011/5045/pdf/sir2011-5045.pdf

Feng Z, LR Leung, S Hagos, RA Houze, Jr, CD Burleyson, and K Balaguru. 2016. “More frequent intense and long-lived storms dominate the trend in central U.S. rainfall.” *Nature Communications* 7:13429. doi: 10.1038/ncomms13429

Fritsch J, R Kane, and C Chelius. 1986. “The contribution of mesoscale convective weather systems to the warm-season precipitation in the United States.” *Journal of Applied Meteorology and Climatology* 25:1333–1345

Fry LM, AD Gronewold, V Fortin, S Buan, AH Clites, C Luukkonen, D Holtschlag, L Diamond, T Hunter, F Seglenieks, D Durnford, M Dimitrijevic, C Subich, E Klyszejko, K Kea, and P Restrepo. 2014. “The Great Lakes Runoff Intercomparison Project Phase 1: Lake Michigan (GRIP-M).” *Journal of Hydrology* 519:3448-3465. http://dx.doi.org/10.1016/j.jhydrol.2014.07.021

Gaborit E, V Fortin, B Tolson, L Fry, T Hunter, AD Gronewold. 2017. Great Lakes runoff inter-comparison Project, phase 2: Lake Ontario (GRIP-O). *Journal of Great Lakes Research* 43, 217-227, https://doi.org/10.1016/j.jglr.2016.10.004

Gensini VA and TL Mote. 2014. “Estimations of hazardous convective weather in the United States using dynamical downscaling.” *Journal of Climate* 27:6581-6589. doi: 10.1175/JCLI-D-13-00777.1.

GLC (The Great Lakes Commission). 2003. *Toward a Water Resources Management Decision Support System for the Great Lakes-St. Lawrence River Basin – Status of Data and Information on Water Resources, Water Use, and Related Ecological Impacts*. The Great Lakes Commission for the Great Lakes States and Provinces. https://www.glc.org/library/2003-toward-a-water-resources-management-decision-support-system

GLC (The Great Lakes Commission). 2017. *Strategic Plan for the Great Lakes Commission 2017–2022*. http://www.glc.org/wp-content/uploads/2013/07/GLC-strategic-plan_Final_Adopted-Jan-13-2017.pdf

GLC (The Great Lakes Commission). 2019. ”About Us. The Great Lakes Commission website.” https://www.glc.org/about/

Gronewold AD and CA Stow. 2014. ”Water Loss from the Great Lakes.” *Science*, 343(6175):1084-1085.

Gronewold AD, J Bruxer, D Durnford, JP Smith, AH Clites, F Seglenieks, SS Qian, TS Hunter, and V Fortin. 2016. ”Hydrological drivers of record-setting water level rise on Earth’s largest lake system.” *Water Resources Researech* 52:4026–4042. doi:10.1002/2015WR018209

Gronewold AD, TS Hunter, J Allison, LM Fry, KA Kompoltowicz, RA Bolinger, and L Pei. 2017. *Project Documentation Report for Great Lakes seasonal and interannual water supply forecasting improvements project Phase I: Research and Development*. NOAA Great Lakes Environmental Research Laboratory, U.S. Army Corps of Engineers Detroit District and the University Corporation for Atmospheric Research, Ann Arbor, Mich., 233 pp. https://www.glerl.noaa.gov/pubs/fulltext/2018/20180020.pdf

Hamlet AF, MM Elsner, G Mauger, S-Y Lee, I Tohver, RA Norheim. 2013. “An overview of the Columbia Basin climate change scenarios project: Approach, methods, and summer of key results.” *Atmosphere and Ocean* 51(4):392-415. doi:10.1080/07055900.2013.819555

Hoogewind KA, ME Baldwin, and RJ Trapp. 2017. “The impact of climate change on hazardous convective weather in the United States: Insights from high-resolution dynamical downscaling.” *Journal of Climate* 30:10081-10100. doi: 10.1175/JCLI-D-16-0885.1

Houze RA. 2004. “Mesoscale convective systems.” *Reviews of Geophysics* 42(4):RG4003.

IUGLSB (International Upper Great Lakes Study Board). 2012. *Lake Superior regulation: addressing uncertainty in Upper Great Lakes Water Levels*. Final Report to the International Joint Commission by the International Upper Great Lakes Study Board. ISBN: 978-1-100-20324-9.

Kain JS, SJ Weiss, DR Bright, ME Baldwin, JJ Levit, GW Carbin, CS Schwartz, ML Weisman, KK Droegemeier, DB Weber, and KW Thomas. 2008. “Some practical considerations regarding horizontal resolution in the first generation of operational convection-allowing NWP.” *Weather Forecasting* 23:931–952. https://doi.org/10.1175/WAF2007106.1

Kendon EJ et al. 2017. “Do convection-permitting regional climate models improve projections of future precipitation change?” *Bulletin of the American Meteorological Society* 98:79–93.

Kooperman GJ, MS Pritchard, and RCJ Somerville. 2013. “Robustness and sensitivities of central U.S. summer convection in the super-parameterized CAM: Multi-model intercomparison with a new regional EOF index.” *Geophysical Research Letters* 40:3287–3291. doi: 10.1002/grl.50597

Kooperman GJ, MS Pritchard, and RCJ Somerville. 2014. “The response of U.S. summer rainfall to quadrupled CO_2 climate change in conventional and superparameterized versions of the NCAR community atmosphere model.” *Journal of Advances in Modeling Earth Systems* 6:859–882. doi:10.1002/2014MS000306

Kunkel KE, D Arndt, H Brooks, et al. 2013a. “Monitoring and understanding trends in extreme storms: State of knowledge.” *Bulletin of the American Meteorological Soc*iety 94:499-514. doi: 10.1175/BAMS-D-11-00262.1

Kunkel KE, MA Palecki, L Ensor, D Easterling, KG Hubbard, D Robinson, and K Redmond. 2009. “Trends in twentieth-century U.S. extreme snowfall seasons.” *Journal of Climate* 22:6204-6216.

Kunkel KE, DA Robinson, S Champion, X Yin, T Estilow, and RM Frankson. 2016. "Trends and extremes in Northern Hemisphere snow characteristics." *Current Climate Change Reports,* 2:65-73. http://dx.doi.org/10.1007/s40641-016-0036-8

Kunkel KE, LE Stevens, SE Stevens, L Sun, E Janssen, D Wuebbles, SD Hilberg, MS Timlin, L Stoecker, NE Westcott, and JG Dobson. 2013b. "Regional Climate Trends and Scenarios for the U.S. National Climate Assessment. Part 3. Climate of the Midwest U.S." *NOAA Technical Report NESDIS 142-3*. 103pp. National Oceanic and Atmospheric Administration, National Environmental Satellite, Data, and Information Service, Washington, D.C. http://www.nesdis.noaa.gov/technical_reports/NOAA_NESDIS_Tech_Report_142-3-Climate_of_the_Midwest_U.S.pdf.

Kunkel KE, DR Easterling, DAR Kristovich, B Gleason, L Stoecker, and R Smith. 2012. "Meteorological causes of the secular variations in observed extreme precipitation events for the conterminous United States." *Journal of Hydrometeorology* 13:1131–1141. https://doi.org/10.1175/JHM-D-11-0108.1

Laird NF and DAR Kristovich. 2002. "Variations of sensible and latent heat fluxes from a Great Lakes buoy and associated synoptic weather patterns." *Journal of Hydrometeor*ology 3:3-12.

Lehmann J, D Coumou, K Frieler, V Eliseev, and A Livermann. 2014. "Future changes in extratropical storm tracks and baroclinicity under climate change." *Environmental Research Letters* 9:084002.

Lin Y, W Dong, M Zhang, Y Xie, W Xue, J Huang, and Y Luo. 2017. "Causes of model dry and warm bias over central U.S. and impact on climate projections." *Nature Communications* 8:881. doi: 10.1038/s41467-017-01040-2

Liu AQ and GWK Moore. 2004. "Lake-effect snowstorms over Southern Ontario, Canada, and their associated synoptic-scale environment." *Monthly Weather Review* 132:2595–2609.

Lofgren BM and TA Hunter. 2011. *Final Report: NOAA Great Lakes Environmental Research Laboratory's Contributions to the Activity "Comparative Analysis of Net Basin Supply Components and Climate Change Impacts on the Upper Great Lakes."* NOAA Great Lakes Environmental Research Laboratory, Ann Arbor, Michigan. http://www.iugls.org/project/Comparative%20Analysis%20of%20Net%20Basin%20Supply%20Components%20and%20Climate%20Change%20Impacts%20on%20the%20Upper%20Great%20Lakes%20Using%20CHARM. Accessed February 16, 2018

Lofgren BM, TA Hunter, and J Wilbarger. 2011. "Effects of using air temperature as a proxy for potential evapotranspiration in climate change scenarios of Great Lakes basin hydrology." *Journal of Great Lakes Research* 37:744–752. doi:10.1016/j.jglr.2011.09.006

Lofgren BM and J Rouhana. 2016. "Physically plausible methods for projecting changes in great lakes water levels under climate change scenarios." *Journal of Hydrometeorology* 17:2209-2223. doi: 10.1175/JHM-D-15-0220.1.

Lombard F. 1987. "Rank tests for changepoint problems." *Biometrika* 74:615-624.

Lopez H, R West, S Dong, G Goni, B Kirtman, S-K Lee, and R Atlas. 2018. "Early emergence of anthropogenically forced heat waves in the western United States and Great Lakes." *Nature Climate Change* doi:10.1038/s41558-018-0116-y.

Lu J, GA Vecchi, and T Reichler. 2007. "Expansion of the Hadley cell under global warming." *Geophysical. Research Letters* 34:L06805. doi:10.1029/2006GL028443

MacKay M and F Seglenieks. 2013. "On the simulation of Laurentian Great Lakes water levels under projections of global climate change." *Climatic Change* 117:55-67. doi:10.1007/s10584- 012-0560-z

Maddox RA. 1980. Mesoscale convective complexes. *Bulletin of the American Meteorological Society* 61:1374-1387.

Mallakpour I and G Villarini. 2015. "The changing nature of flooding across the central United States." *Nature Climate Change* 5:250-254.

Mallakpour I and G Villarini. 2016. "Investigating the relationship between the frequency of flooding over the central United States and large-scale climate." *Advances in Water Resources* 92:159-171.

Mascioli NR, M Previdi, AM Fiore, and M Ting. 2017. "Timing and seasonality of the United States 'warming hole'." *Environmental Research Letters* 12:34008. http://dx.doi.org/10.1088/1748-9326/aa5ef4

Melillo JM, TC Richmond, and GW Yohe (eds.). 2014. *Climate Change Impacts in the United States: The Third National Climate Assessment*. U.S. Global Change Research Program, 841 pp. doi:10.7930/J0Z31WJ2

MNDNR (Minnesota Department of Natural Resources). 2018. *Historic Mega-Rain Events in Minnesota*. http://www.dnr.state.mn.us/climate/summaries_and_publications/mega_rain_events.html. Accessed February 12, 2018.

Mueller ND, EE Butler, KA McKinnon, A Rhines, M Tingley, NM Holbrook, and P Huybers. 2016. "Cooling of U.S. Midwest summer temperature extremes from cropland intensification." *Nature Climate Change* 6:317-322. http://dx.doi.org/10.1038/nclimate2825

NASEM (National Academies of Sciences, Engineering, and Medicine). 2018. *Review of the Draft Fourth National Climate Assessment*. Washington, D.C.: The National Academies Press. doi: https://doi.org/10.17226/25013.

Nash JE and JV Sutcliffe. 1970. "River flow forecasting through conceptual models part I – A discussion of principles." *Journal of Hydrology* 10(3):282–290. doi:10.1016/0022-1694(70)90255-6

NCEI (National Centers for Environmental Information). 2016a. *U.S. Climate Atlas*. http://www.ncdc.noaa.gov/climateatlas/

NCEI (National Centers for Environmental Information). 2016b. *Comparative Climatic Data For the United States Through 2015*. NOAA NCEI, Ashville, North Carolina. http://www1.ncdc.noaa.gov/pub/data/ccd-data/CCD-2015.pdf

Niyogi D, P Pyle, M Lei, SP Arya, CM Kishtawal, M Shepherd, F Chen, and B Wolfe. 2011. "Urban modification of thunderstorms: an observational storm climatology and model case study for the Indianapolis urban region." *Journal of Applied Meteorology and Climatology* 50:1129-1144.

NOAA (National Oceanic and Atmospheric Administration). 2019. "What is a Lake Effect Snow?" National Weather Service. https://www.weather.gov/safety/winter-lake-effect-snow

NOAA GLERL (National Oceanic and Atmospheric Administration Great Lakes Environmental Research Laboratory). 2018a. Archieved Water Level Brochures. https:///www.glerl.noaa.gov/data/wlevels/archivedLevelBrochures.html

NOAA GLERL (National Oceanic and Atmospheric Administration Great Lakes Environmental Research Laboratory). 2018b. "Great Lakes Water Levels – February 2018." https://www.glerl.noaa.gov/pubs/brochures/lakelevels/lakelevels.pdf

Notaro M, V Bennington, and B.Lofgren. 2015. "Dynamical downscaling–based projections of Great Lakes water levels." *Journal of Climate* 28:9721–9745. doi:10.1175/JCLI-D-14-00847.1

Novotny EV and HG Stefan. 2007. "Stream flow in Minnesota: Indicator of climate change." *Journal of Hydrology* 334:319-333.

NRC (U.S. Nuclear Regulatory Commission). 2016. Guidance for Activities Related to Near-Term Task Force Recommendation 2.1, Flooding Hazard Reevaluation; Focused Evaluation and Integrated Assessment. Interim Staff Guidance JLD-ISG-2016-01. https://www.nrc.gov/docs/ML1609/ML16090A140.pdf

NRC (U.S. Nuclear Regulatory Commission). 2017. *Information Digest, 2017-2018*. NUREG-1350, Volume 29, Revision 1. Accession No. ML17228A057. Accessed December 19, 2017 at https://www.nrc.gov/reading-rm/doc-collections/nuregs/staff/sr1350/.

NWS (National Weather Service). 2018. *Historic Flooding Event – 28-30 April 2017.* https://www.weather.gov/sgf/28-30AprilHistoricFloodingEvent. Accessed February 13, 2018.

Peterson TC, RR Heim, R Hirsch, DP Kaiser, H Brooks, NS Diffenbaugh, RM Dole, JP Giovannettone, K Guirguis, TR Karl, RW Katz, K Kunkel, D Lettenmaier, GJ McCabe, CJ Paciorek, KR Ryberg, S Schubert, VBS Silva, BC Stewart, AV Vecchia, G Villarini, RS Vose, J Walsh, M Wehner, D Wolock, K Wolter, CA Woodhouse, and D Wuebbles. 2013. "Monitoring and understanding changes in heat waves, cold waves, floods and droughts in the United States: State of knowledge." *Bulletin of the American Meteorological Society* 94:821-834. doi:10.1175/BAMS-D-12-00066.1

Pierce DW, DR Cayan, and BL Thrasher. 2014. Statistical downscaling using Localized Constructed Analogs (LOCA). *Journal of Hydrometeorology* 15, 2558–2585, doi: 10.1175/JHM-D-14-0082.1.

Prein AF, C Liu, K Ikeda, R Bullock, RM Rasmussen, GJ Holland, and M Clark. 2017a. "Simulating North American mesoscale convective systems with a convection-permitting climate model." *Climate Dynamics* https://doi.org/10.1007/s00382-017-3947-8.

Prein AF, RM Rasmussen, K Ikeda, C Liu, MP Clark, and GJ Holland. 2017b. "The future intensification of hourly precipitation extremes." *Nature Climate Change* 7:48–52. doi: 10.1038/nclimate3168

Prein, AF, C Liu, K Ikeda, SB Trier, RM Rasmussen, GJ Holland, and MP Clark. 2017c. Increased rainfall volume from future convective storms in the US. *Nature Climate Change* 7:880-884. doi: 10.1038/nclimate/s41558-017-0007-7.

Pritchard MS, MW Moncrieff, and RCJ Somerville. 2011. "Orogenic propagating precipitation systems over the United States in a global climate model with embedded explicit convection." *Journal of the Atmospheric Sciences* 68(8):1821–1840.

Pryor SC, D Scavia, C Downer, M Gaden, L Iverson, R Nordstrom, J Patz, and GP Robertson. 2014. "Chapter 18: Midwest." *Climate Change Impacts in the United States: The Third National Climate Assessment*, JM Melillo, Terese (TC) Richmond, and GW Yohe, (eds.). U.S. Global Change Research Program, 418-440. doi:10.7930/J0J1012N

Raymond C, D Singh, and RM Horton. 2017. "Spatiotemporal patterns and synoptics of extreme wet-bulb temperature in the contiguous United States." *Journal of Geophysical Research: Atmospheres* 122:13,108–13,124. https://doi.org/10.1002/2017JD027140

Romps DM, JT Seeley, D Vollaro, and J Molinari. 2014. "Projected increase in lightning strikes in the United States due to global warming." *Science* 346:851–854.

Saide PE, SN Spak, RB Pierce, JA Otkin, TK Schaack, AK Heidinger, AM da Silva, M Kacenelenbogen, J Redemann, and GR Carmichael. 2015. "Central American biomass burning smoke can increase tornado severity in the U.S." *Geophysical Research Letters* 42:956–965. doi:10.1002/2014GL062826

Schumacher RS, and RH Johnson. 2006. "Characteristics of U.S. extreme rain events during 1999-2003." *Weather Forecasting* 21:69-85. doi: 10.1175/WAF900.1

Seeley JT and DM Romps. 2015. "The effect of global warming on severe thunderstorms in the United States." *Journal of Clim*ate doi:10.1175/JCLI-D-14-00382.1.

Smith JP and AD Gronewold. 2018. "Development and Analysis of a Bayesian Water Balance Model for the Large Lake System." Cooperative Institute for Great Lakes Research and Great Lakes Environmental Research Laboratory, Ann Arbor, Michigan. https://arxiv.org/abs/1710.10161

Song F, LR Leung, J Lu, and L Dong. 2018a. "Seasonally dependent responses of subtropical highs and tropical rainfall to anthropogenic warming." *Nature Climate Change 8*(9):787. https://www.nature.com/articles/s41558-018-0244-4

Song F, LR Leung, J Lu, and L Dong. 2018b. "Future changes in seasonality of the North Pacific and North Atlantic subtropical highs." *Geophysical Research Letters 45*(21):11-959. https://agupubs.onlinelibrary.wiley.com/doi/10.1029/2018GL079940

Stevenson SN and RS Schumacher. 2014. "A 10-year survey of extreme rainfall events in the central and eastern United States using gridded multisensory precipitation analyses." *Monthly Weather Review* 142:3147-3162. doi: 10.1175/MWR-D-13-00345.1

Swanston CW, LA Brandt, MK Janowiak, SD Handler, P Butler-Leopold, L Iverson, FR Thompson, TA Ontl, and PD Shannon. 2017. "Vulnerability of forests of the Midwest and Northeast United States to climae change." *Climatic Change* 146(1-2):103-116. doi:10.1007/s10584-017-2065-2

Taylor KE, RJ Stouffer, and GA Meehl. 2012. "An overview of CMIP5 and the experiment design." *Bulletin of the American Meteorological Society* 93:485–498.

Teng H and G Branstator. 2017. "Causes of extreme ridges that induce California droughts." *Journal of Climate* 30(4):1477–1492. https://doi.org/10.1175/jcli-d-16-0524.1

Tippett MK, C Lepore, and JE Cohen. 2016. "More tornadoes in the most extreme U.S. tornado outbreaks." *Science* 354:1419-1423. doi: 10.1126/science.aah7393

Tippett MK, AH Sobel, and SJ Camargo. 2012. "Association of U.S. tornado occurrence with monthly environmental parameters." *Geophysical Research Letters* 39, doi:10.1029/2011GL050368.

Trapp RJ and KA Hoogewind. 2016. "The realization of extreme tornadic storm events under future anthropogenic climate change." *Journal of Climate* 29, doi: 10.1175/JCLI-15-0623.1.

Trapp RJ, NS Diffenbaugh, HE Brooks, ME Baldwin, ED Robinson, and JS Pal. 2007. "Changes in severe thunderstorm environment frequency during the 21st century caused by anthropogenically enhanced global radiative forcing." *Proceedings of the National Academy of Sciences Dec 2007* 104(50):19719–19723. doi:10.1073/pnas.0705494104

USACE (U.S. Army Corps of Engineers). 2015a. *Recent U.S. Climate Change and Hydrology Literature Applicable to U.S. Army Corps of Engineers Missions – South Atlantic-Gulf Region 03*. Civil Works Technical Report, CWTS 2015-03, USACE, Washington, D.C. Accessed February 1, 2017 at http://corpsclimate.us/docs/rccvarreports/USACE_REGION_03_Climate_Change_Report_CWTS-2015-03_Hi.pdf.

USACE (U.S. Army Corps of Engineers). 2015b. *Red River of the North at Fargo, North Dakota, Pilot Study, Impact of Climate Change on Flood Frequency Curve*. Available at: http://www.corpsclimate.us/docs/Red_River_of_the_North_Adaptation_Pilot.pdf.

USACE (U.S. Army Corps of Engineers). 2016. *Guidance for Incorporating Climate Change Impacts to Inland Hydrology in Civil Works Studies, Designs, and Projects*. Engineering and Construction Bulletin, No. 2016-25, Corps of Engineers Civil Works, Washington, D.C.

USACE (U.S. Army Corps of Engineers). 2017. *Responses to Climate Change*. Available at http://corpsclimate.us/index.cfm.

USACE (U.S. Army Corps of Engineers). 2018. Monthly Bulletin of Great Lakes Water Levels. USACE Detroit District. Available at http://www.lre.usace.army.mil/Missions/Great-Lakes-Information/Great-Lakes-Water-Levels/Water-Level-Forecast/Monthly-Bulletin-of-Great-Lakes-Water-Levels/. Accessed February 14, 2018.

USGCRP (U.S. Global Change Research Program). 2017. *Climate Science Special Report: Fourth National Climate Assessment, Volume I*, Wuebbles DJ, DW Fahey, KA Hibbard, DJ Dokken, BC Stewart, and TK Maycock (eds.), Washington, D.C., USA, 470 pp., doi: 10.7930/J0J964J6.

USGCRP (U.S. Global Change Research Program). 2018. *Impacts, Risks, and Adaptation in the United States: Fourth National Climate Assessment, Volume II*, Reidmiller, DR, CW Avery, DR Easterling, KE Kunkel, KLM Lewis, TK Maycock, and BC Stewart (eds.), Washington, DC, USA, 1515 pp. doi: 10.7930/NCA4.2018.

USGS (U.S. Geological Survey). 2005. Uncertainty in the Great Lakes Water Balance. USGS Scientific Investigations Report 2004-5100, USGS, Reston, Virginia. https://pubs.usgs.gov/sir/2004/5100/

USGS (U.S. Geological Survey). 2007. Lake-Level Variability and Water Availability in the Great Lakes. USGS Circular 1311, USGS, Reston, Virginia. https://pubs.usgs.gov/circ/2007/1311/

USGS (U.S. Geological Survey). 2010. *Flooding in the United States Midwest*, 2008. USGS Professional Paper 1775, USGS, Reston, Virginia. https://pubs.usgs.gov/pp/1775/

USGS (U.S. Geological Survey). 2011a. "General Weather Conditions and Precipitation Contributing to the 2011 Flooding in the Mississippi River and Red River of the North Basins, December 2010 through July 2011." Chapter B of *2011 Floods of the Central United States*. USGS Professional Paper 1798-B.

USGS (U.S. Geological Survey). 2011b. "Peak Streamflows and Runoff Volumes for the Central United States, February through September, 2011." Chapter C of *2011 Floods of he Central United States*. USGS Professional Paper 1798-C.

USGS (U.S. Geological Survey). 2011c. "Annual Exceedance Probabilities and Trends for Peak Streamflows and Annual Runoff Volumes for the Central United States During the 2011 Floods." Chapter D of *2011 Floods of he Central United States*. USGS Professional Paper 1798-D.

USIAC (U.S. Interagency Advisory Committee on Water Data). 1982. "Guidelines for determining flood flow frequency." Bulletin 17-B of the Hydrology Subcommittee, U.S. Geological Survey, Office of Water Data Coordination, Reston, Virginia. 183 p. Available from the National Technical Information Service, Springfield, Virginia as report no. PB 86 157 278 or from the Federal Emergency Management Agency at http://www.fema.gov/mit/tsd/dl_flow.htm.

Watras CJ, JS Read, KD Holman, Z Liu, Y-Y Song, AJ Watras, S Morgan, and EH Stanley. 2014. "Decadal oscillation of lakes and aquifers in the upper Great Lakes region of North America: Hydroclimatic implications." *Geophysical Research Letters* 41:456–462. doi:10.1002/2013GL058679

Wood AW, LR Leung, V Sridhar, and DP Lettenmaier. 2004. "Hydrologic implications of dynamical and statistical approaches to downscaling climate model outputs." *Climate Change* 62(1–3):189–216. doi:10.1023/B:CLIM.0000013685.99609.9e

Vose RS, S Applequist, M Squires, I Durre, MJ Menne, CN Williams Jr., C Fenimore, K Gleason, and D Arndt. 2014. "Improved Historical Temperature and Precipitation Time Series for U.S. Climate Divisions." *Journal of Applied Meteorology and Climatology* 53:1232-1251. doi: 10.1175/JAMC-D-13-0248.1

Vose RS, DR Easterling, KE Kunkel, AN LeGrande, and MF Wehner. 2017. "Temperature changes in the United States." In: *Climate Science Special Report: Fourth National Climate Assessment, Volume I*, Wuebbles DJ, DW Fahey, KA Hibbard, DJ Dokken, BC Stewart, and TK Maycock (eds.). U.S. Global Change Research Program, Washington, D.C., USA, pp. 185-206. doi: 10.7930/J0N29V45

Pacific Northwest
NATIONAL LABORATORY

www.pnnl.gov

902 Battelle Boulevard
P.O. Box 999
Richland, WA 99352
1-888-375-PNNL (7665)

U.S. DEPARTMENT OF
ENERGY